

SEMIANNUAL REPORT NO. 2

DEVELOPMENT OF COMPRESSOR END SEALS,
STATOR INTERSTAGE SEALS, AND STATOR PIVOT
SEALS IN ADVANCED AIR BREATHING
PROPULSION SYSTEMS

Prepared for

NATIONAL AERONAUTICS AND SPACE ADMINISTRATION

July 20, 1966

CONTRACT NAS3-7605

Technical Management
NASA Lewis Research Center
Cleveland, Ohio
Air Breathing Engine Division
D. P. Townsend
Project Manager
L. P. Ludwig
Research Advisor

Written by: R. M. Hawkins
R. M. Hawkins
Assistant Project Manager

Approved by: C. A. Knapp
C. A. Knapp
Project Manager

R. P. Shevchenko
R. P. Shevchenko
Senior Project Engineer

Pratt & Whitney Aircraft

DIVISION OF UNITED AIRCRAFT CORPORATION



EAST HARTFORD, CONNECTICUT

#32

PREFACE

This report describes the progress of work conducted between 1 January 1966 and 30 June 1966 by the Pratt & Whitney Aircraft Division of United Aircraft Corporation, East Hartford, Connecticut on Contract NAS3-7605, Development of Compressor End Seals, Stator Interstage Seals, and Stator Pivot Seals in Advanced Air Breathing Propulsion Systems, for the Lewis Research Center of the National Aeronautics and Space Administration.

Charles A. Knapp is Project Manager for Pratt & Whitney Aircraft for this program.

The following National Aeronautics and Space Administration personnel have been assigned to this project:

Contract Officer	- J. H. DeFord
Project Manager	- D. P. Townsend
Research Advisor	- L. P. Ludwig
Contract Administrator	- T. J. Charney

SUMMARY

This report describes the work completed during the second six month period of an analytical, design, and experimental program directed at developing compressor end seals, stator interstage seals, and stator pivot seals for advanced air breathing propulsion systems.

The objective of this contract is to achieve a means of increasing compressor efficiency by providing compressor seals with significantly lower air leakage rates than those currently in use while not incurring undue penalties in reliability and weight.

The program involves a screening study of all potential types of seals and a detailed feasibility analysis of those recommended for further evaluation. This feasibility analysis is to be followed by design and procurement of seals for rig evaluation. Test rigs simulating advanced engine construction, where applicable, will be procured for evaluation of these seals under specified operating conditions. Mechanical Technology Incorporated, under subcontract to Pratt & Whitney Aircraft, is to conduct an analytical program contributing to the feasibility analysis (Tasks I and III) of the prime contract.

Pratt & Whitney Aircraft is supplying MTI with information required to evaluate engine application of various seal concepts and is monitoring MTI's efforts through periodic meetings, as required under terms of the prime contract.

As mentioned in the monthly Progress Reports of March, April, and May 1966, Pratt & Whitney Aircraft feels that the similarity of the two floated shoe seal designs recommended for final design and evaluation will leave the program without a backup of radically different concept. This problem was discussed in a joint NASA-P&WA-MTI meeting held at NASA on March 17th. Three new concepts appear worthy of feasibility analysis: a ring-mounted flexure shoe design, an "OC" diaphragm thin strip design, and a semi-rigid one-piece seal design. NASA is presently considering the recommendation covering this work.

A NASA-Pratt & Whitney Aircraft meeting was held on 19 May 1966 to review the compressor seal program. At this meeting, Pratt & Whitney Aircraft submitted layout drawings for NASA approval to commence final design of the one side floated shoe compressor seal and two versions of a stator vane pivot seal. Also presented at this meeting were preliminary design layouts of test rigs in which Task I compressor seals and Task III vane pivot seals will undergo experimental evaluation. NASA approval of these seals was granted in a letter dated 31 May 1966. Design work was initiated immediately.

Mechanical Technology Incorporated (MTI) of Latham, New York submitted a Summary Report which is included in the text of this report.

Pratt & Whitney Aircraft is utilizing a computer program to evaluate primary seal performance for off-design conditions. A review of coil and wave spring designs for the one side floated shoe seal is being conducted. The thermal characteristics of this seal are being studied, with particular emphasis on thermal shunt requirements.

Design work was continued on test rigs in which Task I compressor seals and Task III vane pivot seals will undergo experimental evaluation.

Milestone charts are presented at the end of this report.

SEMIANNUAL REPORT NO. 2

DEVELOPMENT OF COMPRESSOR END SEALS,
STATOR INTERSTAGE SEALS, AND STATOR PIVOT
SEALS IN ADVANCED AIR BREATHING
PROPULSION SYSTEMS

by

H. L. Northup, R. M. Hawkins, and C. A. Knapp

ABSTRACT

The design of compressor end seals, stator interstage seals and stator pivot seals is discussed in detail. One-side floated shoe seals, two-side floated shoe seals, and thin strip seal designs are considered. Each design is analyzed with respect to mechanical, thermal, and fluid-flow conditions which affect sealing properties. The performance of each design is compared to the performance of seals currently in use.

TABLE OF CONTENTS

	<u>Page</u>
PREFACE	ii
SUMMARY	iii
ABSTRACT	v
LIST OF ILLUSTRATIONS	x
LIST OF TABLES	xv
NOMENCLATURE	xvii
INTRODUCTION	1
I. TASK I	2
A. SUMMARY	2
B. MTI FEASIBILITY ANALYSIS	2
1. INTRODUCTION	7
2. SUMMARY AND CONCLUSIONS	7
a. Compressor End and Interstage Seals	7
b. Vane Pivot Seals	19
3. PRIMARY SEALS	19
a. Rayleigh Step	19
b. Primary Seal Analysis for Multiple Pad Design	34
4. ANALYSIS OF THE TWO-SIDE FLOATED SHOE SEAL	38
a. Description	38
b. Primary Seal Selection	43
c. Force and Moment Balancing	44
d. Leakage	45
e. Tracking Capability	48
f. Thermal Distortion Effects	50
g. Mechanical Distortions	53
h. Wear and Rubbing Life	54
i. Stress Considerations	54
j. Tolerance to Dirt	54

TABLE OF CONTENTS (Cont'd)

	<u>Page</u>
k. Maneuvering Loads	55
l. Fail-Safe Considerations	55
m. Materials	55
n. Off-Design Operation	56
5. ANALYSIS OF THE ONE-SIDE FLOATED SHOE SEAL	56
a. Description	56
b. Selection of Primary Seal Type	60
c. Moment and Force Balance	63
d. Leakage	63
e. Dynamics	64
f. Thermal Distortion Effects	69
g. Mechanical Distortion	72
h. Wear and Rubbing Life	73
i. Stress and Fatigue	74
j. Tolerance to Foreign Particles	75
k. Maneuvering Loads	75
l. Fail-Safe Considerations	77
m. Materials	77
n. Off-Design Operation	78
6. DESIGN OF THE THIN-STRIP PLUS PISTON RING CONCEPT	78
a. Description	78
b. Design Criteria for Thin-Strip Seal	78
c. Primary Seal Concepts Considered for Thin-Strip Seal	82
d. Force and Moment Balance	87
e. Flexibility Requirements	88
f. Other Considerations	94
7. DESIGN OF THE THIN-STRIP PLUS C DIAPHRAGM CONCEPT	97
a. Description	97
b. Force and Moment Balance	97
c. Flexibility Requirements	98
d. Other Considerations	99
8. OPERATION UNDER ENGINE CONDITIONS	101
a. Rebalancing	101
b. Lift-Off Speed	102
c. Off-Design Operation	103

TABLE OF CONTENTS (Cont'd)

	<u>Page</u>
d. Thermal Transient Effects	103
e. Inertia Effects	103
f. Back-Up Design	104
II. TASK II	110
A. SUMMARY OF TASK II EXPERIMENTAL EVALUATION	110
B. TEST SEAL DESIGNS	110
C. TEST RIG DESIGNS	112
III. TASK III	113
A. SUMMARY OF TASK III FEASIBILITY ANALYSIS	113
B. MTI FEASIBILITY ANALYSIS - TASK III	113
1. CONCLUSIONS AND RECOMMENDATIONS	113
2. BELLOWS-LOADED FACE SEAL	115
a. Introduction	115
b. Description	115
c. Leakage Calculations	117
d. Actuation Torque	119
e. Life	120
f. Comparison of Bellows-Loaded Face Seal with Current Vane Pivot Seal Practice	120
3. SPHERICAL SEAT FACE SEAL	125
a. Introduction	125
b. Description	125
c. Leakage	125
d. Actuation Torque	127
e. Life	127
f. Comparison with Current Vane Pivot Seal Practice	128
IV. TASK IV	131

TABLE OF CONTENTS (Cont'd)

	<u>Page</u>
A. SUMMARY OF TASK IV EXPERIMENTAL EVALUATION	131
B. TEST SEAL DESIGNS	132
C. TEST RIG DESIGN	132
PROGRAM SCHEDULE & MILESTONE CHART	135
APPENDIX A Fortran Listing for the Rayleigh Pad Seal	139
APPENDIX B Analysis of Spiral Groove Orifice Hybrid Seal	149
APPENDIX C Face & Moment Balancing	160
APPENDIX D Thermal Analysis of the Two-Side Floated Shoe Seal	176
APPENDIX E Thermal Analysis of the One-Side Floated Shoe Seal	198
APPENDIX F Effective Polar Moment of Inertia of Thin Open Section	211
APPENDIX G Leakage Rate Calculations of Present Labyrinth Seals for Test Rig Conditions	212
BIBLIOGRAPHY	217
REFERENCES	218
DISTRIBUTION LIST	219

LIST OF ILLUSTRATIONS

<u>Figure No.</u>	<u>Title</u>	<u>Page No.</u>
1	One-Side Floated Shoe Compressor End Seal. Ref. P&WA Dwg. L-70329	3
2	One-Side Floated Shoe Stator Interstage Seal. Ref. P&WA Dwg. L-70328	5
3	Compressor End Seal Concept Scheme A. Ref. P&WA Dwg. L-67714 and MTI Sketch-D-2116	8
4	Compressor End Seal Concept Scheme C. Ref. P&WA Dwg. L-67714 and MTI Sketch-D-2134	9
5	Compressor End Seal Concept Scheme D. Ref. P&WA Dwg. L-67714 and MTI Sketch-D-2132	10
6	Compressor End Seal Concept Scheme E. Ref. P&WA Dwg. L-67714 and MTI Sketch-D-2118	11
7	Stator Interstage Heat Concept Scheme A. Ref. P&WA Dwg. L-67713 and MTI Sketch-D-2116	12
8	Stator Interstage Seal Concept Scheme C. Ref. P&WA Dwg. L-67713 and MTI Sketch-D-2134	13
9	Stator Interstage Seal Concept Scheme D. Ref. P&WA Dwg. L-67713 and MTI Sketch-D-2132	14
10	Overall Test Rig Pressure Levels	15
11	Rayleigh Step Seal Designs	20
12	Typical Flow Matching of Rayleigh Step and Orifice	26
13	Dimensionless Load Vs. Film Thickness for Various Orifices with Pocket Depth = 0.5×10^{-3} Inches	29
14	Dimensionless Load Vs. Film Thickness for Various Orifices with Pocket Depth = 0.3×10^{-3} Inches	29

LIST OF ILLUSTRATIONS (Cont'd)

<u>Figure No.</u>	<u>Title</u>	<u>Page No.</u>
15	Rayleigh Step Seal Loading	30
16	Effect of Length-to-Width Ratio on Performance	31
17	Computation of Pad Tilting Effect	35
18	Double Orifice Primary Seal with Special Groove	35
19	Double Pad Seals with Central Vent Groove	36
20	Load Vs. Film Thickness for Multiple Pad Design	37
21	Dimensionless Mass Flow-Hydrostatic Step, $\bar{b}_1 = 0.35$	46
22	Schematic of One-Side Floated Shoe Seal	57
23	Dynamic Model of One-Side Floated Shoe Seal	64
24	Thin-Strip Plus Piston Ring Seal	79
25	A Ring Element of the Thin-Strip Plus Piston Ring Seal	81
26	Single Pad, Double Orifice Spiral-Groove Seal	83
27	Double Pad, Spiral Groove Seal	84
28	Model of Double Pad Seal Surface	85
29	Loading of Double Pad Seal	87
30	Forces on Primary Seal Ring	88
31	Thin-Strip Plus Piston Ring Seal	89
32	Forces Acting on the Seal in a Tilting Position, $\Delta \alpha = -0.001$ rad.	91
33	Forces Acting on the Seal in a Tilting Position, $\Delta \alpha = +0.001$ rad.	92

LIST OF ILLUSTRATIONS (Cont'd)

<u>Figure No.</u>	<u>Title</u>	<u>Page No.</u>
34	Two Common Restrictions	93
35	Layout of Thin Strip Plus C Diaphragm Seal	95
36	Forces Acting on the Primary Seal	98
37	Center of Pressure - Hydrostatic Step, $\overline{b_1} = .25$	102
38	Thin Strip OC Diaphragm	105
39	Hoop-Mounted Flexure Shoe	108
40	One-Piece Semi-Rigid Seal	109
41	Single Bellows Vane Pivot Seal	116
42	Vane Pivot Seal Test Rig	121
43	Spherical Seat Vane Pivot Seal	126
44	Seal Test Rig Schematic	133
45	Geometry of Spiral Groove - Orifice Hybrid Seal	149
46	Preliminary Design of Two-Side Floated Shoe Seal	163
47	Force and Moment Balancing of Two-Side Floated Shoe Seal	167
48	Load Curve for Hydrostatic Step Seal, $\overline{b_1} = 0.35$	174
49	Center of Pressure for Hydrostatic Step Seal, $\overline{b_1} = 0.35$	174
50	Temperature Distribution in Two-Side Floated Shoe Seal. Thermal Conductivity 7.1 BTU/hr. ft. ² °F/ft. throughout, 1200°F Core Machine. Temperatures Shown in °F.	178

LIST OF ILLUSTRATIONS (Cont'd)

<u>Figure No.</u>	<u>Title</u>	<u>Page No.</u>
51	Temperature Distribution in Two-Side Floated Shoe Seal. Thermal Conductivity 7.1 BTU/hr. ft. ² °F/ft. throughout, 1300°F Core Machine. Temperatures Shown in °F.	179
52	Temperature Distribution in Two-Side Floated Shoe Seal. Thermal Conductivity 7.1 BTU/hr. ft. ² °F/ft. throughout, 1100°F Core Machine. Temperatures Shown in °F.	180
53	Temperature Distribution in Two-Side Floated Shoe Seal. Thermal Conductivity 13.0 BTU/hr. ft. ² °F/ft. throughout, 1200°F Core Machine. Temperatures Shown in °F.	181
54	Temperature Distribution in Two-Side Floated Shoe Seal with Thermal Shunt in Runner. Thermal Conductivities 26.0 BTU/hr. ft. ² °F/ft. in Shunt, 13.0 BTU/hr. ft. ² °F/ft. elsewhere; 1200°F Core Machine. Temperature Shown in °F.	182
55	Temperature Distribution in Two-Side Floated Shoe Seal with Thermal Shunt in Runner. Thermal Conductivities 26.0 BTU/hr. ft. ² °F/ft. in Shunt, 13.0 BTU/hr. ft. ² °F/ft. elsewhere; 1300°F Core Machine. Temperatures Shown in °F.	183
56	Temperature Distribution in Two-Side Floated Shoe Seal with Thermal Shunt in Seal Block. Thermal Conductivities 26.0 BTU/hr. ft. ² °F/ft. in Shunt, 13.0 BTU/hr. ft. ² °F/ft. elsewhere; 1200°F Core Machine. Temperatures Shown in °F.	184
57	Temperature Distribution in Two-Side Floated Shoe Seal with Thermal Shunt in Seal Block. Thermal Conductivities 26.0 BTU/hr. ft. ² °F/ft. in Shunt, 13.0 BTU/hr. ft. ² °F/ft. elsewhere; 1300°F Core Machine. Temperatures Shown in °F.	185

LIST OF ILLUSTRATIONS (Cont'd)

<u>Figure No.</u>	<u>Title</u>	<u>Page No.</u>
58	Temperature Distribution in Two-Side Floated Shoe Seal with Thermal Shunt in Seal Block. Thermal Conductivities 26.0 BTU/hr. ft. ² °F/ft. in Shunt, 13.0 BTU/hr. ft. ² °F/ft. elsewhere; 1100°F Core Machine. Temperatures Shown in °F.	186
59	Hydrostatic Step Seal Parameters	191
60	Original and Final Clearances of One-Side Floated Shoe Face Seal	198
61	Node Number System for One-Side Floated Shoe Face Seal	199
62	Temperature Distribution for Case A	200
63	Temperature Distribution for Case B	201
64	Temperature Distribution for Case C	202
65	Pressures in One-Side Floated Shoe Face Seal Gap	206
66	Labyrinth Seal Leakage Curves	213
67	Flow Coefficient Curve	213
68	Current Engine End Seal	214
69	Current Engine Interstage Seal	215

LIST OF TABLES

<u>Table No.</u>	<u>Title</u>	<u>Page No.</u>
I	Performance of Rayleigh Step Seal with Through Pocket	21
II	Performance of Rayleigh Step Seal with Orifice Feeding (Pocket Depth = 0.5×10^{-3} in.)	22
III	Performance of Rayleigh Step Seal with Orifice Feeding (Pocket Depth = 0.3×10^{-3} in.)	23
IV	Performance of Rayleigh Step Seal with Side Feeding	24
V	Performance of Rayleigh Step Seal with Shrouded Steps	24
VI	Dimensionless Flow \bar{Q}_{ORIFICE}	25
VII	Performance of Pad with Orifice of Pocket Depth = 0.5×10^{-3}	27
VIII	Performance of Pad with Orifice of Pocket Depth = 0.3×10^{-3}	28
IX	Performance of Rayleigh Step Seal at Take-Off Condition	31
X	Performance of Rayleigh Step Seal, Interstage Seal at Cruise	32
XI	Stiffness of Various Rayleigh Pads	33
XII	Performance of Rayleigh Step Seal at Tilting Position	34
XIII	Contract Seal Operating Conditions	39
XIV	Comparison of Two-Side Floated Shoe Seal with Labyrinth Seal	40

LIST OF TABLES (Cont'd)

<u>Table No.</u>	<u>Title</u>	<u>Page No.</u>
XV	Summary of Reliability Considerations for Two-Side Floated Shoe Seal	42
XVI	Leakage Flow Tabulation	45
XVII	Comparison of One-Side Floated Shoe Seal with Labyrinth Seal	61
XVIII	Summary of Reliability Considerations for One-Side Floated Shoe Seal	62
XIX	Dynamic Response of Rayleigh Step Seal	66
XX	Vane Pivot Seal Characteristics	114
XXI	Seal Balancing for Two-Side Floated Shoe Seal	165
XXII	Seal Parameters	169
XXIII	Seal Balancing for One-Side Floated Shoe Seal	171
XXIV	Physical Properties of Inconel-X, the Thermal Shunts, and the Air Used in the Thermal Analysis	187
XXV	Adiabatic Temperature Drop	208

NOMENCLATURE

- α coefficient of linear expansion
- α relative angular displacement between rotor and seal face in milliradians
- α_D angular twist between rotor and seal ring face, radians
- β groove angle, radians
- $\delta_{f, 2}$ changes in film thickness resulting from center spring change and runout of runner, inches
- δ_{WARP} warping due to thermal distortion, inches
- δ_C centrifugal growth, inches
- δ_s linear growth of seal width, inches
- δ_t differential growth due to temperature and material differences, inches
- δ_b radius increase due to thermal bowing, inches
- $\Lambda = \frac{6\mu bU}{P_1 h^2}$
- λ eigen value of Eq. (85)
- μ viscosity of air, pound-seconds per square inch
- ν_h torsional natural frequency, cycles per second
- ν_0 lowest torsional natural frequency, cycles per second
- ρ mass density, lb-sec²/in⁴
- \bar{P} radius of curvature inches
- ω rotating speed, radians per second
- ω_0 transverse natural frequency, radians per second

- $\bar{\omega}$ imposed vibration frequency on a vibrating system, radians per second
- $A_{1, 2, 3}$ dynamic displacements in simulated spring-mass system, inches
- A cross-sectional area of orifice controlled leakage path, square inches
- A_p pad area per inch of circumference, square inches per inch
- B surface finish of mating surfaces, rms
- C damping coefficient in equations of motion
- C_D discharge coefficient, dimensionless
- C_m radial clearance as manufactured, inches
- E modulus of elasticity, pounds per square inch
- F thrust, pounds
- G shear modulus, pounds per square inch
- $G(r_{12})$ dimensionless orifice flow
- \bar{H} height ratio = $h_1/(h_2 - h_1)$
- J effective polar moment of inertia of seal section, inches⁴
- J mechanical equivalent of heat = 778 ft-lb/BTU
- K_S stiffness, pounds per inch per inch of circumference
- \bar{K}_α dimensionless angular stiffness at constant load
- \bar{K}_S dimensionless stiffness = $K_S h_1 / (p_2 - p_1)(\bar{H}b)$
- K'_{S1} K'_{S2} stiffness per unit area of sealing surface
- $K_{1, 2, 3}$ spring rate, pounds per inch
- \bar{M} dimensionless flow $m / \left(\frac{h_1^3}{24\mu b} \right) \left(\frac{P_2^2}{RT_2} \right)$
- M moment, inch-pounds
- M Mach number of gas in seal

- M mass of the seal segment
- N rotor speed, rpm
- Q_T total weight flow
- Q weight flow per pad = $m c g$
- $\bar{Q} = Q / \frac{P_1^2 h^3}{12 \mu R T_1}$
- R gas constant, $\text{in}^2 / ^\circ\text{R sec}^2$
- R_f radius of seal path, inches
- T torque, inch-pounds
- T_1 inlet temperature, degrees Rankine
- T_S surface temperature of segment, degrees Fahrenheit
- T_r surface temperature of rotor, degrees Fahrenheit
- ΔT_{S-s} temperature difference between seal segments and support structure, degrees Fahrenheit
- ΔT temperature change across t, degrees Fahrenheit
- U surface velocity, inches per second
- V volumetric flow rate, cubic feet per minute
- W load per unit circumference, pounds per inch
- \bar{W} dimensionless load = $W / (P_2 - P_1) b$
- X_C position of center of pressure of sealing surface, inches
- \bar{X}_C dimensionless center of pressure X_C / b
- X displacement of element in a vibrating system or relative angular displacement between rotor and seal face, inches

X, Y, Z coordinates

a' half length of object under thermal distortion, inches

α_r thermal expansion coefficient of rotor, inches per inch-degree Fahrenheit

α_s thermal expansion coefficient of segment, inches per inch-degree Fahrenheit

a orifice radius, inches

b width of sealing surface or shoe face, inches

\bar{b}_1 step width ratio = b_1 / b

C circumferential length of one pad, inches

e strain, inches/inch

f coefficient of friction

f_1 half amplitude of runner disturbance, inches

g gravitational constant, 386 in/sec^2

h_1, h_2 gas film thickness, inches

h_1, h_2 height, inches; also film thickness of downstream and upstream sections respectively, inches

h_m mean gas film thickness, inches

i $\sqrt{-1}$

k_f stiffness of the fluid film, pounds per inch

k_s stiffness of seal back-up springs, pounds per inch

l cross flow length of seal, inches; thickness of object under thermal distortion, inches

m mass flow rate per unit circumferential length, lb-sec/in^2

m mass of seal

n number of surface oscillations per revolution

n number of pads in complete seal

- P_1, P_2 Downstream and upstream pressure respectively, lb/in²
- q rate of heat generation or dissipation, BTU's per hour
- q restoring force per unit length
- q_α restoring moment per unit length
- r_{12} pressure ratio P_1/P_2
- t thickness of object or mean runner thickness, inches
- v mean velocity in vibration excursion, feet per second
- w weight flow, pounds per second
- \bar{Y} Y/b
- Y transverse displacement, inches

INTRODUCTION

High performance, modern multistage axial flow compressors built with state-of-the-art features, incorporate several air leak paths which are detrimental to compressor performance. Elimination or significant reduction of these leaks would result in a compressor of higher efficiency and possibly smaller size. Some typical areas of leak paths with estimates of percent air loss and potential effect on compressor performance are:

	% Air Loss	<u>Effect on Compressor Efficiency</u>
End Seal	0.6%	1.0%
Interstage Stator Seals (ten stages)	0.9%	1.0%
Vane Pivot Seals (variable stator)	0.2% per stage	0.2% per stage

Increases in compressor efficiency are traditionally sought by means of compressor geometry redesign. A few extra points in efficiency often mean the difference between a successful or an unsuccessful engine design. These increases as a result of geometry change are always very expensive and not always successful. On the other hand, the losses to efficiency as a result of air leaks are strikingly large and real gains are within reach at a relatively low cost. The gains in efficiency however, must be balanced against any detrimental effect that improved sealing may have on the engine, such as lower reliability or increased weight.

This program will provide for a research, analytical, and test program having as its goal the development of compressor end seals, stator interstage seals, and vane pivot seals which exhibit lower air leakage rates than those currently in use. This will be accomplished using components of such size, materials, and designs as to be considered applicable to compressors for engines capable of supersonic aircraft propulsion.

I. TASK I - CONCEPT FEASIBILITY ANALYSIS
PROGRAMS FOR COMPRESSOR END SEALS
AND FOR COMPRESSOR STATOR
INTERSTAGE SEALS

A feasibility analysis program was conducted on seals for application in stator interstage and end seal systems. The first phase of this program was a preliminary analysis and screening of various seal concepts prior to the selection of concepts for the detailed feasibility analysis. The analytical effort included a comparison of the selected concepts to current practice and all calculations, analyses, and drawings necessary to establish feasibility of these selected concepts. This analytical effort was subcontracted to Mechanical Technology Inc. (MTI) of Latham, New York and was monitored by Pratt & Whitney Aircraft as required under the terms of the NASA contract.

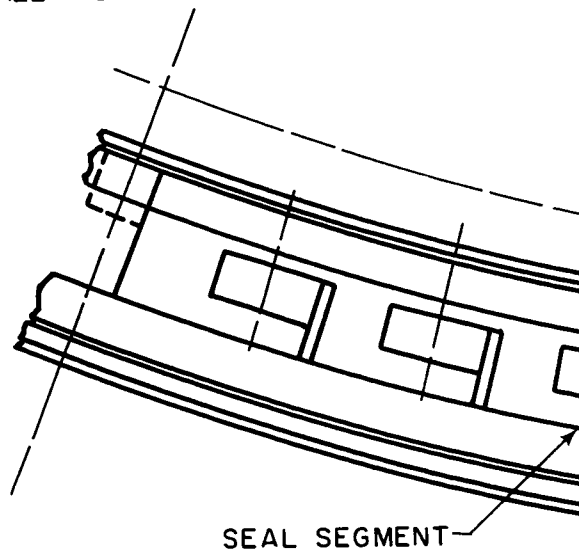
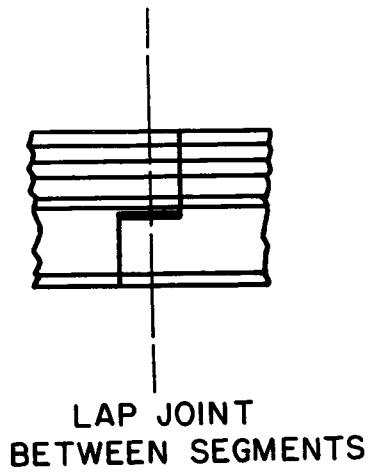
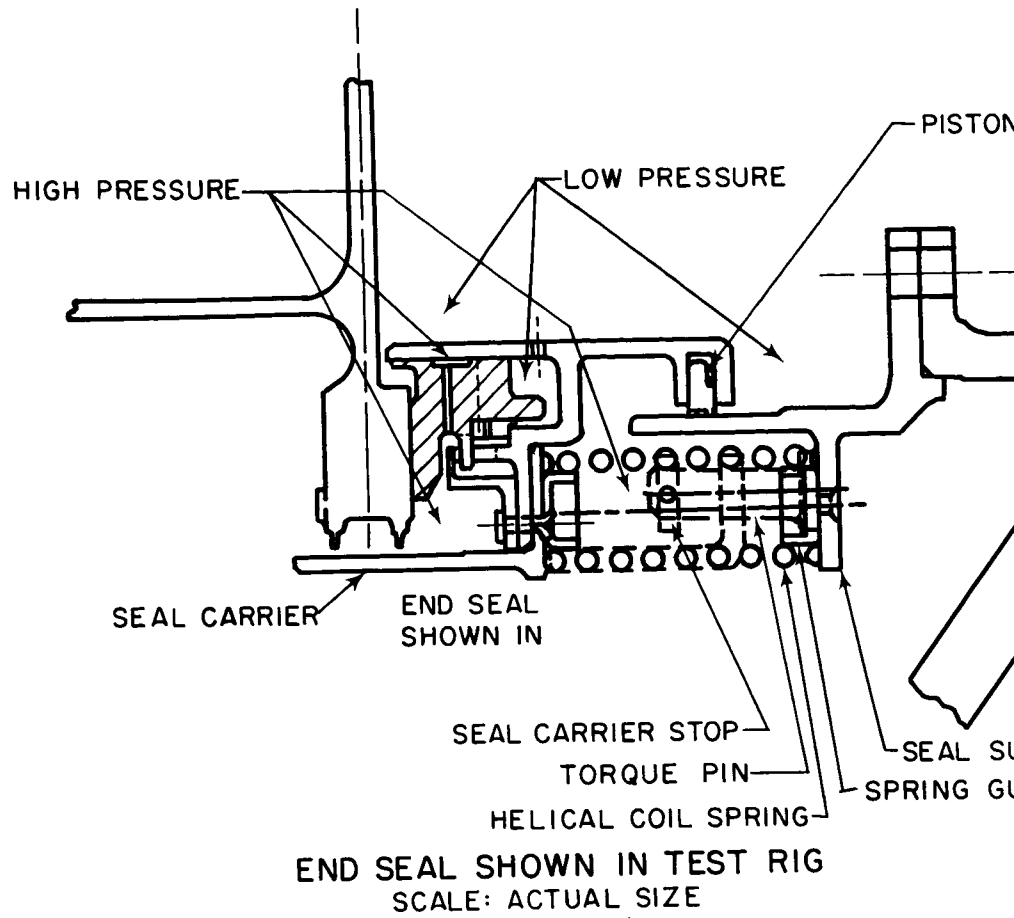
A. SUMMARY OF TASK I FEASIBILITY ANALYSIS

MTI completed the feasibility analysis on the four compressor seal concepts remaining from the original screening studies. Two seal concepts were considered feasible and adequate for recommendation to NASA: the one side and two side floated shoe seals. Pratt & Whitney Aircraft submitted the latest designs of the one side floated shoe compressor end seal and stator interstage seal concepts to NASA on 19 May 1966 requesting approval to start final design under Task II (see Figures 1 and 2). An effort was made to ensure compatibility of the seal with current engine practice without making major changes in the basic seal concepts shown on the MTI drawings. Approval was granted in a letter from NASA dated 31 May 1966.

The results of the feasibility analysis indicated that the two side floated shoe (a radial seal) was also worthy of final design and manufacture. However, the recommendation of this seal was held in abeyance, since it was felt that the similarity of the two floated shoe seal designs would leave the program without a backup of radically different concept. Three new concepts appear to be worthy of feasibility analysis: a ring-mounted flexure shoe design, an "OC" diaphragm, a thin strip design, and a semirigid one piece seal design. NASA is presently considering the recommendation covering this work.

B. MTI FEASIBILITY ANALYSIS

The feasibility analysis of compressor end seal and stator interstage seal concepts conducted by MTI is presented in this section of the report. The material presented in this section was prepared by D. Wilcock, H. Cheng, J. Bjerklie, C. Chow, R. Newell, R. Thorkildsen, and K. Wachman.



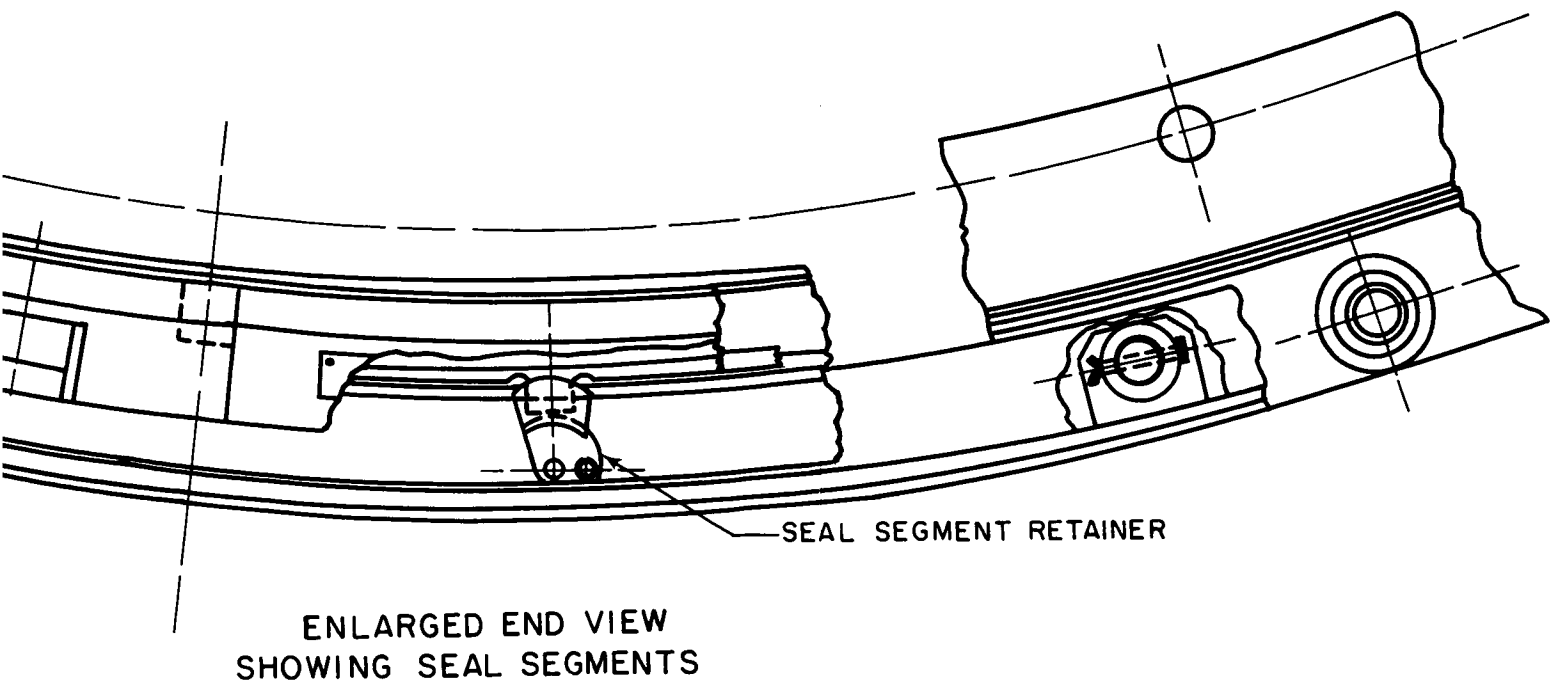
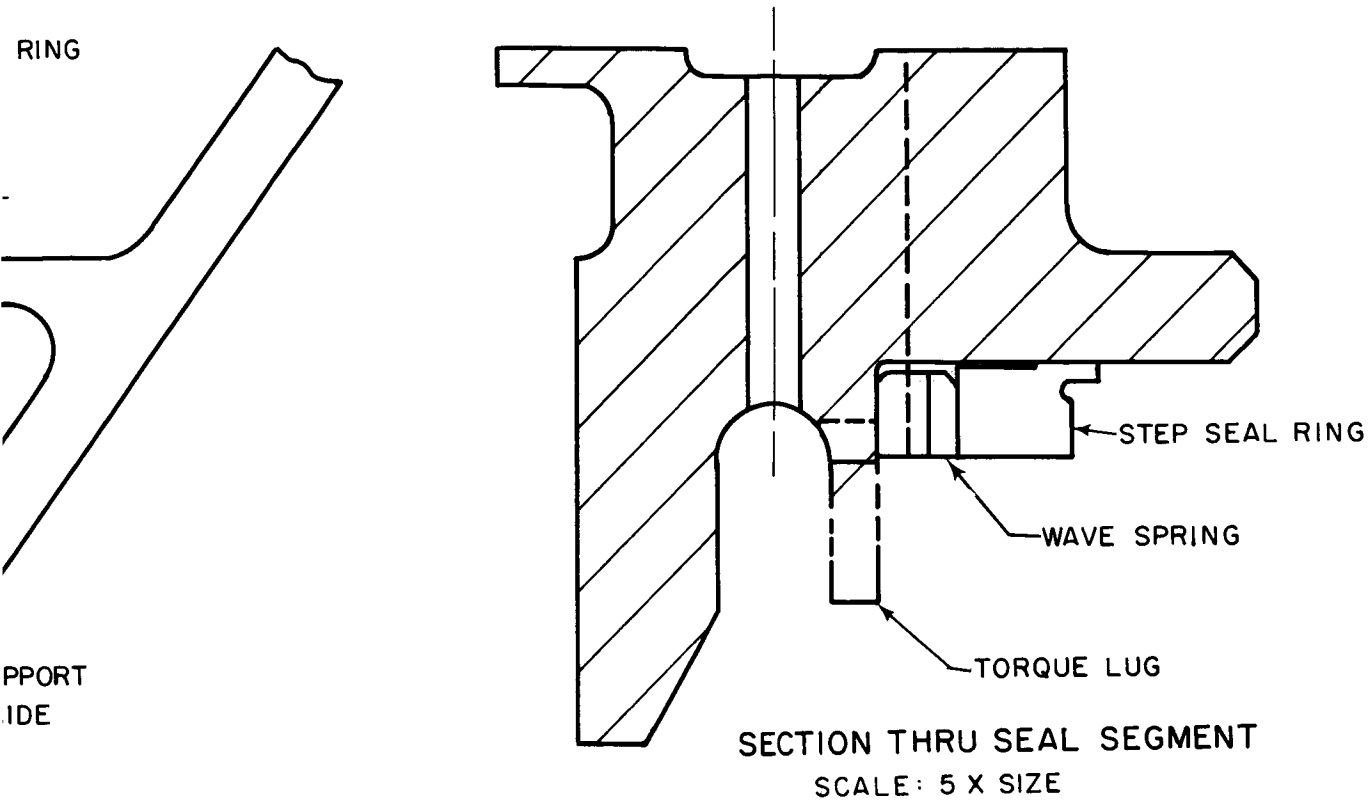
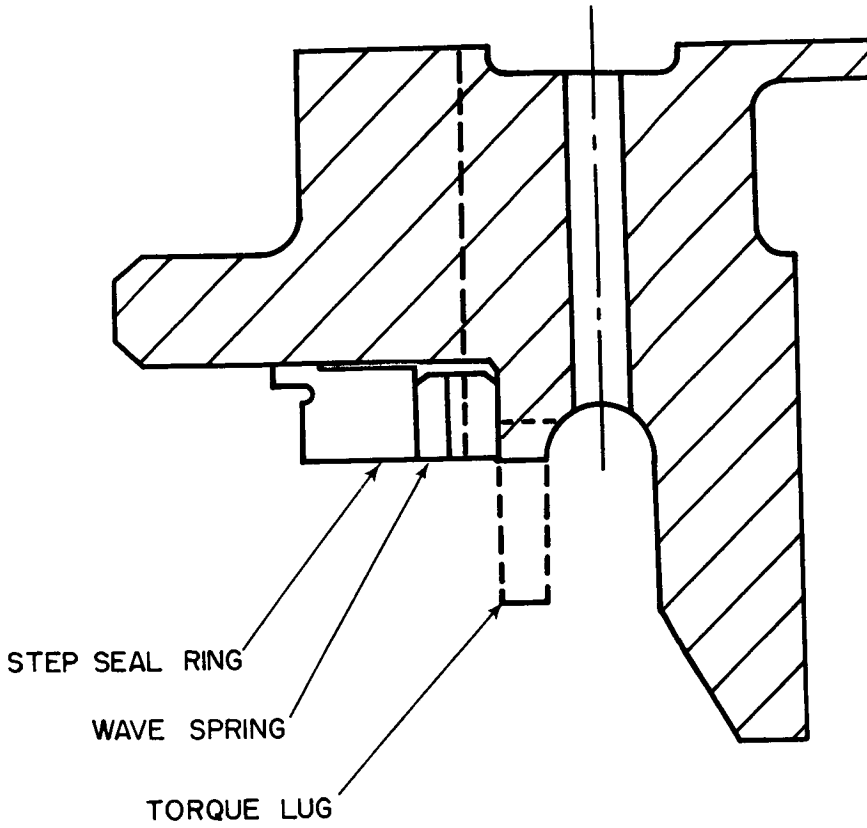
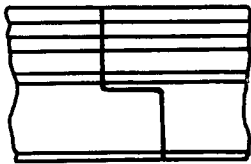


Figure 1 One-Side Floated Shoe Compressor End Seal. Ref. P&WA Dwg. L-70329

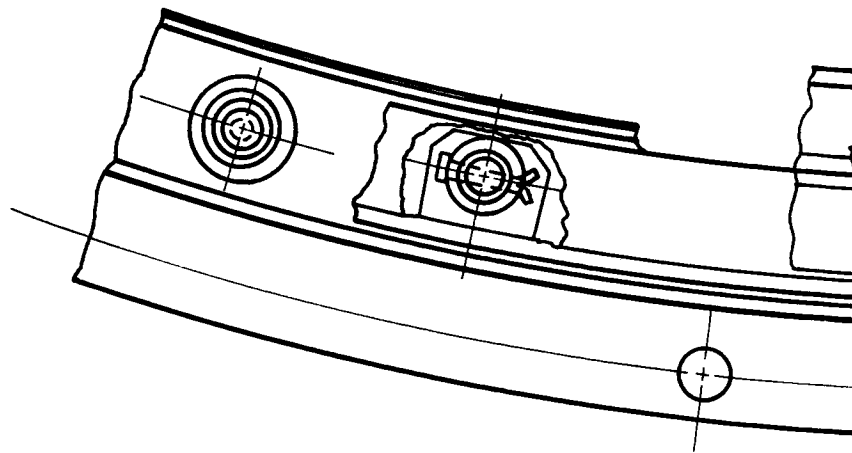


SECTION THRU SEAL SEGMENT

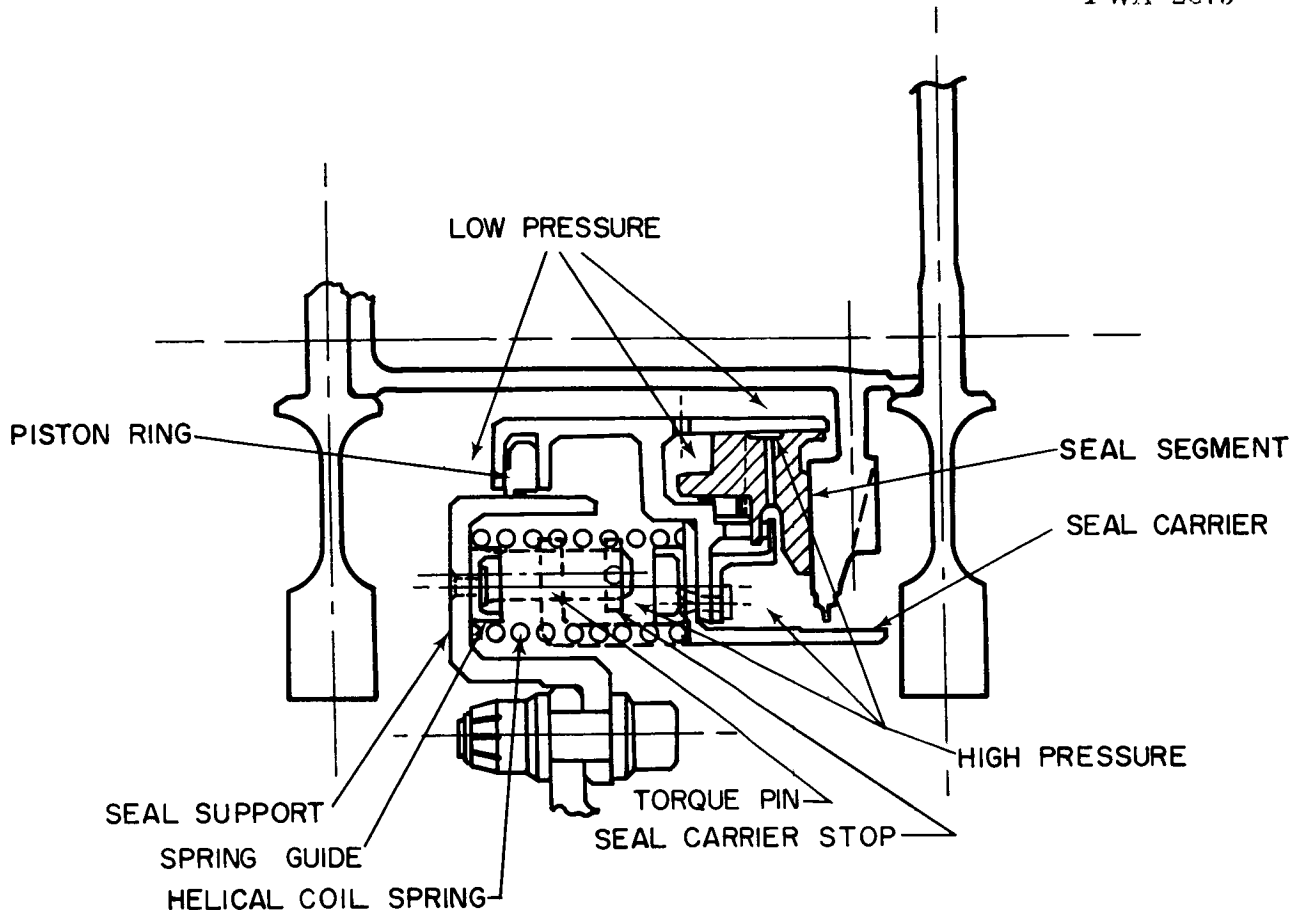
SCALE : 5X SIZE



LAP JOINT
BETWEEN SEGMENTS

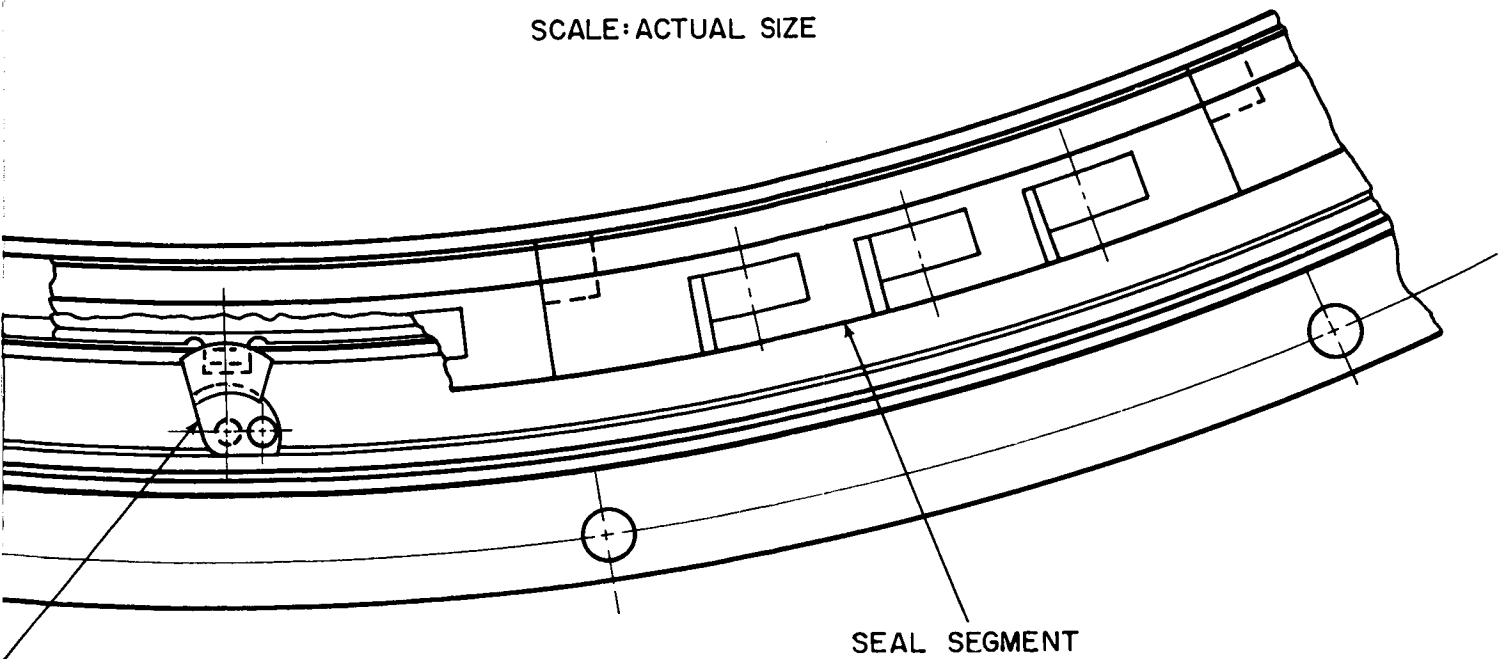


SEAL SEGMENT R



INTERSTAGE SEAL
SHOWN IN TEST RIG

SCALE: ACTUAL SIZE



RETAINER

Figure 2 One-Side Floated Shoe Stator Interstage Seal. Ref. P&WA Dwg. L-70328

ENLARGED END VIEW
SHOWING SEAL SEGMENTS

1. INTRODUCTION

This report concludes the feasibility analysis on compressor end seals and stator interstage seals for advanced air breathing propulsion systems.

The first Semi-Annual Report (PWA 2752) dated January 20, 1966, summarized the screening of a large number of concepts and the selection of the four best concepts for a detailed feasibility analysis. For the compressor end and interstage seals, it described the detailed analysis of primary seal performance, and the dynamics of seal tracking of runner motion.

This report brings the feasibility analysis to a conclusion, and contains duplications of material in the first Semiannual Report only when essential.

2. SUMMARY AND CONCLUSIONS

a. COMPRESSOR END AND INTERSTAGE SEALS

As a result of the screening study reported in the first Semiannual Report (PWA 2752) four seal concepts were selected for a further feasibility analysis,

- The Two-Side Floated Shoe (A Radial Seal)
- The One-Side Floated Shoe (A Face Seal)
- The Thin Strip Plus Piston Ring (A Face Seal)
- The Thin Strip Plus C Diaphragm (A Face Seal)

These designs are illustrated in Figures 3 to 6 for the compressor end seal, and in Figures 7 to 9 for the interstage seal.

1) TEST RIG CONDITIONS

The specifications for this study defined the air pressure and temperature conditions for both cruise and take-off as follows:

	<u>End Stage</u>		<u>Interstage</u>	
	<u>Cruise</u>	<u>Take-off</u>	<u>Cruise</u>	<u>Take-off</u>
Pressure Differential, psi	80	150	25	50
Upstream Temperature, °F	1200	680	1200	680
Seal Sliding Speed, ft/sec.	850	785	850	785

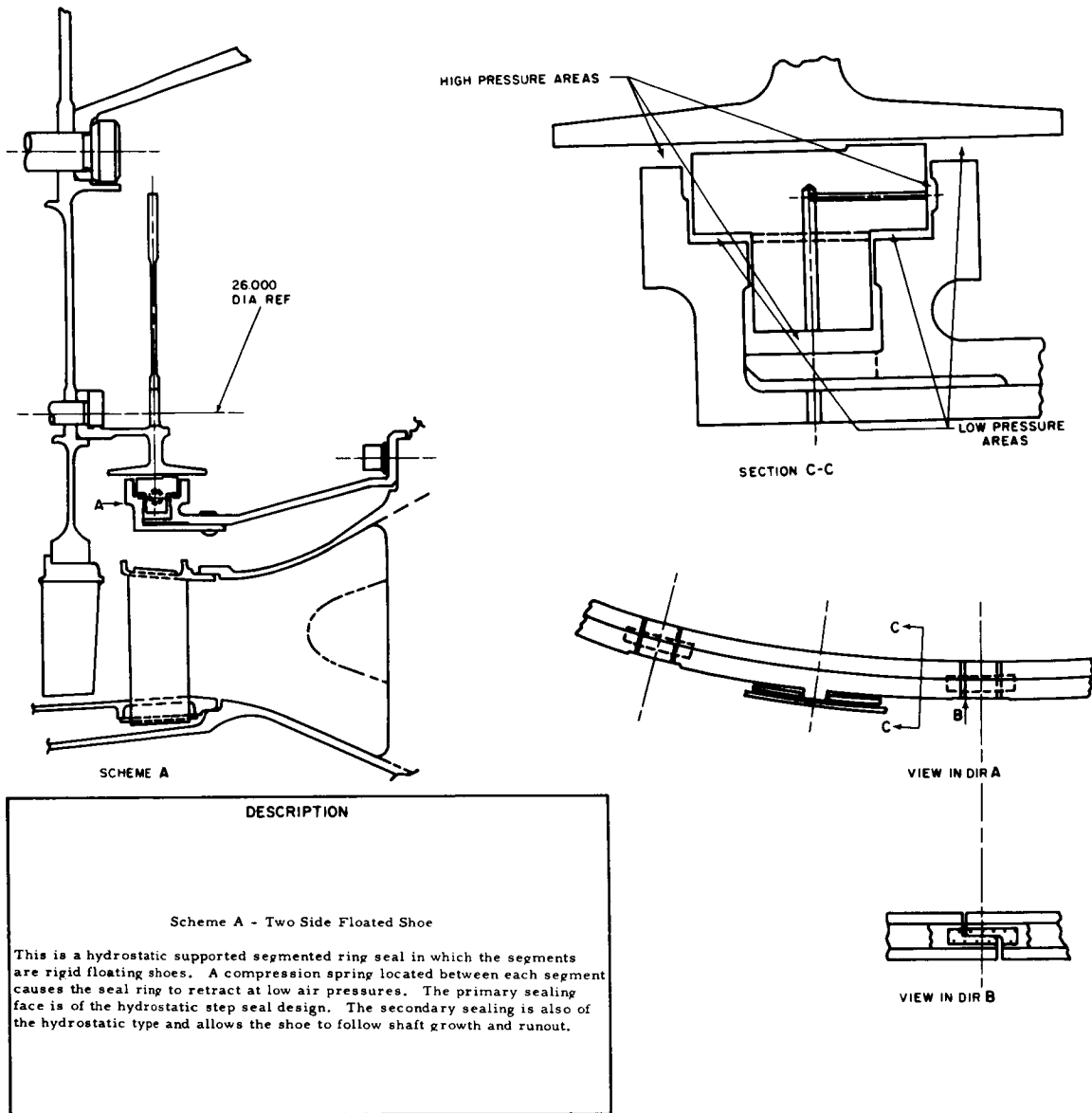
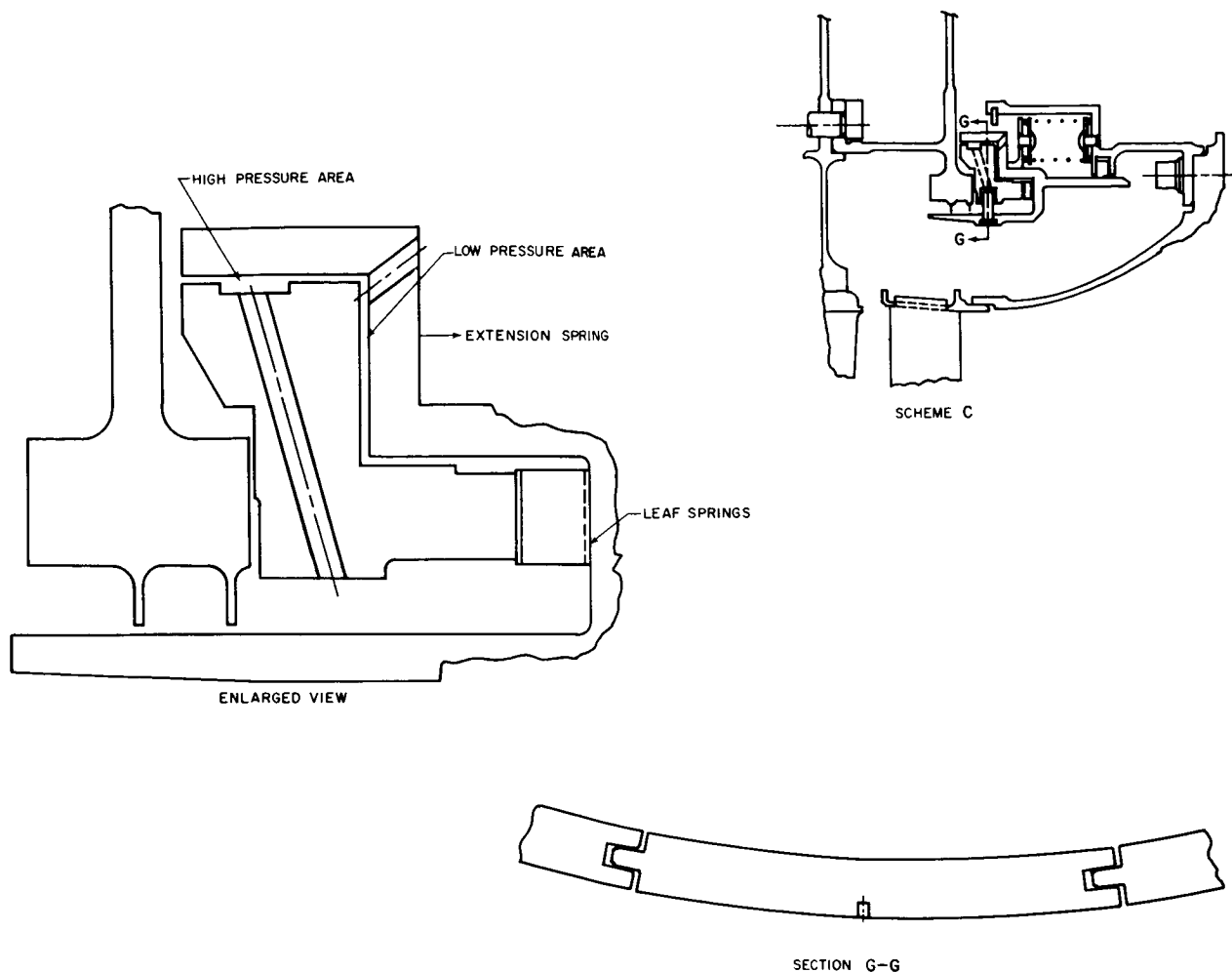


Figure 3 Compressor End Seal Concept Scheme A. Ref. P&WA Dwg. L-67714 and MTI Sketch D-2116

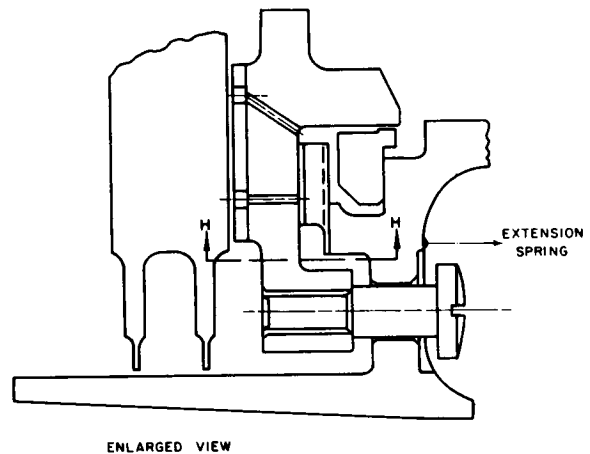
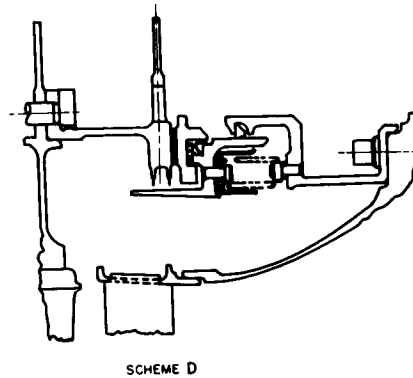
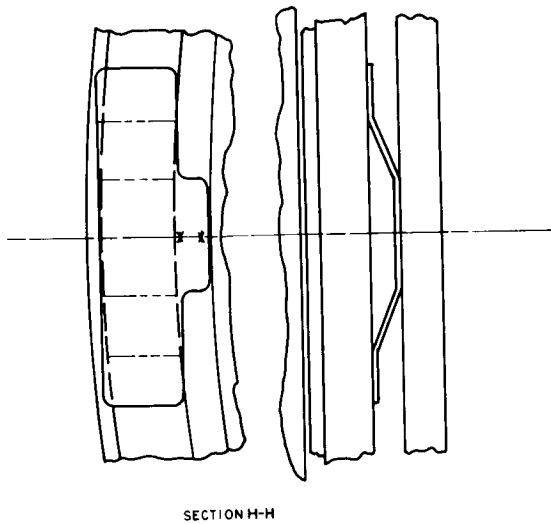


DESCRIPTION

Scheme C - One Side Floated Shoe

This seal is a hydrostatic supported segmented face seal in which the segments are rigid floating shoes. The floating shoes are retained in the seal carrier by an anti-rotation pin which also maintains a light compressive load on the leaf springs. The light duty leaf springs and hydrostatic secondary sealing between the shoe and carrier allows the shoe to follow low magnitude high frequency motion. The seal carrier which has a piston ring for the secondary seal will follow the full 0.4 inches of axial motion required. The extension spring ties the seal carrier to the fixed housing and causes the seal carrier to retract at low air pressures. When the primary seal is open a labyrinth seal produces the required pressure differential to close the seal at the desired engine operating condition.

Figure 4 Compressor End Seal Concept Scheme C. Ref. P&WA Dwg. L-67714 and MTI Sketch D-2134

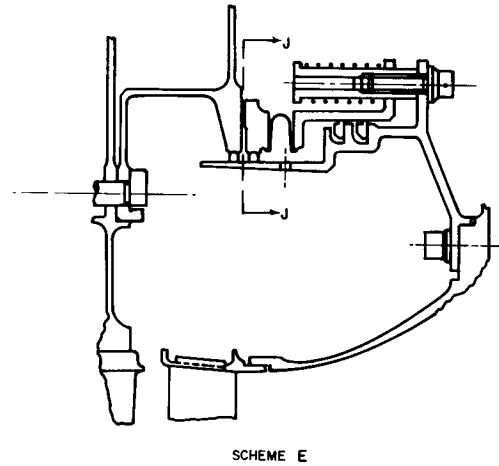
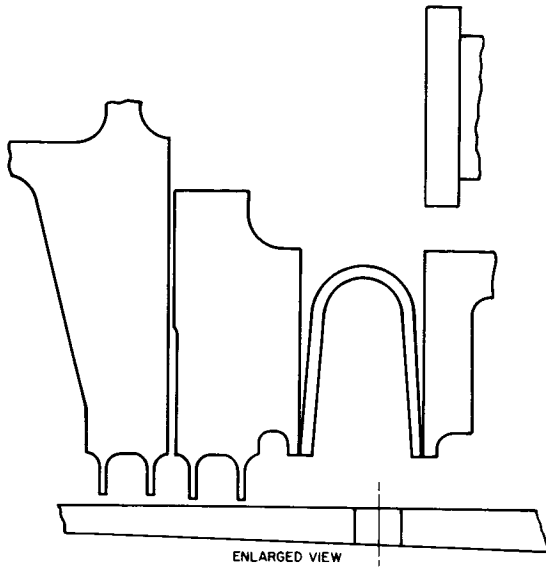


DESCRIPTION

Scheme D - Thin Strip - One Piece

The primary seal in this design is an orifice compensated hydrostatic supported one piece continuous thin strip face seal. A leaf spring is attached to the seal carrier and exerts a compressive force on the thin strip which is attached to the seal carrier by guide pins. Secondary sealing between the thin strip and the carrier consists of a fully floated piston ring which permits the thin strip to follow any runout or wobble of the face. A coating is shown which provides a better rubbing surface in case the thin strip contacts the face. The balance of the construction is similar to the one side floating shoe.

Figure 5 Compressor End Seal Concept Scheme D. Ref. P&WA Dwg. L-67714 and MTI Sketch D-2132



DESCRIPTION

Scheme E - Thin Strip - C Diaphragm

This seal is similar to the one piece thin strip seal, the method of secondary sealing being the primary change. This design utilizes a C diaphragm as the secondary seal between the thin strip and seal carrier in place of the piston ring and leaf springs. The design has been changed to incorporate compression springs in place of the extension springs used in two other face seal designs, but the operation of the seal is similar.

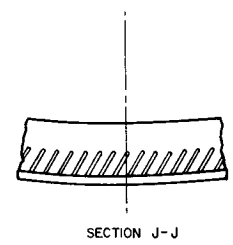
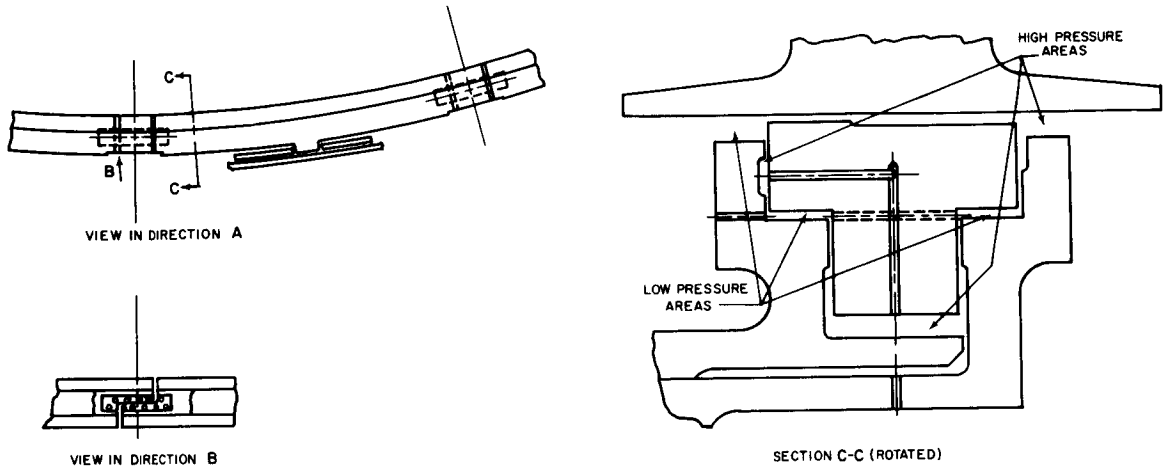


Figure 6 Compressor End Seal Concept Scheme E. Ref. P&WA Dwg. L-67714 and MTI Sketch D-2118



DESCRIPTION

Scheme A - Two Side Floated Shoe

This is a hydrostatic supported segmented ring seal in which the segments are rigid floating shoes. A compression spring located between each segment causes the seal ring to retract at low air pressures. The primary sealing face is of the hydrostatic step seal design. The secondary sealing is also of the hydrostatic type and allows the shoe to follow shaft growth and runout.

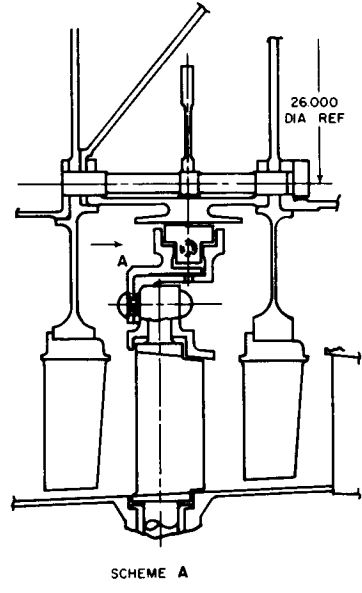
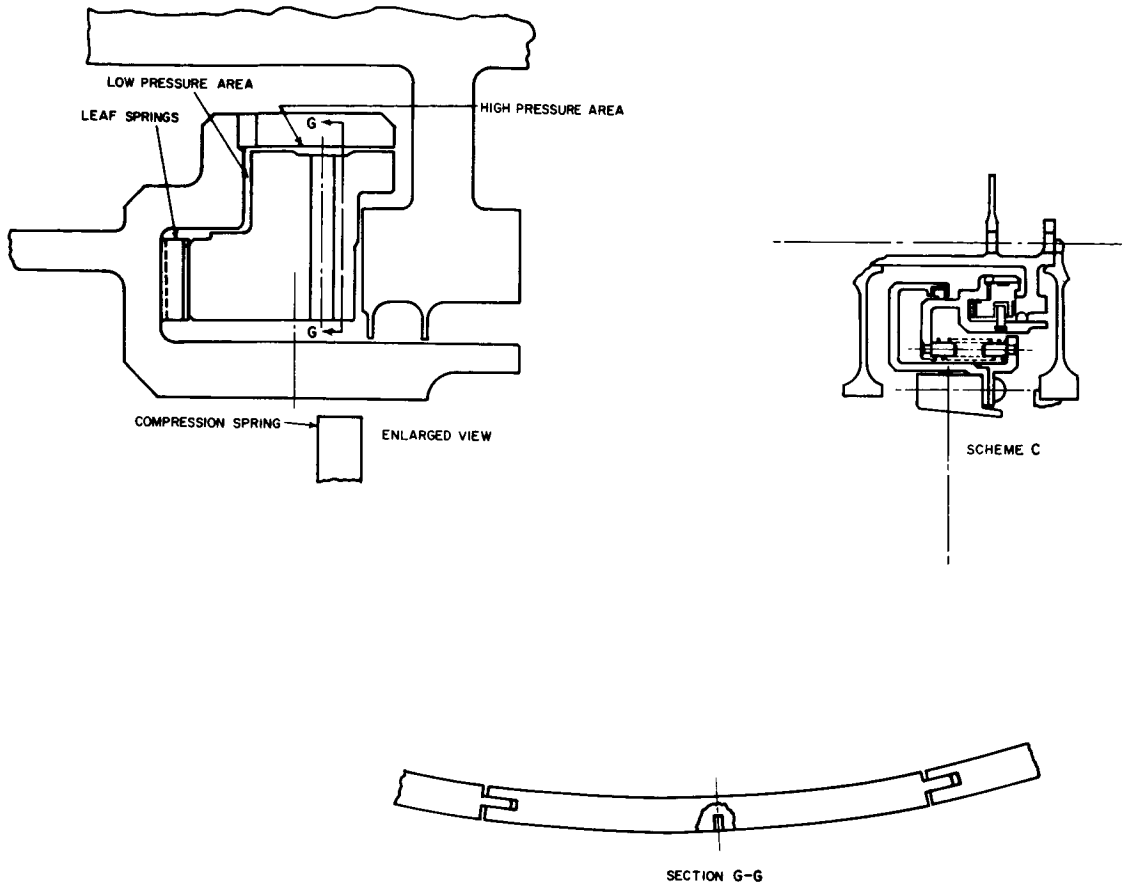


Figure 7 Stator Interstage Heat Concept Scheme A. Ref. P&WA Dwg. L-67713 and MTI Sketch D-2116

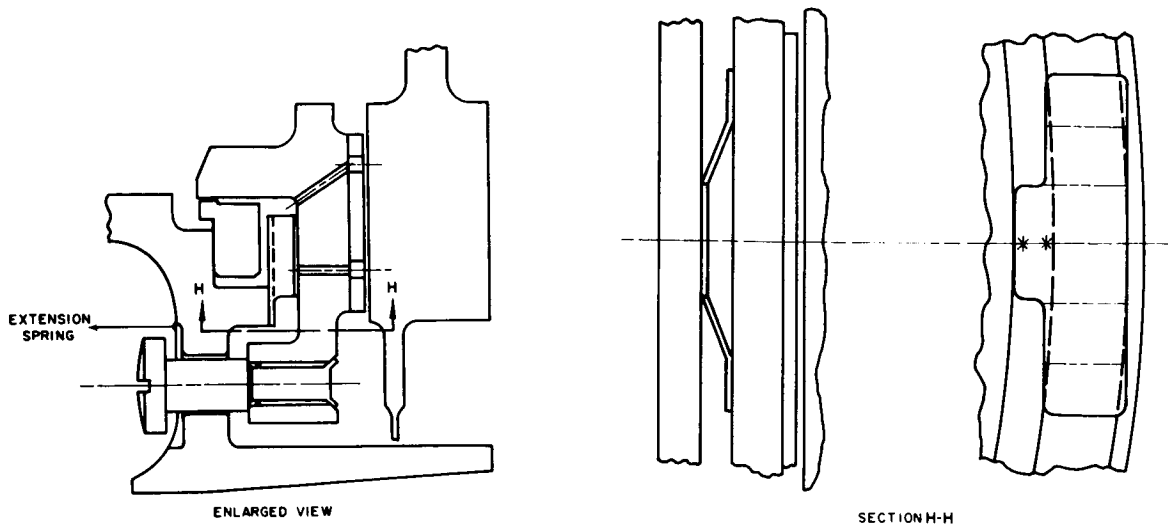


DESCRIPTION

Scheme C - One Side Floated Shoe

This seal is a hydrostatic supported segmented face seal in which the segments are rigid floating shoes. The floating shoes are retained in the seal carrier by an anti-rotation pin which also maintains a light extension load on the leaf springs. The light duty leaf springs and hydrostatic secondary sealing between the shoe and carrier allows the shoe to follow low magnitude high frequency motion. The seal carrier which has a piston ring for the secondary seal will follow the full 0.4 inches of axial motion required. The extension spring ties the seal carrier to the fixed housing and causes the seal carrier to retract at low air pressures. When the primary seal is open a labyrinth seal produces the required pressure differential to close the seal at the desired engine operating conditions.

Figure 8 Stator Interstage Seal Concept Scheme C. Ref. P&WA Dwg. L-67713 and MTI Sketch D-2134



DESCRIPTION

Scheme D - Thin Strip - One Piece

The primary seal in this design is an orifice compensated hydrostatic supported one piece continuous thin strip face seal. A leaf spring is attached to the seal carrier and exerts a compressive force on the thin strip which is attached to the seal carrier by guide pins. Secondary sealing between the thin strip and the carrier consists of a fully floated piston ring which permits the thin strip to follow any runout or wobble of the face. A coating is shown which provides a better rubbing surface in case the thin strip contacts the face. The balance of the construction is similar to the one side floating shoe.

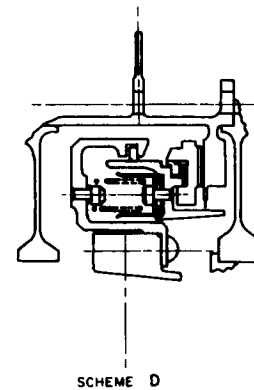


Figure 9 Stator Interstage Seal Concept Scheme D. Ref. P&WA Dwg. L-67713 and MTI Sketch D-2132

The actual pressure level was not specified, and will be, among other things, a function of altitude and vehicle speed. Simulated testing is planned to use a lower pressure of 20 psia. See Figure 10 for overall test rig pressure levels.

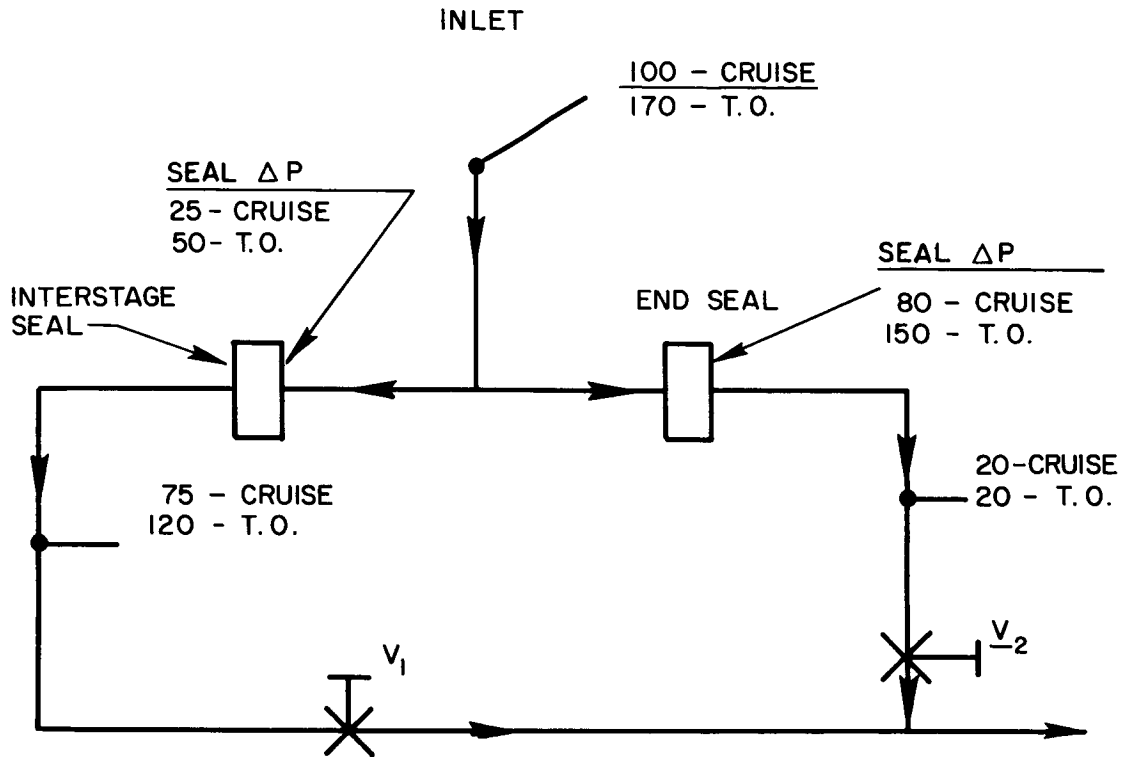


Figure 10 Overall Test Rig Pressure Levels

The seals are designed for test rig conditions, recognizing that these pressure levels are lower than could be experienced in an engine, and that the pressure ratios are therefore higher (see Section I. B. 2. a)8)). Redesign will be required for engine conditions to account for the influence of higher density and lower pressure ratios.

2) LABYRINTH LEAKAGE RATES

A standard four-tooth engine labyrinth, operating with a clearance of 0.018 inches under simulated end seal cruise conditions, is calculated to have a leakage rate of 1.07 pounds per second. Standard interstage seal leakage at cruise conditions is 2.02 pounds per second at 0.040 inches clearance. Comparisons of calculated seal leakage rates are made with these numbers.

3) TWO-SIDE FLOATED SHOE RADIAL SEAL

A feasibility analysis and preliminary layout of this seal have been completed. The design is shown in detail on Figures 3 and 7. Leakage rate for the end seal under test rig cruise conditions is calculated to be 0.076 pounds per second, less than one tenth that of the comparable labyrinth seal. The primary seal gas film is stiff enough to maintain its thickness to better than 0.0007 inches during maximum expected runout of the runner surface. A Rayleigh step configuration on the primary seal surface of the shoe provides additional hydrodynamic protection.

This seal contains 24 segments which are lightly spring loaded in one version, and which have retraction springs in another version. The shoes are floated in a close-fitting carrier by hydrostatic action. Some thermal shunting is required in order to minimize warping due to thermal gradients.

This design requires that a number of close tolerances be held during manufacture. In addition, both the runner and the shoe holder must be designed to minimize warping due to stress or thermal gradients, in order to keep the primary seal surfaces parallel.

4) ONE-SIDE FLOATED SHOE FACE SEAL

A feasibility analysis and preliminary layout of this seal have been completed. The design is shown in detail on Figures 4 and 8. The calculated leakage rate for the end seal under test rig cruise conditions is 0.028 pounds per second, less than one tenth of that of the comparable labyrinth seal. Film thickness change during tracking of runner wobble is less than 10 percent of that of the two-side floated shoe design. This is because face runout is about one tenth of the anticipated radial runout. Each shoe carries a Rayleigh step pattern on the primary surface for additional hydrodynamic protection.

In order to accommodate the anticipated relative axial motion, which may be as much as 0.4 inches, the 24 shoes are supported by a carrier ring which in turn is supported by soft springs. Stiffer springs support the shoes in the carrier and permit the shoes to track any unevenness in the runner surface as well as runner face runout. Secondary sealing is obtained by a floated one-piece piston ring between the carrier and the engine support structure, as well as by hydrostatic action between the floating shoe and carrier. Some thermal shunting is required for this seal.

This design is expected to be easier to manufacture than the two-side floated shoe. It requires fewer close tolerances and highly finished surfaces for proper functioning.

5) THIN STRIP PLUS PISTON RING FACE SEAL

The thin strip concepts inherently offer desirable features which could never be achieved with the shoe designs. These seals (Figure 5) are envisioned as being in one piece, not requiring inter-segment sealing. They can be simpler than the others, in that fewer pieces would be required. In addition, the inherent flexibility could make the application of low speed retraction easier, by providing better conformity during touchdown. A great amount of effort was expended on these concepts. The analysis has been complex and time consuming and has not produced an acceptable design. Results of the studies to date indicate that further efforts will probably not meet with success.

One major problem is to obtain the proper angular stiffness, so that the effects of initial angular warping and of residual moment errors will not result in an inadequate film thickness. Applying the criterion that the minimum film thickness shall be at least 70 percent of the design value in order to minimize local overheating, one finds that for a one inch strip, the combined rotor and seal angular warping must be no more than 0.0005 inches per inch. Manufacturing a flexible strip to such tolerances and guaranteeing that the flatness at rest will remain good is a problem that must be resolved. The most serious problem is to have complete assurance that warping will not occur after repeated cycling to 1200 degrees Fahrenheit and back to ambient, so that the film will remain uniform within 0.0005 inches per inch, particularly in the radial direction.

A second major problem in this design is that the torsional rigidity of the thin strip is greatly increased by the structure required to carry the piston rings, which carry the full pressure difference across the seal.

6) THIN STRIP PLUS C DIAPHRAGM FACE SEAL

This concept, shown in Figure 6, retains the flat, thin strip of the Thin Strip plus Piston Ring design - but adds a small spline, to which a C diaphragm is attached. Serious uncertainties in the flexibility of the diaphragm about a radial axis, and in the consistency of the moment transfer from the diaphragm to the strip have led to the abandonment of this design.

7) NEED FOR BACKUP DESIGNS

In any development program it is obviously desirable to have an alternate design which approaches the problem through an entirely different concept. The two floated shoe designs, while different in shoe orientation (face and radial), are still very similar. During evaluation they may both suffer from the same problem: both are extremely limited in their acceptance of angular deviations caused by thermal and elastic coning of the rotor and elastic rotation of the shoe carrier. It would be in the best interest of the overall program to have a backup involving a different concept.

Three new concepts have evolved since the completion of the screening studies. These have been the result of the extended effort to achieve acceptable thin strip designs. The three concepts are:

- The use of multiple diaphragm support for a thin strip to provide better control of the residual moment.
- A multiple shoe design in which the shoes are flexibly mounted to a supporting hoop which is flexible in bending about a radial axis.
- A one-piece semi-rigid seal, held to flatness tolerances as good as the runner face (0.0005 inches total indicator reading).

It is recommended that serious consideration be given to a feasibility analysis of these additional concepts, so that an alternate approach to the problem may be made available.

8) OPERATION UNDER ENGINE CONDITIONS

The two floated shoe designs, which have been completed as summarized above, are based on test rig pressure levels and pressure ratios. These pressures are considerably lower than could be experienced in an engine, and the pressure ratios could be much higher as a result. There are a number of additional factors which will enter into actual engine operation which will require further careful analysis.

The factors which should be subjected to further analysis and study to permit sound design of the seal for engine application may be summarized as follows:

- Pressure ratio: rebalance of the seal.
- Start, idle, and stop conditions: seal operation including lift-off performance where a non-retracting seal is used.
- Thermal transient effects during a full engine cycle of start-idle-take-off-cruise-idle-shutdown.
- Gas inertia effects: at the higher density experienced at engine operating pressures, inertia effects on pressure profile through the seal and on turbulence in the seal flow, must be predicted since both seal balance and heating will be affected. The present analysis is in the laminar region, but close to turbulence.
- Effects of compressor surge and seal action during windmilling.

b. VANE PIVOT SEALS

Two vane pivot seals have been recommended for final design. Since finishing the screening study, considerable design work has been carried out on both candidate designs. The two concepts have been completed and layout designs prepared. The designs have been submitted to potential vendors so that minor final changes could be made to conform to their practice.

Both seals have the potential to be eminently satisfactory from points of view of leakage, tolerance to cocking and dirt, and low actuation force. The potential problem areas are nearly the same for both seals. It will undoubtedly be a matter of exact final design technique and results of testing that will prove which seal is best.

Since the seals appear to be so evenly matched, it is recommended that both seals be built and tested. It is also recommended that consideration be given to the evaluation of carbon, electrofilm, and ceramic seal materials.

3. PRIMARY SEALS

As was indicated in the first Semiannual Report (PWA-2752), additional work on primary seal behavior was necessary and has been completed. This has included work on Rayleigh step characteristics, and on multiple pad configurations necessary for thin-strip tracking. This section summarizes this additional information.

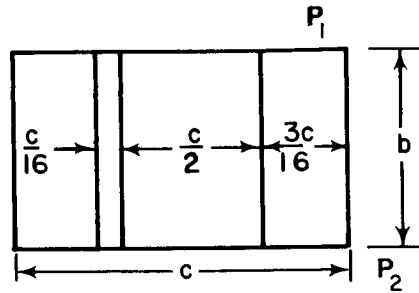
a. RAYLEIGH STEP

The Rayleigh step designs of interest here are hybrid hydrostatic-hydrodynamic seals. Several designs have been studied in search for a pattern offering high stiffness and low leakage flow. Four designs have been examined, as follows:

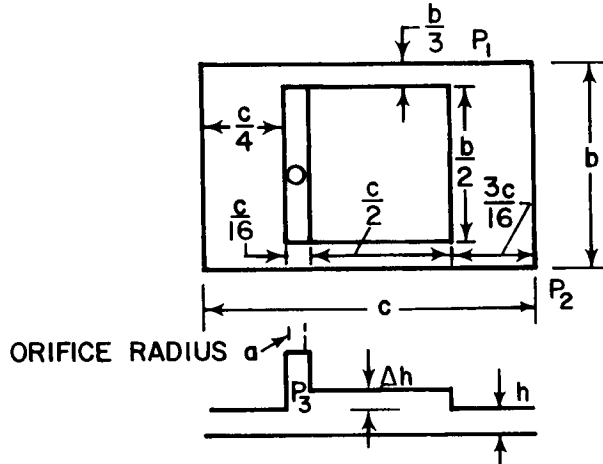
- Full width pocket (Figure 11-a)
- Orifice fed shrouded pocket (Figure 11-b)
- Side fed pocket (Figure 11-c)
- Shrouded pocket (Figure 11-d)

1) DESIGN SELECTION BASED ON CRUISE CONDITION

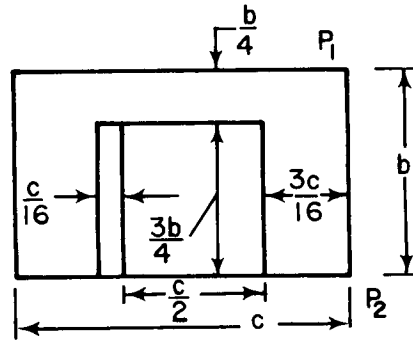
The performance was computed with the G. E. Model 625 computer. A boundary condition was imposed which simulated the condition of a number of steps on an annulus. The condition of operation of the seal was at $\mu = 5.9 \times 10^{-9}$ lb-sec/in²; $U = 10,000$ in/sec; $P_1 = 20$ psia; $P_2 = 100$ psia, and $T = 1200^\circ\text{F} = 1660^\circ\text{R}$. The seal geometry, pocket depth, film thickness and/or the feeding pressure to the orifice were variables. The results are tabulated in Tables I through V.



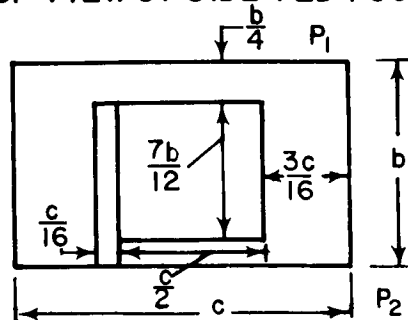
(a) TOP VIEW OF FULL WIDTH POCKET



(b) ORIFICE FED SHROUDED POCKET



(c) TOP VIEW OF SIDE FED POCKET



(d) TOP VIEW OF SHROUDED POCKET

Figure 11 Rayleigh Step Seal Designs

TABLE I
 PERFORMANCE OF RAYLEIGH STEP SEAL WITH THROUGH POCKET
 (Ref. Fig. 11-a)

Λ	c/b	b	$h_1 \times 10^3$	Pocket depth $\times 10^3$	\bar{H}	\bar{W}	$1-\bar{X}_c$	\bar{Y}_c	\bar{Q}^*
17.7	1.0	1.0	1.0	1.0	1.0	0.856	0.557	0.492	284
17.7	1.5	1.0	1.0	1.0	1.0	0.802	0.569	0.489	235
17.7	2.0	1.0	1.0	1.0	1.0	0.766	0.577	0.488	209
21.9	1.0	1.0	0.9	1.0	1.11	0.862	0.557	0.493	334
21.9	1.5	1.0	0.9	1.0	1.11	0.808	0.569	0.491	277
21.9	2.0	1.0	0.9	1.0	1.11	0.770	0.577	0.491	246
64.9	1.0	0.33	0.3	0.3	1.0	0.938	0.551	0.503	234
64.9	1.5	0.33	0.3	0.3	1.0	0.888	0.561	0.503	281
64.9	2.0	0.33	0.3	0.3	1.0	0.851	0.569	0.504	250
146.0	1.0	0.33	0.2	0.3	1.5	1.02	0.546	0.506	706
146.0	1.5	0.33	0.2	0.3	1.5	0.977	0.556	0.506	599
146.0	2.0	0.33	0.2	0.3	1.5	0.950	0.560	0.505	542

*
$$\bar{Q} = \frac{12 \mu RT}{P_1^2 h^3} Q_x \quad Q_x = \text{weight flow in x direction, \#/sec - per pad}$$

TABLE II
 PERFORMANCE OF RAYLEIGH STEP SEAL WITH ORIFICE FEEDING
 (Pocket Depth = 0.5×10^{-3} in)

$h \times 10^3$	P_3/P_1	Λ	\bar{W}	$1-\bar{X}_c$	\bar{Y}_c	$\bar{Q}_{ORIFICE}$ (to pad)
1	2.5	17.7	0.519	0.624	0.518	-19.2
	3.0	17.7	0.570	0.612	0.514	-12.0
	3.5	17.7	0.625	0.601	0.510	- 3.70
	4.0	17.7	0.680	0.592	0.506	5.58
0.8	2.5	27.7	0.520	0.621	0.514	-20
	3.0	27.7	0.578	0.608	0.512	-11.5
	3.5	27.7	0.639	0.597	0.510	- 2.06
	4.0	27.7	0.700	0.588	0.509	8.45
0.5	2.5	70.8	0.524	0.615	0.509	-21.7
	3.0	70.8	0.606	0.599	0.508	- 9.37
	3.5	70.8	0.687	0.587	0.509	4.22
	4.0	70.8	0.768	0.577	0.509	19.1
	4.5	70.8	0.848	0.570	0.510	35.3
0.3	3.5	197.0	0.760	0.576	0.504	14.9
	4.0	197.0	0.865	0.567	0.506	36.8
	4.5	197.0	0.970	0.561	0.507	60.9
	5.0	197.0	1.07	0.556	0.508	87.2

TABLE III

PERFORMANCE OF RAYLEIGH STEP SEAL WITH ORIFICE FEEDING

(Pocket Depth = $.3 \times 10^{-3}$ in)

$h \times 10^3$	P_3/P_1	Λ	\bar{W}	$1-\bar{X}_c$	\bar{Y}_c	\bar{Q}_{ORIFICE} (to pad)
1.0	2.5	17.7	0.517	0.629	0.517	-18.1
	3.0	17.7	0.565	0.617	0.512	-11.5
	3.5	17.7	0.615	0.606	0.508	- 4.03
	4.0	17.7	0.667	0.597	0.504	4.33
0.8	2.5	27.7	0.514	0.628	0.513	-19.1
	3.0	27.7	0.569	0.614	0.511	-11.5
	3.5	27.7	0.625	0.603	0.508	- 3.02
	4.0	27.7	0.683	0.594	0.506	6.35
0.5	2.5	70.8	0.507	0.625	0.505	-22.1
	3.0	70.8	0.584	0.607	0.505	-11.3
	3.5	70.8	0.660	0.594	0.506	0.665
	4.0	70.8	0.734	0.584	0.507	13.7
	4.5	70.8	0.809	0.576	0.507	27.9
0.3	3.5	197.0	0.720	0.583	0.501	8.33
	4.0	197.0	0.818	0.573	0.502	26.3
	4.5	197.0	0.915	0.566	0.503	47.1
	5.0	197.0	1.09	0.560	0.504	69.3

TABLE IV

PERFORMANCE OF RAYLEIGH STEP SEAL WITH SIDE FEEDING

 $C/b = 2.125$, Pocket Depth = 1×10^{-3} in

$h \times 10^3$	Λ	\bar{W}	$1-\bar{X}_C$	\bar{Y}_C	\bar{Q}
5.0	0.71	0.739	0.564	0.486	58.0
1.0	17.7	0.835	0.550	0.505	85.6
0.8	27.6	0.865	0.547	0.508	93.6
0.6	49.2	0.910	0.542	0.510	107.0
0.4	111.0	0.990	0.537	0.509	128.0
0.2	444.0	1.098	0.532	0.504	165.0

TABLE V

PERFORMANCE OF RAYLEIGH STEP SEAL WITH SHROUDED STEPS

 $P_2/P_1 = 5.0$, Pocket Depth = 0.001 inches, $b = .5$, cruise condition
at various C/b ratios

C/b	$h \times 10^3$	Λ	\bar{W}	$1-\bar{X}_C$	\bar{Y}_C	\bar{Q}
1.0	1.0	8.85	0.865	0.558	0.500	44.7
1.5	1.0	8.85	0.835	0.563	0.499	40.8
2.125	1.0	8.85	0.802	0.568	0.499	37.1
1.0	0.9	10.9	0.873	0.557	0.501	45.8
1.5	0.9	10.9	0.845	0.561	0.501	42.1
2.125	0.9	10.9	0.814	0.566	0.501	38.5
1.0	0.4	55.3	0.948	0.549	0.509	56.0
2.125	0.4	55.3	0.959	0.551	0.517	55.8
1.0	0.3	98.3	0.983	0.547	0.507	60.3
2.125	0.3	98.3	1.026	0.547	0.516	64.3

a) Orifice Fed Types

It should be noted that the computer program shown in Appendix A of the first Semiannual Report did not have provision for orifice feeding. Therefore the flow matching between the Rayleigh-Step seal and the orifice is accomplished separately by a graphical method. The dimensionless flow at several values of P_3/P_1 and orifice radii was calculated and is tabulated in Table VI. A typical example of flow matching may be seen in Figure 12. Finally, the matched conditions were obtained at various orifice radii, pocket depths, and film thicknesses as shown in Tables VII and VIII. The load curves are plotted in Figures 13 and 14.

TABLE VI

DIMENSIONLESS FLOW $\bar{Q}_{ORIFICE}$

$a \times 10^2$ $h \times 10^3$	P_3/P_1	1.0 \bar{Q}_{ORIF}^*	1.15 \bar{Q}_{ORIF}^*	1.3 \bar{Q}_{ORIF}^*	1.5 \bar{Q}_{ORIF}^*
1.0	4.0	3.28	4.43	5.58	7.39
	4.5	2.48	3.27	4.22	5.58
	4.8	1.62	2.13	2.75	3.64
0.8	4.0	6.41	8.46	10.9	14.4
	4.5	4.85	6.4	8.24	10.9
	4.8	3.16	4.15	5.38	7.11
0.5	4.0	26.2	34.7	44.6	59.0
	4.5	19.8	26.2	33.7	44.6
	4.8	12.9	17.2	22.0	29.1
0.3	4.0	121.0	160.0	206.0	272.0
	4.5	91.2	121.0	156.0	206.0
	4.8	59.8	79.0	102.0	135.0
	4.9	42.9	56.7	73.0	96.5
	4.95	30.6	40.4	52.0	68.8

* Note:

$$\bar{Q}_{ORIF} = \frac{12 \times 0.62 \pi a^2}{P_i h^3} \sqrt{\frac{2 g k R T}{k-1}} \left[\frac{P_3}{P_1} \right]^{1/k} \left[\frac{P_2}{P_1} \right] \left[1 - \left(\frac{P_3}{P_2} \right)^{\frac{k-1}{k}} \right]^{1/2}$$

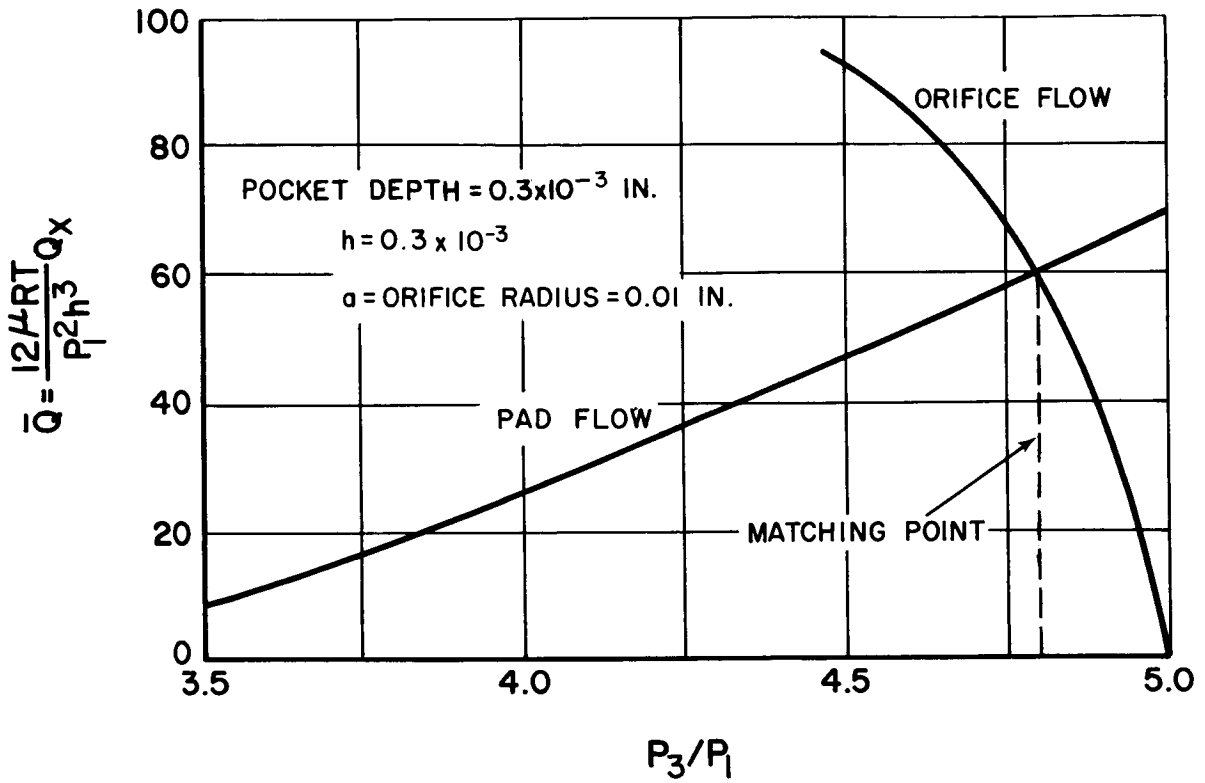


Figure 12 Typical Flow Matching of Rayleigh Step and Orifice.

Pad Dimension $b = 1.0$, $c = 1.5$.
 One Orifice per Pad.

TABLE VII

PERFORMANCE OF PAD WITH ORIFICE AT POCKET DEPTH = 0.5×10^{-3}

$a \times 10^2$	$h \times 10^3$	P_3 / P_1	\bar{W}	Q_{ORIF}^*	$1 - \bar{X}_c$	\bar{Y}_c
1.0	1.0	3.89	0.666	3.4	0.594	0.507
1.0	0.8	3.92	0.68	6.2	0.589	0.509
1.0	0.5	4.18	0.797	24.5	0.574	0.610
1.0	0.3	4.71	1.01	72.0	0.559	0.507
1.3	1.0	4.00	0.680	5.58	0.592	0.506
1.3	0.8	4.09	0.71	10.5	0.587	0.508
1.3	0.5	4.48	0.843	34.3	0.570	0.610
1.3	0.3	4.88	1.05	80.0	0.557	0.508
1.5	1.0	4.09	0.69	7.1	0.591	0.505
1.5	0.8	4.19	0.722	13.3	0.585	0.508
1.5	0.5	4.62	0.865	39.6	0.569	0.510
1.5	0.3	4.93	1.06	83.0	0.557	0.508

* Note:

$$\bar{Q}_{ORIF} = \frac{12 \times 0.62 \pi a^2}{P_i h^3} \sqrt{\frac{2 g k RT}{k-1}} \left(\frac{P_3}{P_1} \right)^{1/k} \left(\frac{P_2}{P_1} \right) \left[1 - \left(\frac{P_3}{P_2} \right)^{\frac{k-1}{k}} \right]^{1/2}$$

TABLE VIII

PERFORMANCE OF PAD WITH ORIFICE AT POCKET DEPTH = 0.3×10^{-3}

$a \times 10^2$	$h \times 10^3$	P_3 / P_1	\bar{W}	Q_{ORIF}^*	$1 - \bar{X}_C$	\bar{Y}_C
1.0	1.0	3.95	0.663	3.4	0.598	0.504
1.0	0.8	3.99	0.68	6.42	0.594	0.506
1.0	0.5	4.32	0.78	22.5	0.578	0.507
1.0	0.3	4.80	0.97	60.0	0.562	0.504
1.15	1.0	4.0	0.666	4.3	0.597	0.504
1.15	0.8	4.08	0.69	8.2	0.592	0.506
1.15	0.5	4.47	0.804	27.0	0.576	0.507
1.15	0.3	4.87	0.984	63.2	0.561	0.504
1.5	1.0	4.14	0.682	6.9	0.595	0.503
1.5	0.8	4.23	0.71	11.7	0.600	0.505
1.5	0.5	4.71	0.843	35.0	0.573	0.507
1.5	0.3	4.95	1.00	67.0	0.560	0.504

* Note:

$$Q_{ORIF} = \frac{12 \times 0.62 \pi a^2}{\rho_1 h^3} \sqrt{\frac{29KRT}{K-1} \left(\frac{P_3}{P_1}\right)^{1/K} \left(\frac{P_2}{P_1}\right) \left[1 - \left(\frac{P_3}{P_2}\right)^{\frac{K-1}{K}}\right]^{1/2}}$$

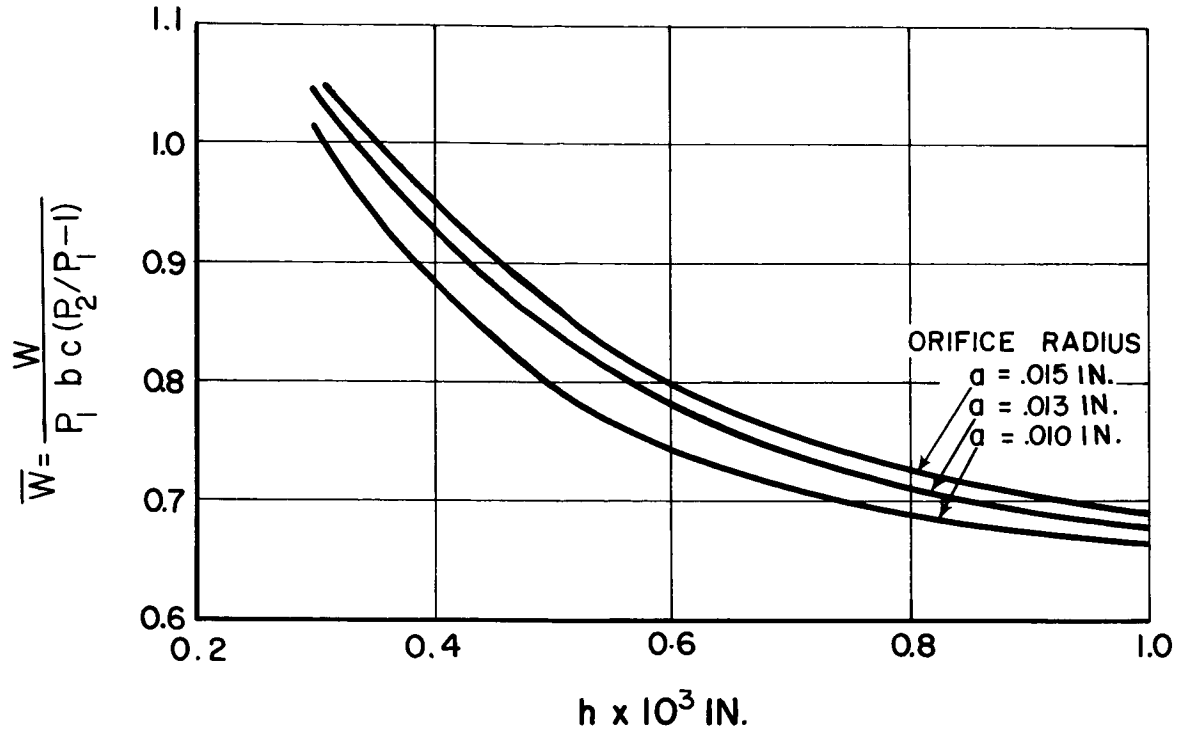


Figure 13 Dimensionless Load Vs. Film Thickness for Various Orifices with Pocket Depth = 0.5×10^{-3} Inches

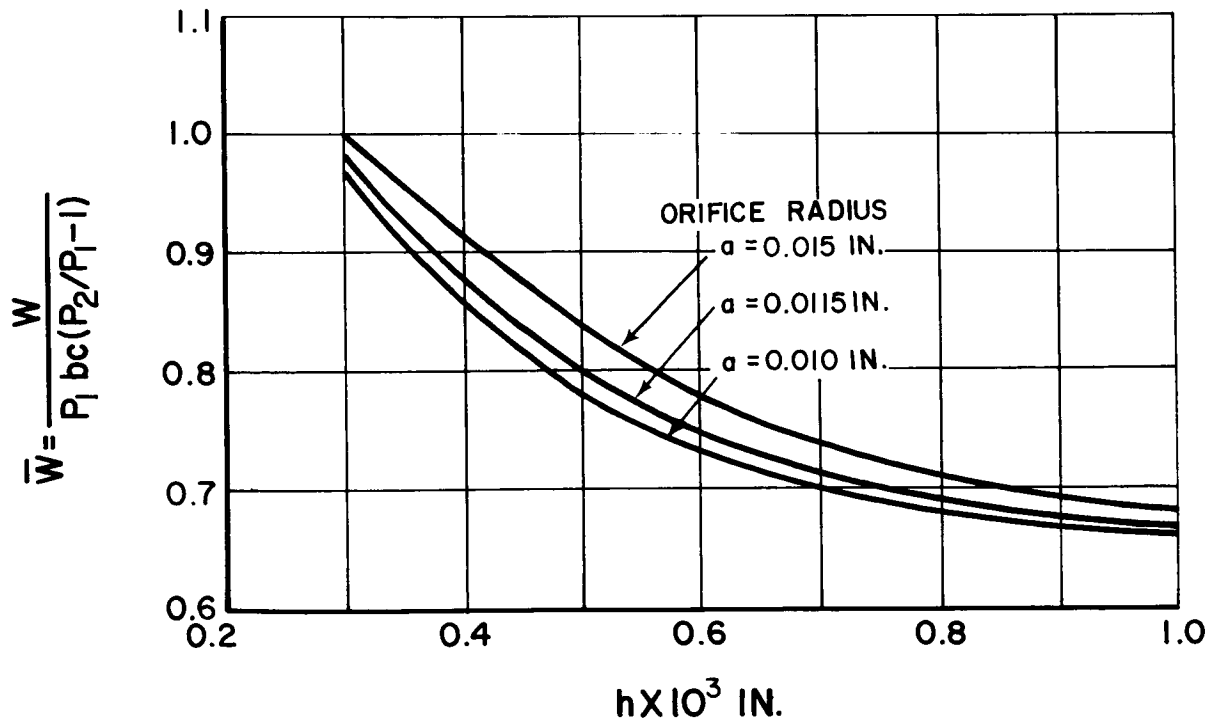


Figure 14 Dimensionless Load Vs. Film Thickness for Various Orifices with Pocket Depth = 0.3×10^{-3} Inches

b) Load Capacities

The load carrying capabilities of the Rayleigh-Step seal with different feeding arrangements are plotted in Figure 15. It was found that the shrouded pocket and the orifice feed types were the most stiff designs. For simplicity, the former was chosen for further analysis.

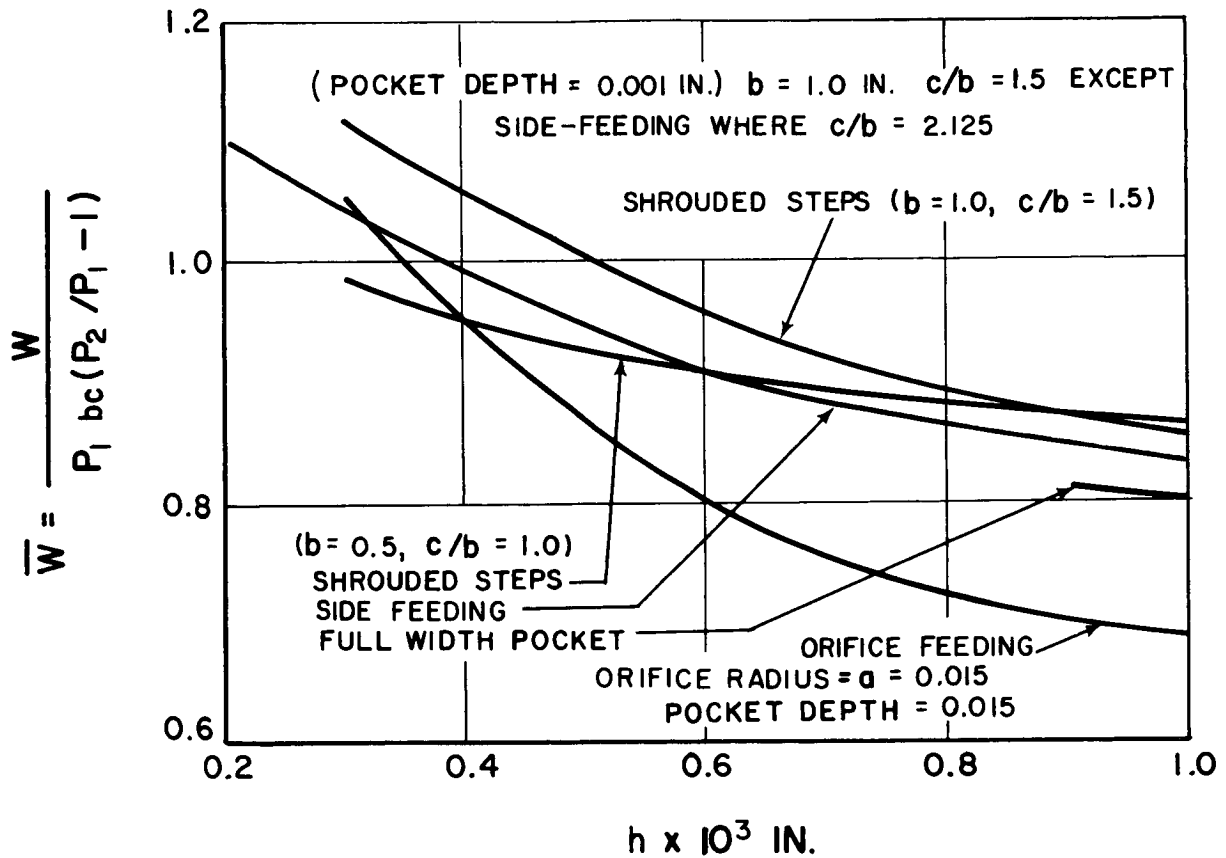


Figure 15 Rayleigh Step Seal Loading

2) PERFORMANCE OF SHROUDED STEP SEAL

The effect on performance of different length to width ratios may be seen in Figure 16. Maximum stiffness occurs at $c/b = 2.125$.

When take-off is simulated with the end seal in the test rig, the pressures are 170 and 20 psia for the high and low pressure sides, respectively. The computer results are listed in Table IX.

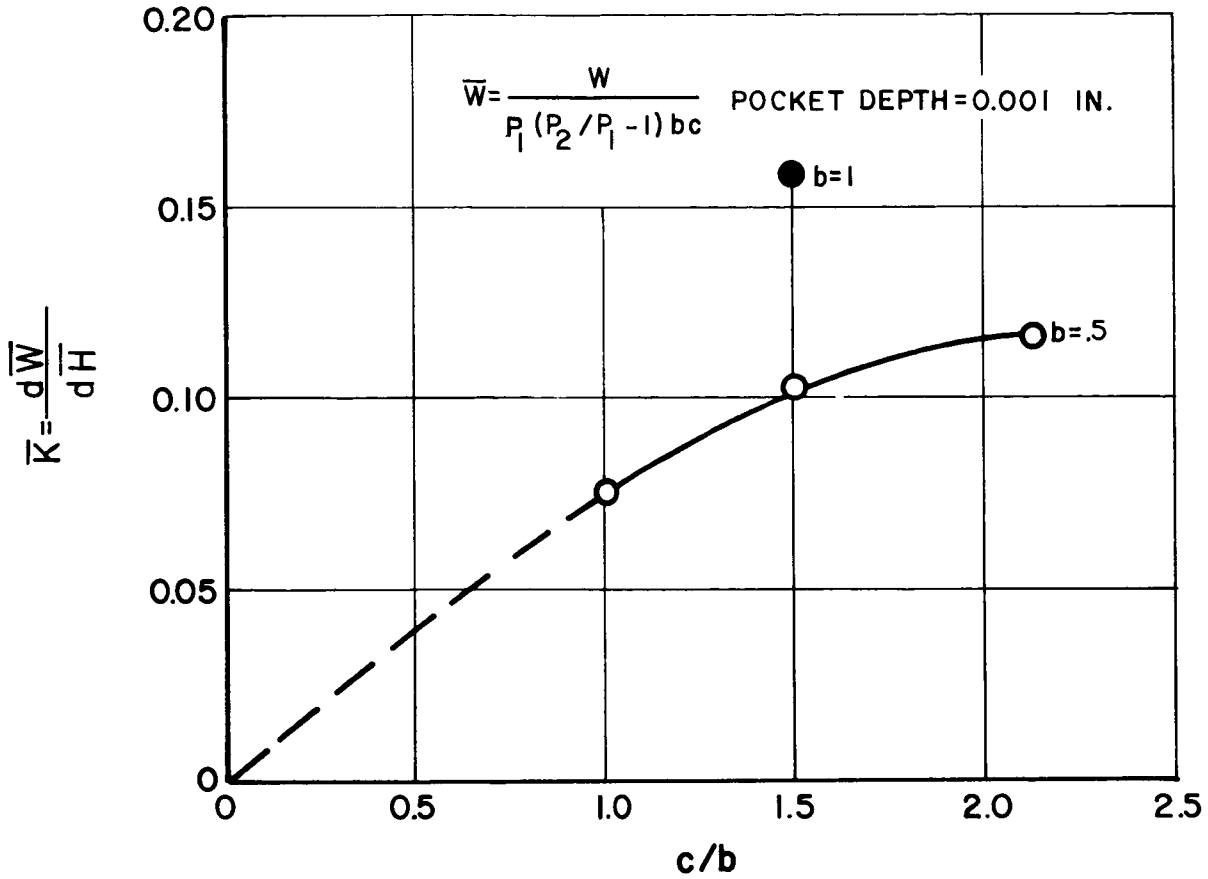


Figure 16 Effect of Length-to-Width Ratio on Performance

TABLE IX

PERFORMANCE OF RAYLEIGH STEP SEAL AT TAKE-OFF CONDITION

$P_2 / P_1 = 8.5$, Pocket Depth = 10^{-3} in., $b = 15$, $c/b = 2.125$

$h \times 10^3$	Λ	\bar{W}	$1 - \bar{X}_c$	\bar{Y}_c	\bar{Q}
1.0	6.75	0.8	0.565	0.494	114.3
0.9	8.34	0.808	0.564	0.496	117.6
0.3	75.0	0.925	0.551	0.514	164.5

The geometry of the interstage seal was the same as that selected for the primary seal. A set of calculations were made at the cruise condition with $P_1 = 75$ psia and $P_2 = 100$ psia. The results are listed in Table X.

TABLE X
PERFORMANCE OF RAYLEIGH STEP SEAL, INTERSTAGE SEAL
AT CRUISE

$P_2/P_1 = 1.333$, Pocket Depth = 10^{-3} in, $b = .5$, $c/b = 2.125$,
 $P_2 = 100$ PSIA, $P_1 = 75$ PSIA
(per pad)

$h \times 10^3$	Λ	\bar{W}	$1 - \bar{X}_c$	\bar{Y}_c	\bar{Q}
1.0	2.36	0.785	0.581	0.505	1.12
0.9	2.91	0.810	0.578	0.511	1.18
0.3	26.2	1.34	0.546	0.534	2.39

3) TABULATION OF STIFFNESSES OF VARIOUS DESIGNS

The stiffness of the seal under operating conditions was computed from the slope of the load curve. Table XI shows the values obtained.

4) PERFORMANCE OF PRIMARY SEAL WHEN TILTED DURING CRUISE

Table XII shows the performance of the primary seal (shrouded step) when tilted under cruise conditions. From the load and the center of pressure, one can find the angular stiffness at constant load from the equation.

$$K_\alpha = \frac{-\bar{W} [(\bar{X}_c)_2 - (\bar{X}_c)_1]}{\alpha}$$

Where the subscripts 1 and 2 refer to the conditions before and after tilting, respectively.

TABLE XI
STIFFNESS OF VARIOUS RAYLEIGH PADS

$$\bar{K} = \frac{d\bar{W}}{dH}$$

$$K_1 = \frac{\bar{K}}{h_1} (P_2 - P_1)$$

$$K \text{ (PER PAD)} = K_1 b C$$

Application	Operation	P ₂ PSIA	P ₁ PSIA	b	c/b	h x 10 ³	h _m x 10 ³	A	(\bar{K}/h_1) x 10 ⁻³	K ₁ x 10 ⁻³
Shrouded-Step	Cruise	100	20	0.5	1.0	1.0	0.95	7.95	0.0759	6.06
Shrouded-Step	Cruise	100	20	1.0	1.5	1.0	0.95	15.9	0.1586	12.7
Side Feeding	Cruise	100	20	1.0	2.125	1.0	0.90	14.3	0.150	12.0
Shrouded-Step	Cruise	100	20	0.5	1.5	1.0	0.95	7.95	0.1027	8.23
Full Width Pocket	Cruise	100	20	1.0	1.0	1.0	0.95	15.9	0.0496	3.97
Full Width Pocket	Cruise	100	20	1.0	1.5	1.0	0.95	15.9	0.0489	3.91
Orifice "Feeding a = .015"	Cruise	100	20	1.0	1.5	1.0	0.90	14.3	0.16	12.8
Shrouded-Step	Cruise	100	20	0.5	2.125	1.0	0.95	7.95	0.116	9.28
Shrouded-Step	Cruise	100	20	0.5	1.0	1.0	0.35	72.5	0.329	26.3
Shrouded-Step	Cruise	100	20	1.0	1.5	1.0	0.35	145.0	0.600	48.0
Orifice "Feeding a = .015"	Cruise	100	20	1.0	1.5	1.0	0.4	110.5	0.975	78.0
Full Width Pocket	Cruise	100	20	0.33	1.0	0.3	0.25	93.5	0.841	67.3
Full Width Pocket	Cruise	100	20	0.33	1.5	0.3	0.25	93.5	0.885	70.7
Side "Feeding"	Cruise	100	20	1.0	2.125	1.0	0.3	197.0	0.540	43.2
Shrouded-Step	Cruise	100	20	0.5	2.125	1.0	0.35	72.5	0.672	53.8
Shrouded-Step	Take-off	170	20	0.5	2.125	1.0	0.95	7.95	0.0830	12.5
Shrouded-Step	Cruise	100	75	0.5	2.125	1.0	0.95	2.62	0.244	6.09
Interstage Seal										

TABLE XII

PERFORMANCE OF RAYLEIGH-STEP SEAL AT TILTING POSITION

$b = .5$, $c/b = 2.125$, $P_2/P_1 = 5$, Pocket Depth = 10^{-3} in, Condition Cruise

$h \times 10^3$	α	Λ	\bar{W}	$1-\bar{X}_c$	\bar{Y}_c	\bar{Q}
1.1	0.001	7.31	0.845	0.556	0.500	23.2
1.1	-0.001	7.31	0.736	0.577	0.491	49.9
0.9	0.001	10.9	0.862	0.554	0.504	24.5
0.9	0	10.9	0.814	0.566	0.501	38.5
0.9	-0.001	10.9	0.762	0.575	0.496	54.4

Figure 17 provides curves of \bar{W} versus h and \bar{X}_c versus h . Since the stiffness is desired at constant load, stiffness may be obtained, for example, for the load of $\bar{W} = 0.845$ at a tilt of $+0.001$ radians at $h = 1.1$ mils, and for a parallel film at $h = 0.66$ mils. The stiffness is then

$$\bar{K}_\alpha = \frac{0.845 (0.560 - 0.556)}{0.001} = 3.4 \text{ per radian}$$

In dimensional terms this amounts to 68 in-lbs/in/rad, which is quite low. Additional data can be computed in the manner shown to further show the effect of tilt. The film thickness change is large.

b. PRIMARY SEAL ANALYSIS FOR MULTIPLE PAD DESIGN

As indicated in the first Semiannual Report, two primary seal configurations were considered for the multiple-pad design: the double orifice design, and the double pad design.

An analysis was made to discover the pressure distribution of a double orifice design with spiral grooves on both sides. This design is shown in Figure 18. Numerical results indicate that the angular stiffness of this primary seal design is still too low in spite of the dual orifice design. Consequently, the double orifice design was abandoned in favor of the double pad design. Either the spiral groove-orifice type of primary seal or the Rayleigh-step can be employed in the double pad design. Both are shown in Figure 19. Detailed analysis and results for the Rayleigh-step primary seal can be found in the section concerning primary seals.

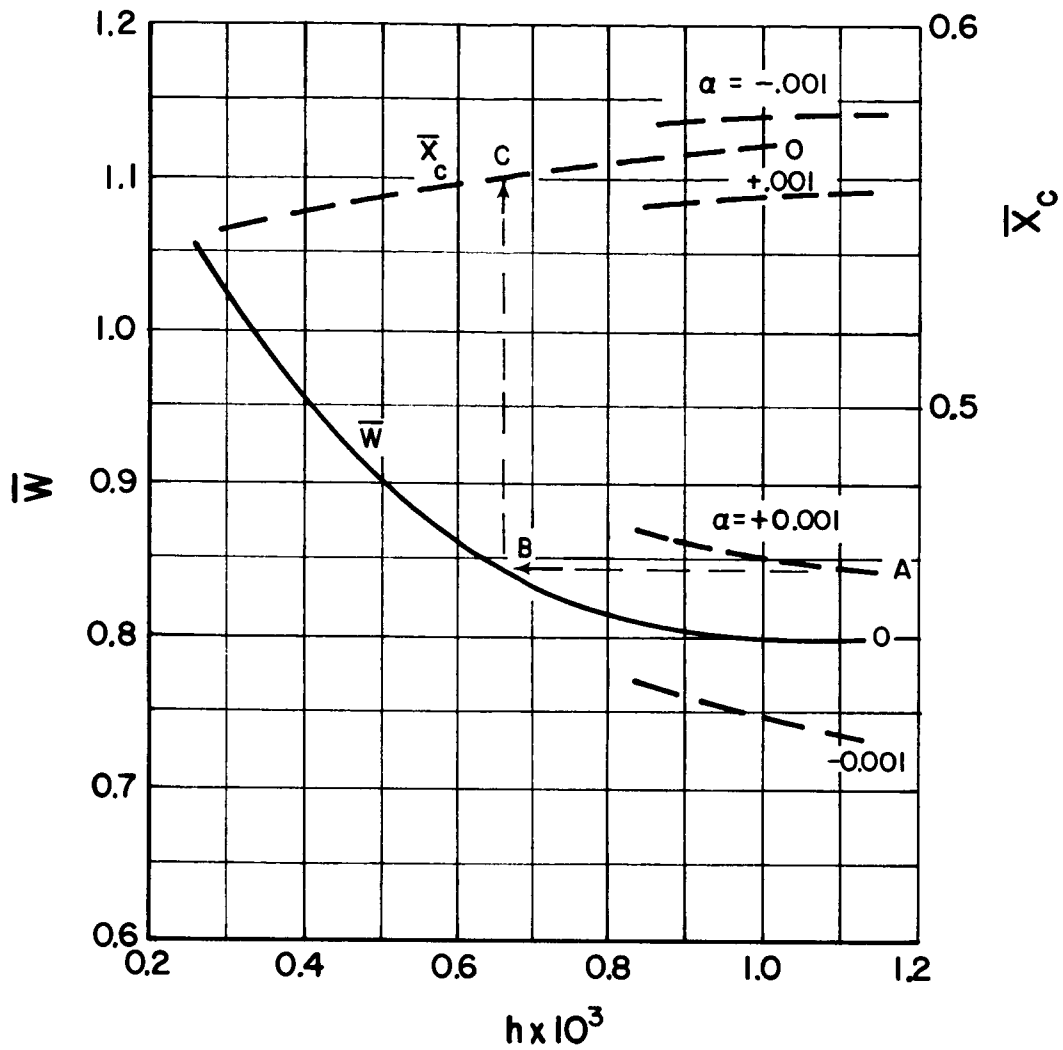


Figure 17 Computation of Pad Tilting Effect

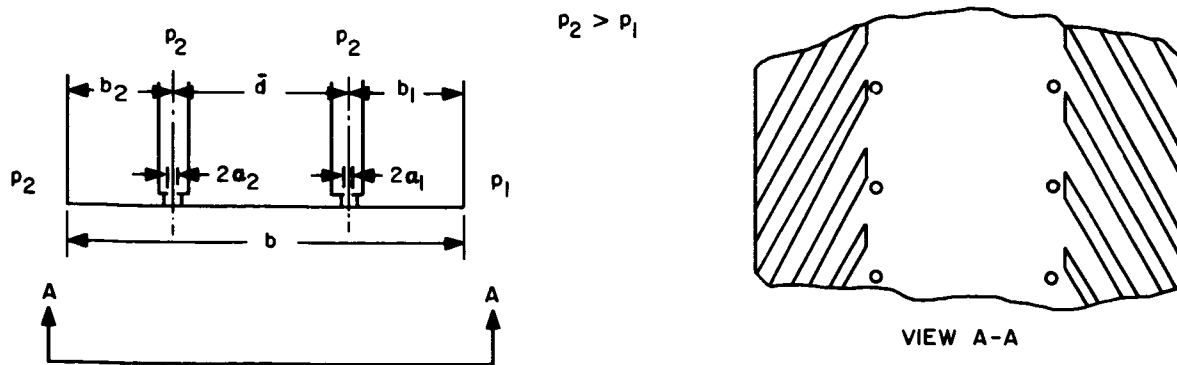


Figure 18 Double Orifice Primary Seal with Special Groove

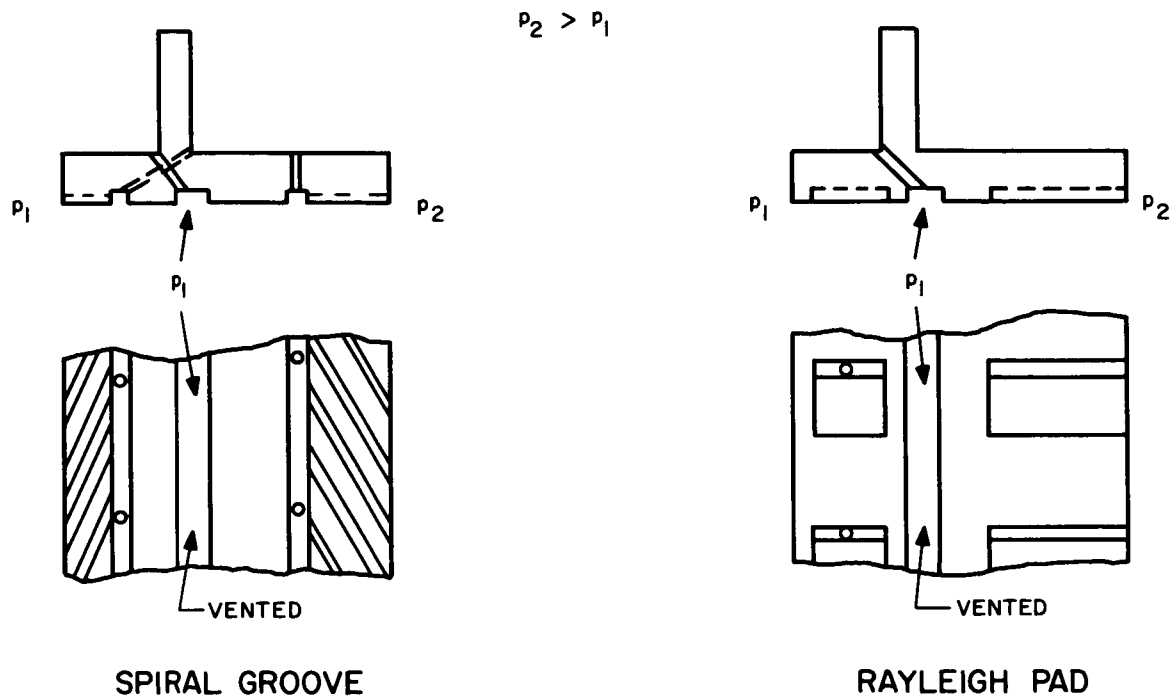


Figure 19 Double Pad Seals with Central Vent Groove

To study the behavior of the spiral groove orifice type of double pad seal, it is necessary to develop an analysis for a single pad first and then to use this analysis for obtaining the performance of double pads. To this end, the analysis of the double orifice design was modified to permit the calculation of results for the new geometry. Details of this analysis are included in Appendix A.

Numerical results for one set of seal dimensions are shown in Figure 20, and are plotted as the load vs. the film thickness. This curve is for a seal with a parallel gas film operating at the test rig cruise condition. It is seen that the hydrodynamic action of the groove is very effective at small film thickness; however, it is believed that this action will be greatly reduced if the gas film becomes non-parallel. The analysis and computer program developed are capable of calculating the exact performance for a non-parallel film, and this effect should be examined in the future.

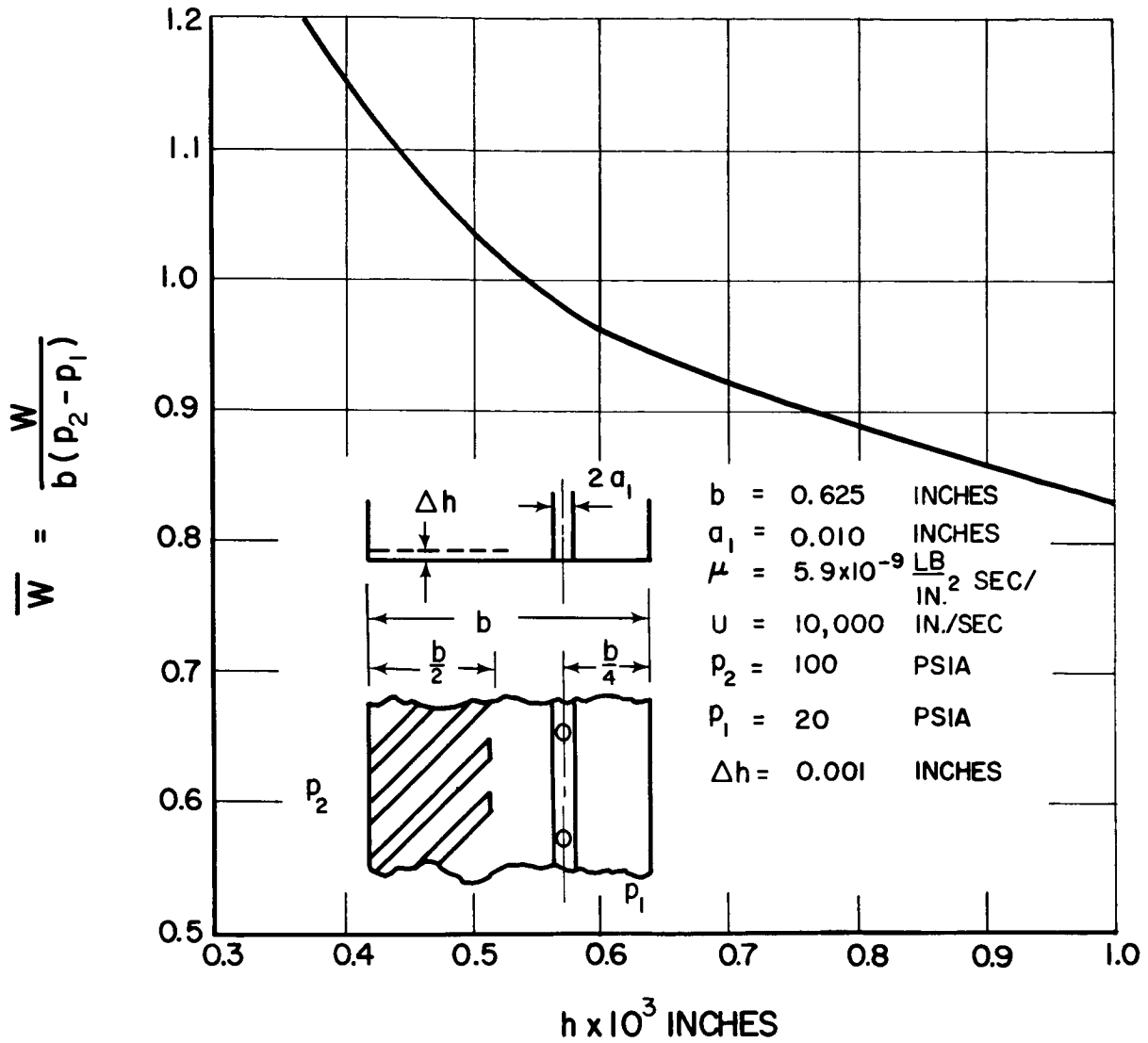


Figure 20 Load Vs. Film Thickness for Multiple Pad Design

4. ANALYSES OF THE TWO-SIDE FLOATED SHOE SEAL

a. DESCRIPTION

The two-side floated shoe seal is a circumferential seal in which rigid seal segments (shoes) are pressure balanced in a radial direction between high pressure on the outside diameter and a gas film between the rotating runner and the seal inner surface. They are balanced in the axial direction by hydrostatic bearings which allow the shoes to move freely between the two containing surfaces to account for rotor vibration, runout and initial waviness. These guide bearings form the secondary sealing surfaces. This concept is illustrated in Figure 3. A ring of shoes is used instead of a continuous ring so that centrifugal and thermal growth, conformation to the runner, and minor distortions of the holder can be accommodated.

The ring of shoes is formed by butting one against the other, all contained in the support ring attached to the fixed structure of the engine. The joint between segments can be a true butt joint. Springs are used to provide a tare force for the shoe against the runner.

Sealing is accomplished by using inherent balancing to maintain a close clearance between the shoes and the runner. Since slight radial movements of the shoes must be allowed for, the shoes must be sealed against the support ring with controlled gaps. The leakage paths are, then, through the primary seal, through the secondary seals on each side of the shoe, and through the gaps between the ends of the shoes.

The objective was to design a seal that would allow less than 0.10 pounds per second leakage when operating under pressures and temperatures given in Table XIII. The seal must have dynamic tracking ability and sufficiently small distortions to insure a constant film thickness on all sealing surfaces within 30 percent to 50 percent while accommodating radial runout of ± 0.008 inches and an axial motion of ± 0.2 inches.

TABLE XIII
CONTRACT SEAL OPERATING CONDITIONS

	<u>End Seal</u>		<u>Interstage Seal</u>	
	<u>Cruise</u>	<u>Take-Off</u>	<u>Cruise</u>	<u>Take-Off</u>
Sliding speed, ft/sec.	850	785	850	785
Air temperature, °F	1200	680	1200	680
Pressure differential, psi	80	150	25	50
*Air pressure, high pr. side, psia	100	170	45	70
*Air pressure, low pr. side, psia	20	20	20	20
*Pressure ratio	5	8.5	2.25	3.5

* Determined by test rig capability, and does not simulate engine pressure levels.

Both the interstage and end seals can be assembled in their support rings outside the engine, and installed as units during the assembly of the engine compressor. Tables XIV and XV compare all the pertinent points between the two side floated shoe seal (end and interstage) and the current labyrinth seal.

TABLE XIV
COMPARISON OF TWO-SIDE FLOATED SHOE SEAL
WITH LABYRINTH SEAL

<u>Item</u>	<u>End Seal</u>	<u>Interstage Seal</u>	<u>Current Seal (Labyrinth)</u>
Reliability	Excellent*	Excellent*	Excellent
Wear life	Indefinite*	Indefinite*	Indefinite
Weight penalty	Five lbs. (segments)	Same	Zero (by definition)
Tolerance to elastic and thermal growth	Accommodated by intersegment gap	Same	Accommodated by wear
Tolerance to manufacturing dimensional variations	Up to 0.0003" on segments & support. Up to ± 0.008 " on runner runout.	Same	Up to clearance value
Tolerance to foreign particles	Up to 0.0006" will pass through	Same	Up to clearance dimension will pass.
Tolerance to load deflections			
pressure loading	Subject to design	Same	Subject to design
maneuvering loading	13g - any direction	Same	Subject to design
Tolerance to contact:			
rubs-primary seal	(can be made tolerable by proper material selection)		Contact damage is tolerable.
-secondary seal	(can be made tolerable by proper material selection)		No seal
start-stop	(No contact if retractable)		No contact

* Subject to experimental verification.

TABLE XIV (Cont'd)

<u>Item</u>	<u>End Seal</u>	<u>Interstage Seal</u>	<u>Current Seal (Labyrinth)</u>	
			<u>End</u>	<u>Interstage</u>
Space requirements	Torus 13.75"R x 0.9" x 1.1"	Same cross-section, radius depends on stage.	No space penalty	
	No space penalty		No space penalty	
Film thickness			<u>End</u>	<u>Interstage</u>
cruise	0.001"	0.001"	0.018"	0.040"
take-off	0.001"	0.001"	0.020"	0.047"
Leakage rate	Test Rig Condition			
cruise	0.090 lbs/sec	0.032 lbs/sec	1.07 lb/sec	2.02 lb/sec
take-off	0.2385 lbs/sec	0.0799 lbs/sec	2.50 lb/sec	5.20 lb/sec
Heat generation (cruise)	9600 BTU/hr	9600 BTU/hr	Zero	
Tracking capability				
radial	Min. design film thickness with max. runner runout = 0.0007 inches		No interaction between runner and seal	
Maximum stress				
springs	(No important stresses in either end or interstage seals)		None	
seal support segments			Subject to design	
			None	

TABLE XV

SUMMARY OF RELIABILITY CONSIDERATIONS FOR TWO-SIDE
FLOATED SHOE SEAL

<u>Factors Under Consideration</u>	<u>Description</u>
Static and Dynamic Film Stability	Film does not break down - the smaller the primary seal film thickness, the greater the film stiffness.
Internal and External Damping	None considered. None needed to stay within amplitude variation limits. Some exists in thin films.
Compensation for Gross Centrifugal Growth and Thermal Growth	Accommodated simultaneously. The seal segments have 0.009 inch gaps between segments at cruise. Initial gap at low temperature and non-operating engine is essentially zero. The 0.009" gap (0.216" total gap in the circumference) accounts for a diametral centrifugal growth of 0.077" runner minus (up to) 0.008" differential thermal growth between the segments and runner (the segments are hotter than the runner).
Compensation for Runout and Distortions	Runout of up to ± 0.008 " can be tolerated by the allowable variation in film thickness along the length of a segment. Distortions can be as much as 1/3 the film thicknesses without serious detriment. Design allows thermal and mechanical distortions to be less than this.
Fatigue and Creep Rupture Limits of Stressed Members	No major stresses exist. Support structure and runner stresses can be fixed by design at a reasonable value.
Tolerance to Start-Stop Contact	Spring loaded design has hydrodynamic profile for low lift-off speed, and wear resistant face materials. Retractable alternate design utilizes spring action to achieve retraction at low engine speed.

Tolerance to High Speed Rubs in Operation

Any such contact should be only momentary. Materials are available which can be used at the seal faces to prevent severe damage. The choice must be made after establishment of method of thermal conductivity augmentation in the shoes and after obtaining better definition of the ability of various materials to be used.

Thermal Map and Effects of Heat Generation

Thermal distortions are less than 1/3 the film (secondary or primary) thicknesses if shoes have augmented thermal conductivity. Appendix D reports the calculated temperature distributions.

b. PRIMARY SEAL SELECTION

Three candidate primary face seal types were considered - hydrostatic step, spiral groove, and Rayleigh step. All initial design was done with the hydrostatic step concept. However, this concept introduces a problem because there is a peak film stiffness. This means that as the film thickness decreases there will be a distance at which a very slightly greater perturbing force will cause the seal to touch the runner. This condition must be avoided.

The other two seal types exhibit an increasing stiffness as film thickness decreases. This is desirable in order to have the best chance of avoiding high speed rubs. The spiral groove type of seal, however, loses quite a bit of its effectiveness when used on segments as is required here. Only a few grooves can be placed in a segment, and the segment ends are lost for this purpose, because they must be terminated in a land. Thus, only a fraction of the total ring can be covered with effective spiral grooves.

The Rayleigh step seal was eventually selected since it exhibits the major attributes required for a primary face seal:

- Good lifting force at low clearance
- Increasing stiffness as clearance decreases
- Low leakage rate
- Relative ease in forming the steps on the surface.

c. FORCE AND MOMENT BALANCING

The design procedure for both the compressor end seal and the interstage seal requires the balancing of forces and moments due to the pressure loads. The forces and centers of pressure were found by using the design curves and tables shown in the first Semiannual Report (PWA-2752) and in Section I. B. 3 of this report. They are summarized in Appendix C. The geometries of all balanced conditions are given in Appendix C, Table XXI. The leakage flows for primary and secondary sealing surfaces plus dynamic tracking responses are given in Appendix C, Table XXII.

The final design was arrived at in the following manner. Starting with a seal section of 0.50 inches x 0.50 inches the pressure forces and the moments caused by these forces were balanced by changing the lengths of the secondary sealing surfaces. This initial balanced condition required one secondary sealing surface to be 0.056 inches long. Since this was a very inefficient use of the total length available, additional geometries were balanced in order to more nearly match lengths of the secondary seals. The design initially selected was case 7C in Table XXI and Cases J, K and L in Table XXII. This design met all the goals for the compressor end seal and all requirements except dynamic tracking for the interstage seals.

After reviewing this design, it was agreed that the relief step adjacent to the primary sealing surface y_1 and y_4 on Table XXI should be a minimum of 0.08 inches instead of 0.04 inches. This change would allow additional clearance between the stationary carrier and the rotating runner.

In order to increase this step, the seals had to be redesigned to be pressure balanced. A relief step of 0.100 inches was chosen, and the overall height had to be increased to 0.80 inches to keep the secondary seal lengths long enough to seal effectively. The result of this redesign is presented as Case 19C in Table XXI and meets all design objectives for the compressor end seal. An alternate method to arrive at a balanced condition was to introduce a step on both sides of the seal. This case (Case 17C, Table XXI) would add a great deal of difficulty in manufacturing, because it requires four surfaces to be controlled to extremely close tolerances instead of three, and therefore was not selected.

An end seal using a Rayleigh step for the primary seal and hydrostatic step seals for the secondary seals was selected and balanced in the same manner as the previous designs (Table XXI, Case 22C and Table XXII, Case N). This seal met all design requirements and is shown in Figure 3.

The differences between the interstage seals and the end seals are slight changes in dimensions to maintain force and moment balance, and a different holding ring, so that the interstage seal will fit in the available space. The dimensional differences between the two seals are as follows:

<u>Dimension of Surface</u>	<u>End Seal</u>	<u>Interstage</u>
b_3 (see Appendix C)	0.384"	0.386"

The weights and volumes of the two seals are essentially the same.

d. LEAKAGE

The calculated total leakage for the seals is as given in Table XVI.

TABLE XVI

LEAKAGE FLOW TABULATION

	<u>End Seal **</u>	<u>Interstage Seal</u>	<u>Labyrinth*</u>	
			<u>End</u>	<u>Interstage</u>
<u>Cruise</u>				
Primary	0.0142	0.00248		
Secondary	0.0130	0.00263		
Segment Gaps	<u>0.0630</u>	<u>0.02650</u>		
Total	0.0902	0.03161	1.07	2.02
<u>TAKE-OFF</u>				
Primary	0.0825	0.0145		
Secondary	0.0716	0.01213		
Segment Gaps	<u>0.1294</u>	<u>0.05330</u>		
Total	0.2835	0.0799	2.5	5.20

* See Appendix G.

** See below for sample calculations.

Primary seal (shrouded Rayleigh steps, $c/b = 2.125$, $r_{12} = 0.2$, $h = 0.001''$)

$$Q = \bar{Q} \frac{p_1^2 h^3}{12 \mu RT_1} n \text{ lbs/sec where } n = \text{number of pads}$$

$$n = 24 \times \left\lceil \frac{27.5 \pi}{24 \times c/b \times b} \right\rceil \quad \text{where } \lceil \cdot \rceil \text{ indicates: rounded off to nearest whole value under calculated value.}$$

$$n = 72$$

\bar{Q} from Table V = 37.1

$$\therefore Q = \frac{37.1 \times (20)^2 \times (0.001)^3 \times 72}{12 \times 5.9 \times (10)^{-9} \times 12 \times 53.3 \times 1660} = 0.0145 \text{ lbs/sec}$$

Secondary seal (hydrostatic step, $b_1/b = 0.35$, $\bar{H} = 1$, $r_{12} = 0.2$, $h_1 = 0.0003$ inches)

$$m = \bar{M} \frac{h_1^3}{24 \mu b} \frac{P_2^2}{R T_2} \quad \text{pound-seconds per square inch}$$

From Figure 21, $\bar{M} = 2.22$. Further details are in the Semiannual Report (PWA-2752), pp. 59 ff.

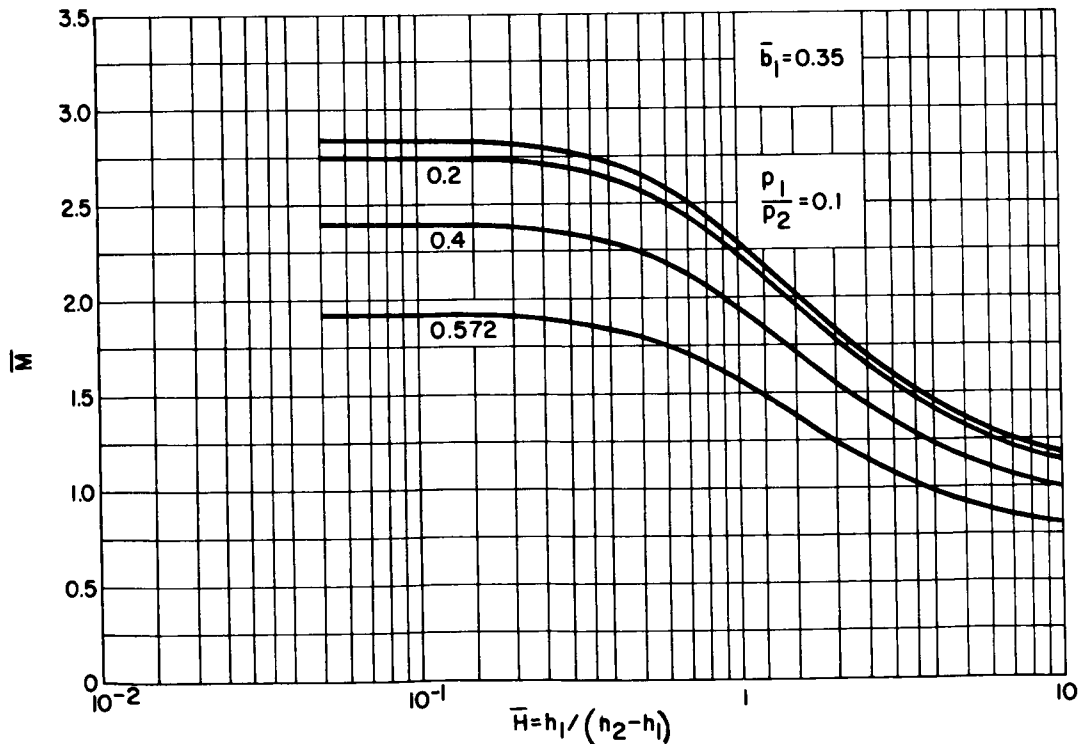


Figure 21 Dimensionless Mas Flow-Hydrostatic Step, $\bar{b}_1 = 0.35$

Five leakage paths, 3 at $b = 0.120$ inches, 1 at $b = 0.110$ inches, 1 at $b = 0.250$ inches

$$\therefore W_{\text{TOTAL}} = \frac{3}{0.120} + \frac{1}{0.110} + \frac{1}{0.250} \times \frac{2.22 (0.0003)^3 (100)^2 (27.5\pi)}{(24) (5.9) (10)^{-9} (12) (53.3) (1660)} =$$

0.013 pounds per second

Segment Gaps (gap thickness = 0.009 inches)

For a slit

$$M = \frac{h^3 \Delta p (p_2 + p_1) \ell n}{24 \mu b R T_2} \quad \text{pound-seconds per square inch}$$

where n = number of gaps = 24
 ℓ = width of slit

For two paths: from y_4 to y_1 (see figure in Table C-1)
 from b_3 to y_3

the estimate summation of y/b for these paths is

$$\frac{0.040}{0.5} + \frac{0.24}{0.36} = 0.746$$

$$\therefore W_T = 0.746 \times 24 \times \frac{120 \times 80 \times (0.009)^3}{24 \times 5.9 \times 10^{-9} \times 12 \times 53.3 \times 1660} =$$

0.835 pounds per second

For an orifice

$$W_T = \frac{ng C_D A p_2 G(r)}{\sqrt{R T_2 g}} \quad \text{pounds per second}$$

where $G(r)$ is found on Figure 12 of PWA-2752:

$$W_T = \frac{24 \times 386 \times 0.8 \times (0.240 + 0.040) \times 0.009 \times 100 \times 0.683}{\sqrt{12 \times 53.3 \times 1660 \times 386}} =$$

0.0630 pounds per second

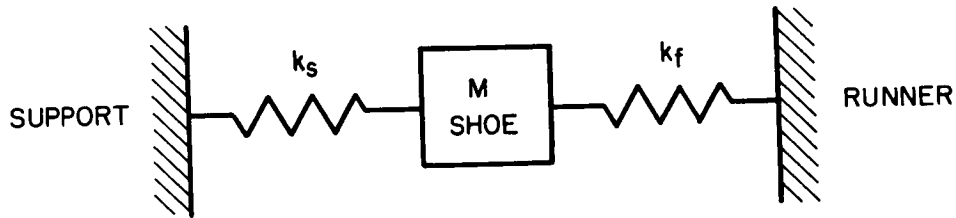
Since the orifice flow is smaller than for viscous flow in a slit, it will be the type of flow prevailing. Then the segment gap leakage is 0.0630 pounds per second.

For other conditions, values of \bar{Q} for the primary were extrapolated from previously calculated data. \bar{H} of secondary seals is always the same, since the seal is axially trapped. Then W_T for other conditions can be obtained from the above values by setting up ratios with respect to \bar{Q} , ΔP , P_1 , P_2 , T_1 , and μ for the desired cases.

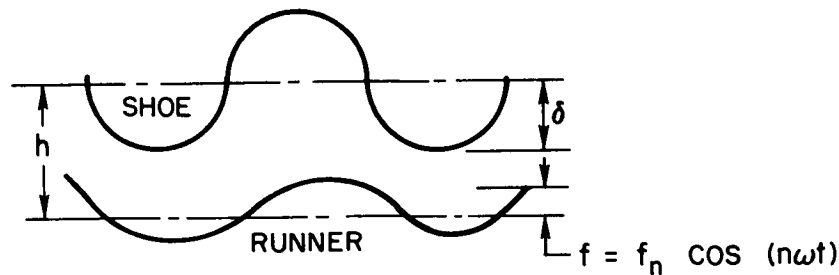
In order to reduce leakage between segments, several types of joints were studied. A simple butt joint is the least complex and seals effectively. The effect of tolerances on leakage flows and dynamic tracking response is given as Cases J, K and L in Table C-2.

e. TRACKING CAPABILITY

The dynamic response of this system is very simply formulated. The model is as shown below.



However, k_s can be so small that for all practical purposes k_f is the only significant spring. The analysis for this system was presented in the Semi-annual Report. Note that the runner movement can be as high as $f_1 = \pm 0.008$ inches, that the allowable relative movement between runner and seal is only $\delta = 0.0003$ inches, that the nominal film, h , is about 0.001 inches, the allowable $\frac{\delta}{h} = 0.3$, and $\frac{f_1}{h} = 8.0$. This is shown in the diagram below:



where $f_n = 1/2$ amplitude of runner disturbance.

For the selected Rayleigh step configuration:

$$\bar{K} = 0.116 \text{ (from Table XI)}$$

$$\frac{\delta}{h} = \left(\frac{\delta}{f_n} \right) \left(\frac{f_n}{h} \right)$$

and for a radial shoe seal the single amplitudes defined for the runner are:

$$f_1 = 0.008$$

$$\therefore \frac{f_1}{h} = 8.0$$

We have
$$\omega^* = \frac{n^2 \omega^2 M - k_s}{k_f}$$

where
$$k_f = \bar{K} b (P_2 - P_1) \times 10^3 \text{ AND } k_s \approx 0$$

so
$$\omega^* \approx \frac{n^2 \omega^2 M}{k_f}$$

For

$$P_2 - P_1 = 80 \text{ pounds per square inch}$$

$$n = 1$$

$$\bar{K} = 0.116$$

$$Mg = 0.0553 \text{ pounds per inch of circumference}$$

$$\omega^2 = \left(\frac{2\pi 8000}{60} \right)^2 \text{ (radians/sec)}^2$$

$$b = 0.5 \text{ inches}$$

$$k_f = (0.5) (0.116) (80) \times 10^3 = 4640 \text{ pounds per square inch}$$

$$\omega^* \approx \frac{\eta^2 \omega^2 M}{k_f} = \frac{1^2 \left(\frac{2778000}{60} \right)^2 (0.0553)}{(4640) (386)} = 0.0216$$

Using Figures 61 and 62 from the first Semiannual Report,

$$\frac{\delta}{f_n} = 0.024$$

$$\frac{\delta}{h} = \left(\frac{\delta}{f_n} \right) \left(\frac{f_n}{h} \right) = (0.024) (8) = 0.19$$

Thus, the response for the end seal is well within limits.

Similarly, for the interstage seal, $\bar{K} = 0.244$; $(p_2 - p_1) = 25$, from Table XI

$$\therefore k_f = 0.244 \times 25 \times 0.5 \times 10^3 = 3,050 \text{ pounds per square inch}$$

$$\omega^* = \frac{\left(\frac{2778000}{60} \right)^2 \times 0.0553}{3,050 \times 386} = 0.033$$

$$\frac{\delta}{f_n} = 0.0362 \text{ from Figures 61 and 62 of the first Semiannual Report}$$

$$\text{and } \frac{\delta}{h} = 0.0362 \times 8 = 0.290, \text{ within limits.}$$

f. THERMAL DISTORTION EFFECTS

Appendix D shows the temperature distributions for the seal under various conditions:

- Metal of low conductivity, 1200°F core
- Metal of low conductivity, 1300°F core
- Metal of low conductivity, 1100°F core
- Metal of moderate conductivity, 1200°F core
- Highly conductive shunt in runner, moderately conductive metal elsewhere, 1200°F core
- Highly conductive shunt in shoe, moderately conductive metal elsewhere, 1200°F core

- Highly conductive shunt in shoe, moderately conductive metal elsewhere, 1300°F core
- Highly conductive shunt in shoe, moderately conductive metal elsewhere, 1100°F core

The axial distortion in the shoes cannot exceed 0.0006 inches, or all the available clearance is taken up. The radial distortion in the shoes should not exceed about 30 percent of the operating clearance, or 0.0003 inches, for good operation. Using these clearance tolerances, the allowable temperature gradients are determined from the following equation:

$$\Delta T = \frac{2 \ell \delta}{(\alpha')^2}$$

where α' is 1/2 the length of the subject perpendicular to ℓ .

Then the allowable gradients are:

axial:

$$\Delta T = \frac{2 \times 0.5 \times 0.0006}{9 \times 10^{-6} \times \left(\frac{27.5}{24 \times 2}\right)^2} = 20.5 \text{ degrees Fahrenheit}$$

radial:

$$\Delta T = \frac{2 \times 0.8 \times 0.0003}{9 \times 10^{-6} \times \left(\frac{27.5}{24 \times 2}\right)^2} = 16.4 \text{ degrees Fahrenheit}$$

The cases with gradients falling within the allowable limits are the shunted shoe cases where the effective conductivity is twice normal. The same conductivity will also allow the 1100 degree Fahrenheit core and 1300 degree Fahrenheit core conditions to meet the thermal gradient requirements.

If the difference between the temperature of the shoe face and the temperature of the support bridge between the two secondary sealing surfaces of the ring is too much, the gap between the secondary seals will close. With an otherwise undistorted seal, the limiting temperature difference is:

$$\Delta T_{s-s} = \frac{\delta \ell}{\alpha b} = \frac{0.0006}{9 \times 10^{-6} \times 0.5} = 133.5 \text{ degrees Fahrenheit}$$

This is more than any of the calculated differences and should lead to little trouble by itself. However, when this distortion is superimposed on the axial distortion of the segment, the allowable difference is reduced according to

available clearance - clearance taken up by distortion = linear growth,
or $0.0006 - \delta = \delta_l = \alpha b \Delta T_{s-s}$

$$\text{Then } \frac{\left[0.0006 - \left(\frac{\Delta T_{\text{AXIAL}} \alpha (\alpha')^2}{2l} \right) \text{SHOE} \right]}{\alpha b} = \frac{0.0006 - \frac{6 \times 9 \times 10^{-6} \times \left[\frac{27.5 \times}{24 \times 2} \right]^2}{1.0}}{9 \times 10^{-6} \times 0.5} =$$

= 94 degrees Fahrenheit where ΔT_{AXIAL} is assumed to be 6 degrees Fahrenheit.

This is greater than any calculated differences, also, so that no problems are anticipated.

The runner distortion is primarily a bulge on the runner surface under the shoe. This can be due to a mean temperature difference between the inside and the outside of the runner, or to differential growth in circumference due to unrestrained thermal growth of the surface. The latter is an ultraconservative viewpoint, however. The differential growth of various parts of the surface as measured from that part of the runner web just outside the skirt, superimposed on the curvature caused by differential mean temperature from the outside to the inside of the runner, will be taken as the effective distortion. Thus,

$$\delta = \frac{\Delta T_{\text{OD-ID}} \alpha (\alpha')^2}{2l} + \left[(T_{\text{SURF MAX}} - T_{\text{WEB}}) - (T_{\text{SURF MIN}} - T_{\text{WEB}}) \right] \alpha (R_{\text{SURF}} - R_{\text{WEB}})$$

where

$\Delta T_{\text{OD-ID}}$ = mean temperature difference from outside to inside of runner under the shoe

R_{SURF} = radius of runner surface

R_{WEB} = radius of runner disc at narrow point just outside of skirt

T_{WEB} = temperature at R_{WEB}

$T_{\text{SURF MAX}}$ = maximum temperature of runner surface

$T_{\text{SURF MIN}}$ = minimum temperature of runner surface under the shoe.

Thus, for moderate conductivity, 1200°F core,

$$\delta = \frac{(1236 - 1232) \times 9 \times 10^{-6} \times 0.5^2}{2 \times 0.125} + (11 + 1) \times 0.25 \times 9 \times 10^{-6} =$$

$$0.000036 + 0.000027 = 0.000063 \text{ inches}$$

The total bulge is, therefore, well below any dimensional change that can be considered serious. The only potential thermal problem area in this seal is, therefore, the temperature gradients within the shoes. Use of a material with two to three times the normal conductivity of Inconel will relieve even this zone of potential problems. The required conductivity augmentation in the shoe can be obtained with silver or beryllium-copper. These materials may be clad, plated, impregnated, or imbedded in the shoe. Probably the easiest method (in concept) is to use a 0.010 inch to 0.015 inch layer of silver sandwiched between Inconel structural members, and silver plating the outside of the whole shoe except the face, which has to have a hard coating for other reasons. In practice the silver plate may come off at these temperatures, and the only way to face the surfaces with silver would be to silver braze it on. Again, at 1200°F some risk is entertained with silver brazing. Probably the best solution would be to use porous (or sintered) Inconel which has been vacuum impregnated with silver.

g. MECHANICAL DISTORTIONS

The only mechanical distortions of serious concern for this design are those caused by pressure differentials across the "sides" of the holder ring, by the centrifugal growth of the runner, and by runout of the runner. The first need not be of much concern, since bending stiffness can easily be increased to any level conceivably needed.

For whatever centrifugal growth is present, the only seal design requirement is to prevent the intersegment gap from becoming too large or too small. The gap between segments at the cruising condition should be kept less than 0.009 inches to prevent leakage from becoming excessive. The gap in a cold, non-operating engine can be virtually that of the finish of the butting surfaces. When the runner is designed, this can be taken into account. The less design growth, the less the intersegment gap will be, and the less the leakage will be. Because the gap flow is orifice-controlled, leakage will be directly proportional to the gap width.

Runout should be low enough so that the instantaneous clearance at one end of a segment differs from that of the other by less than 2/3 of the nominal film thickness. This maximum difference in allowable clearance multiplied by 1/2 the

number of segments is the maximum allowable runout over 1/2 the circumference of the seal, since the clearances are cumulative. The other half of the circumference provides space to let the seal return to normal position. Therefore, the total allowable runout is ± 0.008 inches.

It is assumed that the accuracy of the face seal will be held within 0.0003 inches and the accuracy of the secondary seals to within 0.0003 inches to prevent binding.

h. WEAR AND RUBBING LIFE

Under ideal conditions with a retractable seal, there should be no wear or rubbing, since the seal and runner theoretically never touch. With a lift-off type of seal, which rubs until lift-off occurs, materials at the seal faces must be properly chosen to ensure sufficient life. In practice, however, there may be momentary contact between the runner and the surface of either type of seal at high speeds, a condition which requires optimum material compatibility to minimize wear.

The seal segments must have augmented conductivity as mentioned previously. One method suggested was to use a silver layer sandwiched between Inconel outer pieces. This leaves Inconel facing Inconel at the seals. If these surfaces are well oxidized, they may resist wear and rubbing satisfactorily. Flame spray coating a carbide or oxide on the shoes will provide a wear-resistant coating, but it should run against a similar coating on the runner. Since the runner expands and contracts, there is a question about the ability of such a coating to stay on. Another solution would be to coat the runner with a thin layer of solid lubricant, such as a eutectic mixture of CaF_2 and BaF_2 .

If the sintered Inconel shoe impregnated with silver is used for thermal reasons, it will probably serve as an adequate protection against wear and rubbing at high temperature. Then, in all probability, the facing surface will not need a coating or special treatment, especially if it is naturally oxidized.

i. STRESS CONSIDERATIONS

Except for the runner (which is considered part of the compressor rotor), the only part of the seal subjected to any significant stress is the support structure. This structure can easily be made to support the compressive pressure loading with as little stress as desired. In addition, the support structure is similar to that required for any seal, so it was not considered as a controlling factor in the seal design.

j. TOLERANCE TO DIRT

Dirt in the primary seal can be passed quite readily if it is small enough. The limiting size will correspond to a particle at the trailing edge sufficiently large

to cause the shoe to tip until it touches the containing walls. The maximum size of the particle is then the normal gap at the trailing edge plus the amount required to tip the shoe by 0.0003 inches (the operating clearance). Since the shoe has a nearly square cross section, this gives 0.0013 inches as a tolerable particle size, assuming that no embedding occurs. The secondary seals cannot pass any larger particle than the total available shoe travel, or 0.0006 inches.

k. MANEUVERING LOADS

The only parts of this seal subject to g-loading and whose tolerance to such loading cannot be established elsewhere in the engine are the shoes. Thus, the shoes can stand g-loading in any direction up to the point where they touch. For all practical purposes, since the shoe weights are quite small, the allowable g-loads are higher than will ever be encountered. Considering that the shoes weigh about 0.0553 pounds per inch, and that the mean film stiffness of the secondary seals between normal position and touching is about 2400 pounds per square inch, for a movement of 0.0003 inches (the normal operating gap) the required g-load to close the gap is $\frac{0.0003 \times 2400}{0.0553} = 13 \text{ g.}$

It will be even greater in the radial direction since the average film stiffness of the Rayleigh step seal is far greater than for the hydrostatic step used on the secondary seals.

l. FAIL-SAFE CONSIDERATIONS

If the springs on the shoes fail and they are normally retracted, the seal will function normally until the engine stops and the shoe will not retract. Slow speed touching of the seals should have no serious effects on the structure or seals. It is assumed that maintenance will take place after such an incident. Thus, using a conservative approach to selection of coating materials, the seals can be made fail-safe as far as rubbing is concerned.

Cocking of the shoes is discouraged by the small allowable movements. With cocking, the potentiality of serious effects will exist because of the high runner speed, but properly chamfered corners and leading edges of the primary face material should prevent any scraping or gouging of the runner.

A more thorough evaluation of the fail-safe properties of the seal will have to await testing.

m. MATERIALS

Except for coatings the entire assembly will be made from Inconel X-750. The shoe construction technique has not yet been established, however. As dis-

cussed previously, it is necessary to have an effective thermal conductivity in the shoe of two to three times that of Inconel X-750. This can be achieved by several methods, but the two most probable ones are:

- Sintered Inconel X-750 impregnated with silver
- Inconel X-750 structure with silver slabs sandwiched in between.

If a nonretracting seal with hydrodynamic lift-off is to be used, the seal face material will probably be a flame-sprayed oxide or carbide ground to the proper shape and finish. The runner, too, may be coated with a thin layer of dry lubricant. Best coating materials or surface treatment will be established after the basic decision of shoe structure is made.

n. OFF DESIGN OPERATION

The operation at take-off requires primarily that the seal remain balanced, or that only slight cocking occur, and that the primary seal gap remain sufficiently large. Leakage is not so important during take-off as during cruise. The unbalance that can occur during take-off is only about 0.003 inch-pounds per inch of circumference: insufficient to be of consequence.

5. ANALYSES OF ONE-SIDE FLOATED SHOE SEAL

a. DESCRIPTION

The one side floated shoe seal is a face seal consisting of a ring of segments acting against a rotating surface attached to the compressor rotor. Figure 22 is a schematic drawing of the concept. Since this is a face seal, (the primary seal faces against a radial surface), the flow is radial - from outside surface to the inside surface. The primary seal is between the stationary ring of shoes and the rotating face. The secondary seals are between the shoes and the carrier ring and between the carrier ring and the mounting ring. Referring to Figure 22, the runner, (A) is attached to the compressor rotor, and is the surface against which the seal works. The segmented shoes, (B) face against (A) so that the primary seal is surface (BQ). The shoes are held in position against the runner by the secondary ring seal (D) and the ring seal spring (C) which butts against the carrier ring (E). Slight movement must be allowed between B and D, hence surface Bb is nearly a static seal. Sealing of D against E is also essentially static. The carrier (E) is supported from the frame (H) by the carrier springs (G). A nearly static seal is formed between H and E by the carrier ring seal, F.

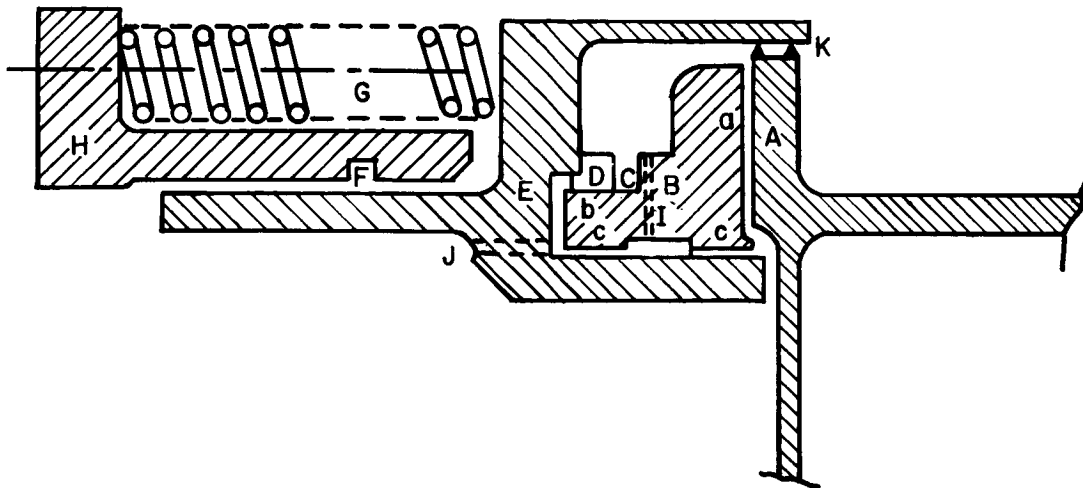


Figure 22 Schematic of One-Side Floated Shoe Seal

The shoe must be floated, since it has to move to accommodate most of the oscillating motion between the runner and frame induced by runout and misalignment. A passage (I) is provided through the shoe so that high pressure air can be used to support it. This air flow is kept from being excessive by the sealing surfaces Bc. This, again, is nearly a static seal. There can be some leakage past surfaces Bc, Bb, and between D and to the low pressure zone. A hole (J) is provided to communicate to the compressor rotor core to maintain this low pressure.

The seal at Bg works only when in close clearance from A. Therefore, to accommodate conditions when B is considerably removed from A, the labyrinth seal (K) could be provided so that engine leakage can be held as low as it is in present engines.

The large, nearly steady state motions of the seal are ± 0.2 inches in the axial direction, and up to about 0.15 inches in the radial direction. These movements are due to elastic and differential thermal growth as the engine heats up and cools down during the operating cycle. Slight axial motions due to manufacturing inaccuracies are superimposed on this. Radial inaccuracies tend to be inconsequential with the face seal.

The shoes only have to be floated on the inside surface, the outside surface being exposed almost entirely to the high pressure air. Hydrostatic pockets on the inside surface provide for floating the shoes. Lands (Bc) on the same surface provide for sealing the radial gap between segments and carrier.

Because of the presence of few confining surfaces and few surfaces requiring high precision in axial, radial, or angular position, the effects of thermal distortion can be minimized. Only the flatness and squareness of the primary face on the segment and the radius of curvature of the floated face need be preserved. This can be done by holding down the axial and radial thermal gradients in the segments.

The completely circular parts are subject to existing manufacturing methods which can achieve the tolerances required here. A set of segments would probably be made as precision-ground matched segments with the ends ground to a precision butt joint.

The 24 shoe segments are confined by a secondary sealing ring (D) which seals the gap between the segments and carrier (E). Twenty-four shoes were selected as a compromise between allowable distortion and manufacturing error on the one hand, and number of parts on the other. The seal ring has only one split to allow for differential thermal growth and other slight radial movements of the segments with respect to the carrier. The seal ring is balanced in the radial direction so that there will be minimum rubbing force between shoes and ring. There is only partial pneumatic balance in the axial direction so that there is contact between carrier and ring. A spring (C) between the segments and the seal ring takes up the low amplitude high frequency movement between the carrier and the segments.

The carrier is a complete ring and is designed to accommodate the gross axial movement of the compressor caused by thermal growth. Thus, the carrier is free to slide axially. A split ring (F) is used to seal between the carrier and the seal support (H). This ring accommodates any slight out of roundness of the ring or support so that good sealing can be achieved. Springs are mounted between the support and carrier.

In its normal (inoperative) position, the active face can be pressed against the runner, or it can be retracted. Each has its advantages and disadvantages. The seal that rests against the runner when standing still must be lifted off the face before it can function as designed. This can be accomplished by hydrodynamic lift-off or by using jacking air. Hydrodynamic lift-off requires that some rubbing occur when the compressor starts rotating - thus raising the question of surface wear. Jacking requires that an external air source be supplied along with a valve and its control, and does not lend itself to aircraft applications.

The normally retracted design assures that surface wear at low speed will not occur. However, means of achieving the retraction will undoubtedly cause a

certain amount of design complication. One scheme to accomplish this is to design the carrier spring non-operational length to be just enough to keep the carrier retracted from the disc. The carrier could be pressure unbalanced so that at operating pressure the carrier would experience a small force toward the runner. The seal would then function normally. At part speed the carrier would tend to pull away from the runner. The carrier ring must be well guided in its movement so that the segments can remain parallel when close to the runner.

The choice of approach can await design for an actual application. What is required now is to obtain sufficient data on lift-off speed, wear rates, and reliability of surface adhesion to allow the simplest approach to be evaluated.

The concept shown in Figure 22 can provide several basic desirable characteristics. The secondary seal ring C is a springy member whose cross section is relatively easy to dimensionally control. The only parts of the carrier requiring close tolerance control are the small radial surface against which the seal ring pushes, and the surface on which the segments float. The first has to be smooth (about a 16 microinch finish), and the latter has to be smooth and round (0.0025 inches total indicator reading or better). The segments must be smooth (16 microinch finish) on all sealing surfaces, flat on the primary seal face (to within 0.0002 inches or less), and circular on the floated surface and seal ring surface. The segment's inner surface and face must be square. The runner must be smooth (16 microinch finish). These surfaces are relatively easy to control, however.

The relative motions to be accommodated are due to -

- axial growth of the compressor with respect to the case: ± 0.2 inches.
- relative radial growth of the runner and seal rings: ± 0.15 inches.
- runner out of axial flatness and axially misalignment: ± 0.0025 inches.

In addition, the carrier ring and support ring may be slightly out of round.

The pressure varies from compressor pressure to core pressure across the primary face seal, the secondary seal ring (both the side facing the carrier and the side facing the segments), and the lands at the floated surface. A leakage path is provided to the core from the cavity between the carrier and shoes at the low pressure side of the seals to keep the low pressure downstream of the secondary sealing surfaces.

For end and interstage applications, the primary seal with the Rayleigh step face operates with a design point nominal clearance of 0.001 inches and a step height of 0.001 inches. The face configuration is shown on Figures 4 and 8. The secondary seals operate with a nominal clearance of 0.0003 inches, and have hydrostatic steps of 0.0003 inches. The secondary seal rings butt against the carrier, and the carrier piston rings butt against the support and the carrier ring grooves. The segments are sealed between each other with butted smooth flat surfaces. The split points of the secondary seal ring and the carrier ring seals are overlapping smooth surfaces.

The secondary seal ring spring (C in Figure 22) has a stiffness of about 100 pounds per inch per inch of circumference. The carrier springs are about 3 pounds per inch per inch of circumference. If an unbalanced carrier is used for retraction purposes, the undisturbed primary gap will be about 0.4 inches. Then, except for the unbalance method, all seal characteristics will be the same for hydrodynamic lift off or initial retraction schemes. Tables XVII and XVIII show the pertinent features of the design and points of comparison between the one side floated shoe seal (end and interstage) and the current seal type.

The interstage seal is essentially similar to the end step seal except that it faces aft instead of forward and the inside diameter of the shoe is slightly smaller. The pressure differential is less than for the end seal, also, since it is only the differential across a single compressor stage rather than across all compressor stages. The mounting ring is necessarily different for the interstage seal because of the short space between compressor disks. However, the springs and piston rings are similar.

The basic simplicity of the seal design allows the seal to be assembled outside the engine and then fitted onto the support ring, which has already been mounted in the engine.

Servicing will consist of complete disassembly and inspection of primary face seals, floated surface faces, and seal ring face for wear, inspection of anti-rotation pins and lugs and seal rings for wear, and inspection of seal ring spring and carrier springs for checking or fretting.

b. SELECTION OF PRIMARY SEAL TYPE

The best candidate primary seal types were the hydrostatic step, the shrouded Rayleigh step, and the spiral groove. These are the same as those considered for the two side floated shoe. For the same reasons as discussed for that design, the shrouded Rayleigh step was selected for the final design. Essentially, the leakage is low, the film stiffness is good (and gets better at low clearance so that actual rubbing of the primary face is difficult to induce), and the configuration can be easily adapted to the segmented shoe concept.

TABLE XVII
COMPARISON OF ONE-SIDE FLOATED SHOE SEAL WITH LABYRINTH SEAL

<u>Item</u>	<u>End Seal</u>	<u>Interstage Seal</u>	<u>Current Seal (Labyrinth)</u>	
Reliability	Excellent*	Excellent*	Excellent	
Wear life	Indefinite*	Indefinite*	Indefinite	
Weight penalty	36 lbs.	36 lbs.	Zero (by definition)	
Tolerance to elastic thermal growth	Virtually no differences in growth between segments and carrier ring		Accommodated by wear	
Tolerance to mfg. dimensional variations	Up to 0.0003" on three faces of segments and two faces of carrier ring		Up to clearance value	
Tolerance to foreign particle	Up to 0.001", without imbedment, can be passed		Up to clearance value will pass	
Tolerance to load deflections				
- pressure loading	Subject to design	same	Subject to design	
- maneuvering load	30g axial, indefinite radial	same	Subject to design	
Tolerance to contact:				
rubs - primary seal	(can be made tolerable by proper material selection)		Contact is tolerable	
- secondary seal	(no contact for retracted system; can be made tolerable by proper material selection if non-retractable)		No seal	
start stop			No contact	
Space requirements	Torus: 13.75"R x 1-3/4 x 1-1/4" No Space Penalty	Same cross section. radius depend on stage	Zero (by definition)	
Film thickness			End	Inter
- cruise	0.001"	0.001"	0.018"	0.040"
- take off	0.001"	0.001"	0.020"	0.047"
Leakage rate				
- cruise	0.058 lbs/sec	0.020 lb/sec.	1.07 lb/sec. 2.02 lbs/sec	
- take off	0.2006 lbs/sec	0.063 lb/sec.	2.50 lb/sec. 5.2 lbs/sec	
Heat generation (cruise)	9600 BTU/hr	9600 BTU/hr	zero	
Tracking capability				
- axial	$N_{crit} = 3170$ rpm Minimum design film thickness with maximum runner movement = 0.0007"	$N_{crit} = 3170$ rpm	No interaction between runner and seal	
Maximum stress				
- springs	40,000 psi	40,000 psi	none	
- seal support	Subject to design		Subject to design	
- segments	No important stresses		none	

*Subject to experimental verification.

TABLE XVIII

SUMMARY OF RELIABILITY CONSIDERATIONS FOR ONE-SIDE FLOATED SHOE SEAL

<u>Factors Under Consideration</u>	<u>Description</u>
Static and Dynamic Film Stability	Film does not break down - the smaller the primary seal film thickness, the greater the film stiffness.
Internal and External Damping	No film damping was considered in the accompanying analysis. Damping between the carrier ring and support ring must be built in.
Compensation for Gross Centrifugal Growth and Thermal Growth	Either kind of growth of runner has no affect on seal performance or configuration since a face seal is used. Thermal growth of segments, secondary seal ring, and carrier ring will be nearly the same.
Compensation for Runout and Distortions	Out-of-flatness and out-of-line runner is accommodated by dynamic design of seal; out-of-roundness of runner is of no consequence. Segment distortions as high as 0.0003" are tolerable; design contributes less distortion than this.
Fatigue and Creep Rupture Limits of Stressed Members	Only springs are stressed to a significant degree (40,000 psi). Hertzian stresses are low.
Tolerance to Start - Stop Contact	With hydrodynamic lift off design the susceptibility to damage at start and stop has to be experimentally evaluated. However, wear resistant face coatings are available. With retractable alternate design there will be no contact during start and stop.
Tolerance to High Speed Rubs in Operation	Any such contact should be only momentary. Materials are available which can be used at the seal face to prevent severe damage. The choice must be made after establishment of method of thermal conductivity augmentation in the shoes and after obtaining better definition of the ability of various materials to be used.
Thermal Map and Effects of Heat Generation	Thermal distortions will be less than 1/3 the film (secondary or primary) thicknesses if shoes have augmented thermal conductivity. Appendix D reports the calculated temperature distributions.

c. MOMENT AND FORCE BALANCE

Forces and moments were balanced using \bar{W} and \bar{X}_c curves for Rayleigh step seals. Appendix B gives details of the segment balancing. Since nearly complete freedom can be given to the radial position of the secondary seal ring (D in Figure 22), and axial positions of the floated surface seals (Bc), any type of primary seal can be balanced. The designs shown in Figures 4 and 8 are for a Rayleigh step face seal, however, working with

$$\text{Pressure ratio} = 0.2$$

$$\frac{c}{b} = 2.125,$$

$$\bar{H} = 1.0$$

Minor variations are required in the shoe configuration to maintain force and moment balance. Referring to Table C-3, the dimension h_4 and b_x are compared as follows:

	<u>End Seal</u>	<u>Interstage</u>
b_x (see Appendix C)	0.081"	0.074"
h_4 (see Appendix C)	0.204"	0.288"

For the floated surface on the secondary seal ring (Bb in Figure 22) and the floated surface seals (Bc), $\bar{H} = 1.0$, and $b_{1/b} = 0.35$. The surface of the secondary seal ring butted against the carrier is assumed to cause a linear pressure gradient over its surface as for purely viscous flow in a narrow slit. The axial movement of the seal due to runner runout is a maximum of ± 0.0025 inches. Because the shoes can slide under the secondary seal ring, movement of the seal causes a maximum unbalanced moment on the shoe of 8×10^{-4} ($P_2 - P_1$) inch-pounds. The unbalance can be easily taken up by a slight shift in angle of the Bc surface with respect to the carrier. The required angle change results in a shift in working clearance of $\pm 40 \times 10^{-6}$ inches under each sealing surface.

d. LEAKAGE

Calculated dimensionless leakage for the secondary seals are shown in the first Semiannual Report, Figures 38 through 42. Tables I to X apply to the major cases considered here: hydrostatic step face (secondary seals) and Rayleigh step (primary seal). Using the same methods and equations as used for the two-side floated shoe, the following listing of leakage values was calculated. Note that the gaps between segments have orifice-controlled flow rather than predominately viscous flow.

Test Rig Conditions:

Leakage (pounds per second)

	<u>End Seal</u>	<u>Interstage Seal</u>	<u>Labyrinth*</u>	
			<u>End</u>	<u>Inter</u>
<u>Cruise</u>				
Primary	0.0142	0.0025		
Secondary	0.0050	0.0008		
Segment Gaps	<u>0.0390</u>	<u>0.0165</u>		
TOTALS	0.0582	0.0198	1.07	2.02
<u>Take-off</u>				
Primary	0.0825	0.014		
Secondary	0.0381	0.018		
Segment Gaps	<u>0.0800</u>	<u>0.031</u>		
TOTALS	0.2006	0.063	2.50	5.20

*See Appendix G for method.

These leakage values correspond to the Rayleigh step design used on the primary seal, and hydrostatic step seals between the seal ring and the shoes, and between the shoes and carrier at the floated surfaces (Bc).

e. DYNAMICS

The dynamic model of the seal assembly is represented below in Figure 23.

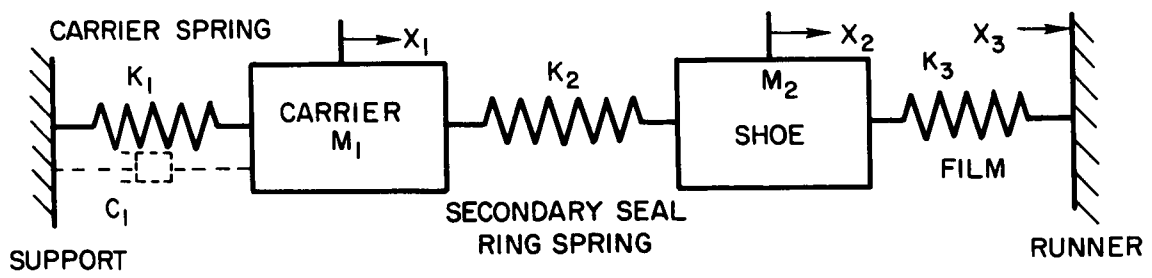


Figure 23 Dynamic Model of One-Side Floated Shoe Seal

The damping, C_1 , is shown dotted since it is not immediately considered.

The solution to natural frequencies and amplitude modes for the undamped system are solved as in Reference 1, where a case is given similar to the above except that $X_3 = 0$. X_3 in our case is the imposed motion of the runner (± 0.0025 inches).

However, solving the equations of motion leads to a solution identical to that given on page 103 of Reference 1.

$$\frac{X_2}{X_3} = \frac{K_3}{K_3 + K_2 \left[1 - \frac{K_2}{K_2 + K_1 - \frac{M_1 \omega^2}{g}} \right] - \omega^2 M_2}$$

$$\frac{X_1}{X_2} = \frac{K_2}{(K_2 + K_1 - M_1 \omega^2)}$$

$$\omega^4 - \omega^2 \left\{ \frac{K_1 + K_2}{M_1} + \frac{K_2 + K_3}{M_2} \right\} + \frac{K_1 K_3 + K_2 K_3 + K_1 K_2}{M_1 M_2} = 0$$

Values of K_1 , K_2 and K_3 were established at 3, 100, and 4640 pounds per inch per inch of circumference, respectively. The value of K_1 was selected as that value required to give a force sufficient at 0.2 inches carrier spring compression to overcome static friction at the carrier seal ring as it presses against the seal support when the engine is at speed. The 0.2 inch spring residual compression at the extreme position allows the nominal force in midposition and at the opposite extreme position to be so small as to have little effect on the film thickness at the primary seal. It should be noted that the spring could be softer, but have more residual compression and maintain the same effect. As will be noted later this spring does not affect the response of the shoe to the runner movement very much, nor does it have much effect on the natural frequencies of the system. Consequently, the real limits of K_1 are those of design ease.

The value for K_2 was established on the basis of natural frequency at around 100 to 1000 pounds per inch per inch of circumference. Small variations in K_2 result in small variation in natural frequency, so the value chosen represents the spring constant within the range of interest that is easiest to achieve.

The value of K_3 is that reported in the section on primary seals (see Table XI).

The mass of the carrier has a large effect on natural frequency, and was selected to provide a low natural frequency far enough removed from engine idle speed to be safe. It would be advisable to pick an even higher weight for the carrier if practical. Despite the fact that larger shoe masses would reduce the lower critical speed, for thermal and response reasons, the size and mass of the shoes should be small. Table XIX shows the undamped response of the system.

TABLE XIX

DYNAMIC RESPONSE OF RAYLEIGH STEP SEAL

$c/b = 2.125$, $h = 0.001$ in., pocket depth = 0.001 in.

N_{rpm}	Displacement			Film Thickness Change
	X_1	X_2	X_3	$\delta = X_2 - X_3$
955	0.002675	0.00251	0.0025	0.000010
1010	0.00379	0.00253		0.000030
2865	0.0128	0.002728		0.000228
3175	0.276	0.00835		0.005850
3820	-0.00515	0.00236		-0.000140
4775	-0.00196	0.00243		-0.000070
5730	-0.0011	0.00246		-0.000040
6685	-0.00073	0.00248		-0.000020
7640	-0.00052	0.00250		0.000000
8590	-0.00040	0.002515		0.000015
9550	-0.000316	0.00254		0.000040

$N_{CRIT} = 48,800$ rpm
3,170 rpm

Within the clearance variation being designed for, the natural frequencies do not approach the imposed frequency. This is, therefore, a safety feature for the seal. However, a low natural frequency occurs at a fraction of design speed so that the engine must accelerate through it. The lower natural frequency can be changed to approximately 3000 rpm by making small changes in the carrier spring constant. However the only practical method of lowering it further would be to increase the weight of the carrier. Since it already weighs 30.25 pounds, it is probably not desirable to do so if it can be avoided. A great reduction in carrier weight and corresponding adjustments in the seal

ring spring constant can allow the critical speed to be increased over the normal running speed. These changes represent a great design challenge however, and the studies have not yet been carried out.

The clearance variation is the critical factor in evaluating performance. For this application it should never be greater than 0.3 times the minimum design film thickness because of the other possible sources of film thickness variation. The undamped amplitude will allow rubbing. Consequently, additional damping must be imposed. The following equation is for the amplitude of δ_f with damping at the carrier spring. Damping was represented in Figure 23 as a dotted dashpot.

The basic equations of motion were modified to include a velocity damping term between the carrier ring mass and the support ring.

Thus:

$$M_1 \ddot{x}_1 + C_1 \dot{x}_1 + K_1 x_1 + K_2(x_1 - x_2) = 0$$

$$M_2 \ddot{x}_2 + K_2(x_2 - x_1) + K_3(x_2 - x_1) = 0$$

Assuming

$$x_1 = X_1 \sin \omega t$$

$$x_2 = X_2 \sin \omega t$$

$$x_3 = X_3 \sin \omega t$$

substituting, and solving for x_2/x_3 we have

$$\frac{X_2}{X_3} = \left\{ \frac{K_3^2 (M_1 \omega^2 - K_1 - K_2)^2 + K_3^2 C_1^2 \omega^2}{\left[[M_1 \omega^2 - K_1 - K_2] [M_2 \omega^2 - K_2 - K_3] - K_2^2 \right]^2 + \omega^2 C_1^2 [M_2 \omega^2 - K_2 - K_3]^2} \right\}^{1/2}$$

and

$$\frac{X_1}{X_3} = \frac{K_2 K_3}{\left\{ [(M_1 \omega^2 - K_1 - K_2) (M_2 \omega^2 - K_2 - K_3) - K_3]^2 + \omega^2 C_1^2 [M_2 \omega^2 - K_2 - K_3]^2 \right\}^{1/2}}$$

and

$$\delta_{\text{FILM}} = X_2 - X_3 = X_3 \left[\frac{X_2}{X_3} - 1 \right]$$

Actual damping in this system is of the Coulomb (friction) type. However, an approximate method of using this in the equations of motion is to evaluate the friction and multiply it by the velocity of the sliding surfaces. This method has been used here.

The inherent damping in just the carrier ring is about

$$C_1 = V \Delta P b f \text{ lb. sec./inch/inch of circumference.}$$

where

$$V = \frac{60 \times 0.707}{\delta \times 2 \times N \times \pi} = \text{mean velocity in vibration excursion, feet per second}$$

ΔP = unbalanced radial pressure difference across piston ring, pounds per square inch

b = width of ring (0.175 inches)

f = friction coefficient (0.2)

δ = excursion of carrier, (assume = 0.120 inches for a limiting case)

π = number of vibrations per revolution (assume $\pi = 1$)

N = 8000 rpm

Then $C_1 = 0.0236$ lb. sec/inch/inch of circumference. This value can be adjusted up or down somewhat by changing the ring configuration. Additional damping can also be built in, if desired, by putting rubbing guide cylinders around or inside the carrier springs.

Using a value of $C_1 = 0.025$ lb sec/in/inch of circumference, the following δ_f was calculated near the lower critical point:

N_{RPM}	δ_{FILM}	x_1 / x_3
2865	0.000195	5.12
2962	0.000250	6.54
3058	0.000305	9.8
3154	0.000140	11.92
3248	-0.000210	9.4
3343	-0.000320	6.48
3440	-0.000278	4.66
3538	-0.000235	3.58

The following chart shows the effect of varying the damping, at the worst N indicated on the above chart (3058 rpm and 3343 rpm):

C_1	δ_{FILM}		x_1 / x_3
	3058 rpm	3343 rpm	3058 rpm
0.0125	0.000495	-0.000465	13.5
0.025	0.000305	-0.000320	9.8
0.0375	0.000177	-0.000220	7.3
0.050	0.000102	-0.000160	5.7

The clearance change approaches the allowable value when the damping level is 1/2 the level easily achievable at normal operating speed. At the speed indicated, however, the pressure ratio across the carrier seal ring is less than 1/4 of the design pressure ratio. This means that the damping due to this pressure difference is reduced to less than 1/4 of the calculated value at the indicated speed. In fact, though, the seal weight will contribute some damping so that the picture is not quite as marginal as it appears. Nevertheless, steps should be taken to increase the damping of the carrier to a level slightly over that readily achieved with one piston ring.

f. THERMAL DISTORTION EFFECTS

The heat generation (q_T), in the seal totals 9560 BTU/hr when operating at design clearance under test rig cruise conditions. Since the seal segments are pressure balanced, the clearance assumed by the seal at the primary face is the design clearance modified only by the amount necessary to counterbalance forces generated by any deflections of the seal ring spring and carrier spring. These clearance changes are slight during cruise. All calculations of heat generation were therefore made at the nominal clearance for evaluating the design.

The fluid motion in the seal is laminar. Therefore, the heat generation can be fairly accurately calculated using laminar shear flow equations. For two surfaces moving past each other in laminar flow, the heat generation is

$$q = LA\omega R/J \quad \text{BTU/second}$$

or

$$q = 0.00955 \frac{R^3 b}{h} \quad \text{BTU/hour}$$

where

- R = mean radius, inches
- Δb = incremental radial length, inches
- h = local gap width, inches
- J = thermal conversion factor = 12 x 778 inch-pounds per BTU
- N = revolutions per minute
- μ = viscosity, pound-seconds per square inch
- L = shear = $\mu \left(\frac{U}{h} \right)$
- U = velocity of moving surface, inches per second
- ω = $2\pi N/60$

and

$$8\pi^3 N^2 \frac{\mu}{J} = 0.01$$

This equation numerically integrated over the face of the seal, results in heat generation of about 9560 BTU/hr.

The effects of this heat generation depend upon the temperature of the core air and upon the effective thermal conductivity of the seal material. Detailed temperature distribution for various assumed conditions are presented in Appendix E, so that at this juncture only the general effects will be discussed. Basically there are three effective heat paths out of the seal face area:

- Down the runner disk to the core air
- Through the runner disk to the compressor exit air
- Through the carrier wall at the runner tip to the compressor exit air

Of these, the second is by far the most effective because the thermal resistance to the air on the upstream face of the runner is small, and there is reasonable stirring action in that air to transfer the heat by convection to the main air stream. The first path has a very good sink, the core air, but must depend on the runner disk to transmit the heat to the core: this is a poor heat conduction path. The third path has high resistance compared to the second.

Calculations indicate that the relatively poor thermal path from disk to runner nearly isolates the seal face from the core: a 100 degree Fahrenheit change in core temperature causes a maximum change in the runner and seal temperatures of only 20 degrees Fahrenheit. Most of the heat follows the second path.

The heat pattern through the seal exhibits considerable gradient within the seal segments and the runner. However, the runner distortion is very small because of the small distances over which the gradients act. Most potential problems arise in the seal segments. The effects of the gradients in the seal segment are to change the curvature of the curved surface and to curve the primary seal face. Assuming that the differences in clearance across the primary seal face should not exceed 0.0003 inches, the maximum allowable temperature gradient in each of the twenty-four segments is

$$\Delta T = \frac{2 l \delta}{\alpha (q')^2} = \frac{2 \times 6 \times 0.0003}{9 \times 10^{-6} \times (1.8)^2} = 12 \text{ degrees Fahrenheit}$$

Without augmented conduction, the gradients are greater than this (as much as 26 degrees Fahrenheit).

Clearly, temperature gradients and consequent thermal distortions can be reduced by increasing the effective conductivity of the seal material. With three times the thermal conductivity of Inconel X-750 in the seal, the differentials drop to a maximum of 4 degrees Fahrenheit (see Appendix E). Augmented conduction is used in this design.

The carrier members tend to reach temperatures very nearly equal to the adjacent seal segment temperature. Therefore, the segments are the only part of the design requiring special treatment. Probably the most easily accomplished conductivity augmentation method is to use a thin layer of a highly conductive material, such as silver (between 0.020 inches and 0.040 inches), sandwiched between Inconel X-750 plates. The whole external surface of the segments (except the primary seal face where ceramic coatings are required to prevent wear due to rubbing) can then be plated to its maximum usable depth (about 0.003 inches to 0.005 inches). Inconel X-750 spacers will be needed across the sandwiched silver to maintain proper segment shape under all conditions since silver has a slightly higher coefficient of expansion than does Inconel X-750. Use of this modification will allow the complete seal to be essentially unaffected in its operation by the surrounding steady state thermal environment.

Other potentially useful methods of augmenting conductivity are to use a sintered Inconel base structure impregnated with silver or to use silver cladding of sufficient thickness. Both of these methods should be explored at a later date.

Since all the seal assembly parts will assume about the same temperature with the augmented conductivity segments, the complete seal will be quite tolerant of thermal growth.

The thermal calculations were conducted for only the hot core and 1200 degrees Fahrenheit core with this design. However, Appendix D shows results for the two sided shoe seal which was analyzed with core temperatures of 1100, 1200, and 1300 degrees Fahrenheit. That seal is isolated from the core about as well as is this design. The general result is that either raising or lowering the core temperature by 100 degrees Fahrenheit will result in a corresponding increase or decrease of the seal temperatures by about 20 degrees Fahrenheit. The gradients are not seriously changed. Consequently, for only nominal core temperature changes this design is satisfactory.

Differential thermal growth is easily taken care of for steady state conditions using augmented conduction in the shoe. Analyses have not been undertaken for transient conditions because this means that detailed analyses have to be made at every point in time of an airplane flight. At this time there is not enough known about the variable air pressure and temperature conditions at the seal position to conduct a meaningful analysis.

g. MECHANICAL DISTORTIONS

It can be stated that the runner can operate essentially independently of the seal for this design, as the only requirement is that the runner face remain axially positioned within about 0.0003 inches across the runner plane. This requirement is easily met for both thermal and stress considerations because the runner is thin enough that it assumes nearly uniform stress and temperature in the axial direction. Also, its radial length is slightly greater than the height of the primary seal face, so that relative movement in the radial direction will cause no change in seal operation.

The thermal growth of the carrier ring under steady state conditions poses no seal operating problems because relative radial motion between seal and runner is allowable.

Small gaps (0.004 inches at cruise assumed for this design) between each segment pair in the seal will accommodate the possible slight differential growth (either thermal or stress induced) between carrier and segments. The gaps

can probably be made smaller in the final design. The secondary seal ring and carrier seal rings are split to allow differential growth, either thermal or stress-induced.

To prevent rubbing of the inner surface of a segment against the carrier ring, the variation in carrier radius under any one seal segment should not exceed 0.0003 inches. Therefore, the total variation in carrier ring radius can be about $12 \times 0.0003 = 0.0036$ inches.

The allowable \bar{h} variation after accounting for the probable seal distortion and seal deflection allows the total variation in the gap between runner and shoe over any one shoe length to be no more than the variation in h minus the maximum possible change in film thickness ($0.001 - 0.00030 = 0.00070$ inches). This variation could lead to 2 waves of 0.005 inches peak-to-peak amplitude in the runner circumference. In other words, the flatness of the runner must be within $\pm 0.0021''$.

These manufacturing tolerances are said to be achievable by standard methods.

h. WEAR AND RUBBING LIFE

Under ideal conditions there should be no wear or rubbing during full speed operation except where the piston rings seal. There will be initial and terminal operation rubbing if hydrodynamic lift-off is used. If seal retraction is used the only rubbing will be at the piston rings. In practice, however, there must be protection against momentary contact, which may occur at high speed. Thus, material at the seal faces must be properly chosen to ensure sufficient life.

The seal segments must have augmented conductivity as mentioned previously. One method suggested was to use a silver layer sandwiched between Inconel outer pieces. This leaves Inconel facing Inconel at the seals. If these surfaces are well oxidized, they may serve as satisfactory surfaces to resist wear and rubbing. Flame spray coating, carbide coating, or oxide coating on the shoes will provide a wear resistant coating, but should run against a similar coating on the runner. Since the runner expands and contracts, there is a question about the ability of such a coating to stay on. Consequently, the runner may have to be coated with a thin layer of solid lubricant such as a eutectic mixture of CaF_2 and BaF_2 .

If the sintered Inconel shoe impregnated with silver is used for thermal reasons, it will probably serve as an adequate protection against wear and rubbing at high temperatures. In all probability, the facing surface will not need a coating or special treatment, especially if it is naturally oxidized.

i. STRESS AND FATIGUE

The runner is the only part of the seal which experiences considerable stress. However, it is usually considered to be part of the compressor structure since it is attached to it and must be designed along with the rest of the compressor. For this reason, its stress will not be considered here.

The carrier ring (E in Figure 22) experiences a compressive stress due to the pressure differential across it. The pressure differential load extends over only about 1-1/2 inch of carrier ring length, however, while the structure supporting the load is the complete ring cross section. Thus, the stress imposed by the pressure load is

$$\text{stress} = \frac{\text{unbalance length of carrier ring} \times \text{mean seal dia.} \times \pi \Delta P}{2 \times \text{cross section area of ring}} = S_{\uparrow}$$

$$\frac{1.5 \times 27.5 \times \pi \Delta P}{2 \times \text{area cross section ring}} = \frac{1.5 \times \pi \times 27.5 \times 80}{2 \times 1.2} = 4330 \text{ psi} = S_{\uparrow}$$

where the area of the ring cross section is sufficient to make the total weight of the carrier come up to 30.25 pounds for controlling the natural frequency. This amount of stress will cause a diameter reduction of $S_{\uparrow} / E \times \text{diameter} = 0.00396$ inches, which is easily taken up by the gaps between shoes. The rupture stress of Inconel-X for 10,000 hour at 1200 degrees Fahrenheit is about 60,000 pounds per square inch, so no real problem is anticipated.

Parts subjected to fatigue and fretting are the carrier ring springs, the secondary seal ring springs, and the surfaces on which they act. The number of cycles to be considered for a 2000 hour life is essentially 2 cycles of motion per revolution, for a total of about 2×10^9 cycles. The springs should be designed to have less than about 40,000 pounds per square inch stress to maintain proper life. This is easily done.

Fretting will tend to cause wear at all points where the springs touch the structure. The actual forces at the carrier ring contact points are about 12.7 pounds per point at maximum deflection (considering that there will be twelve springs), plus ± 1.8 pounds per point caused by maximum possible secondary seal ring spring movement. Assuming the use of a wavy washer having one complete wave length per inch of circumference, the forces at the contact points of the secondary seal ring spring are 1.8 pounds per point ± 0.25 pounds per point. These forces will result in nominal Hertzian stresses of about 10,000 to 100,000 pounds per square inch at the carrier spring's contact points (depending on exact design) and about 2500 pounds per square inch (minimum) at the secondary seal ring spring's contact points. These stresses are low enough so that only very small wear particles will be the product of fretting. Typical particle sizes are in the microinch range, so they can not cause any additional damage to any of the seal surfaces.

j. TOLERANCES TO FOREIGN PARTICLES

Tolerance to foreign particles is a function of allowable movement of a segment in clearing the particle out of the gap. The allowable axial movement of the segment is limited only by the amount of moment unbalance that can be tolerated, since movement of the shoe under the secondary seal ring introduces a moment. The maximum easily tolerable moment corresponds to about 0.005 inches of axial movement. The carrier ring will not deflect to account for the particle because the particle is at one spot and the carrier is a heavy, continuous ring. Thus, particles in the primary seal can equal the above dimension plus the thickness of the gap, giving a tolerable particle size of 0.006 inches diameter.

The other seal surfaces are essentially stationary with respect to each other, so particles of about 0.0003 inches diameter will pass through, and larger ones will be trapped in the hydrostatic air supply pockets or at the leading edge of the secondary seal ring.

Large particles would only cause a slight increase in leakage if it were, by remote chance, possible for them to enter the gaps at the secondary seals.

The entrance passages to the seal can be designed to reduce the possibility of large particles even coming near the seal.

k. MANEUVERING LOADS

Maneuvering loads imposing radial and axial forces on the seal can be substantial. The major effect of radial loads is to press the carrier ring against the support ring. The carrier seal rings will be backed up by wave springs. They will be required to deflect enough to absorb the load without bottoming the seal ring in its groove. Assuming that radial "g" loads can be as high as 8 g's in turbulent air, the carrier seal springs will be required to carry

$$\frac{\text{g's} \times \text{weight}}{\text{mean supporting length}} = \frac{\text{g's} \times W}{\pi \times \frac{\text{diam}}{2} \times 0.707}$$

$$\frac{8 \times 36.3}{\pi \times \frac{27.5}{2} \times 0.707} = 9.5 \text{ pounds per inch of circumference}$$

Thus, these rings could be designed for about 200 pounds per inch per inch of circumference to handle the radial loads (assuming that 0.050 inch deflection can be easily designed for).

Another radial maneuvering load important to consider occurs at the secondary seal. Here, the force due to the shoe weight must be balanced by the secondary seal forces. This follows for either an inward or outward radial loading.

The radial load imposed on the secondary seal by an 8-g maneuver will be

$$(\text{lbs of shoe/inch}) \times \text{g's} = 0.55 \text{ pounds per inch}$$

This must be balanced by an increase or reduction in film thickness such that

$$d\bar{W} = \bar{K}_S d\bar{H}$$

But $d\bar{W} = \frac{0.55}{b(p_1 - p_2)}$, which for test conditions is 0.014.

At nominal conditions $\bar{H} = 1$, $\bar{K}_S = 0.08$, and $\frac{p_1}{p_2} = 0.2$, so

$$d\bar{H} = \frac{0.014}{0.08} = 0.175$$

This means that an increase or reduction in film thickness of about 18 percent will accommodate the radial g load whether directed inward or outward. There will be some variation in \bar{K}_S over the shoe movement, but not enough to cause significant film clearance change difference from the above value.

The secondary seal ring is held in place by the same forces as those described above for the secondary seal of the shoe. Consequently, no touching of either shoe or seal ring due to radial loads is expected.

The rearward axial load, which will approach one g in the worst condition, must be taken by the springs, by a built-in stop for the end seal, or by the primary seal in the interstage seal. To keep the assembly procedure as simple as possible, it is not desirable to make either the carrier springs or secondary seal ring spring operate in tension. The carrier springs have to deflect about 0.140 inches for a one-g load, in addition to any excursion required to absorb the thermal growth of the compressor. This deflection is small enough to be easily accommodated.

The forward g loads, which also can approach one g, must be absorbed by the end primary seal or by the carrier springs of the interstage seal. Reference to the design values shows that the difference in \bar{W} at nominal \bar{H} and at minimum practical \bar{H} (about 0.3) is sufficient to absorb the forward load.

For the Rayleigh step seal

- load carrying ability is 2385 pounds at $\bar{H} = 1$, $\bar{W} = 0.69$.
- load carrying ability is 3650 pounds at $\bar{H} = 0.3$, $\bar{W} = 1.055$.
- excess load = 1265 pounds
- g capacity = $1265/36.3 = 34.8$

where

36.3 lbs. is the weight of the movable portion of the seal.

1. FAIL-SAFE CONSIDERATIONS

Failure of springs will be the main concern for fail-safe operation. Since both carrier and shoes are pressure balanced (unless the unbalanced carrier is used) a spring failure during operation will have little serious effects. If several of the carrier springs break, there will be an effect on critical speed and it will show up when the engine slows down or speeds up. However, this is very improbable. In the case of the initially retracted carrier (unbalanced carrier), the breaking of several springs will only tend to decrease normal operating clearance of the primary seal.

Broken piston rings or seal rings will act to increase damping and leakage, but should not seriously affect an engine's ability to operate at lower performance for long periods of time.

A thorough evaluation of the fail safe properties of the seal will have to await testing.

m. MATERIALS

The design can utilize Inconel X-750. However, the seal segments must have a highly conductive core or impregnation to improve the effective thermal conductivity so that temperature gradients can be held to an acceptable minimum. All nearly stationary parts that could touch any other surface, must have an antigalling surface. Well-oxidized Inconel can serve as this surface, as could a silver-impregnated surface. Silver plating could also serve as a dry lubricant between the Inconel parts if it would perform acceptably.

The primary seal face material should be a high temperature carbide or oxide, especially if hydrodynamic lift-off is used. Use of the NASA sintered nickel-chromium alloy composite impregnated with BaF_2 - CaF_2 eutectic can also be considered. The eutectic alone can be placed in a thin layer on the runner to operate against the face material of the segment.

Experiments will finally determine the proper primary seal face material and type of runner surfacing material if any are to be used.

n. OFF-DESIGN OPERATION

The operation at take-off requires primarily that the seal remain balanced, or that only slight cocking occurs, and that the primary seal gap remain sufficiently large. In this respect, this seal is similar to the two-side floated shoe seal.

At idling conditions, hydrodynamic lift-off may be marginal, although calculations are not sufficiently accurate at this time to definitely state the lift-off speed. At idling speed for the retracted version of the seal, the seal can be designed to maintain a good clearance.

6. DESIGN OF THE THIN-STRIP PLUS PISTON RING CONCEPT

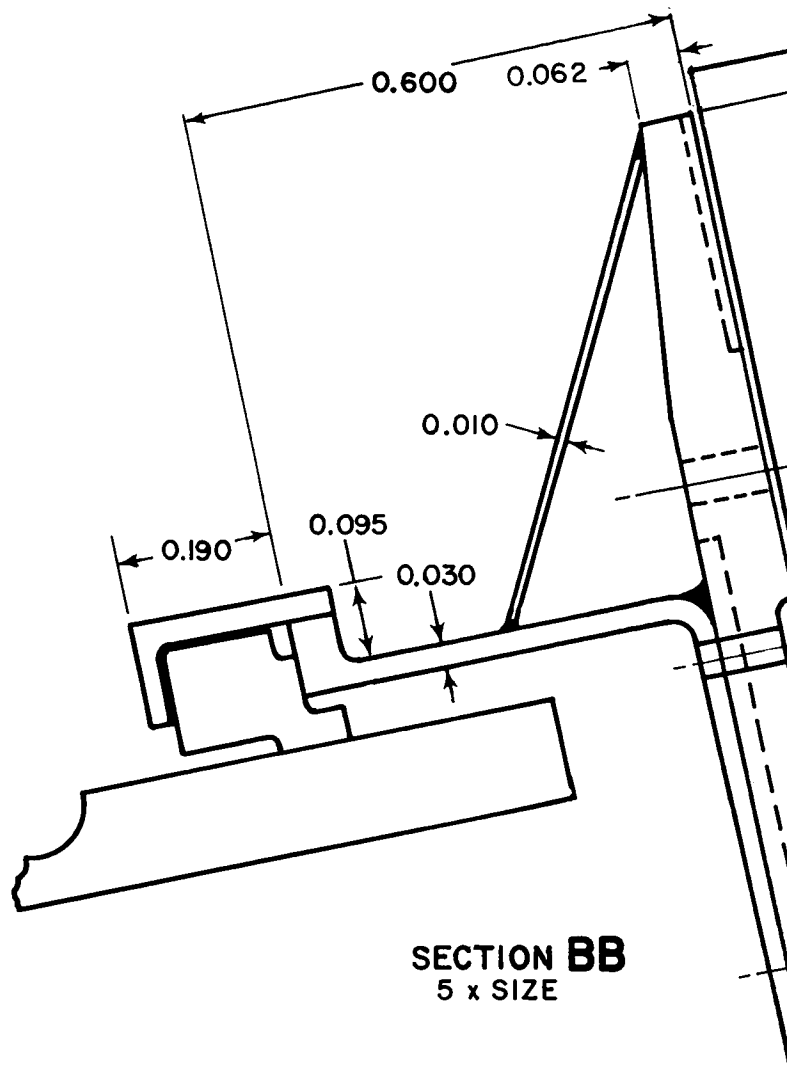
a. DESCRIPTION

One of the end seal concepts proposed for detailed feasibility analysis is the thin-strip one-piece seal. The schematic diagram of this concept is shown in Figure 24. The main design feature is that the primary seal element is a continuous, flexible, thin strip. The thin strip must be extremely flexible so that it can be readily bent or twisted under the action of the gas film forces to follow any mechanical, thermal, or elastic distortions of the rotor face without contacting it. The thin ring, as shown in Figure 24, is flexibly attached to a seal carrier by means of coil springs and guide pins. Secondary sealing between the thin strip and the carrier consists of a fully floated piston ring which permits the thin strip to follow any runout or wobble of the face.

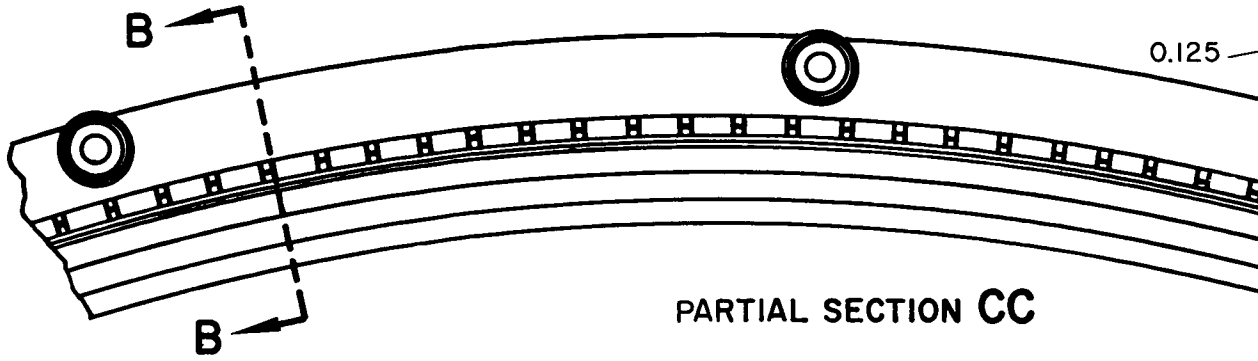
An orifice-compensated hydrostatic gas film is suggested as the means to separate the primary seal face and the rotor face at high speeds. Two rows of orifices are shown in the schematic to provide a greater angular stiffness to keep the edges from rubbing the rotor. The seal carrier design is similar to the one-side floated shoe design.

b. DESIGN CRITERIA FOR THIN-STRIP SEAL

As discussed earlier, the most essential requirement of the thin strip is that the seal be sufficiently flexible to compensate for any initial angular distortion, thermal coning, and residual unbalanced moment. A first order design criterion was presented earlier in the first Semiannual Report. This criterion was based on the assumption that the twist angle, the gas film restoring moment, and other forces acting on the seal ring are all axisymmetrical, i. e., they do not vary in the circumferential direction. In reality, the initial angular distortion, in all likelihood, may contain a considerable degree of asymmetry such as a saddle-shape angular distortion. Therefore, it is necessary to extend the previous criterion to include the case of asymmetrical deformation.



SECTION BB
5 x SIZE



PARTIAL SECTION CC

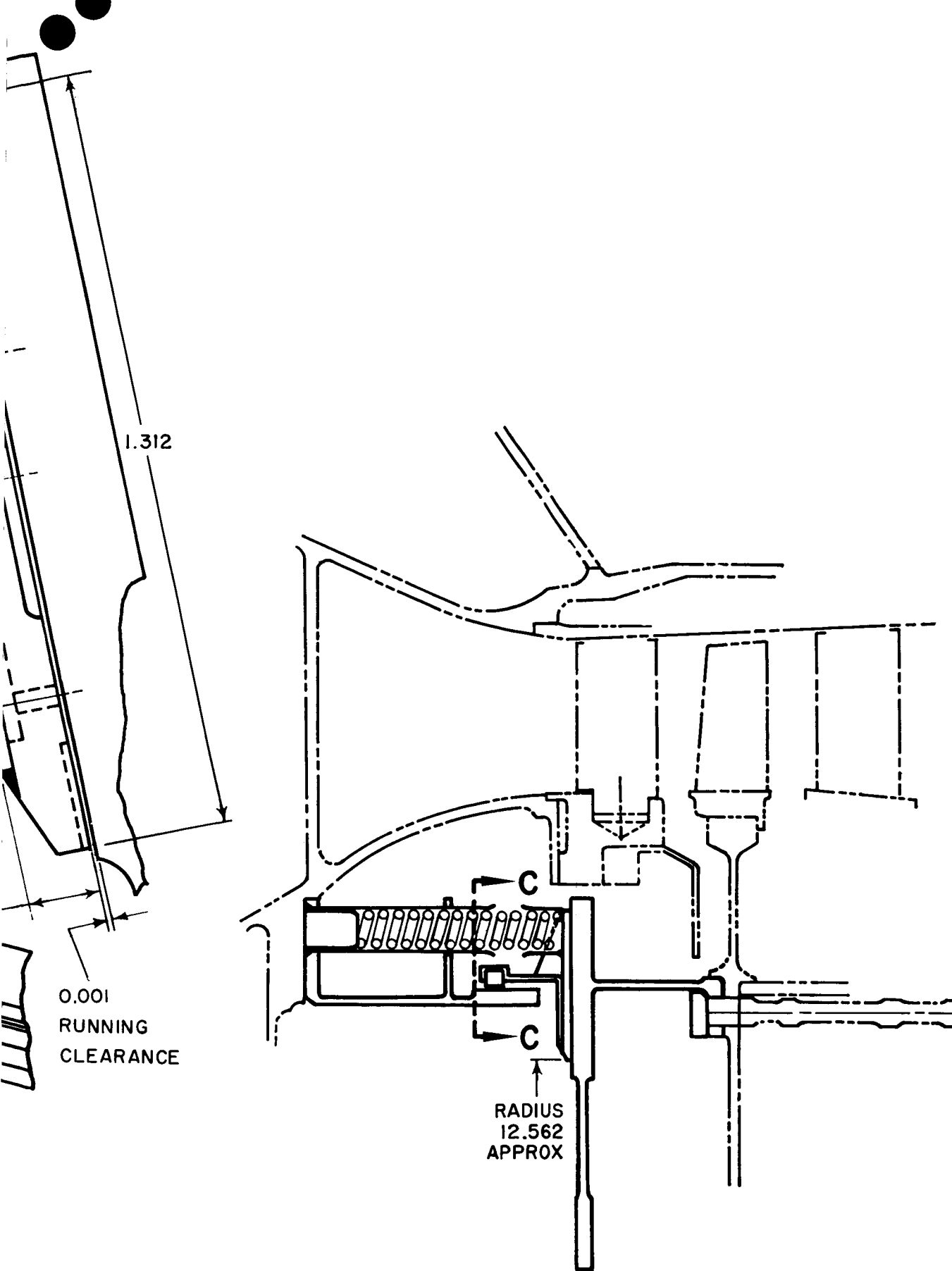


Figure 24 Thin-Strip Plus Piston Ring Seal

Consider an element of the seal ring as shown in Figure 25.

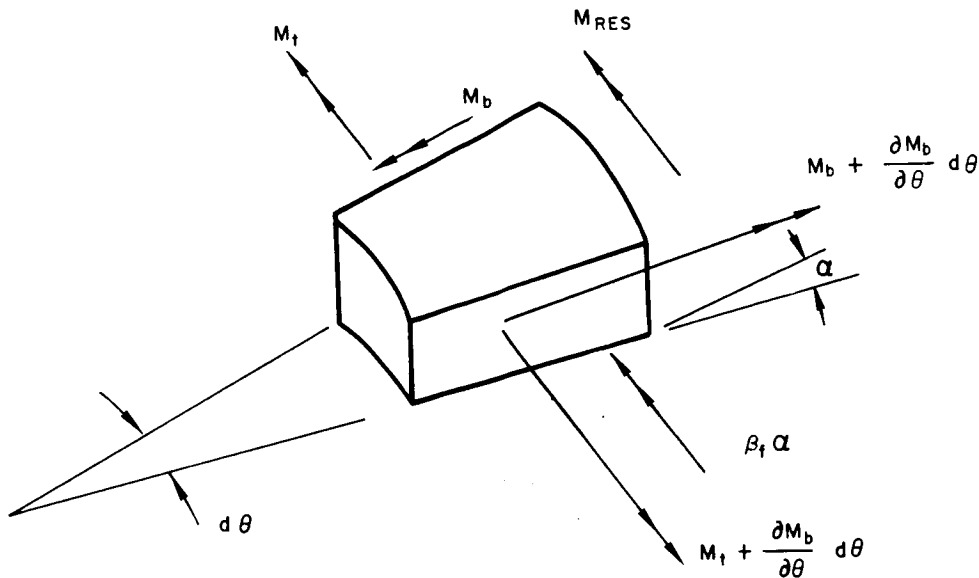


Figure 25 A Ring Element of the Thin-Strip Plus Piston Ring Seal

In this diagram,

- M_b = bending moment, inch-pounds
- M_t = twisting moment, inch-pounds
- α = relative angular displacement between the rotor and seal face, radians
- M_{RES} = unbalance residual moment per unit circumferential length, inch-pounds per inch
- β_f = gas film angular stiffness, inch-pounds per inch-radian

The moment balance of this element requires

$$-\frac{EI_c}{R^2} (\alpha - \alpha_D) + \frac{GJ}{R^2} \frac{\partial^2 (\alpha - \alpha_D)}{\partial \theta^2} = M_{RES} + \beta_f \alpha \tag{1}$$

where

- E = Young's modulus, pounds per square inch
- I_c = area moment of inertia of seal section about its centroid, inches⁴
- R = mean radius of the seal ring, inches
- G = Shear modulus, pounds per square inch
- J = effective polar moment of inertia of the seal section, inches⁴
- α_D = relative angular twist between the rotor and seal ring face due to initial or thermal distortion, radians

Letting

$$\beta_f = \frac{GJ}{R^2}, \quad \beta_e = \frac{EI_c}{R^2},$$

and assuming that α and α_D can be expressed by the Fourier series

$$\alpha_D = \alpha_0 + \sum_{n=1}^{\infty} \alpha_n \cos n\theta, \text{ and } \alpha = \alpha_0 + \sum_{n=1}^{\infty} \alpha_n \cos n\theta, \quad (2)$$

the solution of equation (1) gives the following criterion, where α_0 and α_0 are the rotationally symmetric components of the angular displacements, and α_n and α_n are the high order asymmetric components:

$$\alpha = \sum_{n=0}^{\infty} \left(\frac{n^2 \beta_f + \beta_e}{n^2 \beta_f + \beta_e + \beta_f} \right) \alpha_n - \frac{M_{RES}}{\beta_e + \beta_f} < \alpha_A \quad (3)$$

where α_A is the allowable angle of twist of seal ring face with respect to the rotor face.

Equation (3) is a useful criterion to determine whether the primary seal is sufficiently flexible to follow the rotor. For a given geometry and gas film design of the primary seal, the values of β_e , β_f and β_f can readily be calculated. By assuming a proper value of M_{RES} , equation (3) may be used to evaluate the maximum allowable warping of the ring for safe operation without rubbing. It is evident from equation (3) that in order to keep the left hand side at a minimum, efforts must be made to reduce β_e and β_f , and to increase the gas film stiffness, β_f . The use of equation (3) will be illustrated later in designing the thin-strip seal.

c. PRIMARY SEAL CONCEPTS CONSIDERED FOR THIN-STRIP SEALS

Three types of primary seals have been considered for thin-strip seals. They are:

- The single pad, double orifice spiral groove seals
- The double pad, spiral groove seal
- The double pad, Rayleigh step seal

1) SINGLE PAD, DOUBLE ORIFICE SPIRAL GROOVE SEAL

The static performance of the single pad, double orifice spiral-groove seal shown in Figure 26 has been analyzed. The analysis made use of the basic

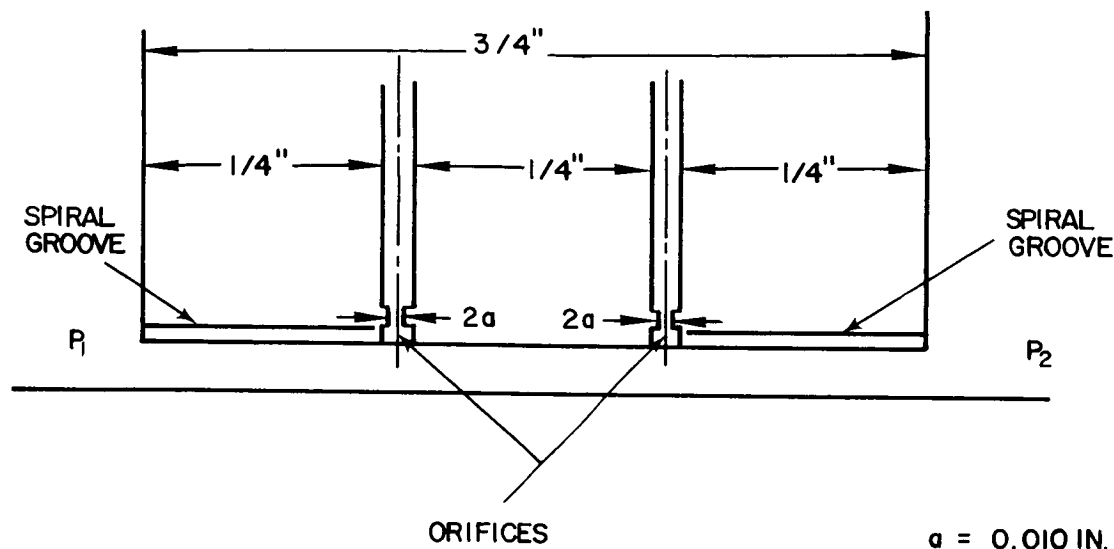


Figure 26 Single Pad, Double Orifice Spiral-Groove Seal

solutions developed for flow through a spiral-groove strip and for flow through an orifice. A numerical iterative procedure is employed to determine the pressure at various points in the gas film by matching flow between orifices and spiral groove passages. A computer program was written to calculate the pressure, load, and center of pressure of this primary seal configuration. The program can also be used to calculate the performance of a divergent or convergent film by assuming the film to be composed of several parallel steps.

Results have been calculated for a typical seal having the dimensions shown in Figure 26. The axial stiffness of this seal was found to be 16,500 pounds per square inch per inch, which is adequate for tracking in the axial direction. The angular stiffness (β_r) of the gas film was found to be 460 inch-pounds per inch-radian. It will be shown later that this value is too low to meet the design criterion outlined in subsection I. B. 6. b. It is unlikely that substantial increase of the angular stiffness can be achieved by improving the geometrical dimension of this primary seal. For this reason, the single-pad design has been abandoned in favor of a double-pad design for the purpose of gaining more angular stiffness.

2) DOUBLE PAD, SPIRAL GROOVE SEAL

The basic design of the double pad, spiral groove seal (Figure 27) is similar to the single pad, double orifice seal. The sealing area is now vented in the middle, forming two pads, and the feeding holes and the spiral grooves are separated by a land in order to increase the groove's pumping action at a thin film thickness. A finite difference method has been used in calculating the performance of this seal. Details of this analysis are presented in Appendix B.

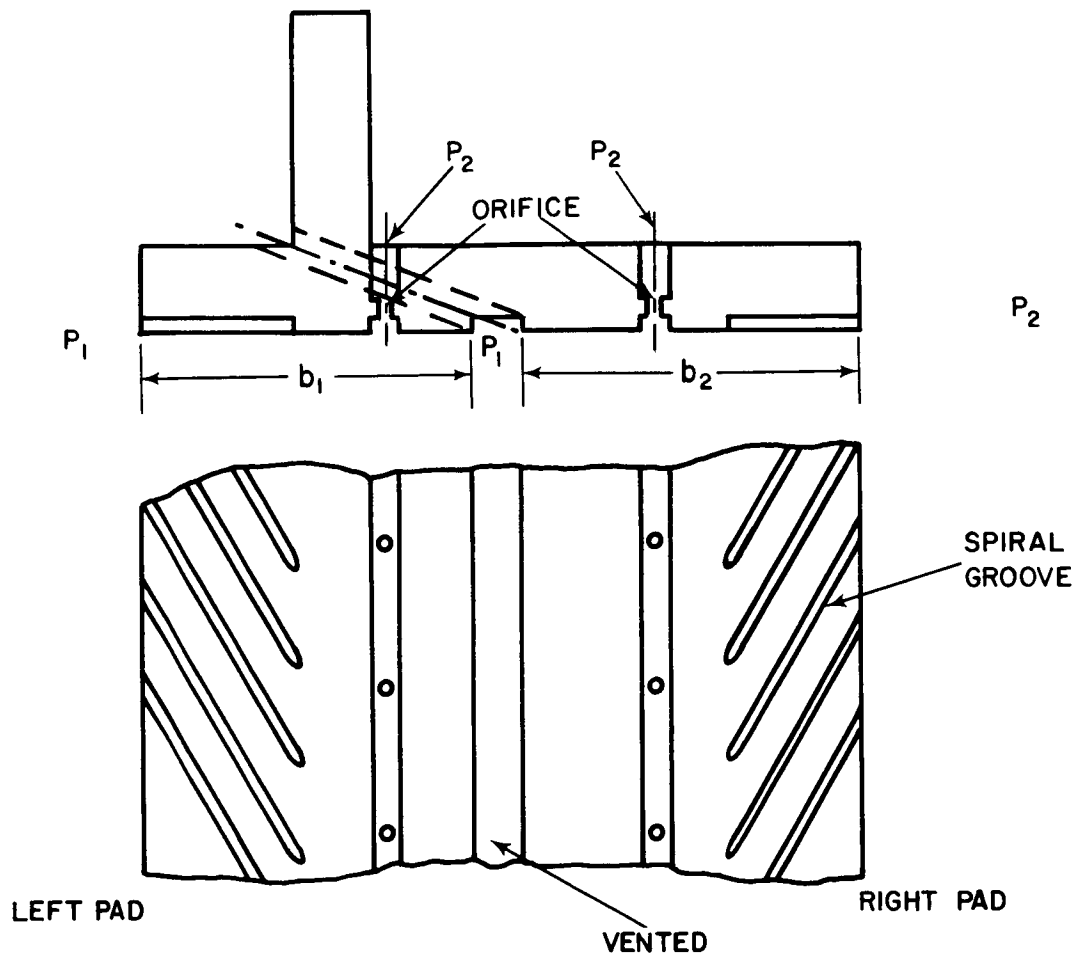


Figure 27 Double Pad, Spiral Groove Seal

The approach gives a very accurate prediction of the pressure distribution and is used to determine the performance for the right pad, which has unequal pressure boundary conditions. The left pad is essentially a thrust bearing: its performance at the operating film thickness can be predicted by existing theories. The theory developed in Reference 2 was used in calculating the load and stiffness for the left pad.

Using the theory developed in Appendix B, the gas film forces and the center of pressure acting on the right pad at a film thickness of 0.001 inch are found to be

$$\frac{W_2}{b_2 (P_2 - P_1)} = 0.832$$

and

$$\frac{x_2}{b_2} = 0.4336,$$

for $p_2 - p_1 = 80$ pounds per square inch and $b_2 = 0.6$ inches

$$W_2 = 0.832 \times 0.6 \times 80 = 40 \text{ pounds per inch}$$

$$x_2 = 0.6 \times 0.4336 = 0.26 \text{ inches}$$

To calculate the load for the left pad, the data by Tang and Gross on page 272 of Reference 2 are used. For $p_2/p_1 = 5.0$, the optimum stiffness requires the bearing parameter, B (as defined in Reference 1), to be in the neighborhood of 15. For $B = 15$, the dimensionless load becomes

$$\frac{W_1}{b_1(p_2 - p_1)} = 0.4375,$$

which gives for $b_1 = 0.4$ and $p_2 - p_1 = 80$ pounds per square inch,

$$W_1 = 0.4375 \times 0.4 \times 80 = 14 \text{ pounds per inch.}$$

For a symmetrical pressure distribution on the left pad in Figure 28,

$$x_1 = 0.5 \times b_1 = 0.5 \times 0.4 = 0.2 \text{ inches.}$$

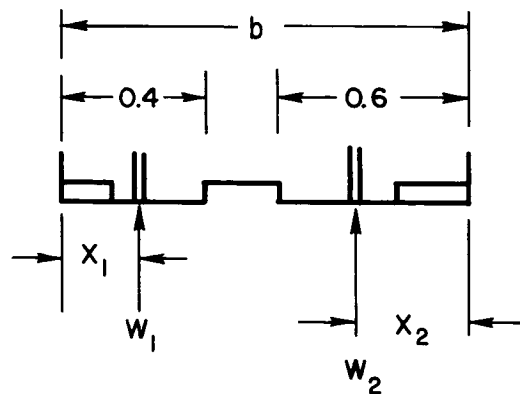


Figure 28 Model of Double Pad Seal Surface

The dimensionless axial stiffness of the left pad can be located on page 272 of Reference 2.

$$\overline{K_{S1}} = \frac{K'_{S1} h}{p_1} \cong 2.0$$

$$\text{for } p_1 = 20 \text{ and } h = 10^{-3}$$

$$K'_{S1} = 2.0 \times 20 \times 10^3 = 40,000 \text{ pounds per square inch per inch,}$$

where K'_{S1} is defined as the stiffness per unit area of the sealing surface.

The axial stiffness of the right pad based on the load curve in Figure 29 is found to be

$$K'_{S2} = 23,700 \text{ pounds per square inch per inch}$$

To summarize, the load, center of pressure, and stiffness of the double pad, spiral groove seal are listed as

$W_1 = 14$	lb/in.
$W_2 = 40$	lb/in.
$x_1 = 0.2$	in.
$x_2 = 0.3$	in.
$K'_{S1} = 40,000$	lbs/in ² /in
$K'_{S2} = 23,700$	lbs/in ² /in

This data will be used later in balancing the primary seal ring.

3) DOUBLE PAD, RALEIGH STEP SEAL

The Raleigh step seal, which has been chosen for the one-side and two-side floated shoe concepts, is also considered here for the thin strip seals. A comparison of the axial stiffnesses shows that the spiral groove seals are much stiffer than the Rayleigh step seals. For example, under the test rig cruise conditions, the Rayleigh step seal has an axial stiffness approximately equal to 15,000 pounds per square inch per inch compared to 23,700 pounds

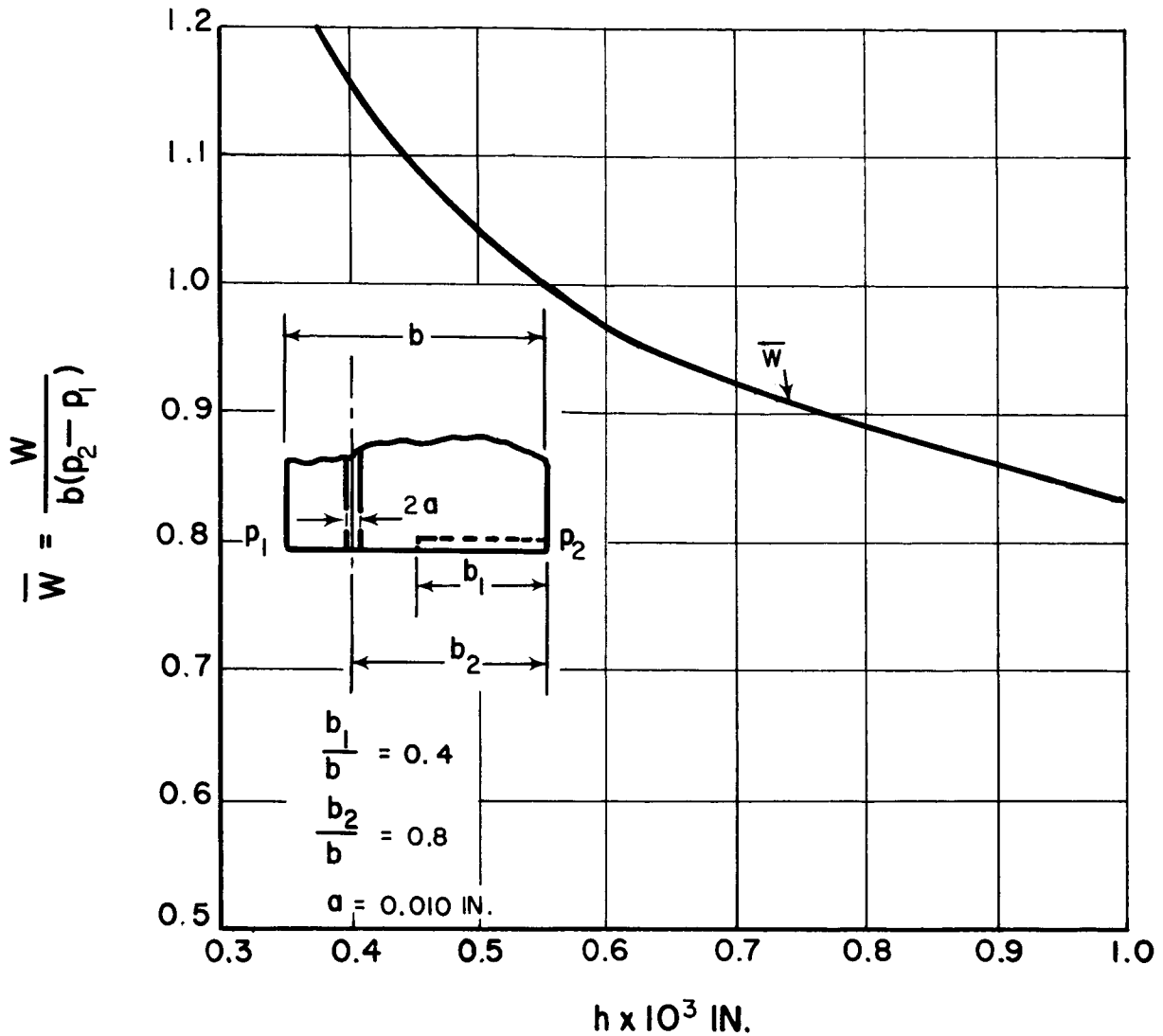
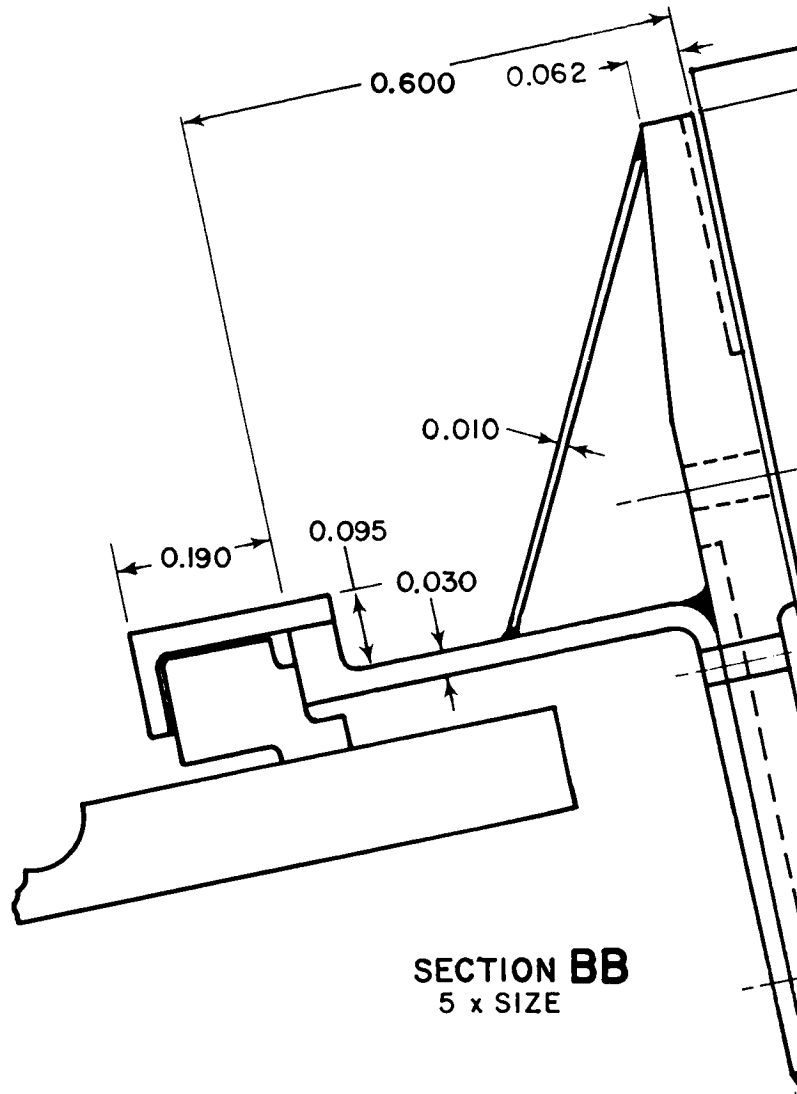


Figure 29 Loading of Double Pad Seal

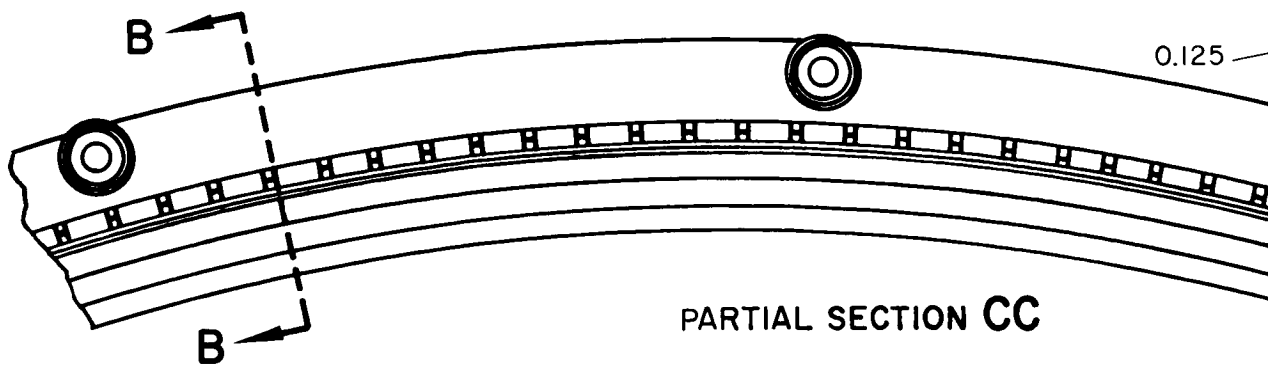
per square inch per inch for the spiral groove seals. Since the one-piece construction of the thin strip permits a continuous spiral groove pattern without any interruption, the spiral groove seal is more favorable and is chosen for the thin strip seals instead of the Rayleigh step seals.

d. FORCE AND MOMENT BALANCE

The forces acting on the primary seal ring are shown in Figure 30.



SECTION BB
5 x SIZE



PARTIAL SECTION CC

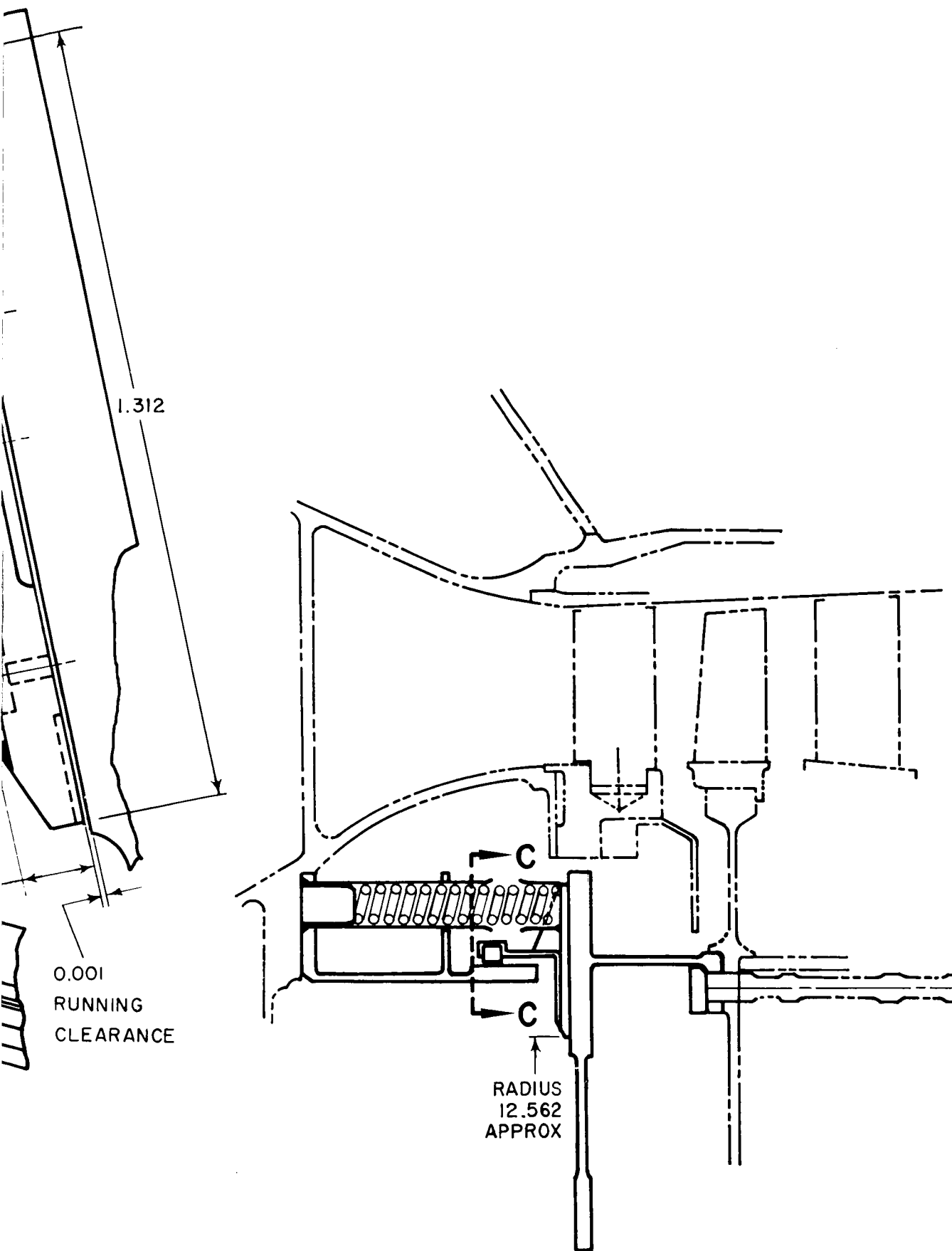


Figure 31 Thin-Strip Plus Piston Ring Seal

$$\begin{aligned}
 J &= \text{effective polar moment of inertia*} \\
 &= 8.8 \times 10^{-4} \text{ inches}^4
 \end{aligned}$$

These sectional properties given for room temperature

$$\beta_e = \frac{EI_c}{R^2} = \frac{30 \times 10^6 \times 31.3 \times 10^{-4}}{(13.75)^2}$$

$$= 498 \text{ inch-pounds per inch-radian}$$

$$\beta_t = \frac{GJ}{R^2} = \frac{12 \times 10^6 \times 8.8 \times 10^{-4}}{(13.75)^2}$$

$$= 56 \text{ inch-pounds per inch-radian}$$

To calculate the angular stiffness of the gas film, it is necessary to study the forces acting on the two pads after the seal cross section is tilted through an angle of ± 0.001 radians. The resulting forces are shown in Figures 32 and 33.

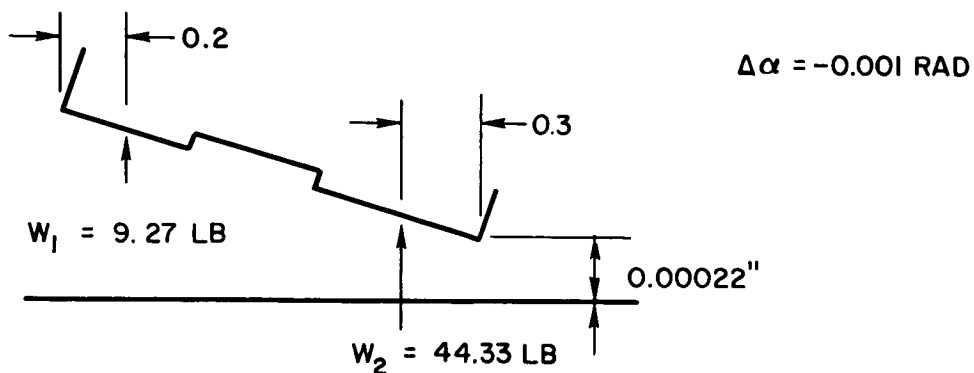


Figure 32 Forces Acting on the Seal in a Tilting Position, $\Delta\alpha = -0.001 \text{ rad}$.

*See Appendix F for discussion of J for slender sections

$$\Delta\alpha = + 0.001 \text{ RAD}$$

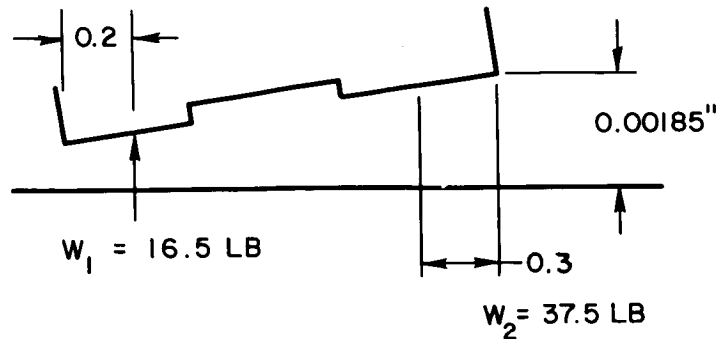


Figure 33 Forces Acting on the Seal in a Tilting Position, $\Delta\alpha = +0.001$ rad.

These data are obtained by using the spiral groove computer program for the right pad at a tilted position and by using the design charts in Reference 2 for the left pad. Changes in the location of W_1 and W_2 are not significant. The angular stiffness using the forces in Figures 32 and 33 become

$$\beta_f = \frac{4.33 \times (0.2 + 0.3 + 0.3125)}{0.001} = 3520 \text{ inch-pounds per inch-radian}$$

for $\Delta\alpha = -0.001 \text{ RAD}$

$$\beta_f = \frac{2.5 \times (0.2 + 0.3 + 0.3125)}{0.001} = 2030 \text{ inch-pounds per inch-radian}$$

for $\Delta\alpha = +0.001 \text{ RAD}$

Taking average of these two values, the angular stiffness at the mid position becomes

$$(\beta_f)_{\text{AVG}} = 2775 \text{ inch-pounds per inch-radian}$$

Now, this angular stiffness is evaluated based on the assumptions that

- The gas film is orifice compensated, and
- There are no pressure variations between orifices

There is a strong likelihood that the consideration of dynamic instability (Pneumatic hammer) may require the use of an inherently compensated film

instead of the orifice-compensated film. (An inherently compensated film is one in which the flow is restricted by the edge of the feeding hole instead of the orifice. Figure 34 shows the difference between these two types of restrictions.)

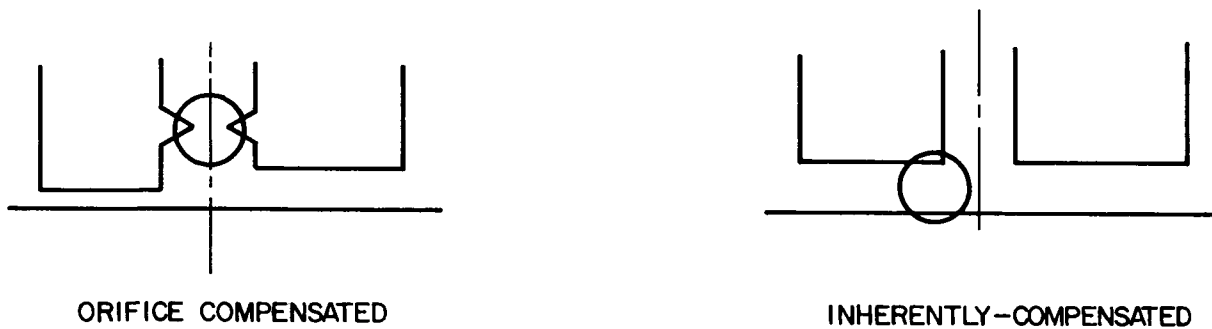


Figure 34 Two Common Restrictions

If the film is inherently-compensated, the stiffness will be reduced by 33 percent. For this reason, the angular stiffness of the film is taken to be 1940 inch-pounds per inch-radian (i. e. $2/3$ of 2910) for calculation of the flexibility requirements.

If we now assume that the initial angular distortion of the primary seal is a saddle-shape ($n = 2$), the design criterion, equation (3), becomes

$$\alpha < \left(1 + \frac{\beta_f}{4\beta_t + \beta_e} \right) \alpha_A$$

Substituting the values of β_e , β_t , and β_f , into the above equation, one obtains

$$\alpha < \left(1 + \frac{1850}{4 \times 56 + 498} \right) \alpha_A$$

$$\alpha < 3.56 \alpha_A$$

The allowable angle of tilt, α_A , is determined by limiting the minimum film thickness to seventy percent of the nominal film thickness. For a nominal thickness equal to 0.001 inch and a seal width equal to 1.3125 inches,

$$\alpha_A = \frac{0.0003 \times 2}{1.3125} = 0.00045 \text{ RADIANS}$$

which means

$$\alpha \leq 3.56 \times 0.00045, \text{ or } \alpha \leq 0.0016 \text{ radians.}$$

Therefore the flatness tolerance for non-parallelism of the saddle-shape must be held to about 0.0016 inches per inch in the radial direction.

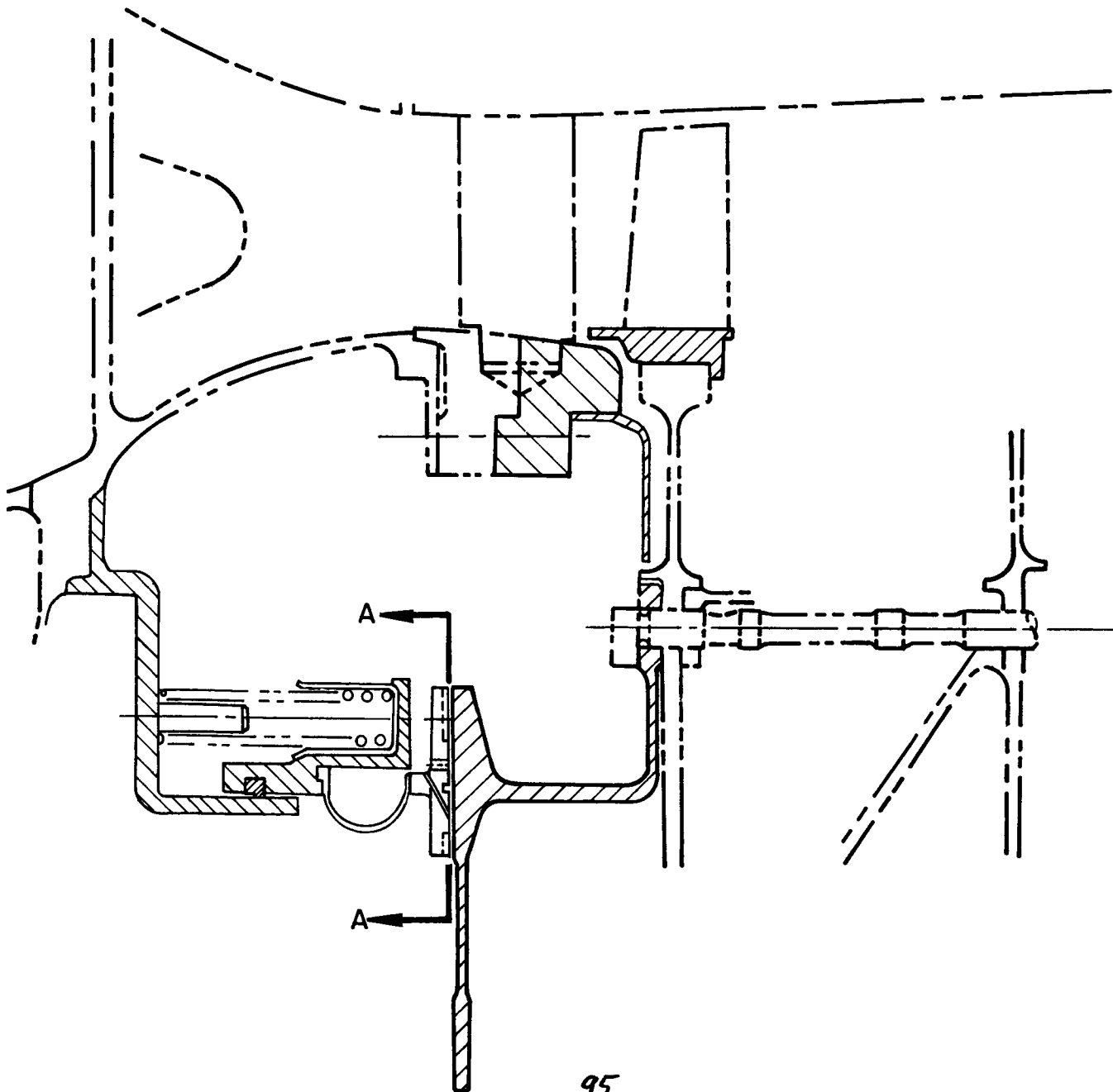
f. OTHER CONSIDERATIONS

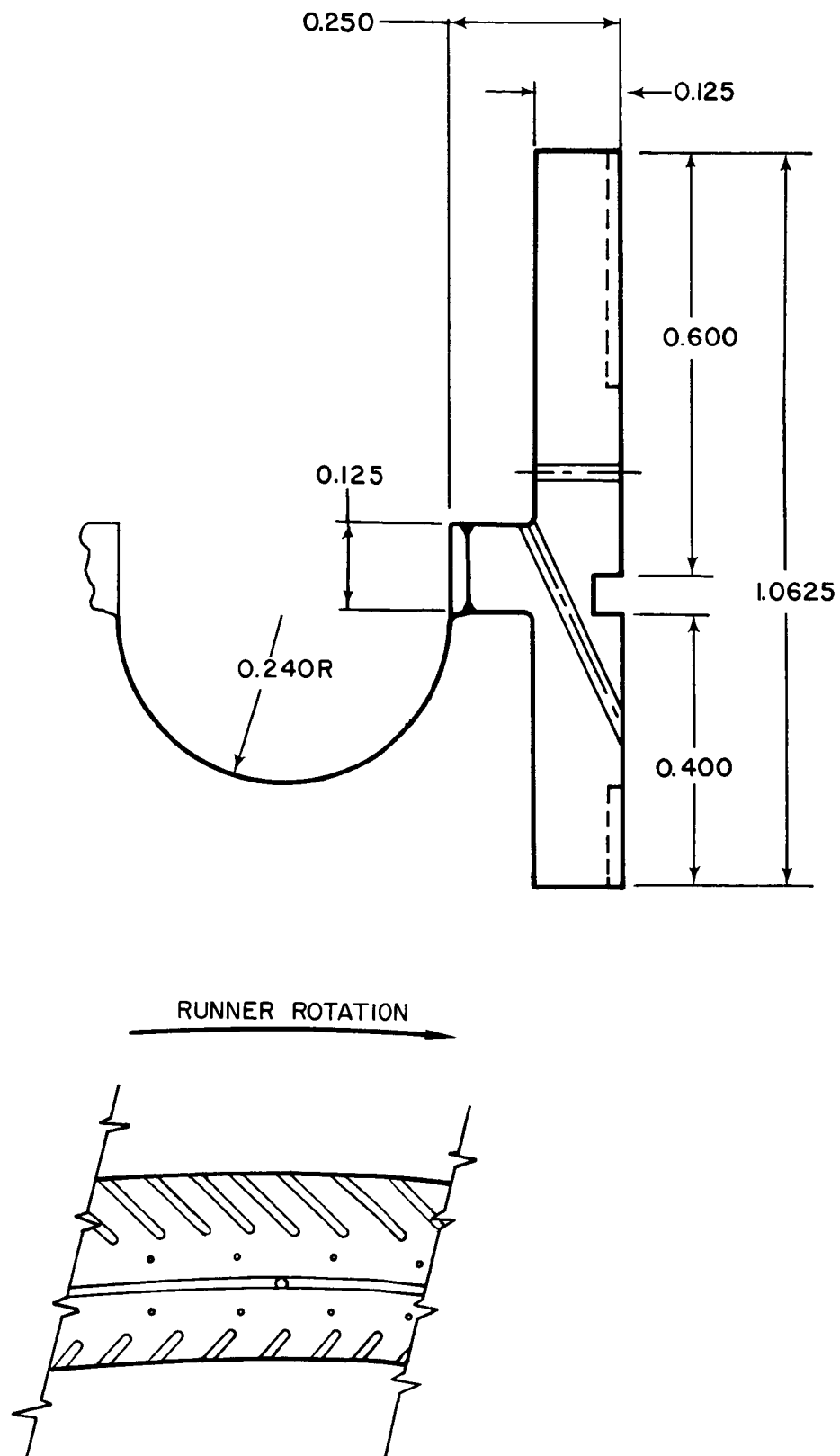
Due to the tendency of the cylindrical spline to collapse under the differential pressure, the bending stress at the joint between the vertical spline and the seal face is estimated to be 120,000 pounds per square inch neglecting the stiffening diagonal. Yield at 1200 degrees Fahrenheit would be expected to reduce this stress.

The welding of the stiffener may present some challenging problems in the fabrication of this ring. The tolerance on the flatness of the seal face when the seal is supported (as in an engine assembly) but not loaded, is as follows:

- At all angular positions, the surface is to be in a single plane within 0.0005 inches per inch, measured in the radial direction.
- At all radii, the surface is to be in a single plane within 0.0008 inches per inch, measured in a circumferential direction.
- At any single radial cross section, the face must be straight within 0.0002 total.

Note the close tolerance required for proper alignment of the seal ring with the rotor face. Whether this tolerance can be achieved for such a large-diameter ring is a serious question that remains to be answered.





SECTION A-A

Figure 35 Layout of Thin Strip Plus C Diaphragm Seal

7. DESIGN OF THE THIN STRIP-C DIAPHRAGM CONCEPT

a. DESCRIPTION

Figure 6 shows the schematic of a thin-strip C diaphragm proposed for detailed feasibility study. This concept is very similar to the thin-strip one-piece concept. The only difference is in the secondary sealing. This design utilizes a C diaphragm as the secondary seal between the thin strip and the seal carrier in place of the piston ring. The cross section of the primary seal is not as deep as the thin-strip one-piece design, and therefore is more flexible. The types of primary sealing surface considered here are identical to the ones for the thin-strip one-piece concept. The double pad, spiral groove seal has been chosen for this design. The data developed in Section I. B. 6. on the load, stiffness and center of pressure are equally applicable here.

b. FORCE AND MOMENT BALANCE

A detailed layout of this concept is shown in Figure 35. The forces acting on the primary seal face are shown in Figure 36.

The moment produced by W_1 , W_2 and W_3 about point A is

$$M_1 = 14 \times .8625 + 40 \times .26 - 54 \times .3375 = 4.3 \text{ inch-pounds per inch}$$

If we let $d = 0.25$, the value of y_C is found to be 0.0765 inches. The moment produced by W_4 and W_5 about point A becomes

$$M_2 = -80R(d - y_C) - 0.250 \times 80 \times \left(\frac{d}{2} - y_C\right) = -13.9R - 0.97$$

For a perfect pressure balance,

$$M_1 + M_2 = 0,$$

and

$$R = \frac{4.3 - 0.97}{13.9} = 0.24''$$

Therefore, a 0.24 inch radius C diaphragm is required for pressure balancing of the primary seal.

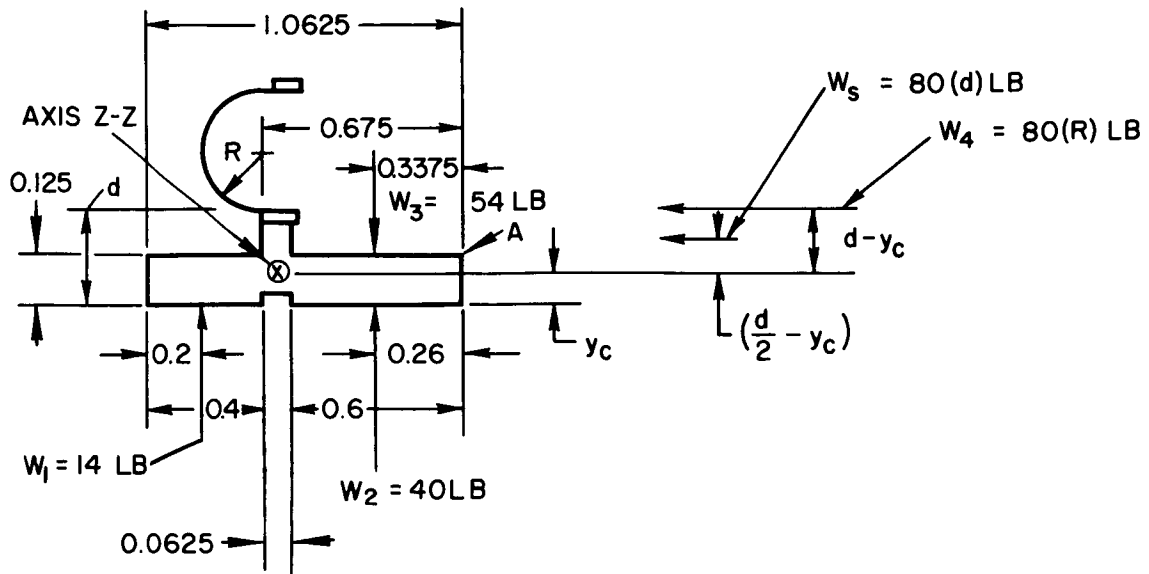


Figure 36 Forces Acting on the Primary Seal

c. FLEXIBILITY REQUIREMENTS

The procedure in this section is similar to the thin-strip one-piece design described in Section I. B. 6. Referring to the geometry of the primary seal shown in Figure 35, the following sectional properties have been calculated.

I_{ZZ} = the area moment of inertia about the centroid

$$= 4.76 \times 10^{-4} \text{ inches}^4$$

J = effective polar moment of inertia

$$= 7.5 \times 10^{-4} \text{ inches}^4$$

These values give

$$\beta_e = 76 \text{ inch-pounds per inch-radian}$$

$$\beta_t = 47.5 \text{ inch-pounds per inch-radian}$$

The angular stiffness of the gas film can be determined in the same way as the thin-strip one-piece design and is found to be

$$\beta_f = 1900 \text{ inch-pounds per inch-radian} \quad \text{for } \Delta \alpha = - 0.001 \text{ radian}$$

$$\beta_f = 870 \text{ inch pounds per inch-radian} \quad \text{for } \Delta \alpha = + 0.001 \text{ radian}$$

Taking the average of these two values and making allowance for the possible application of inherently compensated film, (Section I. B. 6. e) the final angular stiffness becomes 920 inch-pounds per inch-radian.

Substituting the values of β_e , β_i , and β_f into equation (3) for a saddle-shape initial distortion, one finds

$$\alpha < \left(1 + \frac{920}{4 \times 47.5 + 76} \right) \alpha_A$$

$$\alpha < 4.5 \alpha_A$$

The allowable angle of tilt, α_A , is determined by limiting the minimum thickness to 70 percent of the nominal film thickness. For a nominal thickness equal to 0.001 inches and the seal width equal to 1.0625 inches,

$$\alpha_A = \frac{0.0003 \times 2}{1.0625} = 0.00056 \text{ radians.}$$

This gives

$$\alpha < 4.5 \times 0.00056$$

$$\alpha < 0.0025 \text{ radians}$$

The flatness tolerance for non-parallelism of the saddle-shape must be held to about 0.0025 inches per inch in the radial direction which is slightly better than the thin-strip one-piece concept, but still is a difficult task to achieve for such a large diameter ring.

d. OTHER CONSIDERATIONS

The flexibility of the C diaphragm was examined by determining its axial stiffness, assuming that the C section behaves locally like a curved panel. Using

this assumption, the expression for the stiffness of a complete ring is

$$K = \frac{1}{0.149} \left[\frac{EI}{R^3} \right]$$

for derivation of k see reference 3, p. 82, equation 86.

For the C diaphragm, the stiffness would be half of that calculated by the above expression, since the C diaphragm is a half ring section. Using this expression, the axial stiffness for a 0.005 inch thick diaphragm with a radius of 0.25 inch is found to be 67.5 pounds per inch per inch of circumference. It appears that the flexibility of the primary seal is not seriously affected by the C diaphragm.

The bending stress in the C diaphragm for a given axial deflection will be identical to that of a complete ring section.

According to Reference 3, the bending stress can be expressed as

$$\sigma_B = 0.318 \frac{E \delta \dagger}{2R^2}$$

where δ is the axial deflection and \dagger is the thickness of the diaphragm. The direct stress is simply

$$\sigma_{\dagger} = p_2 \frac{R}{\dagger}$$

where p_2 is the sealing pressure.

Using these formulae, the bending and direct stresses were found to be 3800 pounds per square inch and 7500 pounds per square inch respectively for $\dagger = 0.005$ inches and $\delta = 0.01$ inches. These values are certainly not serious.

The C diaphragm can either be welded to the primary seal or seated in a circumferential groove of the seal ring. In either case, the deformation of the seal ring will be partially restrained by the C diaphragm. Consequently, the value of β_e and β_{\dagger} will be slightly affected. The exact influence of the C diaphragm on β_e and β_{\dagger} will require a full analysis of the deformation of half of a toroidal shell under asymmetrical loads. Since the calculation by neglecting the C diaphragm already indicates difficulties in meeting the flexibility requirement, the detailed shell analysis of the C diaphragm has not been considered.

8. OPERATION UNDER ENGINE CONDITIONS

The compressor end seal and interstage seals (on which the feasibility analyses described in the previous sections have been made) are designed specifically for test rig conditions. These conditions are lower than anticipated engine absolute pressures. The greater air density at real engine pressure may require revision and rebalancing of these seals.

In addition to the density factor, several other factors require evaluation prior to designing seals for use in engines. These are:

- Rebalancing, due to the lower pressure ratio
- Lift-off speed, including hydrodynamic effects
- Off-design operation, particularly at idle speed
- Thermal transient effects during a full engine cycle
- Inertia effects due to the greater air density
- Effects of compressor surge and windmilling on seal action (experimental evaluation required)
- Back-up designs

The first three factors involve further application of information or design methods already generated. The fourth and fifth and sixth factors require additional analytical effort.

a. REBALANCING

The conditions set in the test rig are representative of a typical supersonic engine pressure ratio and flight regime. Any change in engine design or aircraft flight profile would require a review of the seal design to determine whether the change in seal pressure ratio is large enough to require unbalancing the seal.

The center of pressure of a seal is a function of the pressure ratio, as shown in Figure 37, so the seal must be reproportioned so that it will be in equilibrium under cruise conditions.

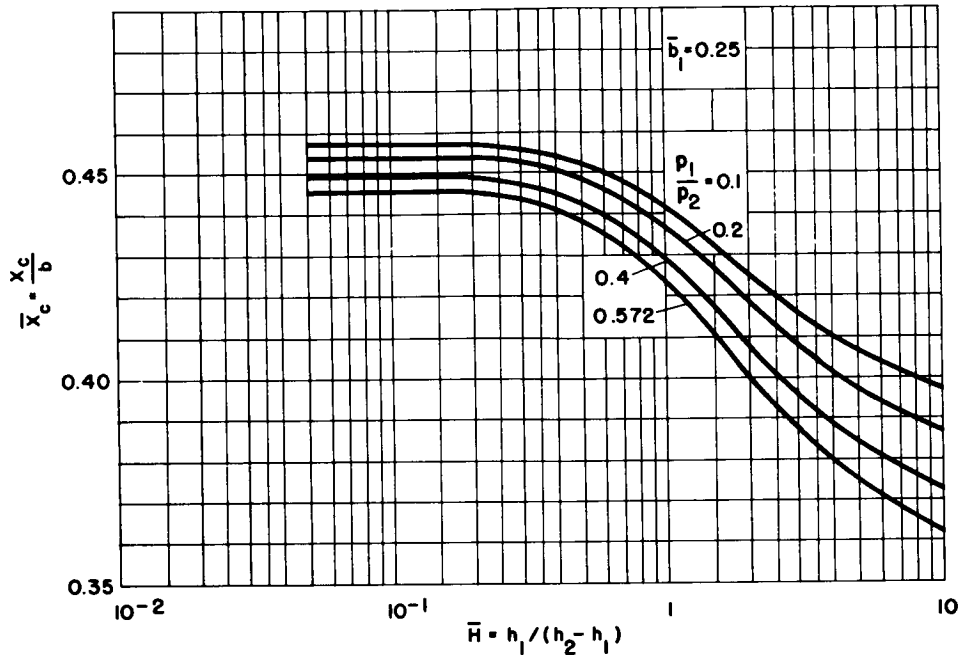


Figure 37 Center of Pressure - Hydrostatic Step, $\bar{b}_1 = .25$

b. LIFT-OFF SPEED

Assuming that the engine pressures are known as a function of engine speed, the speed at which the seal will lift free of the runner (against the locating spring pressure) can be calculated. However, as additional protection against rub, and to hasten lift-off, the floated shoe designs feature a Rayleigh configuration on the primary seal surface, and thin strip designs would be provided with a spiral groove pattern. These patterns provide lift due to hydrodynamic behavior independent of pressure ratio, and as a result can be expected to lower the lift-off speed significantly. Additional computer runs with the Rayleigh step program can furnish the additional information needed.

Experimental verification of lift-off behavior, perhaps using a simplified test rig, is regarded as an important additional task. Such tests should simulate the surface speed, surface configuration, and loading to be expected in starting. Verification of surface rub characteristics as well as hydrodynamic lift-off should be an objective of such tests.

Since it may also be desirable to design seals which are retracted at low speeds in order to minimize rubbing, this experimental phase should if possible include touch-down in nonparallel fashion at a surface speed on the order of idle speed. In this way the resistance to momentary contact on closing the seal can be investigated.

c. OFF-DESIGN OPERATION

In addition to the factor of lift-off and its complementary condition, touch-down, it will be important to check for operation at idle speed. For specific pressure levels, pressure ratios and idle speeds, the seal balance and primary seal film thickness can be calculated.

d. THERMAL TRANSIENT EFFECTS

The thermal analyses described in this report have been for the seal in steady-state operation. This condition will be carefully approached in the test phase of this program. However, in actual engine operation large temperature excursions will occur, from at or below room temperature to 1200 degrees Fahrenheit or more. Shifts in operational mode from idle to take-off to cruise, etc., will cause additional transient effects. It therefore becomes desirable to study the nature and magnitude of the transient temperature distributions in order to ascertain whether conditions may occur which will result in excessive distortion. Such distortion may result in a primary seal rub, or in binding in the secondary seals, unless carefully checked. If such conditions do occur, the seal design will have to be modified to alleviate any aggravated distortions.

It may be possible to explore for transient effects in the experimental phase of this program, at least to a limited extent. When specific engine transient conditions are defined (in particular the rate of change of speed, pressures, and air temperatures) an analytical approach would also be highly desirable.

e. INERTIA EFFECTS

Under the test rig conditions, inertia effects are not expected to be important. The pressure depression (Bernoulli effect) on expansion through the seal at one mil film thickness is minor. The Reynolds number for circumferential shear flow is below the transition range, but close to it.

Operation under engine conditions will raise the effective gas density significantly. This will be to such an extent that both the Bernoulli effect and turbulence should be included in the analysis.

The Bernoulli effect will result in a shift in the center of pressure on the primary seal surface, and hence should be a factor in the seal moment balance.

The turbulence, while in the circumferential direction, will influence the cross-seal flow to some extent, and will also affect the rate of heat generation and hence the temperature distribution.

f. BACK-UP DESIGNS

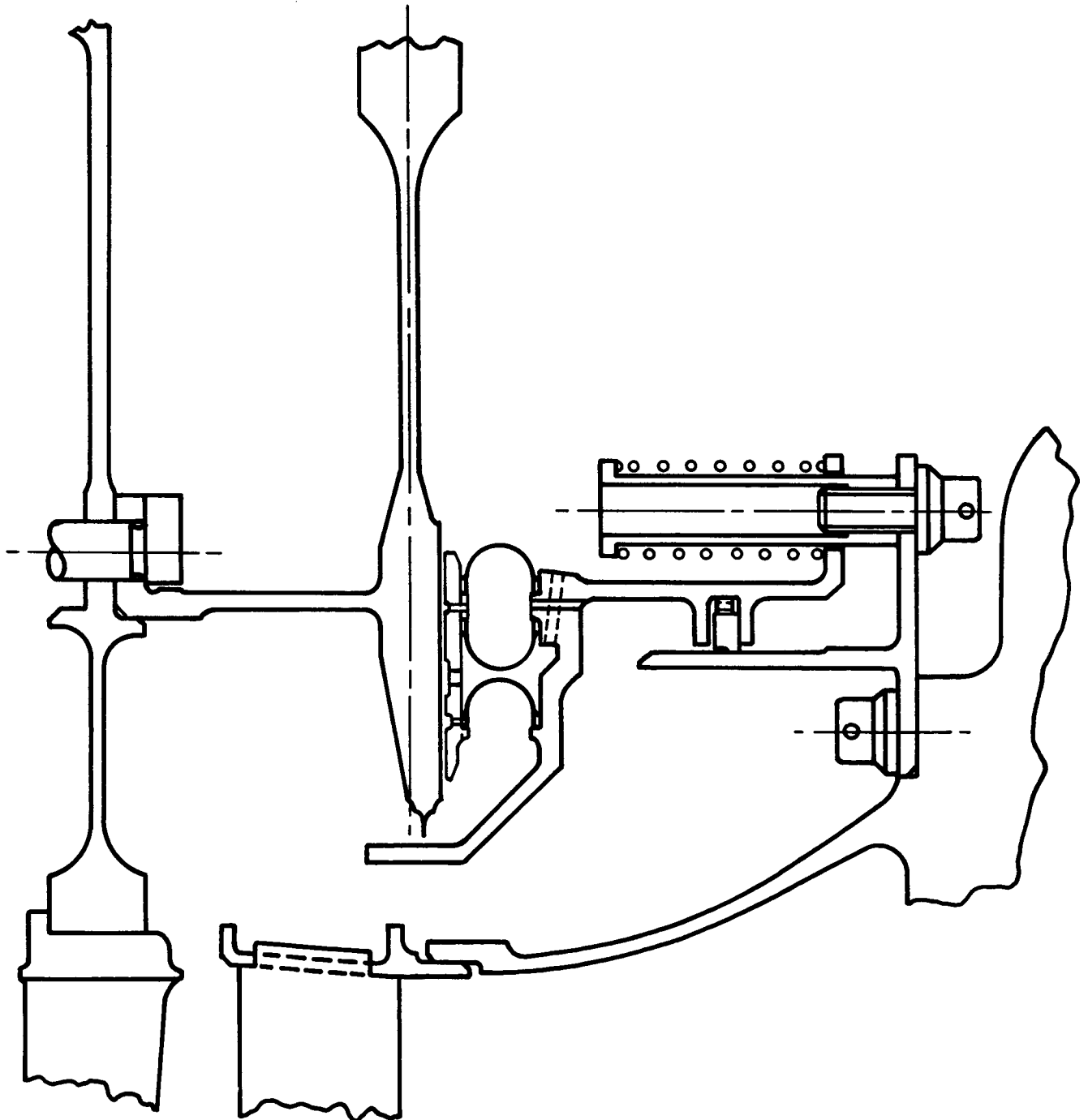
The two floated shoe designs which are regarded as feasible are very similar in principle, although one is a radial seal and one is a face seal. While these designs represent a good technical solution, there are two factors which would make an alternate design worthwhile as a backup. These are (1) the multiple shoes and close tolerances required which may mean high manufacturing cost, and (2) the requirement for maintaining both the runner and the shoe holder in good alignment. In the course of the work on the alternate thin strip designs, three new concepts were generated which appear worthy of detailed analysis. These are:

- A thin-strip flexible-seal design supported on an OC diaphragm.
- A flexible shoe design in which the shoes are mounted flexibly on a hoop which in turn is flexible on a radial axis.
- A one-piece, semi-rigid seal.

1) THIN STRIP OC DIAPHRAGM

This concept employs a thin, flexible one-piece strip as the primary seal element.

The thin strip is supported by three C diaphragms mounted on a floating secondary seal carrier. The secondary carrier permits full axial float with a piston ring seal on the main engine structure. One of the C diaphragms forms a seal between the high pressure and the low pressure areas. This is the bottom one in Figure 38. The other two C diaphragms at the top in the drawing face each other and form a chamber to which the high pressure air is admitted. This design, therefore, permits direct balancing of the moments on the primary seal without the erection of a spine. It also permits a decrease in thickness of the strip with respect to other thin strip designs. Thus, it offers the opportunity of generating a section with increased flexibility and, therefore, better tracking capability. Furthermore, the moment balance is achieved with methods which are more nearly independent of angular displacements of the strip, making low residual moment imbalance easier to achieve. Figure 38 illustrates the proposed construction.



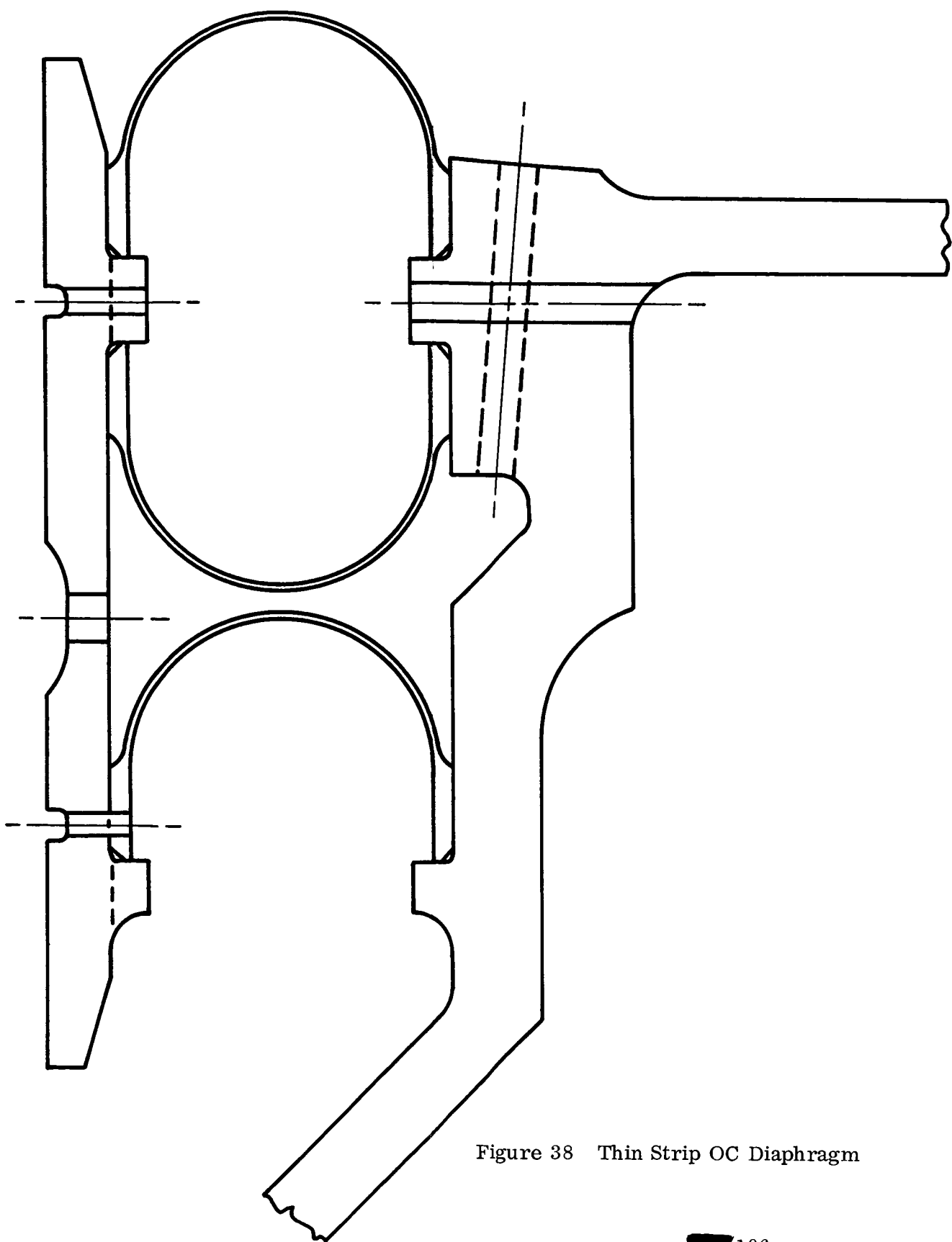


Figure 38 Thin Strip OC Diaphragm

2) HOOP-MOUNTED FLEXURE SHOE

In this concept, the primary seal is in the form of a number of individual shoes, each subtending an arc of about fifteen degrees, which are mounted so that they are relatively free to follow variations in runner contour. Some form of sealing between shoes is required. Each shoe is flexibly mounted to a continuous hoop which provides support in the radial direction but permits angular motion through the mounting. The hoop is stiff in the radial direction, but made thin to provide accommodation to runner motion about a radial axis. Thus, each shoe is free to tilt about both the radial and the circumferential axis. A secondary seal structure is necessary to provide freedom of motion with sealing between the upper part of each shoe and the carrier. The spine on each shoe provides a moment balance. Details of this design are shown in Figure 39.

3) ONE-PIECE SEMI-RIGID SEAL

This concept recognizes the possibility that a semi-rigid one-piece seal may be able to run separated from the runner by a gas film, provided the gas film stiffness is great enough. The possibility of this design rests primarily on the ability to make the one-piece seal to a high degree of flatness, and the ability to generate the flatness of the runner surface that has been specified by Pratt & Whitney Aircraft. Preliminary calculations, assuming a rigid seal member and a twice per revolution waviness of 0.001 inch total indicator reading on the runner face, indicate that a minimum film thickness of 0.5 mils can be maintained for a nominal design film of 1.0 mils; and that the flow will remain within the desired maximum of 10 percent of labyrinth flow. Thus, it would appear that the one-piece seal member would have to be flat within a few tenths of a thousandth of an inch. However, in view of its greater rigidity, it is possible that it can be manufactured to this tight a tolerance. The tracking dynamics of this type of seal should be analyzed, before statements can be made regarding the minimum film thickness to be expected with any of the primary types of gas film for which information is now available. The seal layout is shown in Figure 40.

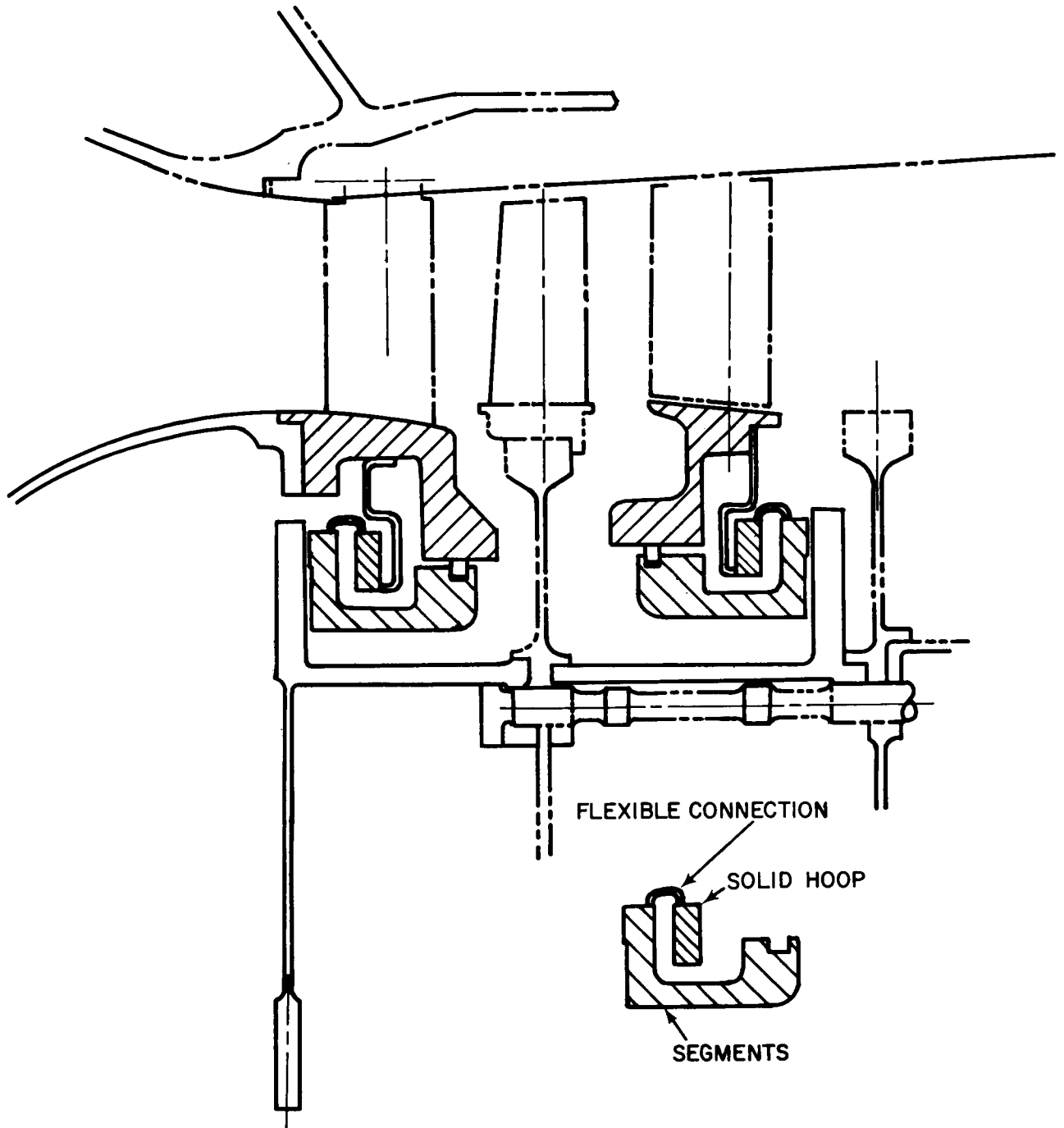


Figure 39 Hoop-Mounted Flexure Shoe

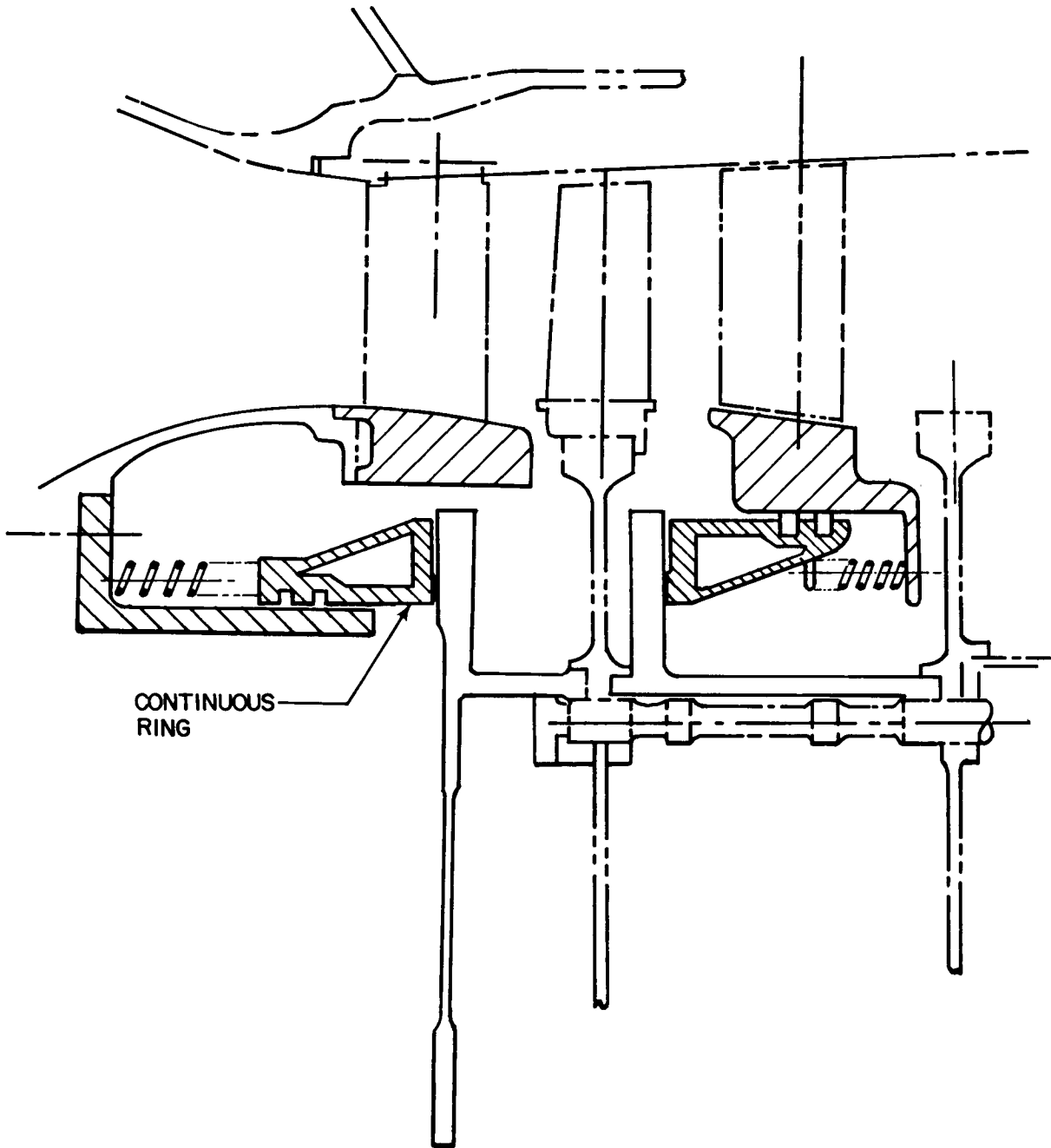


Figure 40 One-Piece Semi-Rigid Seal

II. TASK II - COMPRESSOR END SEAL AND STATOR INTERSTAGE SEAL EXPERIMENTAL EVALUATION

This phase of the program provides for final design and procurement of compressor end seals and stator interstage seals, design and fabrication of a test rig, and experimental evaluation of the compressor seals.

The final design of the four compressor seal concepts selected for experimental evaluation includes all calculations, material determinations, analyses, and drawings necessary for seal optimization, procurement and experimental evaluation.

A test rig will be designed and fabricated to evaluate the selected compressor end seals and stator interstage seals under simulated compressor operating conditions. The test apparatus will simulate the last stages of a full scale compressor including supporting members and bearing system in order to faithfully duplicate structural flexibility and thermal gradients.

The compressor end seals and stator interstage seals will be calibrated in incremental steps at room temperature static conditions, room temperature dynamic conditions, and subsequently over the full speed, pressure, and temperature operating range. Finally, the seals will be subjected to endurance testing.

A. SUMMARY OF TASK II EXPERIMENTAL EVALUATION

Approval was received from NASA to commence final design of the one side floated shoe compressor seal under Task II. Pratt & Whitney Aircraft is using a computer program to evaluate primary seal performance for off-design conditions. A review of coil and wave spring designs for the one side floated shoe seal is being conducted. The thermal characteristics of this seal are being studied, with particular emphasis on thermal shunt requirements.

Design work was continued on a test rig in which Task I compressor seals will undergo experimental evaluation. NASA granted approval to proceed with procurement of long lead time critical raw materials for the test rig.

B. TEST SEAL DESIGNS

In a letter dated May 31, 1966, NASA granted approval to commence final design of the one side floated shoe compressor end seal and stator interstage seals under Task II.

The Rayleigh step computer program and sample input format have been received from M. T. I. The deck is presently being adapted to the Pratt & Whitney Aircraft computer facilities. The contractor will use the program to evaluate primary seal force, center of pressure, and leakage at off-design conditions. It is important that seal performance, particularly seal film thickness, be evaluated over a wide range of operating conditions.

The proposed MTI seal design appears to be unnecessarily heavy and will result in high breakaway and cranking torques. The heavy carrier (30 pounds) is required to reduce the natural frequency of the two mass, three spring system below the operating speed range of the rotor. In a two spool machine, this frequency may have to be reduced below low rotor idle to avoid excitation. The high cranking torque (over 500 in lbs) is required because it is assumed that the spring loads must overcome carrier and piston ring friction with the full pressure differential imposed.

A study of the stress and deflection, (including change in slope) of the carrier indicates that its weight can be reduced by 18-20 pounds from that envisioned by MTI. The heavier weight was used to control the natural frequency of the two-degree-of-freedom system involved. Before the carrier weight can be reduced, the spring system will have to be redesigned. Review of the spring arrangement is in process including the relative advantages of having the natural frequency above or below the operating range. The loading and spring rate of the carrier coil springs is also being reviewed for possible reduction in break-away and engine cranking torque.

Pratt & Whitney Aircraft is considering the light approach in the final design. The seal carrier is being analyzed with the aid of an existing thin shell computer program. Trials to date indicate that the elastic slope control required in the area of the seal shoe can probably be obtained with a reasonably stressed light weight carrier. Preliminary work on a stiff wave spring indicates that adequate deflection can be obtained with reasonable stresses. Efforts will continue toward a solution. The balance of the shoe seal design will be reviewed if changes are required to accept the new spring.

A final study of the thermal characteristics of the one side floated shoe includes thermal shunt requirements. The method of shunting presently being considered is a "sandwich" arrangement with silver 0.030" thick trapped centrally in the primary seal segment. It is felt that some device for decreasing thermal coning is necessary to keep the film thickness variation at a safe level.

C. TEST RIG DESIGN

Design work was continued on a full scale test rig. Improvements were made in a layout drawing showing the hub and disk arrangement, the rig housing, and provisions for a 0.4" axial movement of the housing with respect to the rotor.

The bearings and bearing support system are also shown in the layout. Thermal mapping of the rig was completed for conditions encountered when testing one side floated shoe seals. Schemes have been completed for thrust balancing the rotor, and compartmenting and pressurizing the seals. To maintain a test rig air flow rate within the capacity of the test facility air compressors, modifications were made to labyrinth seal arrangements in the rig. Smaller diameter rig labyrinth seals decrease the air-flow rate considerably, but also increase the thrust imbalance in the rig rotor. The rig design configuration now utilizes a thrust balance piston and larger bearings which are adequate for this application. The most recent design effort has been concentrated on various improvements in the bearing compartments. An investigation is being made of bearing oiling schemes to insure adequate lubrication and scavenging, particularly as related to the two sets of large thrust bearings. Thermal effects and stressing of structural members are being considered in the design of bearing supports and seal arrangements. A concerted effort is being made to incorporate actual engine hardware wherever possible.

Thermal maps, thrust balance diagrams, and the most up-to-date design layout of the test rig were presented at a NASA-P&WA meeting held on May 19, 1966. This layout, while preliminary in many areas, was carried to completion where required to validate a request for approval of advance procurement of critical raw materials. Having received the NASA Contracting Officer's approval in a letter dated June 13, 1966, Pratt & Whitney Aircraft is proceeding with the procurement of critical forgings.

III. TASK III - COMPRESSOR STATOR PIVOT BUSHING AND SEAL CONCEPT FEASIBILITY ANALYSIS

A feasibility analysis program was conducted on stator vane pivot bushing and seal concepts for application in compressors for advanced air breathing propulsion systems. The first phase of this program consisted of a preliminary analysis and a screening of various seal concepts prior to the selection of concepts for the detailed feasibility analysis. The analytical effort included a comparison of the selected concepts to current practice, and all calculations, analysis, and drawings necessary to establish feasibility of these selected concepts. This analytical program was subcontracted to Mechanical Technology Inc. of Latham, New York and was monitored by Pratt & Whitney Aircraft as required under the terms of the NASA contract.

A. SUMMARY OF TASK III FEASIBILITY ANALYSIS

MTI completed the feasibility analysis being conducted on the vane pivot bellows-loaded face seal and spherical seat face seal concepts. Both versions of the seal were considered feasible and adequate for recommendation to NASA. Pratt & Whitney Aircraft submitted the latest designs of these two seals to NASA on 19 May 1966 requesting approval to start final design under Task IV. An effort was made to simplify the seal designs within practical limits without making major changes in the basic seal concepts shown on the MTI drawings. Approval was granted in a letter from NASA dated May 31, 1966. The program objectives under Task III are considered to have been attained, thus completing the work effort. Final design of the seals is currently being accomplished under Task IV.

B. MTI FEASIBILITY ANALYSIS - TASK III

The feasibility analysis of vane pivot seal concepts conducted by MTI is presented in this section of the report. The material in this section was prepared by Dr. D. F. Wilcock, Dr. H. S. Cheng, and J. Bjerklie.

1. CONCLUSIONS AND RECOMMENDATIONS

Table XX summarizes the characteristics of the vane pivot seals that are either under consideration or in use.

TABLE XX

VANE PIVOT SEAL CHARACTERISTICS

	<u>Bellows Loaded Face Seal</u>	<u>Spherical Seat Face Seal</u>	<u>Present Seal</u>
Leakage (specified test rig condition = 135 psi)	0.00079 SCFM	0.0004 SCFM	0.0077 SCFM
Wear rate	Low on flame plate	Extremely low	Very low
Required torque (less bending moment effect)	1.53 in. lbs.	0.54 in. lbs.	3.8 in. lbs.
Accountable size	0.55" diameter	0.65" diameter	0.5"
Accountable weight	0.025 lbs/pivot seal	0.025 lbs/pivot seal	0.025 lbs/pivot seal
Unproven materials	Electrofilm at 1200 F	Carbon at 1200 F	Not suitable at 1200°F
Effect of dirt	Increase in Leakage	None	Increase in leakage and wear
Effect of cocking	Absorbed by bellows	Must reseal	Increased leakage
Separate parts for assembly	Seven	Seven	Five
Ability to install as a cartridge	Possible for bellows assembly	Separate parts	Separate parts
Replacement of seals and seats	Separate	In matched pairs	Separate
Potential problems	Electrofilm integrity Effect of dirt on wear & leakage. Bellows integrity	Ability to remain properly seated when cocked. Other problem same as for bellows loaded seal.	

Table XX illustrates that both new seal designs have the potential to be eminently satisfactory. Also, the potential problem areas are nearly the same. In reality, it remains a matter of judgment and test as to which seal will eventually prove to be better.

Since the seals appear to be so evenly matched, it is recommended that both seals be built and tested. It is also recommended that consideration be given to conducting immediate tests on carbon in a test rig that will provide appropriate temperatures, airflows, loading, and movement to determine the true ability of carbon to serve in these seals as designed. It is recommended that a ceramic back-up material be selected for use instead of carbon in case these tests are negative.

2. BELLOWS-LOADED FACE SEAL

a. INTRODUCTION

The bellows-loaded face seal, as adapted to the vane pivot, offers a relatively simple solution to the problem of preventing leakage of compressed air out of the compressor through the compressor wall. The basic method is adaptable anywhere along the compressor so that it can be used over the whole compressor, or merely at the high pressure stages, as desired.

Since finishing the screening work, considerable preliminary design work has been carried out. The design was submitted to several vendors for their comments. The final design is discussed below.

b. DESCRIPTION

The final design layout of the bellows-loaded face seal is shown in Figure 41. It has a flat face seal held in contact with its seat at all times by the spring action of a slightly loaded bellows. The seat against which the seal face rides is mounted as a separate piece to keep it free from distortion. The seal is formed between a seat fastened to the shaft and a face seal (nose) held to the housing by a bellows. The high pressure thereby is on the outside of the bellows. The thrust caused by the internal pressure of the compressor is taken up on a thrust collar located at the compressor wall. The accomplishment of the final design and final material selection seemed to be the only deterrents to its immediate selection.

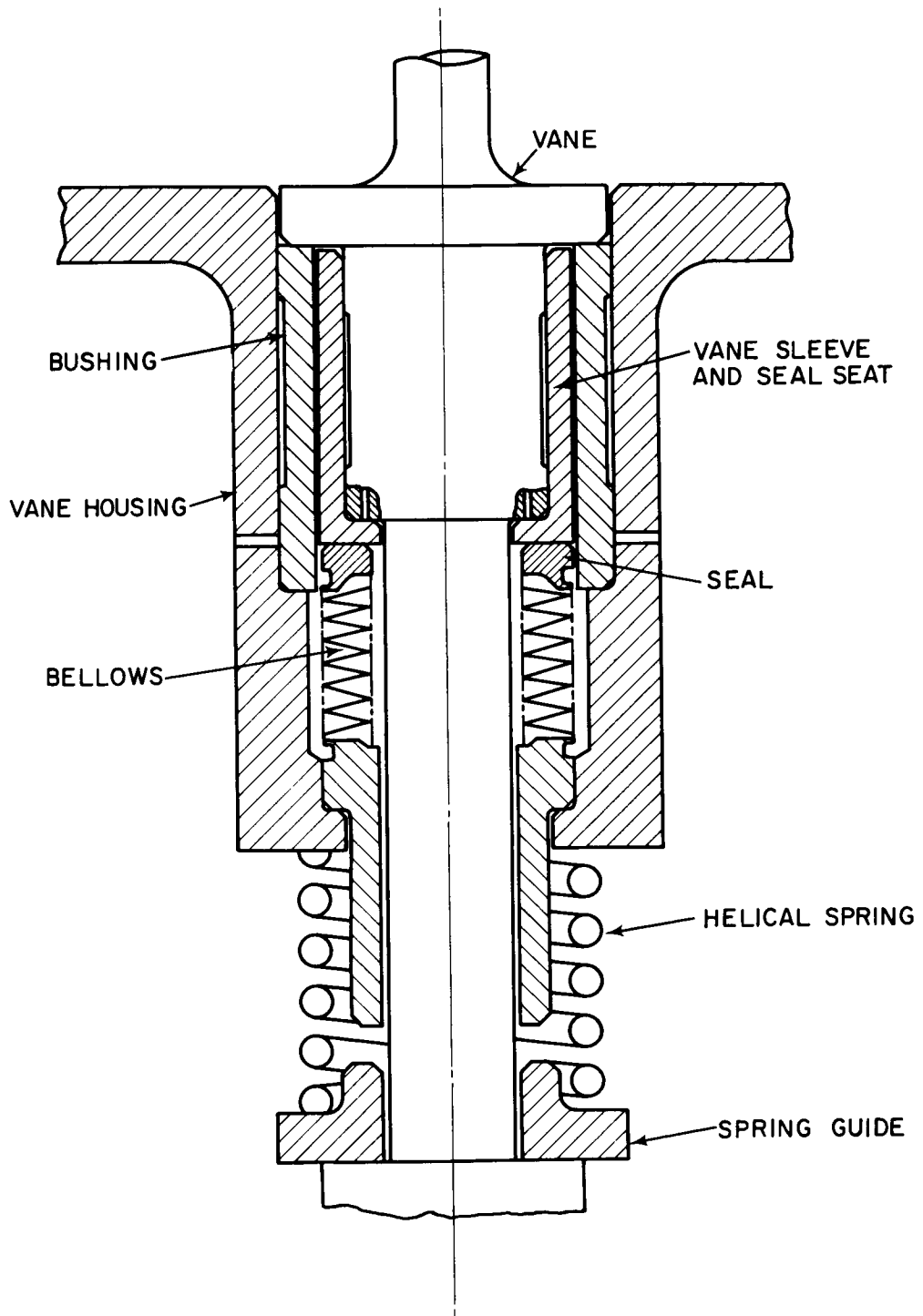


Figure 41 Single Bellows Vane Pivot Seal

c. LEAKAGE CALCULATIONS

The leakage for this seal can be estimated using conventional equations for purely viscous flow.

Referring to the first Semiannual Report (PWA-2752), page 7, equation 6, the leakage rate through a slit is

$$m = \frac{h^3}{24 \mu b} \rho_2 p_2 \left[1 - \left(\frac{p_1}{p_2} \right)^2 \right]$$

where

m = mass flow rate per unit width, lb sec/in²

ρ_2 = mass density of the upstream gas, lb sec²/in⁴

p_2 = pressure of the upstream gas, lb/in²

p_1 = pressure of the downstream gas, lb/in²

h = gap film thickness, inches

μ = viscosity of the upstream gas, lb sec/in²

b = leakage path length, inches

The leakage path thickness in the case of two closely fitting surfaces is taken here to be twice the rms finish (B) of the surfaces. Then

$$m = \frac{8 B^3 \rho_2 p_2}{24 \mu b} \left[1 - \left(\frac{p_1}{p_2} \right)^2 \right] = \frac{8 B^3 \rho_2}{24 \mu b} \left(\frac{p_2 + p_1}{p_2} \right) \Delta p$$

where $\Delta p = p_2 - p_1$

The leakage rate for the vane pivot seal can be calculated using the mean circumference of the seal,

$$R' = \frac{R_0 + R_i}{2}$$

where

R_0 = outer radius of seal, inches

R_i = inner radius of seal, inches

Then,

$$\dot{w} = g \times 2\pi R' m \text{ pounds per second}$$

$$= \frac{2\pi g B^3 \rho_2}{3 \mu b} R' \left(\frac{p_2 + p_1}{p_2} \right) \Delta p = \frac{2\pi}{3} g \frac{B^3 R'}{\mu b} \left(\frac{p_2 + p_1}{p_2} \right) \Delta p \frac{p_2}{R T_2}$$

where

g = acceleration due to gravity, inches per second²

R = gas constant, square inches per degree Rankine-second²

T_2 = seal inlet gas temperature, degree Rankine

Then to find the volumetric flow at standard conditions,

$$V = \frac{w \times 60}{\rho}$$

where ρ = where density of air at standard conditions

$$\rho \approx 0.00237 \frac{\text{lb}_f \text{ sec}^2}{\text{ft}^4}$$

Using the following input for contract-specified test rig conditions,

$$B = (3 \text{ helium light bands}) = 3 \times 11.6 \times 10^{-6} \text{ inches}$$

$$\Delta P = 135 \text{ pounds per square inch}$$

$$R' = \frac{0.75}{4} \text{ inches}$$

$$b = \frac{0.25}{4} \text{ inches}$$

$$\mu = .039 \text{ cp} = 5.65 \times 10^{-9} \text{ pound-seconds per square inch}$$

$$g = 386 \text{ inches per second}^2$$

$$P_2 = 150 \text{ pounds per square inch, absolute}$$

$$P_1 = 15 \text{ pounds per square inch, absolute}$$

$$T_2 = 1200^\circ\text{F} = 1660 \text{ degrees Rankine}$$

$$R = 246500 \text{ square inches per degree Rankine-second}^2$$

Flow rate is:

$$W = 9.86 \times 10^{-7} \text{ pounds per second}$$

$$V = 0.00079 \text{ standard cubic feet per minute}$$

d. ACTUATION TORQUE

The torque required to move the actuator can only be estimated, since accurate friction coefficients are not known. However, if the friction coefficient of tungsten carbide against aluminum oxide is assumed to be 0.3, the following torque is obtained:

$$T = 0.3 R_{M \text{ SEAL}} (F_{\text{THRUST}} + F_{\text{SEAL}}) + \text{bending moment effect, inch-pounds}$$

where

$R_{M \text{ SEAL}}$ is the mean radius of the thrust collar and seal

$$T = 1.53 \text{ in.-lbs.} + \text{bending moment effect}$$

under test rig cruise conditions. This is based on current design dimensions $\Delta P = 135$ pounds per square inch, and seal pressure = 12 pounds per square inch due to the bellows.

e. LIFE

The seal materials are tungsten carbide running against aluminum oxide, for which test data has been obtained at Union Carbide as follows for 500 pounds per square inch:

- rotated part, 43×10^{-6} inches/1000 feet of rubbed distance
- stationary part, 12×10^{-6} inches/1000 feet of rubbed distance

Therefore, anticipated wear is

$$55 \times 10^{-6} \frac{2(20)}{1000} \text{ CPM} \times 360 \times 2\pi \times R' \times t = 0.00072 \text{ inches}$$

where t = operating time, in minutes (for 2000 hours)

The best material reported by Union Carbide would allow wear to be 400×10^{-6} inches. Either of these figures is much less than the flame sprayed coating thickness, but considerably more than the unevenness left on the finished surfaces without flame sprayed coatings. Hence, it becomes a matter of judgment as to which surface combination to use. The wear rates were calculated for 2000 hrs. of ± 20 degree cycling at 10 cycles per minute and for the 500 pounds per square inch test load condition. This is undoubtedly a higher number of cycles than will actually be encountered, the pressure is nearly 2 times as high as will be used, and the real cyclic rate will probably be closer to an average of 1/2 cycle per minute for the full period. Then either material combination would be sufficient. MTI has gathered data on tungsten carbide against aluminum oxide and found the combination to be good for long wear. This familiarity lends confidence in choosing this combination for this application.

f. COMPARISON OF BELLOWS-LOADED FACE SEAL WITH CURRENT VANE PIVOT SEALING PRACTICE

1) SIZE AND WEIGHT

Each seal assembly extends radially outward about 2 inches from the outside of the compressor wall. The distance from the outer surface of the seal to the inside wall of the housing is about 0.55 inches. The weight of the seal, exclusive of vane pivot shaft, actuator arm and bolt, and housing is 0.025 pounds, about the same as the weight of the present seal shown in Figure 42. It should be noted that this seal, while being used for comparison, was not designed for or used under the conditions specified for the current work.

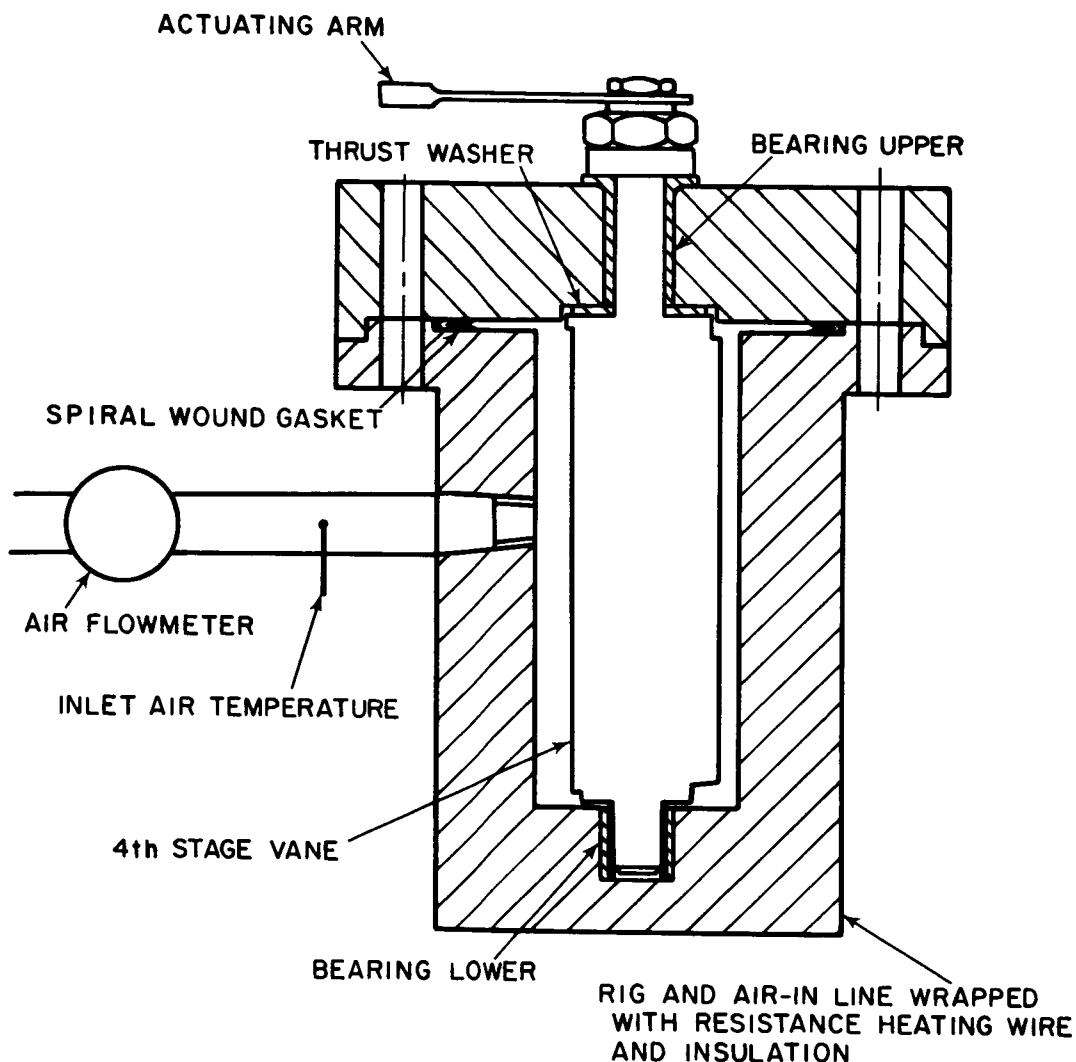


Figure 42 Schematic of Earlier Vane Pivot Seal Test Rig

2) DESIGN SIMPLICITY

The complete unit is assembled in seven parts, considering the actuator assembly and tie-down bolt as one part, the bellows-seal assembly as one part, and not counting the vane pivot shaft or housing.

Steps in assembly are as follows:

- (1) Drop in bellows-seal assembly, press to fit.
- (2) Insert housing sleeve inside of housing. Thrust collar is part of the sleeve.

- (3) Insert vane pivot shaft with seat cylinder attached through housing from the inside.
- (4) Place lower spring guide, spring, and upper spring guide.
- (5) Assemble actuator on shaft.
- (6) Install and tighten bolt on shaft. This will load the thrust collar against the housing, and compress the bellows slightly to make a good seat at the face seal.

Disassembly can be accomplished by using the same steps in reverse. Servicing will consist of inspection for wear and distortion on thrust collar and face, and seal face and seat. The parts can be replaced as necessary, and need not be used as matched parts or in matched pairs.

The basic material used throughout the seal is Inconel X-750. However, several parts require coatings, inserts, or other structural material. The basic requirements of the materials at various points in the seal assembly are to retain dimensional stability at temperatures as high as 1200 degrees Fahrenheit, to provide good wear life at high temperature while in slight motion, to have relatively low coefficient of friction at high temperature and high load, and to be capable of forming a very good static seal between parts at high temperature.

To accomplish these tasks, the following materials and coatings are used:

- Housing sleeve surface: high temperature electrofilm or aluminum oxide plating versus Haynes Alloy N 25 housing sleeve.
- Silver plate on all statically mating parts
- Seal face: 0.0025 to 0.003 inch thick aluminum oxide
- Seal seat: 0.0025 to 0.003 inch thick tungsten carbide (LW-5)

The bellows is Inconel X-750 or 718. The actuator arm, spring and spring guide are AMS 5616. The self-locking nut is AMS 5735. All other parts are Inconel X-750.

The clearances, tolerances, and finishes in specific parts must be held quite closely. The seal face and seat is to be finished to a flatness of 3 helium light bands. The parts that fit over the shaft are 0.0002 inches to 0.0006 inches loose. Stationary mating surfaces are given a 32 microinch (rms) finish. The seal seat has a slight interference fit with the seat housing to assure zero leakage between them.

The coating materials, use of the bellows, and better finishes represent the main difference between this seal and the present seal.

3) TOLERANCE TO FOREIGN PARTICLES AND LOAD DEFLECTIONS

Overall tolerance to dirt and cocking for this seal appear to be good. The seal face and seat are kept in a mating position at all times so that dirt can not ordinarily get between them. The loading force is about 0.9 pounds. The required impact to separate the two faces, therefore, is over 1000 g's. This is such a high level that it will never be encountered in an operational engine.

Since the surfaces are not exactly mated (the 3 helium light bands flatness corresponds to 34.8×10^{-6} inches (variation) there is a possibility that dirt particles up to 69.6×10^{-6} inches diameter can become deposited in the seal. This, then could cause the gap to increase by that amount as the seal rotates. The leakage could then go as high as 8 times the quoted flow. This is still much less than present leakage values. Dirt particles that could get in the gap will tend to be worked out by the reversing motion of the seal face as the actuator moves back and forth. Since the surface materials are very hard, the probability of developing scratches is very low. The wear particles of the surface materials are probably the hardest that will be encountered. These, of course, should be small enough to polish the surfaces as they are being worked out rather than causing damage.

The bellows has good bending flexibility so that a cocked attitude of the shaft should have no effect on the ability of the seal faces to mate. If there is any cocking or misalignment, there will be a tendency for the seal to ride off-center. However, this will only slightly reduce the effective length of the slit rather than cause any serious departure from design performance.

The present seal does not use finishes as smooth as those on the bellows-loaded face seal, so larger dirt particles can enter and cause scratching and wear. Also, the present seal can become unseated when cocked. So leakage rates with the present seal are unavoidably higher than for the new design, and wear can be greater.

4) RELIABILITY

Overall reliability considerations, other than those above, depend largely upon the integrity of the bellows, the flame-sprayed coatings, and the electrofilm coatings. Past experience with similar coatings, has been satisfactory, but design reliability can only be proven by testing. The life and wear of the coatings have already been discussed. The installation of the bellows is predicated upon advice from bellows manufacturers. It has been stated that externally pressurized bellows offer less problem with squirring, and therefore less problem with proper mating, than with internal pressurization. The pressure-induced stress in the walls of the bellows is always less than 17,000 pounds per square inch. The 0.0001 percent creep/hour of Inconel X at 1200 degrees Fahrenheit is about 62,000 pounds per square inch, fully heat treated, thereby realizing sufficient safety factor to account for some bending, squirring and compression-induced stresses.

It is concluded that the only unknown design aspect for over-all reliability is the life of the electrofilm coating. Other points, although better understood, need experimental verification, too. These would include integrity of the flame-plated material; the bellows integrity; the ability of the silver plated parts to resist galling; and the ability of the loaded face seal to resist opening with shock load and cocking loads, and to withstand the action of very small dirt particles which may tend to wear surfaces and open the seal.

5) AIR LEAKAGE RATE AND ACTUATION POWER

Measured leakage rate of the present design is 0.004 standard cubic feet per minute at 94 pounds per square inch pressure drop. This compares to a calculated leakage of 0.00079 standard cubic feet per minute at 135 pounds per square inch pressure drop for the bellows-loaded face seal design. This would be about 0.0004 standard cubic feet per minute at 94 pounds per square inch pressure drop to atmospheric pressure. Thus, it appears that improvement in leakage by a factor of 10 could be realized by using the new design.

The measured actuating torque for the present design when no pressure is applied is 1.5 inch-pounds. The calculated torque required when pressure, but no bending loads, is applied is 3.8 inch-pounds for an assumed friction coefficient of 0.1. This compares to 1.53 inch-pounds calculated torque requirement (without bending moment effects) for the new design.

3. SPHERICAL SEAT FACE SEAL

a. INTRODUCTION

The spherical seat face seal for the vane pivot offers excellent sealing properties at the expense of requiring very fine finishes. This vane sealing method can be utilized anywhere along the compressor.

Since finishing the screening work, considerable preliminary design work has been carried out. The design has been submitted to potential vendors for their comments. The final design is discussed below.

b. DESCRIPTION

The design of the spherical seat face seal is shown in Figure 43. It combines the thrust face and seal face and does not require a bellows. A spring is used to keep the two faces together at all times. The spherical geometry, combined with the lack of restraint on the seal seat permits it to seek its own alignment and therefore stay seated even though there may be some shifting of the axis as a bending moment is applied to the vane. The seal is formed between the spherically concave seat located in the housing and the spherically convex seal held to the shaft. This surface is also the thrust bearing for the vane: the loading due to compressor pressure is taken by the seal. The seat is not tightly confined perpendicular to the vane axis. This permits motion required to keep the sphere seated, as a bending movement is applied to the vane. The high pressure is on the outer diameter of the seal surface. Materials selection appeared to be the biggest technical problem.

c. LEAKAGE

The leakage for this seal is somewhat more difficult to analyze than for the bellows-loaded face seal. The finish is better for the spherical surface and is lapped to fit the seat almost perfectly. If the seal is well seated, an estimate can be made using the rms finish as the half width of the slot. This gives a calculated leakage of about 1/2 of that for the bellows loaded face seal, or

$$v = 0.0004 \text{ standard cubic feet per minute.}$$

at engine conditions. The probable degree of non-seating with this seal is unknown, since there will be friction tending to prevent proper seating. If unseating does actually occur, the leakage rate of this seal will exceed that of the bellows face seal. This effect can be properly evaluated only by testing.

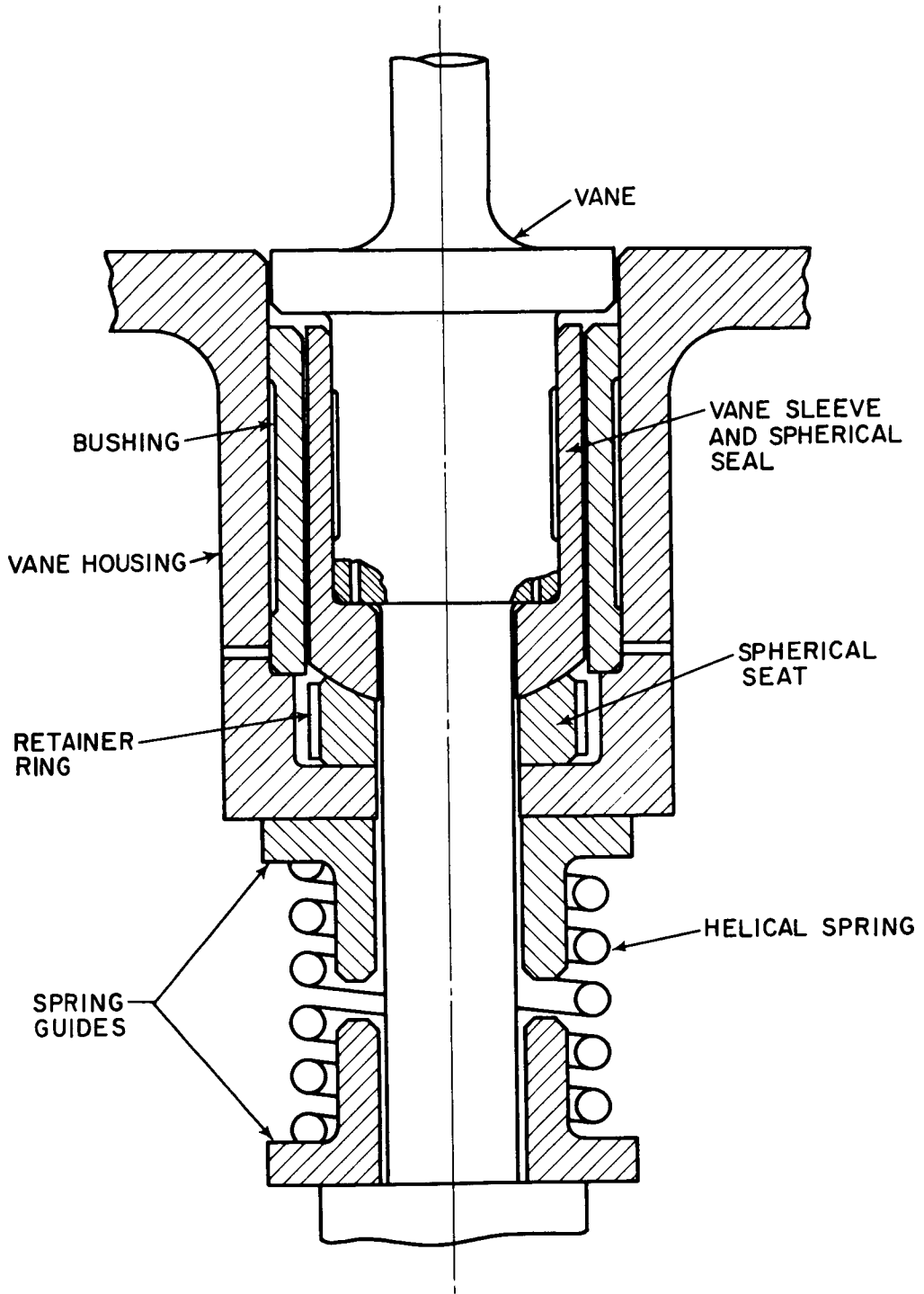


Figure 43 Spherical Seat Vane Pivot Seal

d. ACTUATION TORQUE

The torque requirement for actuation is estimated using an assumed friction coefficient of 0.1 for carbon against tungsten carbide and 0.2 for silver against silver.

Thus

$$T = 0.1 \times R_m \times F_{\text{THRUST}} + \text{bending moment effects} = 0.54 \text{ inch-pounds} \\ + \text{bending moment effects}$$

This is an approximate value for actuation torque under test rig cruise conditions.

e. LIFE

The wear rate on the thrust bearing cannot be calculated directly. However, it has been reported by Purebon Company that the grade of graphite being used here will last 2000 hrs. when p_v is less than 15,000, where p is in pounds per square inch and v is in feet per minute.

The conditions estimated for service of this seal are 20 degrees of rotation at 10 cycles per minute. The thrust force to be taken up is approximately the area inside the outer edge of the seal times the pressure differential

$$F = \pi R_o^2 \Delta P \text{ pounds}$$

where R_o is the outer radius of the high pressure zone.

Then

$$P_{\text{THRUST}} = \frac{\pi R_o^2 \Delta P}{\pi (r_o^2 - r_i^2)} = 210 \text{ pounds per square inch for cruise} \\ \text{conditions,}$$

where r refers to the thrust face. v can be taken as the mean rubbing speed of the seal, or

$$v = \text{CPM} \left(\frac{2Q_{\text{TOTAL}}}{360} \right) (2 \pi R') = 0.218 \text{ feet per minute}$$

where $R' = \frac{r_o - r_i}{2}$
 $\alpha_{TOTAL} =$ rotation angle, degrees

therefore

$$P_{THRUST} v = 46$$

This number is so low that there should be no questions about reaching 2000 hrs. life in the test rig.

The loading on this seal is such that the mean $P_{THRUST} v$ for the carbon is much lower than the recommended upper limit. Therefore, wear should be satisfactory for this seal.

There are no wearing surfaces in this seal made up of one ceramic against another. This fact reduces the uncertainties of allowable wear rate to just that which the Purebon 56-HT can take.

f. COMPARISON WITH CURRENT VANE PIVOT SEALING PRACTICE

1) SIZE AND WEIGHT

The complete assembly extends about 2 inches radially outward from the inside of the compressor wall. The distance from the outer surface of the seal to the inside wall of the seal housing is 0.65 inches. The weight of an individual seal assembly, exclusive of vane pivot shaft, actuator arm and bolt, and seal housing is 0.025 pounds. These sizes and weights are comparable to those for the present seal.

2) DESIGN SIMPLICITY

The complete unit is assembled in seven parts, considering the actuator lever and tie down bolt as one part, considering the seal and retainer ring as one part, and not counting the shaft. Assembly is accomplished as follows.

- (1) Press in housing sleeve.
- (2) Drop in seat and retainer ring until it seats against housing shoulder.
- (3) Press seal onto vane pivot shaft.
- (4) Insert vane pivot shaft through housing from the inside.

- (5) Place spring guide and springs over shaft.
- (6) Assemble actuator on shaft.
- (7) Install and tighten bolt on shaft. This will load the seat to the housing shoulder, thereby making a stationary seal between the primary seal and the housing.

Disassembly is accomplished by reversing the above operations. All faces and seats would be inspected for wear and replaced as necessary. The spherical seat and seal face will have to be replaced as matched pairs.

The basic material of construction is Inconel X-750. As for the bellows loaded seal, however, several faces and surfaces have to be of other materials. The spherical seat will be a shaped carbon mass held in its retainer ring. The housing sleeve will be Inconel 718 surfaced with carbon or high temperature electrofilm. The seal itself is flame-plated with 0.0025 inch to 0.003 inch thick tungsten carbide (Linde LW-5). All Inconel parts required to form a static seal are plated with silver.

Required fits and clearances for a properly functioning seal are as follows:

- Seal: 2 microinch (rms) finish
- Seal and seat lapped together

The main complication of this seal over the present seal is the use of very good finishes on the sealing parts. Some simplification exists with the new design in that the seal also serves as the thrust collar, a separate part in the present design.

3) TOLERANCE TO FOREIGN PARTICLES AND LOAD DEFLECTIONS

This seal resists the action of cocking and misalignment by utilizing a spherical seal and seat. The friction coefficient between the two parts is low, so there will be a great tendency to remain seated with only a small applied force from slight spring compression. Any external vibration will assist in achieving such seating. The force tending to keep the two parts seated is three pounds, but this must act at an angle as low as 22 degrees. This provides centering forces as low as 1.2 pounds. However, the friction force resisting centering is 0.32 pounds, with a friction coefficient of 0.1. There, then, appears to be satisfactory centering and resistance to tilting with cocking loads.

The finishes specified should keep dirt out of the face seal even down to about 4×10^{-6} inches particle diameter. The effect of such small particles on the seal, if they should enter, would be two-fold, 1) a tendency to separate the faces, 2) a tendency to imbed in the carbon. Neither effect is serious since

the increased leakage of such a small lift is negligible as far as absolute amount is concerned, and small imbedded particles will not seriously affect either wear or leakage.

The present seal has a much rougher finish than the spherical seat seal, so large dirt particles can enter and cause scratching and wear. Also, the present seal can become unseated when cocked, so leakage rates and wear are unavoidably higher in the present design than for this new design.

4) RELIABILITY

Overall reliability will depend on the integrity of the carbon inserts, the flame plating, and the ability of the silver plate to resist galling. Past experience of a general sort is available on all of these, but little specific information is available. Basically, it appears that the overall reliability should be good. The design aspects requiring experimental verification are life of the carbon inserts at 1200 degrees Fahrenheit, flame plate integrity, ability of silver plated to resist galling, the ability of the seal to remain seated, and the action of small dirt particles on wear and leakage.

5) AIR LEAKAGE RATE AND ACTUATION POWER

The estimated leakage rate of the new design is 0.0004 standard cubic feet per minute at test conditions, or about 0.0002 standard cubic feet per minute at 94 pounds per square inch pressure drop to atmospheric pressure. This is 1/20 of that measured for the present design at 94 pounds per square inch pressure drop.

The calculated torque requirement is 0.54 inch pounds (without bending moment effects) for the new design, compared to 3.8 inch pounds calculated for the present design without bending moment effects.

IV. TASK IV - PIVOT BUSHING AND SEAL EXPERIMENTAL EVALUATION

This phase of the program provides for final design and procurement of bushings and seals, design and fabrication of a test rig, and experimental evaluation of bushing and seal assemblies.

The final design of the two selected concepts for experimental evaluation includes all calculations, material determinations, analyses, and drawings necessary for pivot bushing and seal optimization, procurement, and experimental evaluation.

A single vane test rig will be designed and fabricated to evaluate the two selected pivot bushing and seal designs under simulated operating conditions for the last compressor stage. The vane and actuating mechanism are to be applicable to current advanced engine practice.

The pivot bushing and seal assemblies will be calibrated in incremental steps over the full pressure and temperature range, with a maximum pressure of 135 psi and a maximum temperature of 1200° F.

The seals will be subjected to a cyclic endurance run of at least 40 hours duration following a test program which provides for simulation of take-off (20 hours) and cruise (20 hours) conditions typical of advanced engine designs through duplication of:

- Compressor stage air temperatures
- Supporting structure geometry
- Supporting structure temperatures
- Pivot movements as required for the vanes
- Pivot loading (mechanical loading to simulate air loading is acceptable)
- Compressor stage pressure drop

The pivot movement will be a minimum of 13 degrees at 10 cycles per minute; the pivot loading will include a vibratory load at a convenient frequency superimposed on the steady load and equal to approximately $\pm 15\%$ of the steady load.

A. SUMMARY OF TASK IV EXPERIMENTAL EVALUATION

NASA granted approval to commence final design of the single bellows and spherical seat vane pivot seals. Final design configurations of these seals are being established, and seal materials and coatings are being further investigated. The basic layout of the vane pivot seal test rig has been completed. Instrumentation requirements are being reviewed.

B. TEST SEAL DESIGNS

In a letter dated May 31, 1966, NASA granted approval to commence final design of the single bellows and spherical seat vane pivot seals. The preliminary designs shown in Figures 41 and 42 are being reviewed to determine the necessary modifications required to establish a final design configuration for each seal. Various high temperature carbons, cermets, and super alloys are being investigated for use as potential seal materials. Hard coat flame platings such as chrome carbide, aluminum oxide and titanium carbide are also being considered for application to mating seal surfaces.

C. TEST RIG DESIGN

Design work was continued on a test rig in which the vane pivot bushing and seal experimental evaluation will be conducted. The basic layout of the rig has been completed. A schematic drawing of this test rig is shown in Figure 44. Work is being done to establish adequate actuation devices for vane pivot movement and for applying the steady state and superimposed vibratory loads on the vane. The vane bending moments have been established at 30 inch pounds for take-off and 10 inch pounds for cruise. Instrumentation necessary to obtain the required experimental data is being specified and incorporated in the rig design. A program has been written outlining the calibration and cyclic endurance experimental testing to be performed on the vane pivot seals.

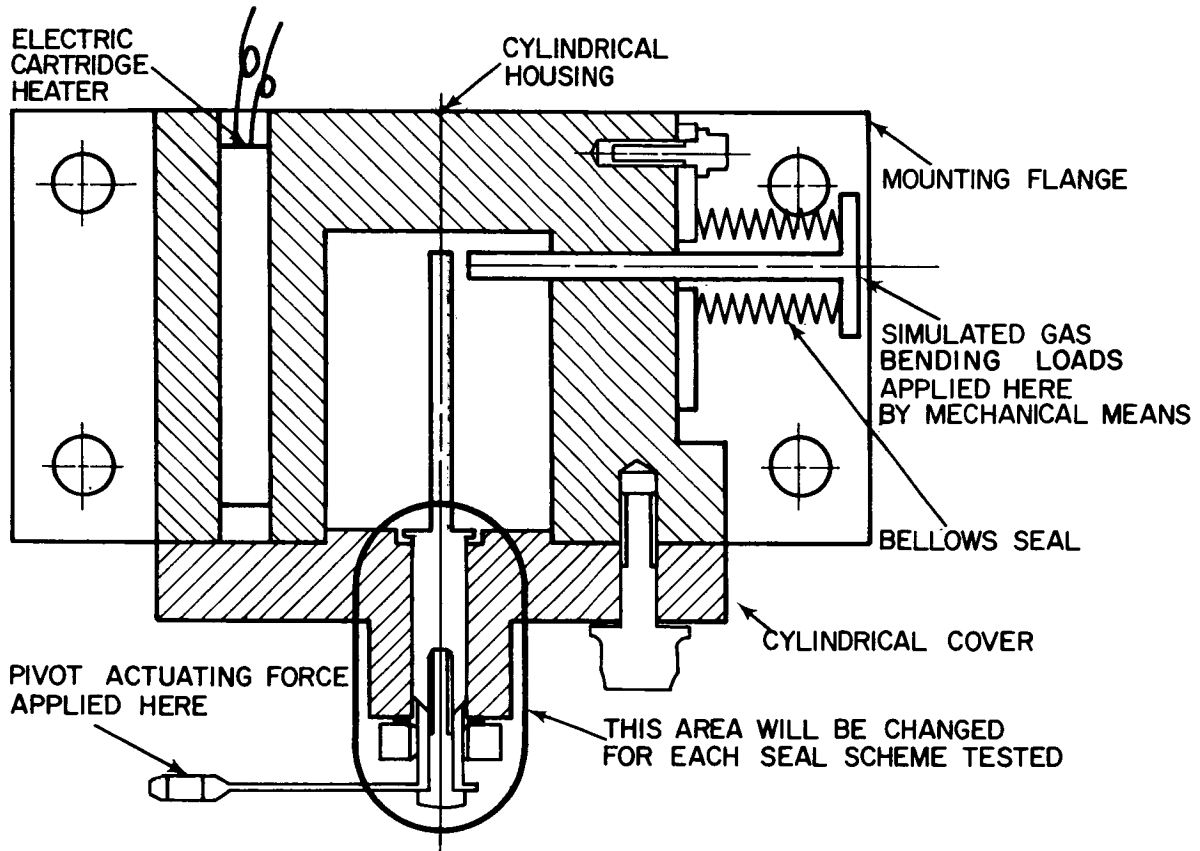
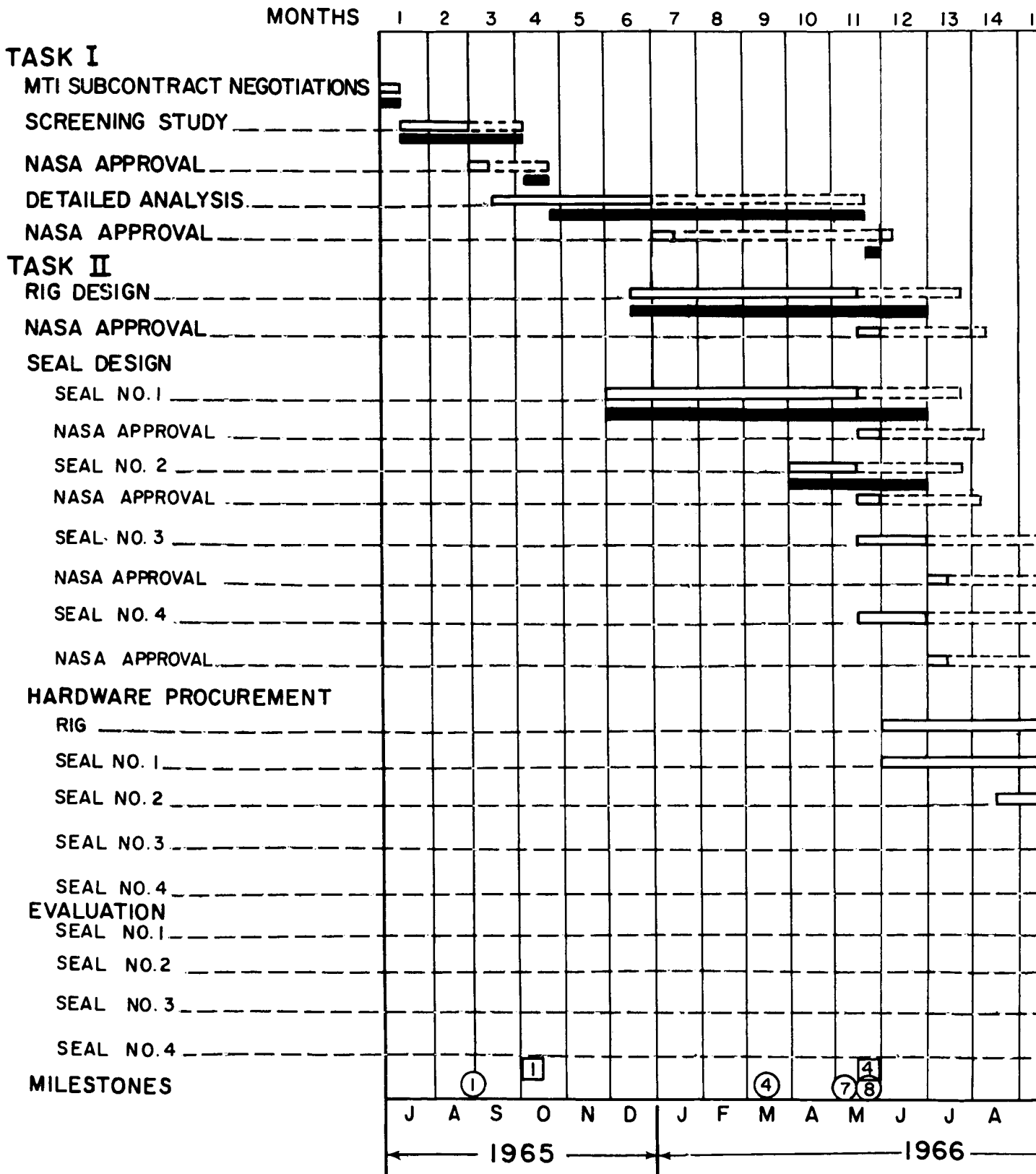
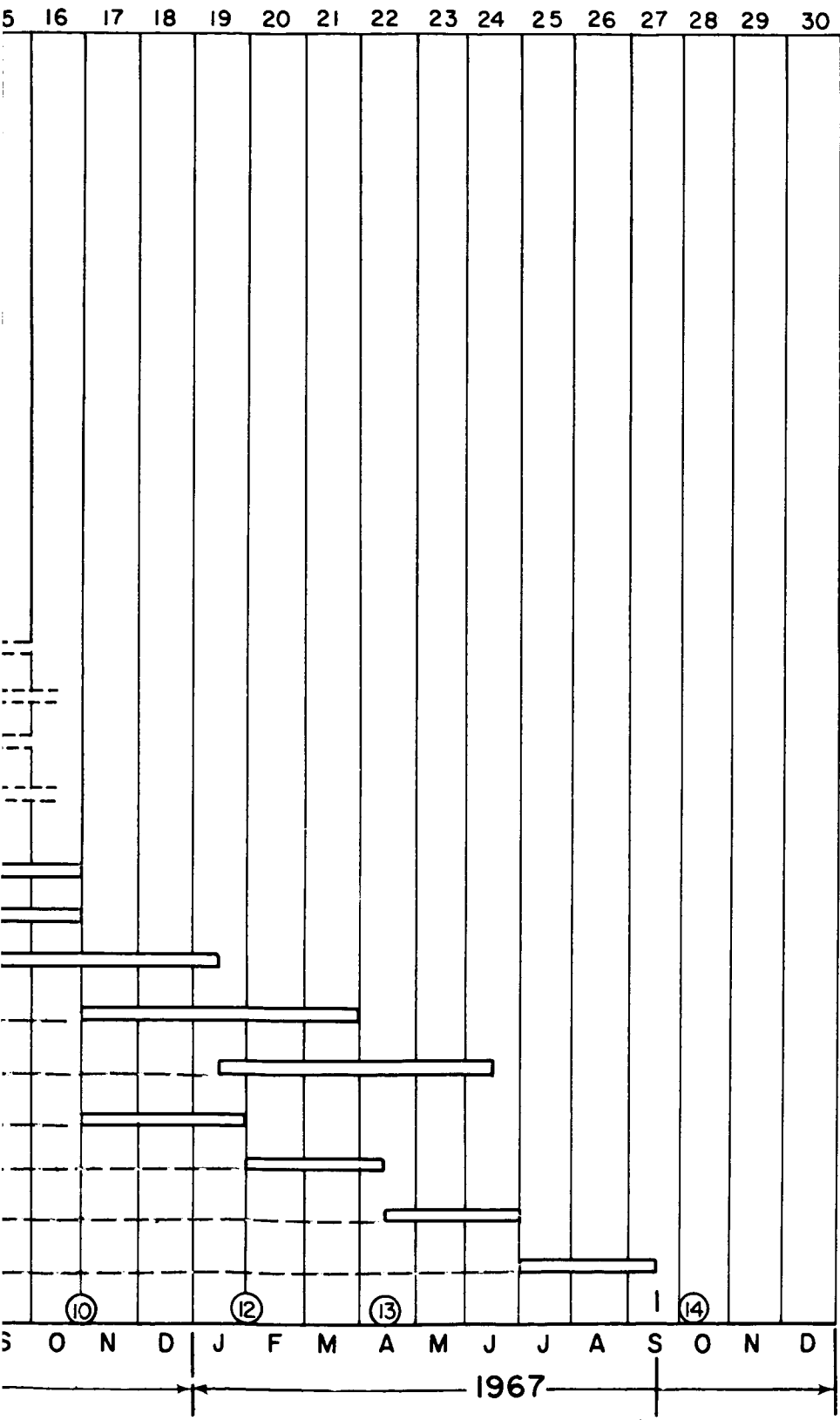


Figure 44 Seal Test Rig Schematic

COMPRESSOR S
PROGRAM SCHEDULE
CONTRACT






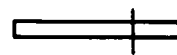


REAL DEVELOPMENT
 E AND MILESTONE CHART
 NAS3-7605



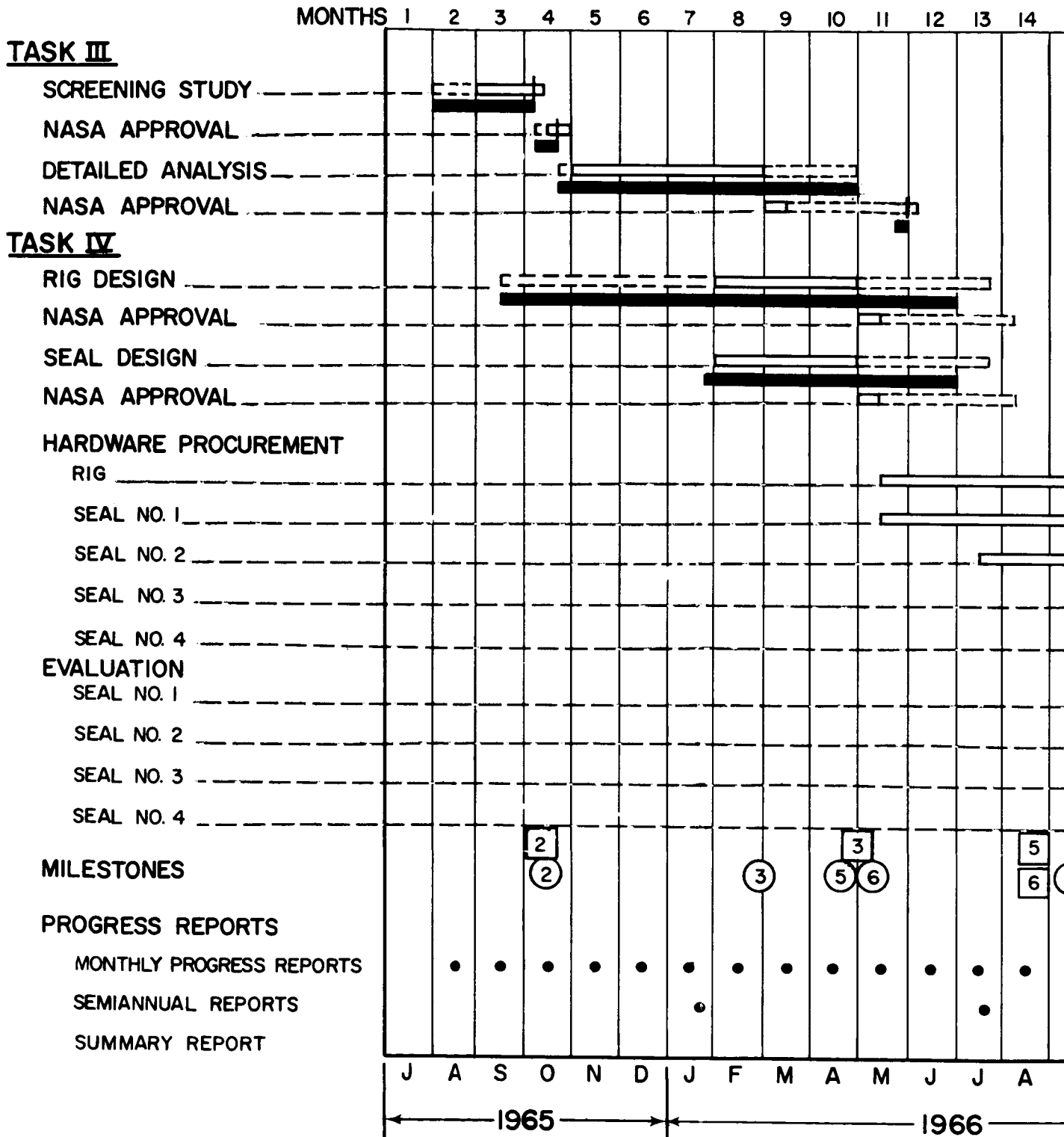
MILESTONES

1. TASK I - COMPLETE SCREENING STUDY
2. TASK III - COMPLETE SCREENING STUDY
3. TASK III - COMPLETE DETAILED ANALYSIS
4. TASK I - COMPLETE DETAILED ANALYSIS
5. TASK IV - COMPLETE RIG DESIGN
6. TASK IV - COMPLETE SEAL DESIGN
7. TASK II - COMPLETE RIG DESIGN
8. TASK II - COMPLETE SEAL DESIGN
9. INITIATE TASK IV TESTING
10. INITIATE TASK II TESTING
11. TASK IV - COMPLETE EVALUATION OF ONE STATOR PIVOT SEAL
12. TASK II - COMPLETE EVALUATION OF ONE COMPRESSOR END SEAL
13. TASK II - COMPLETE EVALUATION OF ONE STATOR INTERSTAGE SEAL
14. SUBMIT SUMMARY REPORT FOR NASA APPROVAL

LEGEND

-  WORK ACCOMPLISHED
-  REVISED WORK PROJECTED
-  WORK ACCOMPLISHED
-  WORK COMPLETED EARLY
-  ORIGINAL MILESTONE
-  MILESTONE ATTAINED

**COMPRESSOR
PROGRAM SCHEDULE
CONTRACT**



SEAL DEVELOPMENT
 SCHEDULE AND MILESTONE CHART
 CONTRACT NAS3-7605







PWA-2875

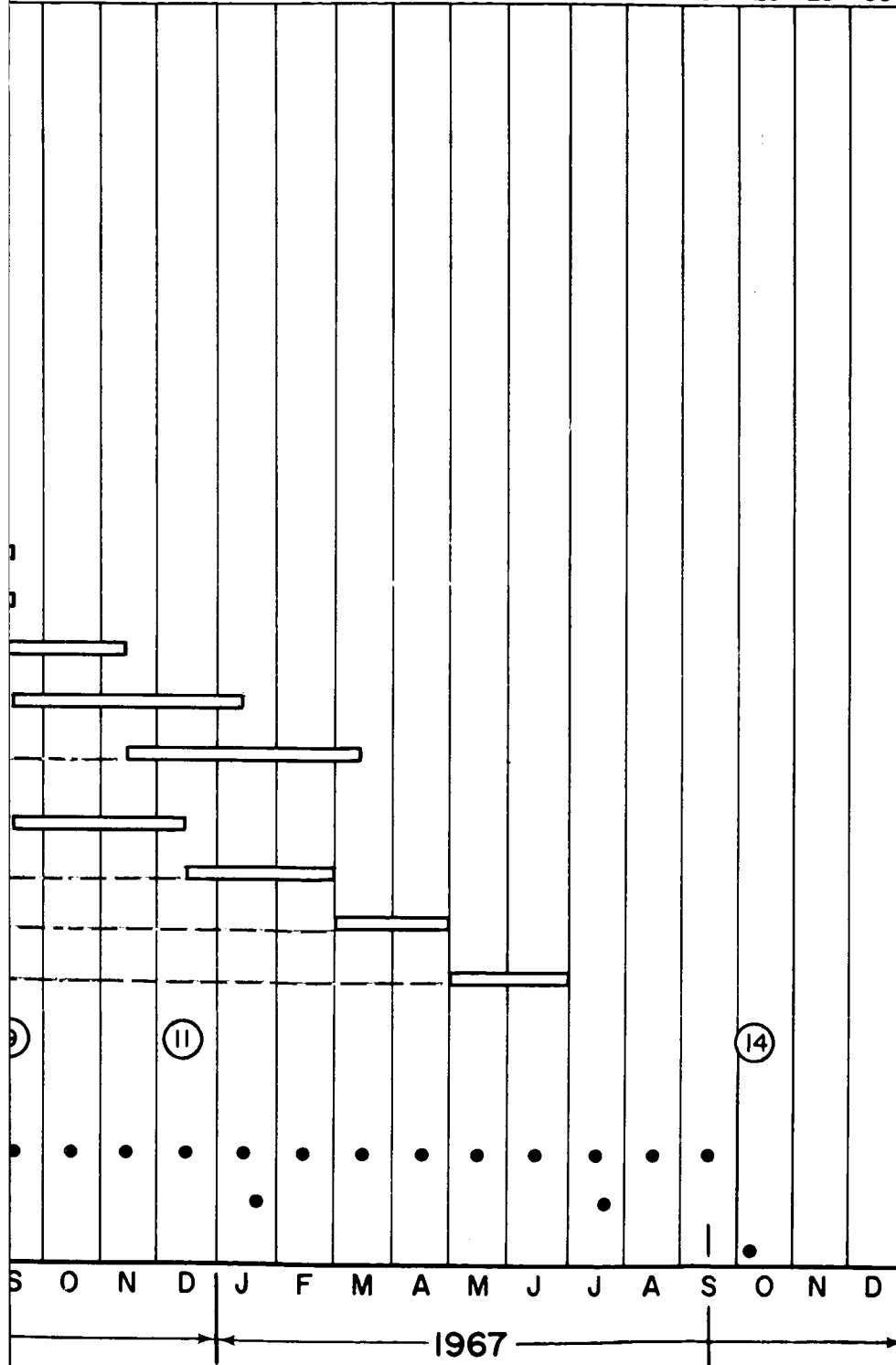
5 16 17 18 19 20 21 22 23 24 25 26 27 28 29 30

MILESTONES

1. TASK I - COMPLETE SCREENING STUDY
2. TASK III - COMPLETE SCREENING STUDY
3. TASK III - COMPLETE DETAILED ANALYSIS
4. TASK I - COMPLETE DETAILED ANALYSIS
5. TASK IV - COMPLETE RIG DESIGN
6. TASK IV - COMPLETE SEAL DESIGN
7. TASK II - COMPLETE RIG DESIGN
8. TASK II - COMPLETE SEAL DESIGN
9. INITIATE TASK IV TESTING
10. INITIATE TASK II TESTING
11. TASK IV - COMPLETE EVALUATION OF ONE STATOR PIVOT SEAL
12. TASK II - COMPLETE EVALUATION OF ONE COMPRESSOR END SEAL
13. TASK II - COMPLETE EVALUATION OF ONE STATOR INTERSTAGE SEAL
14. SUBMIT SUMMARY REPORT FOR NASA APPROVAL

LEGEND

-  WORK PROJECTED
-  REVISED WORK PROJECTED
-  WORK ACCOMPLISHED
-  WORK COMPLETED EARLY
-  ORIGINAL MILESTONE
-  MILESTONE ATTAINED



9/15

APPENDIX AFORTRAN LISTING FOR THE RAYLEIGH PAD SEAL

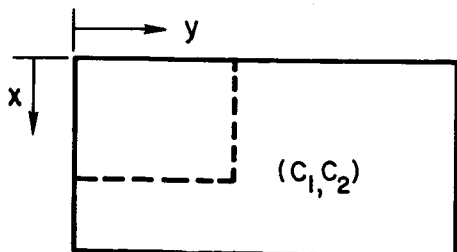
The main program for the Rayleigh pad seal, as listed in Appendix B to the first Semiannual Report (PWA-2752), was modified in order to permit performing additional computations. With the modified program, the flow at the exit of a seal can be computed, and the film shape is not necessarily restricted to a parallel film. Thus a design with an external supply of pressure, such as an orifice in a shrouded pocket, can be examined. The new film thickness functions can provide information on the performance of a tilted seal. The film thickness may be expressed as a polynomial function up to 3rd degree. A further explanation of the film function is given below. The listing contained here are the main program, function HFUN, function HXFUN, and function HYFUN.

1. DESCRIPTION OF FUNCTION HFUN

The purpose of the function HFUN is to define any film shape which may be expressed as a polynomial function of the coordinates x and y up to the 3rd power. The derivative of the local film thickness with respect to x and y can be readily obtained from the film shape. These derivatives are written in subfunction form as functions HXFUN and HYFUN. These three subfunctions are required to compute the pressure distribution and the load.

Defining the nominal film thickness as C_3 at the point ($x = C_1$, $y = C_2$), the local film thickness can be written in a general form with arbitrary coefficients as follows

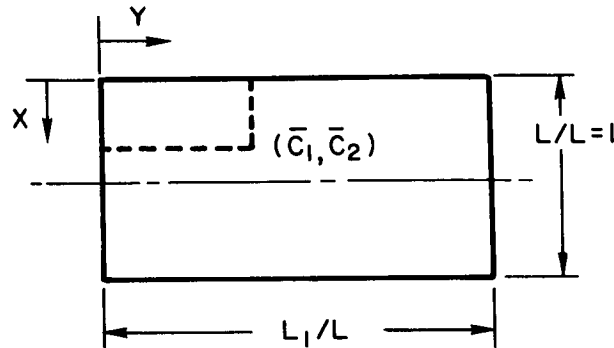
$$h = C_3 + C_4(x - C_1) + C_5(y - C_2) + C_6(x - C_1)^2 + C_7(y - C_2)^2 + C_8(x - C_1)(y - C_2) + C_9(x - C_1)^3 + C_{10}(y - C_2)^3$$



Defining $X = \frac{x}{L}$, $Y = \frac{y}{L}$, $\bar{C}_1 = \frac{C_1}{L}$, $\bar{C}_2 = \frac{C_2}{L}$

$H = \frac{h}{C_3}$ AND $\bar{C}_4 = \frac{C_4}{C_3}$, $\bar{C}_5 = \frac{C_5}{C_3}$, ETC. THUS

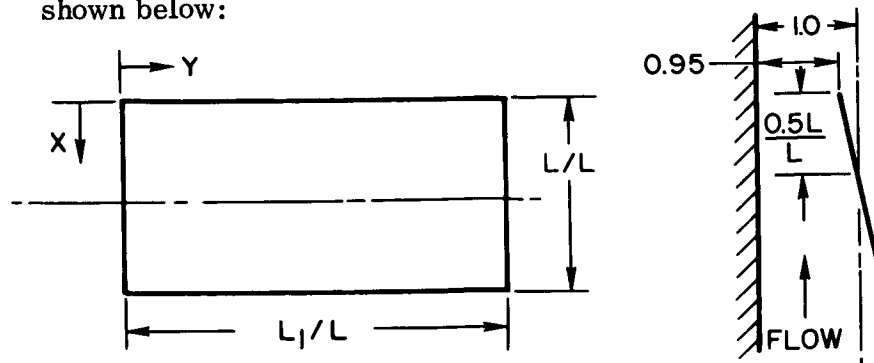
$$H = 1 + \bar{C}_4 (X - \bar{C}_1) + \bar{C}_5 (Y - \bar{C}_2) + \bar{C}_6 (X - \bar{C}_1)^2 + \bar{C}_7 (Y - \bar{C}_2)^2 + \bar{C}_8 (X - \bar{C}_1)(Y - \bar{C}_2) + \bar{C}_9 (X - \bar{C}_1)^3 + \bar{C}_{10} (Y - \bar{C}_2)^3$$



It should be borne in mind that Λ_x and Λ_y depend on the nominal clearance. Also, the origin of the coordinates is located at (0, 0) on the upper left corner of the pad. The local film-thickness as defined in the above equation refers to the land region only. The depth of the recess STEDE is added separately in the main program. The coefficients $\bar{C}_1, \bar{C}_2, \bar{C}_3, \bar{C}_4$, etc. are written as Coe (1), Coe (2), Coe (3), etc. in the program.

Some simple examples are:

- For the constant film: (see sketch above)
 \bar{C}_1 and \bar{C}_2 can be anything but $\bar{C}_3 = 1$
 The other coefficients are zero.
- For a flat plate tilting toward runner at the outer circumference as shown below:



$L_1/L = 1.5$ (EXPRESSED AS YOX IN THE PROGRAM)

2. FORTRAN LISTING

RIN00000

```

S      FORTRAN DECK,LSTOU
C      RIN010 =REVISED BY H CHENG 1/28/66
C      PROGRAM TO SOLVE STEP COMPRESS. BEAR. PROB. WITH FIXED
C      BOUNDARIES, LINES OF SYMMETRY, JOINTS IN ANY DIRECTION.
C      EQUATIONS ARE WRITTEN FOR PARALLEL FACES
C      ONLY. CLEARANCE ALLOWS ONE DEPRESSED AREA
C      ONLY.
C      KUE=0 REGULAR POINT OR CORNER OF DEPRESSED AREA OR LINE OF SUMM
C      KUE=1,2,3 KNOWN PRESSURE= PFIX(1,2,OR 3)
C      KUE=4 VERTICAL LINE OF STEP
C      KUE=5 HORIZONTAL LINE OF STEP
C      KUE=6 TOP JOINT
C      KUE=7 BOTTOM JOINT
C      KUE=8 LEFT JOINT
C      KUE=9 RIGHT JOINT
C      PROBLEM IS SOLVED COLUMNWISE. M (FIRST INDEX)
C      SHOULD BE SMALLER THAN N(SECOND INDEX)
C      X IN I DIRECTION (VERT. DOWN)
C      Y IN J DIRECTION (HOR. LEFT TO RIGHT)
C      PLAMX,PLAMY=X,Y, COMPONENTS OF PLAM
C      (IH,JH),(IHH,JHH) ARE CORNERS OF STOP BOUNDARY
C      STEDE=STEP DEPTH. WHERE NO STEP H=1
C      NDIG= NO OF DIGITS WANTED REPEATED TO TRUNCATE SOLUTION
C      LKOUNT IS THE MAXIMUM ALLOWABLE NUMBER OF ITERATIONS
C      IFLO= I COORDINATE OF THE LINE ACROSS WHICH Y-FLOW IS COMPUTED.
C      JFLO= J COORDINATE OF THE LINE ACROSS WHICH X-FLOW IS COMPUTED.
C      IFLOE=STATION NO FOR EXTRA FLOW CALC
C      COE=CLEARANCE COEFFICIENTS. SEE HFUN, HXFUN, HYFUN.
C      QREP=.TRUE. PUT OUT P2 AFTEREACH ITERATION
C      PPOUT=.TRUE. OUTPUT OF P2 AFTER CONVERGENCE
C      POUT=.TRUE. WANTED OUTPUT OF P.AFTER CONVERGENCE
C      NEWKUE=.TRUE. IF NEW KUE ARRAY IS READ IN
C      DIMENSION PFIX(3),KUE(17,33),QFIX(3),H(17,33),PF(17,33),
1Q(17,33),FF(17,33),F(17),A(17,17),B(17),C(33),E(15,15,34),
1Q SMA(17,17),G(17,34),R(15,15,33),S(17,33),QQ(33),PP(33),PX(33),
1PY(33),D(15,15,34),QQQ(33)
C      LOGICAL JOINT, QREP,PPOUT,POUT,NEWKUE
C      NAMELIST/OUTPUT/QREP,PPOUT,POUT,NEWKUE/INPUT/M,N,PLAMX;
1 PLAMY,YOX,IH,JH,IHH,JHH,STEDE,NDIG,PFIX,NCASE ,LKOUNT,IFLO,JFLO
2,IFLOE,COE
1 FORMAT(1X70I1)
2 FORMAT(70I1)
3 FORMAT( 25H MATRIX IS SINGULAR AT J= 13,16H,CASE ABANDONED./1H1)
4 FORMAT( / 101X,F11.7)
5 FORMAT( //18H CASE CONVERGES TO 13,14H DIGITS AFTER 13,11H ITERATI
-IONS)
6 FORMAT(//23H FINAL RESULTS FOR CASE 15//13H FORCE/AREA =E14.7,
1 64HCOO. OF CENTER OF PRESSURE IN PERCENTAGE OF SIDE
2DIMENSIONS = (E14.7,1H, E14.7,2H).)
7 FORMAT(46HOFLOW PER UNIT LENGTH IN X AT ENT. AND EXIT =(
))H1,7.41EP1 ( = Y NI .L .U REP WOLF42)H1,7.41EP1 ,H2,7.41EP11
8 FORMAT(29HOFINAL PRESSURE DISTRIBUTION. 77)
9 FORMAT(25HOFINAL P**2 DISTRIBUTION. /)
11 FORMAT (6HIINPUT)
NR=5
NW=6
10 READ(NR,INPUT)
WRITE(NW,11)
WRITE(NW,INPUT)
READ(NR,OUTPUT)
WRITE(NW,OUTPUT)

```

```

      IF(.NOT.NEWKUE)GO TO 35
      DO 20 I=1,M
20 READ(NR,2)(KUE(I,J),J=1,N)
      DO 30 I=1,M
      WRITE(NW,1)(KUE(I,J),J=1,N)
      DO 30 J=1,N
30 KUE(I,J)=KUE(I,J)+1
35 KOUNT=0
      NN=N-1
      MM=M-1
      DO 40 K=1,3
40 PFIX(K)=PFIX(K)*PFIX(K)
      DX=1./FLOAT(MM)
      DY=YOX/FLOAT(NN)
      DO 41 I=1,M
41 XX(I)=FLOAT(I-1)*DX
      DO 42 J=1,N
42 YY(J)=FLOAT(J-1)*DY
      SA=1./DX
      SB=1./DY
      SAA=SA*SA
      SBB=SB*SB
      SC=SAA+SBB
      SD=-2.*SC
      SJ=2.*SAA
      SE=PLAMX/(2.*DX)
      SG=PLAMY/(2.*DY)
      SH=2.*SA
      SI=2.*SB
      SK=2.*SBB
      DO 50 I=1,M
      DO 50 J=1,N
50 H(I,J)=HFUN(XX(I),YY(J),COE)
      DO 60 I=IH,IHH
      DO 60 J=JH,JHH
60 H(I,J)=H(I,J)+STEDE
      DO 70 I=1,M
      DO 70 J=1,N
      Q(I,J)=1
      HFX(I,J)=3.*HXFUN(XX(I),YY(J),COE)/H(I,J)
      HFY(I,J)=3.*HYFUN(XX(I),YY(J),COE)/H(I,J)
      ZZZ=-1.0/(H(I,J)*H(I,J))
      F5(I,J)=2./3.0*ZZZ*(HFX(I,J)*PLAMX+HFY(I,J)*PLAMY)
      PFX(I,J)=PLAMX*ZZZ
70 PFY(I,J)=PLAMY*ZZZ
      JOINT=.FALSE.
80 DO 90 I=2,MM
      IF(KUE(I,1).EQ.9.OR.KUE(I,1).EQ.10) JOINT=.TRUE.
90 CONTINUE
100 DO 130 I=1,M
      G(I,1)=0.
      DO 110 K=1,M
110 E(I,K,1)=0.
      IF(.NOT.JOINT)GO TO 130
      DO 120 K=1,M
      D(I,K,1)=0.
      IF(I.EQ.K)D(I,K,1)=1.0
120 CONTINUE
130 CONTINUE
      DO 370 J=1,N
      DO 310 I=1,M

```

```

      FF(I,J)= 1.0/SQRT(ABS(Q(I,J)))
      F(I)=0.
      KU= KUE (I,J)
      GO TO(140,210,210,210,230,250,270,270,140,140),KU
140  SGGG=SGG*(FF(I,J)*PFY(I,J)+HFY(I,J))
      C(I)=SBB+SGGG
      B(I)=SBB-SGGG
      DO 150 K=1,M
      A(I,K)=0.0
      IF(K.EQ.I)A(I,K)=SD +F5(I,J)*FF(I,J)
150  CONTINUE
      IF(JOINT) GO TO 180
      IF(J.NE.1) GO TO 160
      B(I)=0.
      C(I)=SK
160  IF (J.NE.N) GO TO 170
      C(I)=0.
      B(I)=SK
170  IF(I.EQ.1) GO TO 190
      IF(I.EQ.M) GO TO 200
180  SR=SEE*(FF(I,J)*PFX(I,J)+HFX(I,J))
      A(I,I+1)=SAA+SR
      A(I,I-1)=SAA-SR
      GO TO 310
190  A(I,I+1)=SJ
      GO TO 310
200  A(I,I-1)=SJ
      GO TO 310
210  K KU=KUE(I,J)-1
      B(I)=0.
      C(I)=0.
      F(I)=QFIX(KKU)
      DO 220 K=1,M
      A(I,K)=0.
      IF(I.EQ.K) A(I,K)=1.0
220  CONTINUE
      GO TO 310
230  HPLUS=H(I,J)
      HMINUS=H(I,J)
      IF (J.EQ.JH) HMINUS=HMINUS-STEDE
      IF (J.EQ.JHH) HPLUS= HPLUS-STEDE
      HHH=HPLUS**3
      HH=HMINUS**3
      B(I)=-SB*HH
      C(I)= - SB * HHH
      DO 240 K=1,M
240  A(I,K)= 0.
      A(I,I)=SB*(HH+HHH)+PLAMY*( HPLUS-HMINUS)**FF(I,J)
      GO TO 310
250  HPLUS=H(I,J)
      HMINUS=H(I,J)
      IF (I.EQ.IH) HMINUS=HMINUS-STEDE
      IF (I.EQ.IHH) HPLUS= HPLUS-STEDE
      HHH=HPLUS**3
      HH=HMINUS**3
      B(I)=0.
      C(I)=0.
      DO 260 K=1,M
260  A(I,K)=0.0
      A(I,I)=(HH+HHH)/DX=PLAMX*(HMINUS-HPLUS)*FF(I,J)
      A(I,I+1)= -HHH/DX

```

```

      A(I,I-1)= -HH/DX
      GO TO 310
270  SGGG=SGG*(FF(I,J)*PFY(I,J)+HFY(I,J))
      B(I)=SBB-SGGG
      C(I)=SBB+SGGG
      DO 280 K=1,M
      A(I,K)=0.0
      IF(K.EQ.1) A(I,K)=SD+F5(I,J)*FF(I,J)
280  CONTINUE
      SR=SEE*(FF(I,J)*PFY(I,J)+HFY(I,J))
      IF(KU.EQ.8) GO TO 290
      IF(KU.EQ.7) GO TO 300
      GO TO 310
290  A(I,1)=SAA+SR
      A(I,I-1)=SAA-SR
      GO TO 310
300  A(I,M)=SAA-SR
      A(I,I+1)=SAA+SR
      GO TO 310
310  CONTINUE
      DO 320 I=1,M
      DO 320 K=1,M
320  QSMA(I,K)=A(I,K) + B(I)*E(I,K,J)
      CALL MATINV(QSMA,M,BB,C,DET,ID)
      GO TO (340,330),ID
340  DO 360 I=1,M
      G(I,J+1)=J.
      DO 360 K=1,M
      G(I,J+1)=G(I,J+1)+QSMA(I,K)*(F(K)-B(K)*G(K,J))
      E(I,K,J+1)=-QSMA(I,K)*C(K)
      IF(.NOT.JOINT) GO TO 360
      DUM=0.0
      DO 350 KK=1,M
350  DUM=DUM-QSMA(I,KK)*B(KK)*D(KK,K,J)
      D(I,K,J+1)=DUM
360  CONTINUE
370  CONTINUE
      DMA=J.0
      IF(JOINT) GO TO 410
      DO 380 I=1,M
      DMA=AMAX1(DMA,ABS(Q(I,N)-G(I,N+1)))
380  G(I,N)=G(I,N+1)
      DO 400 JJ=2,N
      J=N+2-JJ
      DO 400 I=1,M
      DUM=0.0
      DO 390 K=1,M
390  DUM=DUM+E(I,K,J)*Q(K,J)
      DUM=DUM+G(I,J)
      DMA=AMAX1(DMA,ABS(DUM-Q(I,J-1)))
400  Q(I,J-1)=DUM
      GO TO 560
410  DO 420 I=1,M
      DO 420 K=1,M
      QSMA(I,K)= -D(I,K,N+1)
      IF(I.EQ.K)QSMA(I,K)=QSMA(I,K)+1.0
420  CONTINUE
      CALL MATINV(QSMA,M,BB,C,DET,ID)
      GO TO (430,330),ID
330  WRITE(NW,3) J
      GO TO 10

```

```

430 DO 460 I=1,M
    DU=0.0
    DO 450 K=1,M
    DUM=0.0
    DO 440 KK=1,M
440 DUM=DUM+QSMAT(I,KK)*E(KK,K,N+1)
    R(I,K,N)=DUM
450 DU=DU+QSMAT(I,K)*G(K,N+1)
460 S(I,N)=DU
    DO 490 JJ=2,N
    J= N+2-JJ
    DO 490 I=1,M
    DU=0.0
    DO 480 K=1,M
    DUM=0.0
    DO 470 KK=1,M
470 DUM= D(I,KK,J)*R(KK,K,N)+E(I,KK,J)*R(KK,K,J)+DUM
    R(I,K,J-1)=DUM
480 DU=DU+D(I,K,J)*S(K,N)+F(I,K,J)*S(K,J)
490 ST(I,J-1)=DU+G(I,J)
    DMA=0.0
    DO 500 I=1,M
    DO 500 K=1,M
    QSMAT(I,K)=-R(I,K,1)
    IF(I.EQ.K)QSMAT(I,K)= QSMAT(I,K)+1.0
500 CONTINUE
    CALL MATINV(QSMA,M,BB,0,DET,ID)
    GO TO(510,330),ID
510 DO 530 I=1,M
    DU=0.0
    DO 520 K=1,M
520 DU=DU+QSMAT(I,K)*S(K,1)
    DMA=AMAX1(DMA,ABS(DU-Q(I,1)))
530 Q(I,1)=DU
    DO 550 J=2,N
    DO 550 I=1,M
    DU=0.0
    DO 540 K=1,M
540 DU=DU+R(I,K,J)*Q(K,1)
    DU=DU+S(I,J)
    DMA= AMAX1(DMA,ABS(DU-Q(I,J)))
550 Q(I,J)=DU
560 IF(QREP) WRITE(NW,4)Q
    KOUNT=KOUNT+1
    IF(KOUNT.GE.LKOUNT)GO TO 561
    IF(DMA .GT. 10.0**FLOAT(I-NDIG)
561 WRITE(NW,5)NDIG,KOUNT
    WRITE(NW,11)
    IF(PPOUT)WRITE(NW,9)
    DO 575 I=1,M
    IF(PPOUT)WRITE(NW,4)(Q(I,J),J=1,N)
    DO 570 J=1,N
570 Q(I,J)=SQRT(ABS(Q(I,J)))
575 CONTINUE
    IF(POUT)WRITE(NW,8)
    DO 576 I=1,M
    IF(POUT)WRITE(NW,4)(Q(I,J),J=1,N)
576 CONTINUE
    DO 590 I=1,M
    X=DX*FLOAT(I-1)
    DO 580 J=1,N

```

```

580 QQQ(J)=Q(I,J)-1.0
PP(I)=SUM(QQQ,N,DY)
590 PX(I)=PP(I)*X
DO 610 J=1,N
Y=FLOAT(J-1)*DY
DO 600 I=1,M
600 QQQ(I)=Q(I,J)-1.0
610 PY(J)=SUM(QQQ,M,DX)*Y
FP=SUM(PP,M,DX)
FX=SUM(PX,M,DX)
XF=FX/FP
FY=SUM(PY,N,DY)
YF=FY/FP/YOX
FP=FP/YOX
WRITE(NW,6) NCASE,FP,XF,YF
DO 620 I=1,M
620 PP(I)=Q(I,JFLO)*H(I,JFLO)*(-PLAMY+H(I,JFLO)**2
1*(Q(I,JFLO+1)-Q(I,JFLO-1))/(2.*DY))
FLOY=SUM(PP,M,DX)
NFLO=1
IFLT=IFLO
625 DO 630 J=1,N
630 PP(J)=Q(IFLT,J)*H(IFLT,J)*(-PLAMX+H(IFLT,J)**2
1*(Q(IFLT+1,J)-Q(IFLT-1,J))/(2.*DX))
FLOT=SUM(PP,N,DY)/YOX
GO TO (635,636),NFLO
635 NFLO=2
FLOX=FLOT
IFLT=IFLOE
GO TO 625
636 CONTINUE
WRITE(NW,7) FLOT,FLOX,FLOY
GO TO 10
END

```

315
316

```

FORTRAN ESTOU,DECK
INCODE IBMF
FUNCTION TO EVALUATE CLEARANCE H FROM X,Y AND COEFFICIENTS COE
FUNCTION HFJN(XX,YY,COE)
DIMENSION COE(10)
X=XX-COE(1)
Y=YY-COE(2)
HFUN=COE(3)+COE(4)*X+COE(5)*Y+COE(6)*X*X+
1COE(7)*Y*Y+COE(8)*X*Y+COE(9)*X*X*X+
2COE(10)*Y*Y*Y
RETURN
END

```

```

C FUNCTION HXFUN(XX,YY,COE)
FUNCTION TO EVALUATE X-DERIVATIVE OF H FROM X,Y AND COEFFICIENTS COE
DIMENSION COE(10)
X=XX-COE(1)
Y=YY-COE(2)
HXFUN=COE(4)+2.*COE(6)*X+COE(8)*Y+
13.*COE(9)*X*X
RETURN
END

```

```
C      FUNCTION HYFUN(XX,YY,COE)
      FUNCTION TO EVALUATE Y-DERIVATIVE OF H FROM X,Y AND COEFFICIENTS COE
      DIMENSION COE(10)
      X=XX-COE(1)
      Y=YY-COE(2)
      HYFUN=COE(5)+2.*COE(7)*Y+COE(8)*X+3.*COE(10)*Y*Y
      RETURN
      END
$      ENDJOB
```


APPENDIX B

ANALYSIS OF HYBRID SEAL

The geometry of a hybrid seal which uses both special grooves and orifices is shown in Figure 45. The analysis is quite versatile; it can be applied to cases having grooves on both edges or one edge only.

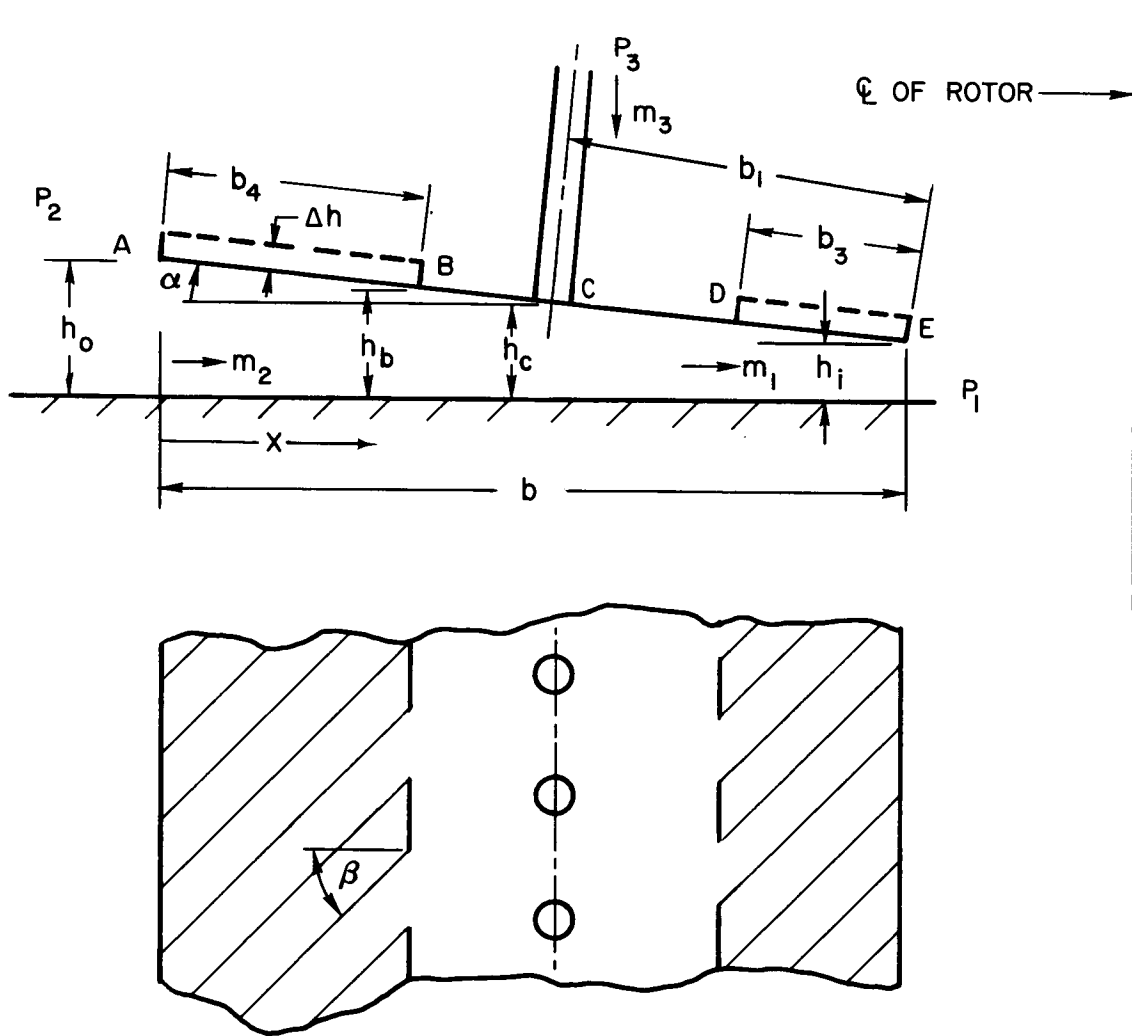


Figure 45 Geometry of Spiral Groove - Orifice Hybrid Seal

The equation governing the pressure distribution in the grooved region AB is:

$$\frac{d\bar{p}}{d\bar{x}} = \Lambda (h_m) \left(\frac{h_m}{h}\right)^2 K_1(h) - \frac{\bar{M}_2}{2} \left(\frac{h_m}{h}\right)^3 \frac{K_2(h)}{\bar{p}} \quad (4)$$

where

$$\bar{p} = p/p_2$$

$$\bar{x} = x/b$$

$$\Lambda = \frac{6\mu Ub}{\rho_2 h_m^2}$$

$$K_1 = \frac{(H^3 - 1)(H - 1) \sin 2\beta}{(H^3 + 1)^2 + 2H^3(A + A^{-1}) + (H^3 - 1)^2 \cos 2\beta}$$

$$K_2 = \frac{2(1 + A^{-1})(H^3 + A)}{(H^3 + 1)^2 + 2H^3(A + A^{-1}) + (H^3 - 1)^2 \cos 2\beta}$$

$$\bar{M}_2 = \left(\frac{24\mu b}{\rho_2 h_m^3}\right) m_2$$

$$H = \frac{\Delta h}{h} + 1$$

U = mean speed, in/sec

$$\mu = \text{viscosity} \frac{\text{lb sec}}{\text{in}^2}$$

$$m_2 = \text{mass flow} \frac{\text{lb sec}}{\text{in}^2}$$

$$\rho_2 = \text{density of upstream gas} \frac{\text{lb sec}^2}{\text{in}^4}$$

A = groove height ratio A_g/A_r

β = groove angle

$$h_m = \frac{h_0 + h_i}{2}$$

Equation (4) can be expressed alternatively by replacing \bar{p}^2 with Q giving

$$\frac{dQ}{d\bar{x}} = 2\Lambda \left(\frac{h_m}{h}\right)^2 K_1(h) \sqrt{Q} - \bar{M}_2 \left(\frac{h_m}{h}\right)^3 K_2(h) \quad (5)$$

When the groove action is weak, equation (5) is preferable, because the non-linear portion is contained in the less dominating hydrodynamic term. If the groove action is strong, equation (4) is more useful, since the hydrodynamic term now becomes dominating.

Approximating equations (4) and (5) by finite difference equations for each grid point, one obtains

$$\bar{p}_j = \bar{p}_{j-1} + f_j - \bar{M}_2 g_j \quad (6)$$

$$Q_j = Q_{j-1} + f'_j - \bar{M}_2 g'_j \quad (7)$$

where

$$f_j = \Delta\bar{x} \left[\Lambda \left(\frac{h_m}{h_{j-1/2}}\right)^2 K_{1,j-1/2} \right]$$

for equation (6),

$$f'_j = \Delta\bar{x} \left[2\Lambda \left(\frac{h_m}{h_{j-1/2}}\right)^2 K_{1,j-1/2} \sqrt{Q_{j-1/2}} \right] \quad (8)$$

for equation (7),

$$g_j = \Delta\bar{x} \left[\frac{1}{2} \left(\frac{h_m}{h_{j-1/2}}\right)^3 K_{2,j-1/2} \frac{1}{p_{j-1/2}} \right] \quad (9)$$

for equation (6), and

$$g'_j = \Delta\bar{x} \left[\left(\frac{h_m}{h_{j-1/2}}\right)^3 K_{2,j-1/2} \right]$$

for equation (7).

In the land region BC, equations (6) and (7) are directly applicable if $K_1 = 0$ and $K_2 = 1$. Likewise, in region CD, equations (6) and (7) are applicable if $K_1 = 0$, $K_2 = 1$ and \bar{M}_2 is replaced by \bar{M}_1 , where

$$\bar{M}_1 = \left(\frac{24\mu b}{\rho_2 h_m^3 \rho_2} \right) m_1$$

In region DE, the pumping action of the groove is reversed, therefore Λ becomes negative. Equations (6) and (7) are also applicable if Λ is made negative and \bar{M}_2 is replaced by \bar{M}_1 .

In equation (6) and (7), f_j, f'_j, g_j, g'_j are considered to be known quantities. The non-linearity in (8) or (9) is solved by iteration.

Identifying the stations underneath the orifice by $j = JC$, and adding equations (6) or (7) from $j=2$ to $j = JC$, one obtains,

$$\bar{M}_2 = \frac{\sum_{j=2}^{JC} f_j - (\bar{p}_{JC} - \bar{p}_1)}{\sum_{j=2}^{JC} g_j}$$

for equation (6),

$$\bar{M}_2 = \frac{\sum_{j=2}^{JC} f'_j - (Q_{JC} - Q_1)}{\sum_{j=2}^{JC} g'_j} \quad (10)$$

for equation (7)

Likewise, equations (6) or (7) from $j = JC$ to the last station $j = JF$ are added together, to give

$$\bar{M}_1 = \frac{\sum_{j=JC+1}^{JF} f_j - (\bar{P}_{JF} - \bar{P}_{JC})}{\sum_{j=JC+1}^{JF} g_j}$$

for equation (6),

$$\bar{M}_1 = \frac{\sum_{j=JC+1}^{JF} f'_j - (\bar{Q}_{JF} - \bar{Q}_{JC})}{\sum_{j=JC+1}^{JF} g'_j} \quad (11)$$

for equation (7),

The flow through the orifice is governed by

$$m_3 = \frac{\pi a^2}{\sqrt{RT_3}} p_3 G \left[\left(\frac{p_2}{p_3} \right)^2 \right] \quad (12)$$

where

$G \left[\left(\frac{p_2}{p_3} \right)^2 \right]$ is the dimensionless flow through the orifice as a function of $\left(\frac{p_2}{p_3} \right)^2$

Match of flow between the orifice and the gas film requires

$$m_1 = m_2 + m_3 \quad (13)$$

Substituting equation (12) into (13) and by virtue of the definition of \bar{M}_1 and \bar{M}_2 one obtains

$$\bar{M}_1 = \bar{H}_m \left(\frac{p_3}{p_2} \right) G \left[\left(\frac{p_2}{p_3} \right)^2 \right] + \bar{M}_2 \quad (14)$$

where

$$\bar{H}_m = \left[\frac{24 \mu b}{\rho_2 h_m^3} \frac{\pi a^2}{\sqrt{RT_3}} \right]$$

Substituting equations (10) and (11) into equations (14), one obtains

$$\frac{\sum_{j=JC+1}^{JF} f'_j - (Q_{JF} - Q_{JC})}{\sum_{j=JC+1}^{JF} g'_j} - \frac{\sum_{j=2}^{JF} f'_j - (Q_{JC} - Q_1)}{\sum_{j=2}^{JC} g'_j} \quad (15)$$

$$- \bar{H}_m \left(\frac{p_3}{p_2} \right) G \left[\frac{Q_{JC}}{\left(\frac{p_3}{p_2} \right)^2} \right] = 0$$

A similar equation can be obtained if \bar{p} is used instead of Q .

Equation (15) can be solved for Q_{JC} numerically by the conventional secant method. Between iterations, the pressure distributions are corrected, i. e., the values of f_j are adjusted during each iteration.

Once Q_{JC} and \bar{p}_{JC} and the pressure at each station are solved after the iterative procedure converges, the load and center of pressure can be determined as follows.

$$\begin{aligned}\bar{W} &= \int_0^b \frac{(p-p_1) dx}{(p_2-p_1) b} \\ &= \frac{l}{\left[1 - \left(\frac{p_1}{p_2}\right)\right]} \int_0^l \left(\frac{p}{p_2} - \frac{p_1}{p_2}\right) d\bar{x} \\ &= \frac{l}{1 - \frac{p_1}{p_2}} \left[\int_0^l \bar{p} d\bar{x} - \frac{p_1}{p_2} \right]\end{aligned}$$

$$\begin{aligned}x_c &= \frac{\int_0^l \frac{(p-p_1) \bar{x} d\bar{x}}{(p_2-p_1)}}{\int_0^l \frac{(p-p_1) d\bar{x}}{(p_2-p_1)}} \\ &= \frac{l}{\bar{W}} \frac{l}{\left(1 - \frac{p_1}{p_2}\right)} \left[\int_0^l \bar{p} \bar{x} d\bar{x} - \left(\frac{p_1}{p_2}\right) \frac{l}{2} \right]\end{aligned}$$

\bar{W} and \bar{x}_c are integrated by Simpson's rule.

```

C   SPRIAL GROOVE - ORIFICE SEAL
C   NRUN - NO. OF RUNS
C   ITMAX - MAX. NO. OF ITERATIONS
C   NHMAX - NO. OF FILM THICKNESSES
C   JB-NO. OF STATIONS IN GROOVE REGION AT HP SIDE,JC-SAME IN SEAL
C   JD=SAME IN SEAL AT LP SIDE, JF-SAME AT EDGE OF LP GROOVE
C   KS-NEW CASE OR LAST CASE OF CALCULATION
C   R - GAS CONSTANT
C   AK - SPECIFIC HEAT RATIO
C   B1B - B1/B
C   B3B - B3/B
C   B4B - B4/B
C   B - WIDTH
C   A1 - ORIFICE RADIUS
C   P1 - P1
C   P2 - P2
C   P3 - P3
C   FL - LENGTH
C   ALFA- TILTING ANGLE IN RADIAN
C   DEL1=GROOVE DEPTH AT HP SIDE, DEL2=SAME AT LP SIDE
C   VIS - VISCOSITY
C   U - SPEED
C   T - TEMP DEG F
C   THE1= SPIRAL ANGLE AT HP SIDE, THE2=SAME AT LP SIDE
C   AF1 - ACC. OR DEACC. FACTORS
C   AF2  DITTO
C   AF3  DITTO
C
C           READ INTEGERS
C   DIMENSION X(90),HM(90),H(90),DUM(90),GX(90),Q(90),FX(90),P(90),
C   IFFM(90),XXC(90),WW(90),STIFN(90)
1111 READ 1,NRUN,ITMAX,NHMAX,JB,JC,JD,JF,KS,NXJ
C           READ VARIABLES
C   READ 2,AF1,AF2,THE1,AX,THE2,AY,VIS,U,T,R,AK,EPS,AF3
C   PUNCH 3
C   PUNCH 8
C   PUNCH 2,AF1,AF2,THE1,AX,THE2,AY
C   PUNCH 5
C   PUNCH 2,VIS,U,T,R,AK,EPS
C   T=T+460.
C   JJB=JB+1
C   JJD=JD+1
C   JJC=JC+1
C   JJF=JF-2
C   JM1=JC-1
C   NNH=NHMAX-1
C   P(1)=1.
C   Q(1)=1.
C   QX=1.0
C   EJE=JF-1
C   DX=1.0/EJE
C   IF (NXJ-1) 16,15,15
15 READ 2, (X(J), J=1,JF)
C   GO TO 17
16 X(1)=0.0
C   DO 20 J=2,JF
20 X(J)=X(J-1)+DX
17 XJC=X(JC)
C   DX2=2.*DX
C   DX3=DX/3.
C   XJFC=X(JF)-XJC
C   DO 1100 NN=1, NRUN

```

```

C          READ GEOMETRY
READ 2,B1B,B3B,B4B,B,A1,DEL1
READ 2,P1,P2,P3,FL,ALFA,DEL2
  RHO2=P2/R/T
PUNCH 6
PUNCH 2,B1B,B3B,B4B,B,A1,DEL2
PUNCH 7
PUNCH 2,P1,P2,P3,FL,ALFA,DEL1
Z1=B*ALFA
Z2=Z1*.5
DXZ1=DX*Z1
ZC1=6.*VIS*B/RHO2
ZC2=ZC1*U /R/T
ZC3=4.*ZC1*3.1416*A1**2/SQRTF(R*T)/FL
P1P2=P1/P2
  IF (P1P2-1.) 23,21,23
23 ZP12=1./(1.-P1P2)
  GO TO 27
21 ZP12=1.
27 P3P2= P3/P2
  QJFX=P1P2
  Q(JF)=QJFX
  QCMAX=AF3*P3P2
  QCMIN= QJFX
  JF1=JF-1
  QC1=.50*(P1P2 +P3P2)
  IF (SENSE SWITCH 1) 22,24
22 PUNCH 2, QC1, QX, QJFX, Z1,Z2,ZC1,ZC2,ZC3,DX2,DX3
24 READ2,(HM(N),N=1,NHMAX)
  DO 1000 N=1,NHMAX
    HMX=HM(N)
    ZHM= Z1/HMX
    HMX2=HMX**2
    HMX3=HMX2*HMX
    H(1)=1.+Z2/HMX
    DO 25 J=2,JF
      DZHM=(X(J)-X(J-1))*ZHM
25 H(J)=H(J-1)-DZHM
    AM=ZC2/HMX2
    HMBAR= ZC3/HMX3
C          CALCULATE DUM(J) AND GX(J)
  IF (SENSE SWITCH 1) 32,34
32 PUNCH 2, HMX,H(1), H(JC), H(JF), AM, HMBAR
34 DO 35 J=2,JD
  DX=X(J)-X(J-1)
  HTM=(H(J)+H(J-1))*0.5
  BH=1.0+DEL1 /HTM/HMX
  HTM2=HTM**2
  IF (J-JB) 37,37,36
36 FX(J)=.0
  EK2=1.
  GO TO 38
37 CALL STIFH(BH,AX,THE1,EK1,EK2)
  FX(J)= EK1/HTM2*DX*AM
38 DUM(J)=DX*EK2/HTM2/HTM*.5
35 CONTINUE
44 IF (JD-JF) 41,50,50
41 DO 45 J=JJD,JF
  DX=X(J)-X(J-1)
  HTM=(H(J)+H(J-1))*0.5
  HTM2=HTM**2

```



```

    BH=1.0+DEL2/HTM/HMX
    CALL STIFH(BH,AY,THE2,EK1,EK2)
    FX(J)=-AM *EK1/HTM2*DX
45  DUM(J)=DX*EK2/HTM2/HTM*.5
    IF (SENSE SWITCH 1) 46,50
46  PUNCH 251
251  FORMAT (11H DUM AND FX
    PUNCH 2, (DUM(J),J=1,JF)
    PUNCH 2, ( FX(J),J=1,JF)
    PUNCH 252
252  FORMAT (16H HTM BH EK1 EK2
    PUNCH 2, HTM, BH, DUM(JF), GX(JF), EK1,EK2
C
50  QC=QC1
    TEMP=(QC1-QX )/XJC
    DO 55 J=2,JC
55  Q(J)=QX +X(J)*TEMP
    QJC=Q(JC)
    IF (SENSE SWITCH 1) 54,57
54  PUNCH 2,TEMP,Q(2),QJC
57  TEMP=(QJFX-QC1)/XJFC
    DO 60 J=JJC,JF
60  Q(J)=QJC +(X(J)-XJC )*TEMP
    NCONV=1
    IT=1
    IF (SENSE SWITCH 1) 59,61
59  PUNCH 2,TEMP,Q(JJC),Q(JF)
61  SMF2=0.0
    SMG2=0.0
    DO 65 J=2,JC
    GX(J)=DUM(J)/ (0.5*(Q(J)+Q(J-1)))
67  SMF2=SMF2+FX(J)
    SMG2=SMG2+GX(J)
65  CONTINUE
    IF (SENSE SWITCH 1) 66,63
66  PUNCH 2,FX(2),FX(JB),FX(JC),SMF2,SMG2
63  SMF1=0.0
    SMG1=0.0
    DO 70 J=JJC,JF
    GX(J)=DUM(J)/ (0.5*(Q(J)+Q(J-1)))
69  SMF1=SMF1+FX(J)
70  SMG1=SMG1+GX(J)
    FM1=(SMF1-QJFX +QC)/SMG1
    FM2=(SMF2-QC +QX )/SMG2
    PXJ=QC
    P(JC)=PXJ
    IF (SENSE SWITCH 1) 72,74
72  PUNCH 2,FX(JJC),FX(JD),FX(JF),SMF1,SMG1,FM1,FM2,PXJ
74  IF (P3P2-PXJ) 77,76,75
75  SIGN=1.
    TEMP= PXJ /P3P2
    GO TO 80
76  SIGN=0.
    G=1.0
    GO TO 85
77  SIGN=-PXJ /P3P2
    TEMP= P3P2/PXJ
80  CALL GNZ (TEMP,AK,G)
85  PHI= FM1-FM2-HMBAR*P3P2*SIGN*G
    IF(IT-1) 81,81,82
81  PUNCH 86

```

```

82 PUNCH 12, QC, PXJ, PHI, IT
   ABPH=ABSF(PHI)
   IF(ABPH-EPS) 150,150,90
90 IF(IT-ITMAX) 95,170,170
95 IF(IT-1) 96,96,97
96 QC1=QC
   F1=PHI
   QC=QC+AF1*QC
   GO TO 105
97 F2=PHI
   QC2=QC
   DPHI=(F2-F1)/(QC2-QC1)
   DQC= -PHI/DPHI
   QC1=QC2
   F1=F2
   QC= QC+DQC
   IF(SENSE SWITCH 1) 104,105
104 PUNCH 11, IT, QC
105 IT=IT+1
   IF(QC-QC MAX) 107,107,106
106 QC=QC MAX
   GO TO 110
107 IF(QC MIN-QC) 110,110,108
108 QC=QC MIN
110 DO 120 J=2, JC
120 Q(J)=Q(J-1)+FX(J)-FM2*GX(J)
   DO 121 J=JJC, JF1
121 Q(J)=Q(J-1)+FX(J)-FM1*GX(J)
   DO 212 J=2, JF
   IF (Q(J)-P1P2) 211,212,212
211 Q(J)=P1P2
212 CONTINUE
   IF (SENSE SWITCH 1) 122,200
122 PUNCH 2, (Q(J), J=2, JF)
200 GO TO (61,201), NCONV
150 NCONV=2
   GO TO 110
201 SUMW=0.0
   SUMX=0.0
   DO 160 J=1, JJF, 2
   DX3=(X(J+1)-X(J))/3.0
   PY4=Q(J+1)*4.
   PJX=Q(J)
   PJ2=Q(J+2)
   SUMW=SUMW+(PJX+PY4+PJ2)*DX3
160 SUMX=SUMX+(PJX *X(J)+ PY4*X(J+1)+ PJ2*X(J+2))*DX3
   WBAR=(SUMW-P1P2)*ZP12
   XBAR=(SUMX-0.5*P1P2)*ZP12/WBAR
   PUNCH 161
   HMBAR=(1./HMBAR)**0.33333
   PUNCH 2, HMX, HMBAR, WBAR, XBAR, FM2, FM1
   PUNCH 162
   PUNCH 2, (Q(J), J=1, JF)
   FFM(N)=FM1
   XXC(N)=XBAR
   WW(N)=WBAR
   GO TO 500
170 PUNCH 171, IT
171 FORMAT(10H DIVERGE , I5)
500 CONTINUE
1000 CONTINUE

```

```

      IF( NHMAX-1)1100,1100,180
180 PUNCH 182
      PUNCH 181
      DO 190 N=1,NNH
      STIFN(N)=(WW(N+1)-WW(N))/(HM(N+1)-HM(N))
190 PUNCH 2,HM(N),WW(N),FFM(N),XXC(N),STIFN(N)
1100 CONTINUE
      IF (KS) 1111,1111,1110
1110 STOP
      1 FORMAT (10I5)
      2 FORMAT (6(1X1PE11.4))
      3 FORMAT (28H SPRIAL GROOVE-ORIFICE SEAL)
      5 FORMAT(72H VISCOSITY          SPEED      TEMP      F      GAS CONST      SPEC. HE
      1AT CONVERG. )
      6 FORMAT(72H B1/B              B3/B        B4/B          B          ORIFICE
      1RAD. DEPTH LP )
      7 FORMAT (72H P1                P2          P3            LENGTH     TILTING
      1ANGEL DEPTH HP )
      8 FORMAT(72H AF1                AF2        ANGLE HP     WIDTH HP   ANGLE
      1 LP WIDTH LP )
      11 FORMAT (13,1X1PE11.4)
      12 FORMAT (3(1X1PE11.4),5X13)
      86 FORMAT(43H QC                ORIFICE PRESS ERROR ITER. NO)
161 FORMAT (72H MEAN FILM FLOW COEF LOAD X-C M2
      1 M1 )
162 FORMAT (23H PRESSURE DISTRIBUTION )
181 FORMAT (60H MEAN FILM LOAD FLOW X-C STIFN
      1ESS )
182 FORMAT (1H1)
      END

```

APPENDIX CFORCE AND MOMENT BALANCING

1. TWO-SIDE FLOATED SHOE

The preliminary design of the shoe seal with two sides floated as shown on Figure 46, consists of a segmented ring with hydrostatic step seals as secondary sealing surfaces. The final primary seal utilizes a Rayleigh step, although the first cases were done with a hydrostatic step seal.

The geometry was arrived at by balancing the forces and moments acting on the surfaces as shown on Figure 47. The results of balancing the section are given in Table XXI. The first six cases were balanced for both take off condition (1T etc.) and cruise condition (1C, etc.). One goal was to arrive at a balanced geometry with one side flat ($b_2 = 0$), in order to simplify manufacture. A 0.50 x 0.50 inch section was the starting point (Case 1) with all dimensions assumed except b_3 and h_3 . These two dimensions were arrived at by balancing forces and moments with the use of the design curves and will be described below. After arriving at the value of 0.064 inches for h_3 for the cruise condition, using a hydrostatic step primary seal, it was evident that this would be unacceptable because one sealing face (face #7) would be only 0.024 inches long. The basic size was changed to a 0.50 x 0.60 inch section, and h_3 was found to be 0.121 inches (Case 2C). The next adjustment was to increase y_2 (in order to increase the clockwise moment) and this adjustment caused h_3 to be increased to 0.206 inches. Cases four and five were attempts to refine the dimensions, but no significant improvement over Case 3C resulted. Case 6C is a record of the dimensions used to calculate leakage flow and the dynamic tracking ability and is actually based on the results of Case 3C balancing.

This table is presented here because of the intimate connection between geometry chosen for leakage, and tracking and the moment and force balancing of the shoe. Note that a value of δ/h of less than about 0.3 is acceptable for tracking.

It was discovered that the 0.020 inches relief on the face was not accounted for on the low pressure side of the primary seal so the seal was balanced again (Table XXI, Case 7C). The balancing of Case 7C is shown below and is similar to all the Cases.

Basic Assumptions:

$$\frac{b_1}{b} = 0.35, \bar{H} = 1.00, \frac{p_1}{p_2} = 0.20$$

Summing Forces:

$$\Sigma F_V = 0 = b\bar{W}(P_2 - P_1) = b_3(P_2 - P_1)$$

$$b_3 = \bar{W}b; \bar{W} = 0.798 \text{ from Figure 17}$$

$$\therefore b_3 = (0.798)(0.48) = 0.384$$

$$\Sigma F_h = 0 = (h - y_1 - y_2 - y_3)\bar{W}(P_2 - P_1) + y_2(P_2 - P_1) - (h - y_4 - y_5)\bar{W}(P_2 - P_1) - y_4(P_2 - P_1)^*$$

$$\text{if } y_1 = y_2 = y_3 = y_4 = 0.04 \text{ and } h = 0.6$$

we have

$$0.48\bar{W} + 0.04 - (0.56 - y_5)\bar{W} - 0.04 = 0$$

$$\therefore y_5 = 0.08$$

Summing Moments:

$$h = 0.600$$

$$h_1 = 0.200$$

$$h_2 = 0.400$$

$$y_1 = y_2 = y_3 = y_4 = 0.04$$

$$y_5 = 0.08$$

$$b = 0.480$$

$$b_2 = 0$$

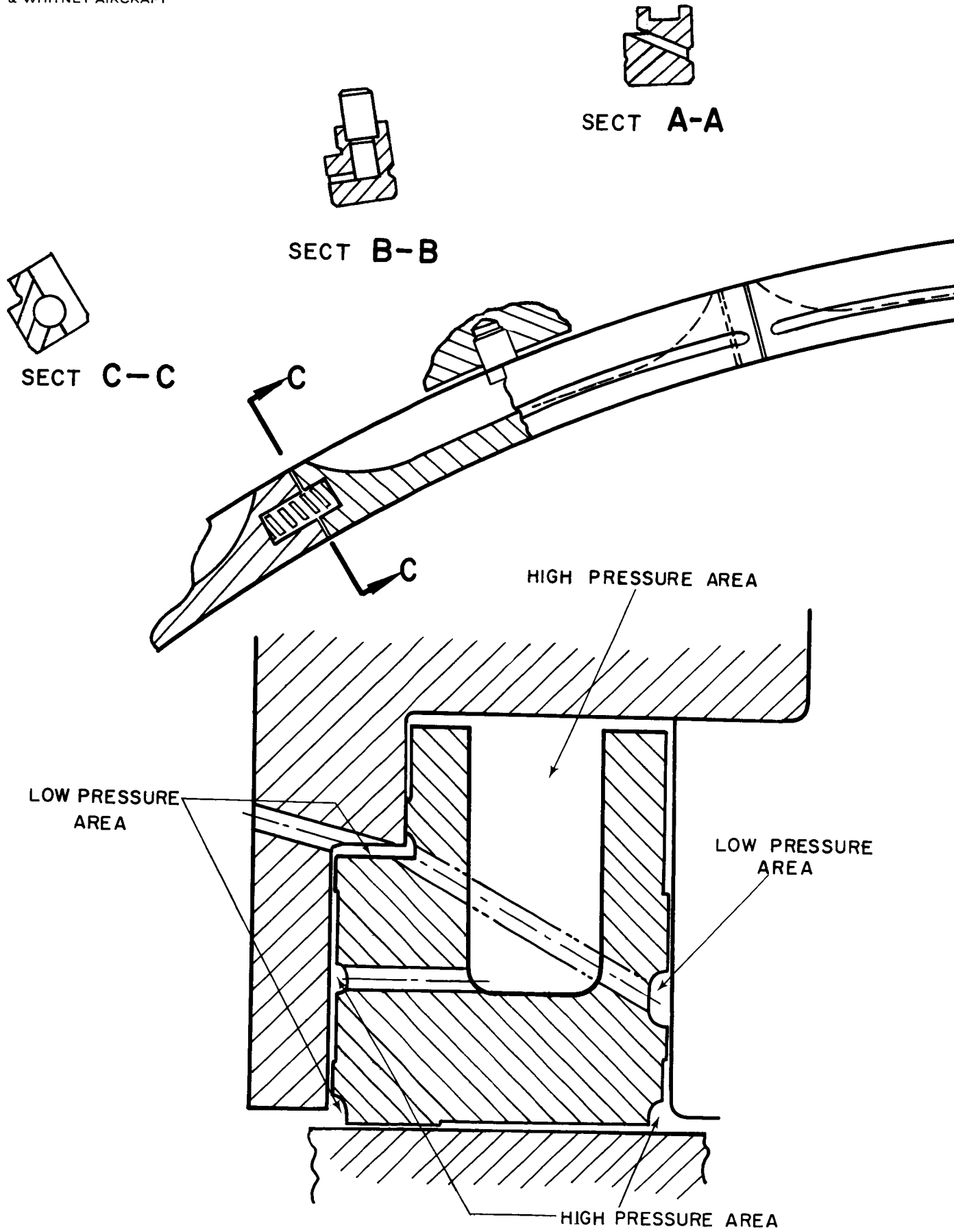
$$b_3 = 0.384$$

Solve for h_3

$$\text{Using: Center of Pressure } \bar{X} = X_{C/b} = 0.426$$

$$\text{Pressure Load } \bar{W} = W/(P_2 - P_1)b = 0.798$$

*Please see Figure 47 for proper interpretation of h , b , and y values used in this Appendix. Note that h and b assume different definitions, according to the figure, then used elsewhere in this report.



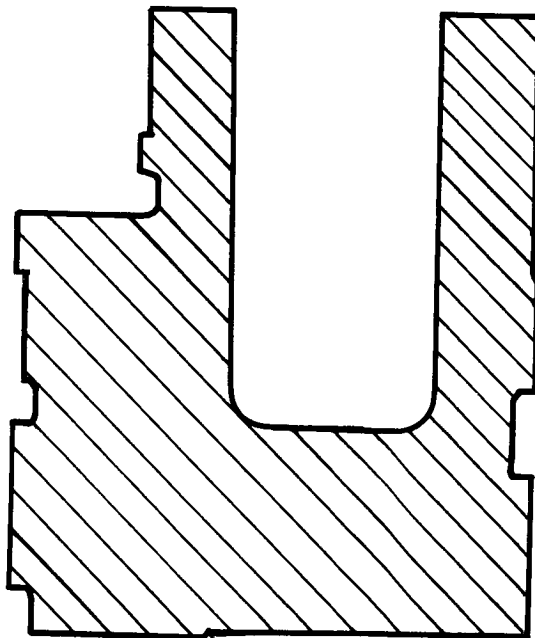
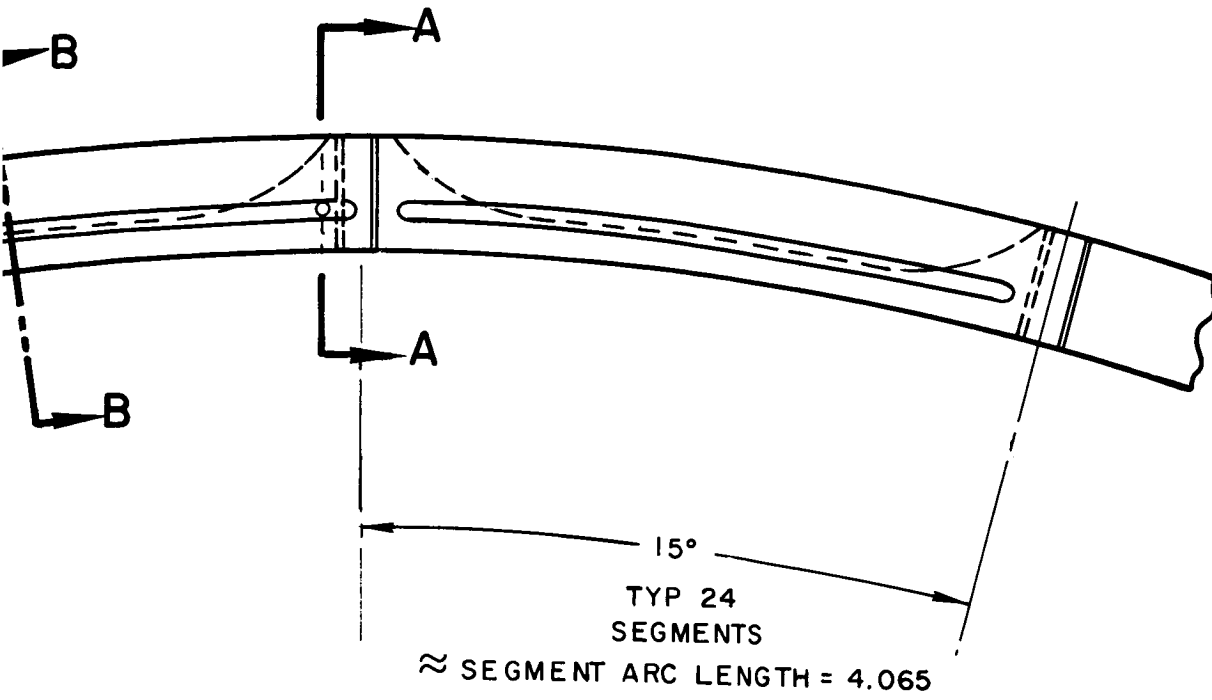
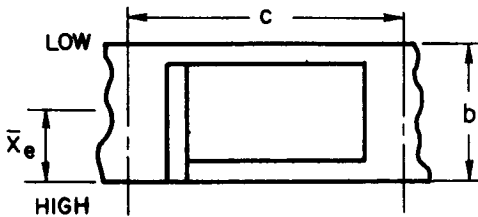


Figure 46 Preliminary Design of Two-Side Floated Shoe Seal

SEAL BALANCING

DIMENSIONLESS QUANTITIES

	\bar{b}_1	\bar{H}	R	\bar{W}	\bar{X}	h	b	b_1	b_2	b_3	n_1
1T	.35	1.00	.118	.810	.431	.500	.500	.175	0	.405	.170
1C	.35	1.00	.20	.798	.426	.500	.500	.175	0	.399	.170
2T	.35	1.00	.118	.810	.431	.600	.500	.175	0	.405	.170
2C	.35	1.00	.20	.798	.426	.600	.500	.175	0	.405	.170
3T	.35	1.00	.118	.810	.431	.600	.500	.175	0	.405	.200
3C	.35	1.00	.20	.798	.426	.600	.500	.175	0	.405	.200
4T	.35	1.00	.118	.810	.431	.600	.500	.175	0	.400	
4C	.35	1.00	.20	.798	.426	.600	.500	.175	0	.400	
5T	.35	1.00	.118	.810	.431	.700	.500	.175	0	.400	.230
5C	.35	1.00	.20	.798	.426	.700	.500	.175	0	.400	.230
6T	.35	1.00	.118	.810	.431	.600	.480	.168	0	.400	.200
6C	.35	1.00	.20	.798	.426	.600	.480	.168	0	.400	.200
7C	.35	1.00	.20	.798	.426	.600	.480	.168	0	.384	.200
8C (2-21-66)	.35	1.00	.20	.800	.426	.660	.480	.168	0	.384	.240
9C (2-21-66)	.35	1.00	.20	.800	.426	.640	.480	.168	0	.384	.220
10C (2-21-66)	.35	1.00	.20	.800	.426	.700	.480	.168	0	.384	.220
11C (2-21-66)	.35	1.00	.20	.800	.426	.700	.480	.168	0	.384	.210
12C (2-21-66)	.35	1.00	.20	.800	.426	.700	.480	.168	0	.384	.240
13C (2-21-66)	.35	1.00	.20	.800	.426	.700	.480	.168	0	.384	.200
14C (2-21-66)	.35	1.00	.20	.800	.426	.720	.480	.168	0	.384	.300
15C (2-21-66)	.35	1.00	.20	.800	.426	.750	.480	.168	0	.384	.360
16C (2-22-66)	.35	1.00	.20	.800	.426	.660	.480	.168	0	.384	.220
17C (2-22-66)	.35	1.00	.20	.800	.426	.660	.480	.168	.041	.384	.220
18C (2-22-66)	.35	1.00	.20	.800	.426	.750	.480	.168	0	.384	.220
19C (2-22-66)	.35	1.00	.20	.800	.426	.800	.480	.168	0	.384	.220



BALANCE USING RAYLEIGH-STEP SEAL ON PRIMARY SURFACE & HYDROSTATIC STEP ON ALL C

	c/b	h_1' (FILM)	\bar{W}_R	\bar{X}_R	\bar{W}_H	\bar{X}_H	h	b	b_1	b_2	b_3	n_1
20C	2.125	.001	.802	.432	.800	.426	.690	.480	---	0	.386	.23
21C	2.125	.001	.802	.432	.800	.426	.750	.480	---	0	.386	.25
22C	2.125	.001	.802	.432	.800	.426	.800	.480	---	0	.386	.22

FINAL GEOMETRY OF CASES 19C and 22C ARE IDENTICAL - EXCEPT FOR DIM b_3 AND CASE 22C USES RAYLEIGH STEP ON PRIMARY SEALING SURFACE.

TABLE XXI

FOR TWO-SIDE FLOATED SHOE SEAL

ENSIONS

CENTERS OF PRESSURE

h_2	h_3	y_1	y_2	y_3	y_4	y_5	C_{p1}	C_{p2}	C_{p3}	C_{p4}	C_{p5}	C_{p6}	C_{p7}	C_{p8}
.330	.096	.04	.03	.04	.04	.082	.216	.114	.256	.444	.2025	.361	.081	.02
.330	.064	.04	.03	.04	.04	.082	.213	.115	.255	.445	.1995	.349	.050	.02
.330	.185	.04	.03	.04	.04	.082	.216	.114	.256	.501	.2025	.457	.102	.02
.330	.121	.04	.03	.04	.04	.082	.213	.115	.255	.502	.2025	.431	.092	.02
.400	.149	.04	.04	.04	.04	.080	.216	.131	.309	.531	.2025	.340	.087	.02
.400	.206	.04	.04	.04	.04	.080	.213	.132	.308	.532	.2025	.466	.111	.02
.400	.200	.04	.04	.04	.04	.080	.216	.187	.365	.531	.200	.462	.109	.02
.400	.200	.04	.04	.04	.04	.080	.213	.213	.389	.532	.200	.464	.108	.02
.460	.307	.04	.04	.05	.04	.090	.216	.148	.352	.618	.200	.585	.155	.02
.460	.391	.04	.04	.05	.04	.090	.213	.149	.351	.619	.200	.603	.189	.02
.400	.200	.04	.04	.04	.04	.080	.2069	.131	.309	.531	.200	.462	.109	.02
.400	.200	.04	.04	.04	.04	.080	.2044	.132	.308	.532	.200	.464	.108	.02
.400	.153	.04	.04	.04	.04	.080	.2044	.132	.308	.532	.192	.444	.088	.02
.480	.101	.100	.100	.04	.100	.140	.2044	.180	.400	.600	.192			.05
.440	.118	.100	.100	.08	.100	.180	.2044	.169	.379	.589	.192			.05
.440	.172	.100	.100	.140	.100	.240	.2044	.169	.379	.649	.192			.05
.420	.173	.100	.100	.170	.100	.270								
.470	.160	.100	.100	.100	.100	.200								
.480	.158	.100	.100	.100	.100	.200						.601	.171	
.520	.155	.100	.100	.100	.100	.180								
.580	.080	.100	.100	.050	.100	.150								
.440	.083	.100	.100	.120	.100	.220								
.440	.220	.100	.100	.100	.100	.200								
.440	.194	.100	.100	.190	.100	.290								
.440	.212	.100	.100	.240	.100	.340								

OTHERS

.460	.146	.100	.100	.100	.100	.200
.500	.156	.100	.100	.100	.100	.200
.440	.212	.100	.100	.240	.100	.340

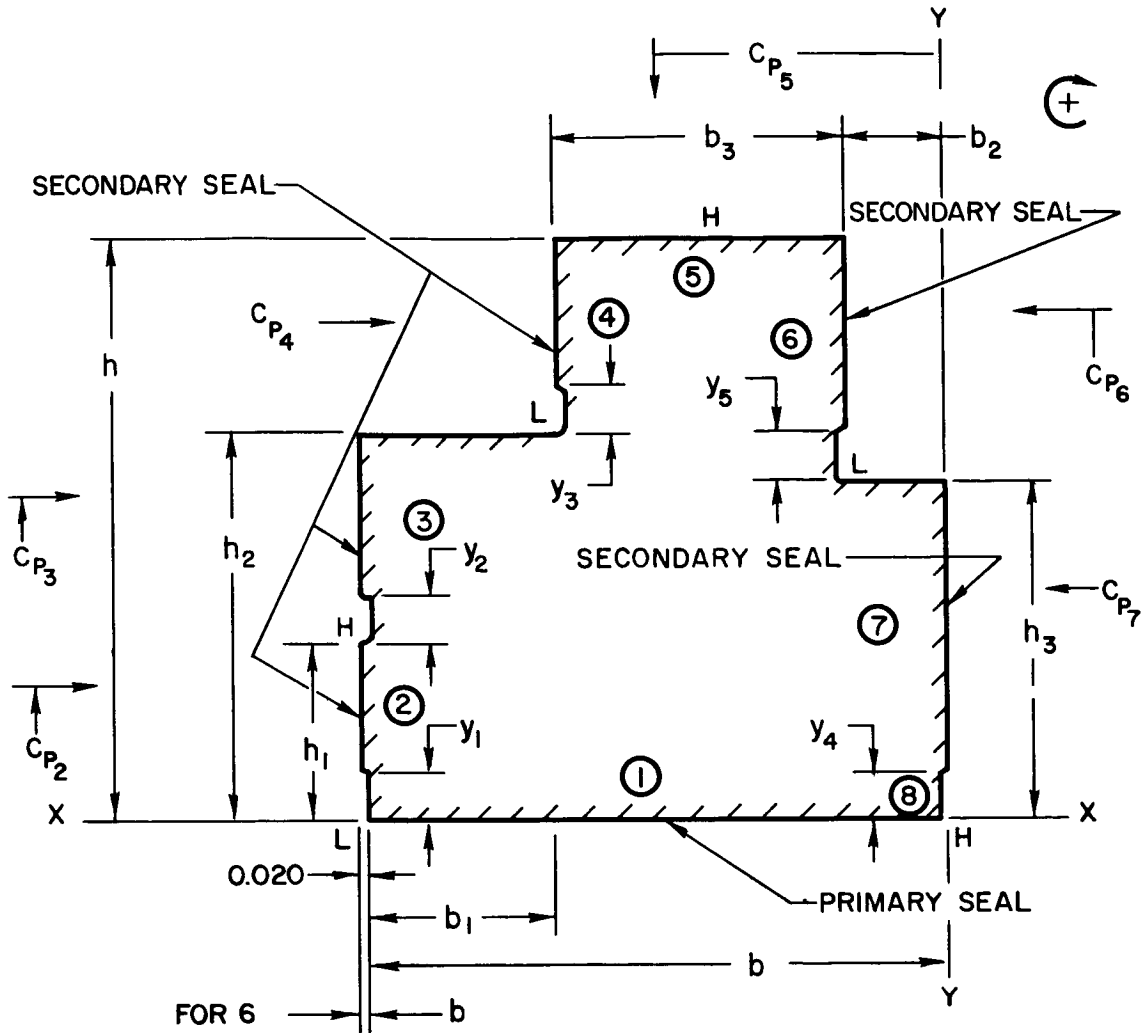


Figure 47 Force and Moment Balancing of Two-Side Floated Shoe Seal

Summing moments about lower righthand corner:

$$\begin{aligned} \Sigma M = 0 = & (\bar{X}b) [\bar{W}b(p_2 - p_1)] + [h_1 - \bar{X}(h_1 - y_1)] [\bar{W}(h_1 - y_1)(p_2 - p_1)] + (h_1 + \frac{y_2}{2}) [y_2(p_2 - p_1)] \\ & + [h_1 + y_2 + \bar{X}(h_2 - h_1 - y_2)] [\bar{W}(h_2 - h_1 - y_2)(p_2 - p_1)] + [h - \bar{X}(h - h_2 - y_3)] \\ & [\bar{W}(h - h_2 - y_3)(p_2 - p_1)] - (\frac{b_3}{2}) b_3 (p_2 - p_1) - [h - \bar{X}(h - h_3 - y_5)] [\bar{W}(h - h_3 - y_5)(p_2 - p_1)] \\ & - [y_4 + \bar{X}(h_3 - y_4)] [\bar{W}(h_3 - y_4)(p_2 - p_1)] - [(\frac{y_4}{2}) y_4 (p_2 - p_1)] \end{aligned}$$

$$\Sigma M = 0 = (0.2044)(0.384) + (0.132)(0.1276) + (0.22)(0.04) + (0.308)(0.1276) + (0.532)(0.1276) - (0.192)(0.384) - [0.60 - 0.426(0.52 - h_3)] [(0.52 - h_3) 0.798] - [0.04 + 0.426(h_3 - 0.04)] [0.798(h_3 - 0.04) - (0.02)(0.04)]$$

$$h_3 = 0.153$$

After the seal had been balanced (Table XXI, Case 7C), the new dimensions were used to calculate leakage flows and tracking ability. The results are presented as Cases J, K, & L in Table XXI.

The hydrostatic step primary seal was eventually discarded in favor of the shrouded Rayleigh step configuration. These cases were evaluated with the results being shown as Cases 20C through 22C on Table XXI and as Case N of Table XXII.

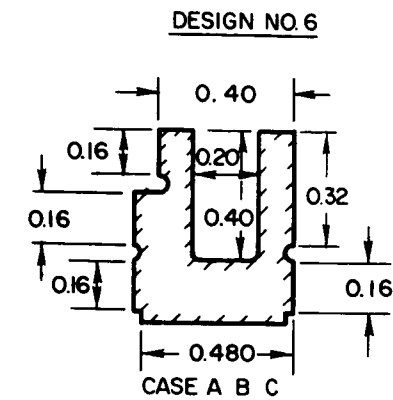
2. ONE-SIDE FLOATED SHOE

The same methods were used to balance the force and moments for this concept as were used for the two-side floated shoe seal. Referring to the sketch on Table XXIII, it will be noted that the only required adjustments are in dimensions b_x and h_1 (or h_4). Preselected values can be used for all dimensions.

Room must be provided between the inner lip of the runner and the shoulder of the b_x extension to allow radial movement of up to about 0.1 inch. This is accounted for in the preselection of h . Likewise, provision must be made to allow the shoe to slip axially under the seal ring. This requires that a slight overhang be provided on the shoe for the purpose. Some clearance room is also required between the carrier lip and the seal ring extension, but this movement is small and is easily preselected.

Table XXIII shows the results of the balancing. Only Cases 3C and 4C are for the Rayleigh step primary seal. There is a small difference in dimensions between the end seal (3C) and the interstage seals (4C).

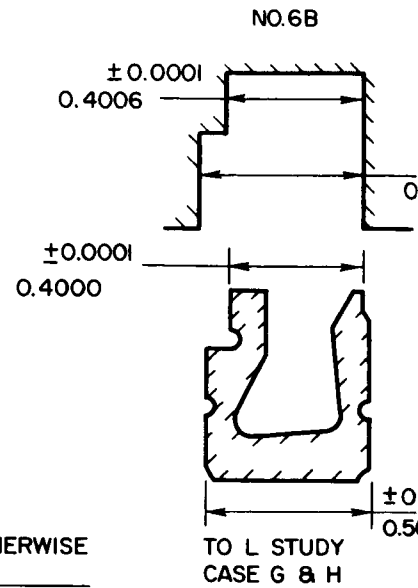
The secondary seal ring is balanced only in the radial direction. High pressure exists across the top, but that on the surface next to the shoe varies from high to low. Therefore, the interface surface is longer than the top surface. Axial balancing is only partial. There is high pressure across the whole face on the seal spring-side, but it varies from high to low on the side that seals against the carrier.



m SOLID = 0.0553
 m₆ = 0.0496
 m_{6A} = 0.0471



REDUCED MASS OTHERWISE
 SAME AS NO. 6
 CASE D E F

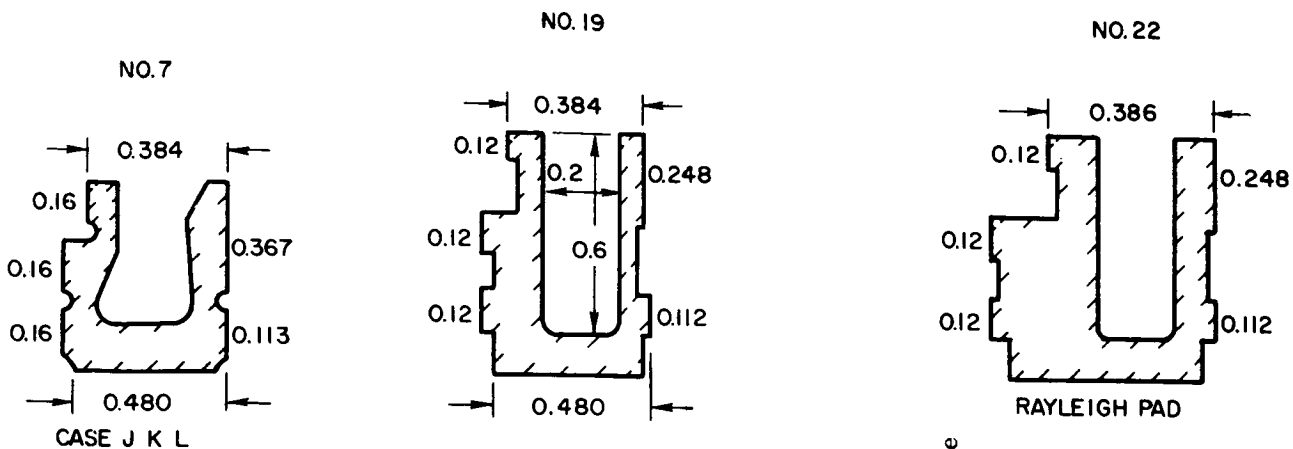


Primary

Case	Description	\bar{W}	\bar{H}	$\frac{h_2 - h_1}{\text{MILS}}$	h_1 MILS
A	End Seal (#6) Cruise Nominal	.798	1.00	1.0	1.0
B	End Seal (#6) Takeoff - Nominal	.810	1.00	1.0	1.0
C	Interstage Seal-Cruise-Nominal	.771	1.00	1.0	1.0
D	Interstage Seal-Cruise-Nominal-Reduced Mass 6A				
E	Interstage Seal-Cruise-Nominal-Increased Film 6A	.705	2.00	1.0	2.0
F	Interstage Seal-Cruise-Nominal-Increased Film 6A	.771	1.00	2.0	2.0
G	End Seal (6B) Cruise-Maximum Flow Cond.	.757	1.560	0.9	1.4
H	End Seal (6B) Cruise-Maximum δ/h Condition	.840	.545	1.1	.6
J	End Seal (7) Cruise-Nominal	.800	.98	1.0	.98
K	End Seal (7) Cruise-Maximum Flow	.797	1.00	1.1	1.10
L	End Seal (7) Cruise-Minimum Flow	.803	.96	.9	.86
M	End Seal (#9) Cruise Nominal	.800	.98	1.0	.98
N	Interstage Seal (#22) Cruise Cond.	.802	--	---	1.00

TABLE XXII

SEAL PARAMETERS



±0.0001
5006

.0001
000

Seal

Secondary Seal

Total Flow
Leakage
not including
segment leakage

R	(P ₂ -P ₁) PSI	\bar{M}	M LB/SEC-IN.	\bar{H}	h_2-h_1 MILS	h_1 MILS	\bar{M}	M LB/SEC-IN.	M _T LBM/SEC	\bar{K}_s	m LB/IN.	δ/f_m	δ/h	h_1 MIN MILS
.200	80	2.22	.3x10 ⁻³	1.00	.3	.3	2.22	.103x10 ⁻³	.035	.082	.0553	.033	.264	.74
.120	150	2.28	1.32x10 ⁻³	1.00	.3	.3	2.28	.61x10 ⁻³	.148					
.445	25	1.85	.05x10 ⁻³	1.00	.3	.3	1.85	.02x10 ⁻³	.006	.095	.0553	.09	.720	.28
										.095	.0471	.077	.640	.36
.445	25	1.45	.31x10 ⁻³	1.00	.3	.3	1.85	.02x10 ⁻³	.035	.050	.0471	.15	.60	.80
.445	25	1.56	.33x10 ⁻³	1.00	.3	.3	1.85	.02x10 ⁻³	.036	.095	.0471	.16	.64	.72
.200	80	1.97	.73x10 ⁻³	2.00	.2	.4	1.80	.20x10 ⁻³	.065	.060	.0471	.035	.200	.72
.200	80	2.60	.076x10 ⁻³	.50	.4	.2	2.64	.036x10 ⁻³	.010	.082	.0471	.031	.41	.66
.200	80	2.24	.31x10 ⁻³	1.00	.3	.3	2.22	.11x10 ⁻³	.030	.082	.0471	.028	.240	.76
.200	80	2.23	.922x10 ⁻³	2.00	.2	.4	1.77	.19x10 ⁻³	.060	.083	.0471	.030	.240	.84
.200	80	2.25	.21x10 ⁻³	.50	.4	.2	2.55	.04x10 ⁻³	.020	.081	.0471		.252	.67
.200	80	2.24	.31x10 ⁻³	1.00	.3	.3	2.22	.141x10 ⁻³	.038	.082	.0638	.04	.320	.67
.445	25	$\bar{Q}=1.12$.84x10 ⁻³	1.00	.3	.3	2.22	.141x10 ⁻³	.072	.244	.0638	.044	.352	.65
			per step											

E XXIII

One-Side Floated Shoe Seal

b_x	h_1	h_2	h_3	F_{s1}	h	C_{p1}	C_{p2}	C_{p3}	C_{p4}	C_{p5}	C_{p6}	C_{p7}	C_{p8}
053	.374	.50	.10	2#/in.	.6	.115	.30	.485	.276	.413	.517	.253	.387
044	.374	.50	.10	2#/in.	.6	.115	.35	.544	.276	.413			.387
0502	.376	.50	.10	2#/in.	.6	.115	.30	.485	.254	.412	.517		.384
074	.312	.50	.10	2#/in.	.6	.115	.30	.485	.338	.444	.544		.373

Moment balancing is not required on the secondary seal ring because it will not easily turn around its circumferential axis, being a continuous ring except for one split. Radially and axially the seal ring is quite flexible. Therefore, it can be expected to conform to the surfaces against which it rides.

The force and moment balance equations are given below for the one side floated shoe seal Case 4C in Table XXIII ($P_1/P_2 = 0.445$).

Vertical force balance

$$\sum F_V = 0 = b_4 (P_2 - P_1) + b_5 (P_2 - P_1) \bar{W} - (b_1 + b_3) \bar{W} (P_2 - P_1) - b_2 (P_2 - P_1)$$

$$\begin{aligned} \text{check } \bar{W} \text{ using} \quad b_1 &= 0.20 \\ b_2 &= 0.20 \\ b_3 &= 0.20 \\ b_4 &= 0.40 \\ b_5 &= 0.150 \end{aligned}$$

$$\therefore 0.40 + 0.15 \bar{W} - 0.2 - 0.4 \bar{W} = 0$$

$$\bar{W} = \frac{0.20}{0.25} = 0.80$$

For hydrostatic step seals with $\bar{W} = 0.8$, $\bar{b}_1 = 0.35$, and $r_{12} = \frac{P_1}{P_2} = 0.445$,

we find that $\bar{H} = 0.7$ from Figure 48. From Figure 49, then, it can be seen that $\bar{X} = 0.424$.

Summing horizontal forces,

$$\sum F_h = 0 = h_1 (P_2 - P_1) + F_{S1} - \bar{W} (h_2) (P_2 - P_1)$$

using $(P_2 - P_1) = 25$ pounds per square inch

$F_{S1} = 2$ pounds per inch of circumference

$\bar{W} = 0.785$ (Rayleigh Step)

$h_1 = 0.312$ inches (from Table XXIII)

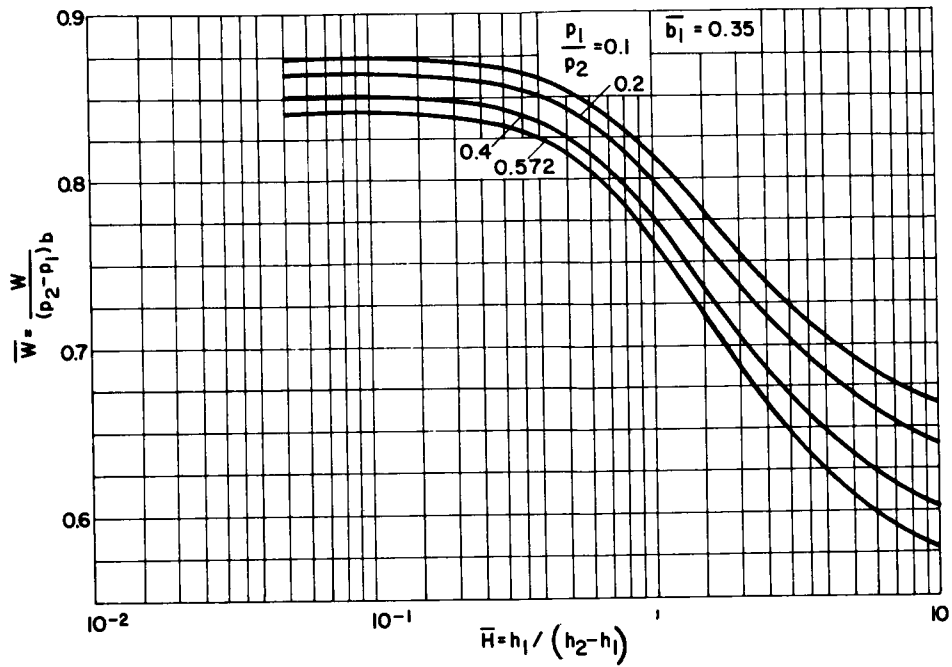


Figure 48 Load Curve for Hydrostatic Step Seal, $\bar{b}_1 = 0.35$

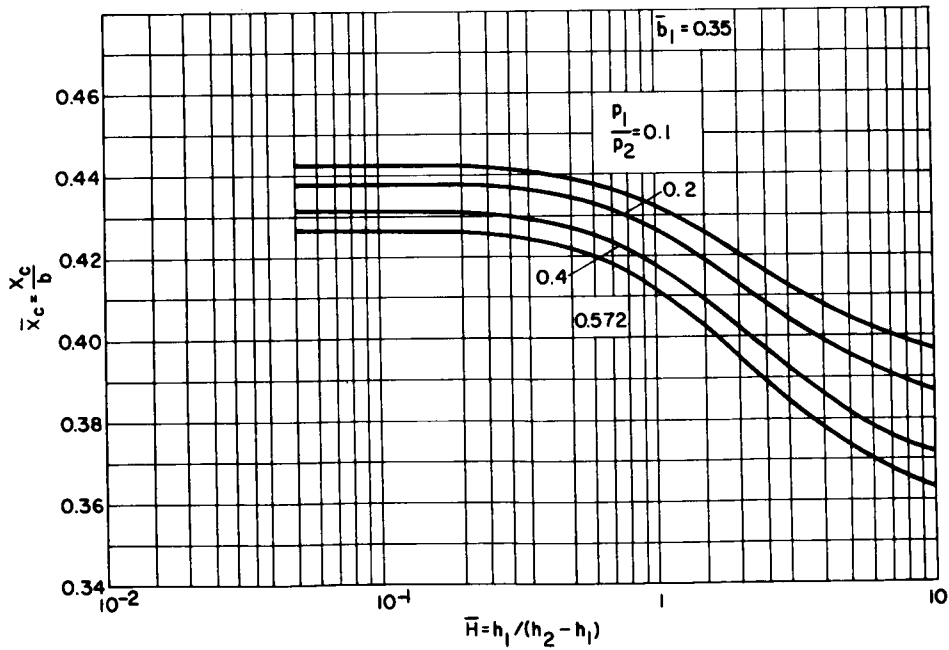


Figure 49 Center of Pressure for Hydrostatic Step Seal, $\bar{b}_1 = 0.35$

Summing moments,

$$\begin{aligned} \Sigma M = 0 = & (C_{p1}) \bar{W} b_3 (P_2 - P_1) + C_{p2} b_2 (P_2 - P_1) \\ & + (C_{p3}) \bar{W} b_1 (P_2 - P_1) + (C_{p4}) F_{s1} + (C_{p5}) h_1 (P_2 - P_1) \\ & - (b_x + b_4 + \bar{X} b_5) \bar{W} b_5 (P_2 - P_1) - \left(\frac{b_4}{2} + b_x \right) b_4 (P_2 - P_1) \\ & - (C_{p8}) \bar{W} h_2 \end{aligned}$$

Solving for b_x we have

$$b_x = 0.074$$

APPENDIX DTHERMAL ANALYSIS OF THE TWO-SIDE FLOATED SHOE SEAL

1. SCOPE

The purpose of the thermal analysis on the two-sided floated shoe seal reported in this appendix is to determine the temperature distribution and consequent thermal distortions, and to recommend certain material properties and design geometries. The thermal analysis and resulting temperature distributions are recorded here.

Steady-state operating conditions were assumed which could be expected during normal flight. Seal block locations were central with respect to the runner. Three temperature regimes were examined:

- (1) 100 pounds per square inch absolute at air delivery and 20 pounds per square inch absolute at the machine core, air and housing temperatures at 1200 degrees Fahrenheit throughout.
- (2) The same air pressures and temperatures as in (1), except a compressor core temperature of 1300 degrees Fahrenheit
- (3) The same air pressures and temperatures as in (1), except a compressor core temperature of 1100 degrees Fahrenheit.

Two thermal conductivities of Inconel-X were considered:

- (1) A conductivity of $7.1 \text{ BTU/hr ft}^2 \text{ }^\circ\text{F}$ representing a cold startup condition.
- (2) The normal high temperature conductivity of $13.0 \text{ BTU/hr ft}^2 \text{ }^\circ\text{F}$ (at 1000 to 1200 degrees Fahrenheit).

The inclusion of thermal shunts to effect more even temperature distribution was investigated. In each case the effective thermal conductivity of the affected component was raised to $26.0 \text{ BTU/hr ft}^2 \text{ }^\circ\text{F}$. Thermal shunts were considered separately in the runner (entire flange facing seal block) and in the seal block (entire block).

This appendix includes also a brief description of the numerical methods involved, details of air flow and heat generation in the gaps surrounding the seal block, and an outline of surface coefficient calculations.

2. RESULTS OF THE THERMAL ANALYSIS

The temperature distributions in the two-sided floated shoe seal are summarized in Figures 50 to 58. The temperatures are given in degrees Fahrenheit. The subvolumes surrounding the nodal points are not shown. The properties of the Inconel X (seal assembly material), the thermal shunts, and the air are given in Table XXIV.

The boundary conditions are defined as 1200 degrees Fahrenheit on the seal holder surface in the delivery duct, in the support adjacent to the seal holder, and in the runner support in contact with the last stage disk. The prescribed air temperatures were 1200 degrees Fahrenheit on the high pressure side, and 1200, 1300, and 1100 degrees Fahrenheit on the low pressure side for the three cases of compressor core temperature investigated.

Figures 50 to 52 present temperatures in the seal assemblies on 1200, 1300 and 1100 degrees Fahrenheit core machines respectively. The thermal conductivities of all components are $7.1 \text{ BTU/hr. ft}^2 \text{ }^\circ\text{F/ft}$. This represents the most adverse case considered.

Figure 53 shows that the temperature distribution of the thermal conductivity is $13.0 \text{ BTU/hr ft}^2 \text{ }^\circ\text{F/ft}$ throughout the seal assembly.

The temperature distributions in the components of the seal assembly are an indication of the severity of the thermal distortions to be expected. Although an increase in the thermal conductivity of the assembly material from $7.1 \text{ BTU/hr ft}^2 \text{ }^\circ\text{F}$ to $13.0 \text{ BTU/hr ft}^2 \text{ }^\circ\text{F}$ effected some improvements, the desirability of further raising the thermal conductivity is apparent. The effect of a thermal shunt in the runner is presented in Figures 54 and 55, and in the seal block in Figures 56 to 58. "Thermal shunt" means the inclusion of a more highly conducting material like beryllium copper or silver to form a sandwich structure, or by vacuum impregnation of silver into the component part. The purpose of the shunt is to reduce temperature gradients. In this analysis, no geometries of the inclusions are presented, but their effects were evaluated by making the thermal conductivity of the affected component twice that of Inconel-X at high temperature: $26.0 \text{ BTU/hr ft}^2 \text{ }^\circ\text{F}$. In all other components of the seal assembly, the thermal conductivity remained at $13.0 \text{ BTU/hr ft}^2 \text{ }^\circ\text{F}$. In the above figures, core temperatures of 1200, 1300 and 1100 degrees Fahrenheit are indicated in the captions. Off-center running of the seal blocks and runner were found to increase temperature inequalities, which is undesirable because of consequent thermal distortion. This factor imposes some additional operating constraints during transients.

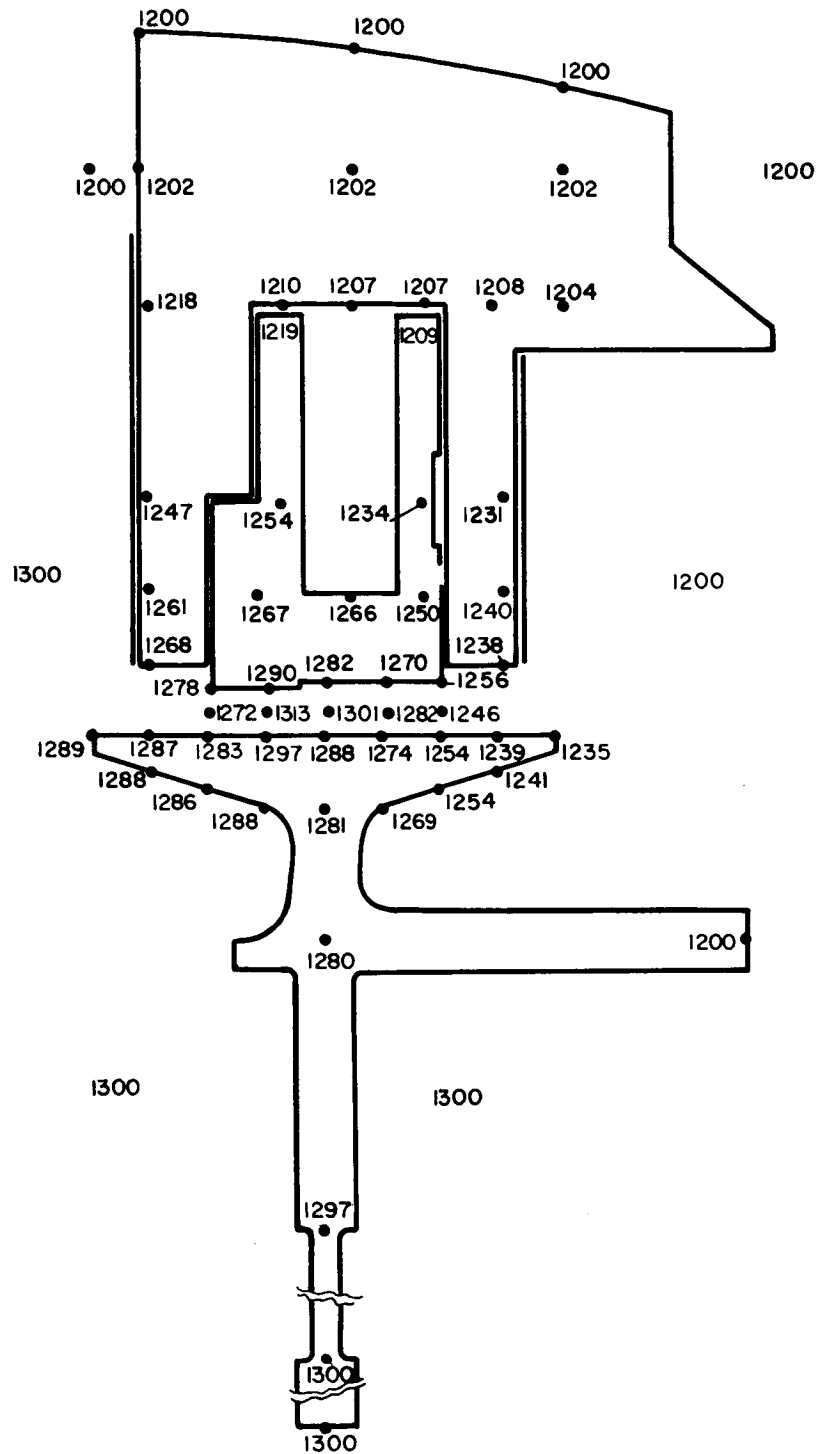


Figure 51 Temperature Distribution in Two-Side Floated Shoe Seal. Thermal Conductivity 7.1 BTU/hr. ft.²°F/ft. throughout, 1300°F Core Machine. Temperatures Shown in °F.

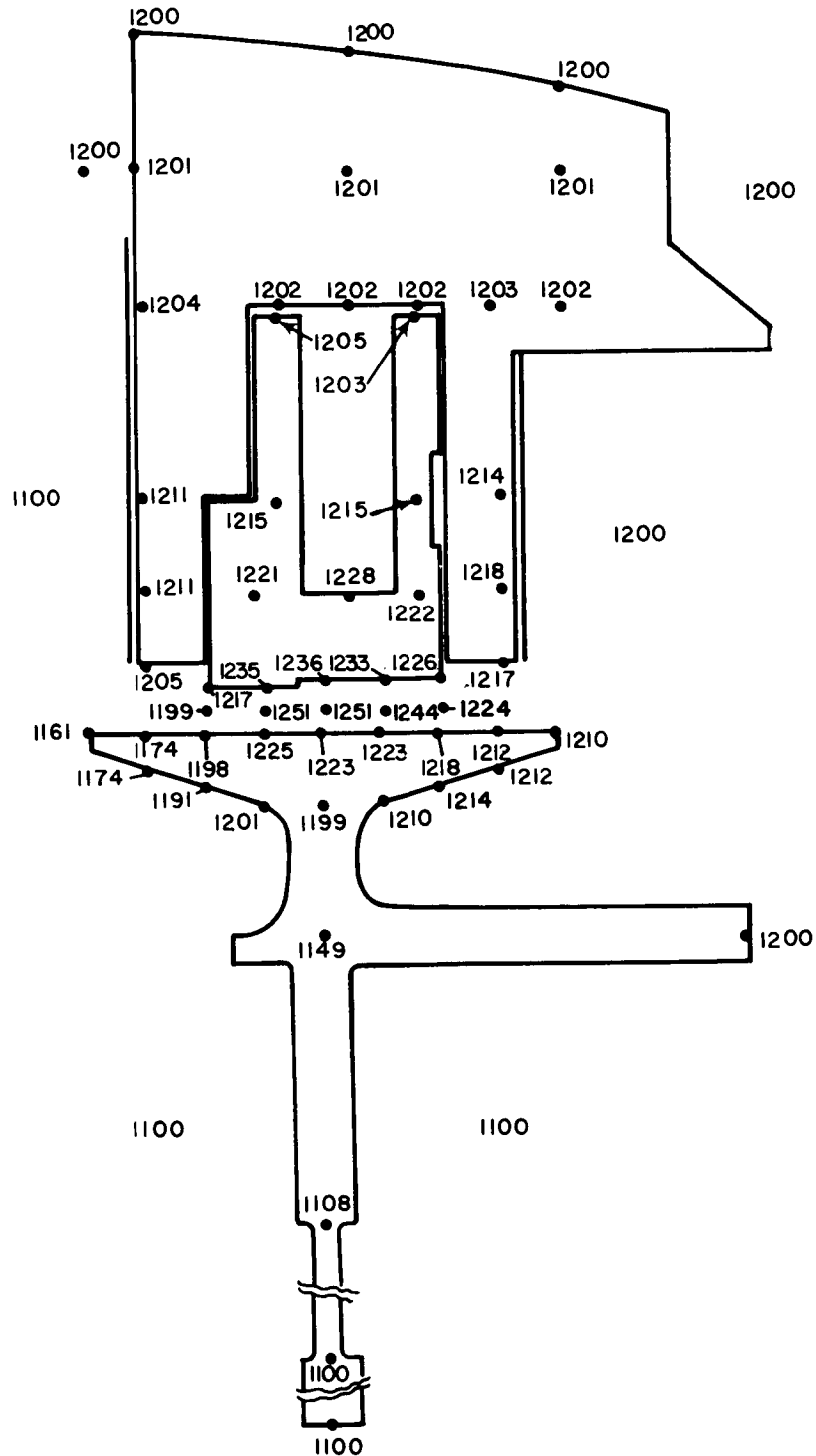


Figure 52 Temperature Distribution in Two-Side Floated Shoe Seal. Thermal Conductivity 7.1 BTU/hr. ft.² °F/ft. throughout, 1100°F Core Machine. Temperatures Shown in °F.

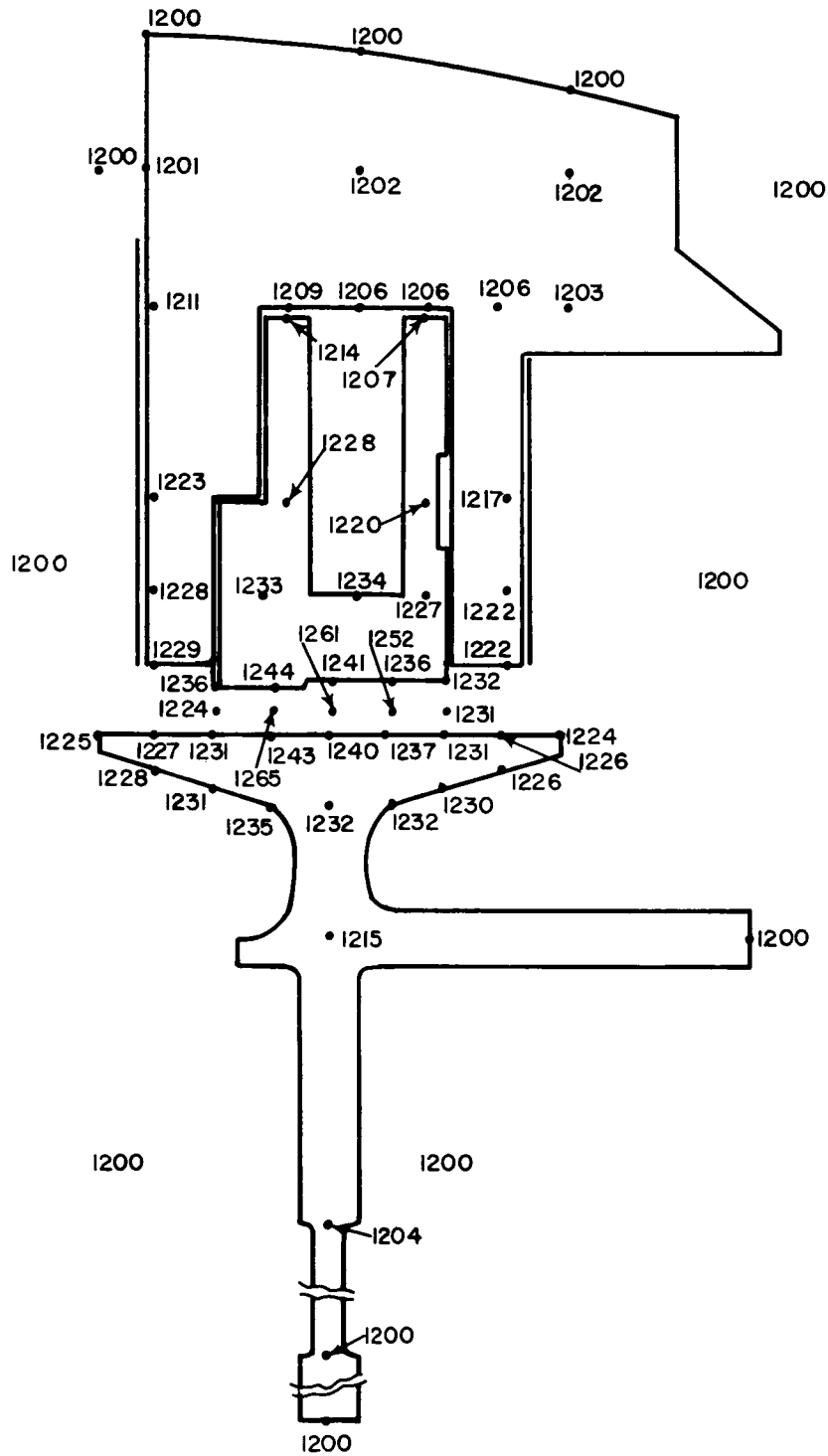


Figure 53 Temperature Distribution in Two-Side Floated Shoe Seal. Thermal Conductivity 13.0 BUT/hr. ft.² °F/ft. throughout, 1200°F Core Machine. Temperatures Shown in °F.

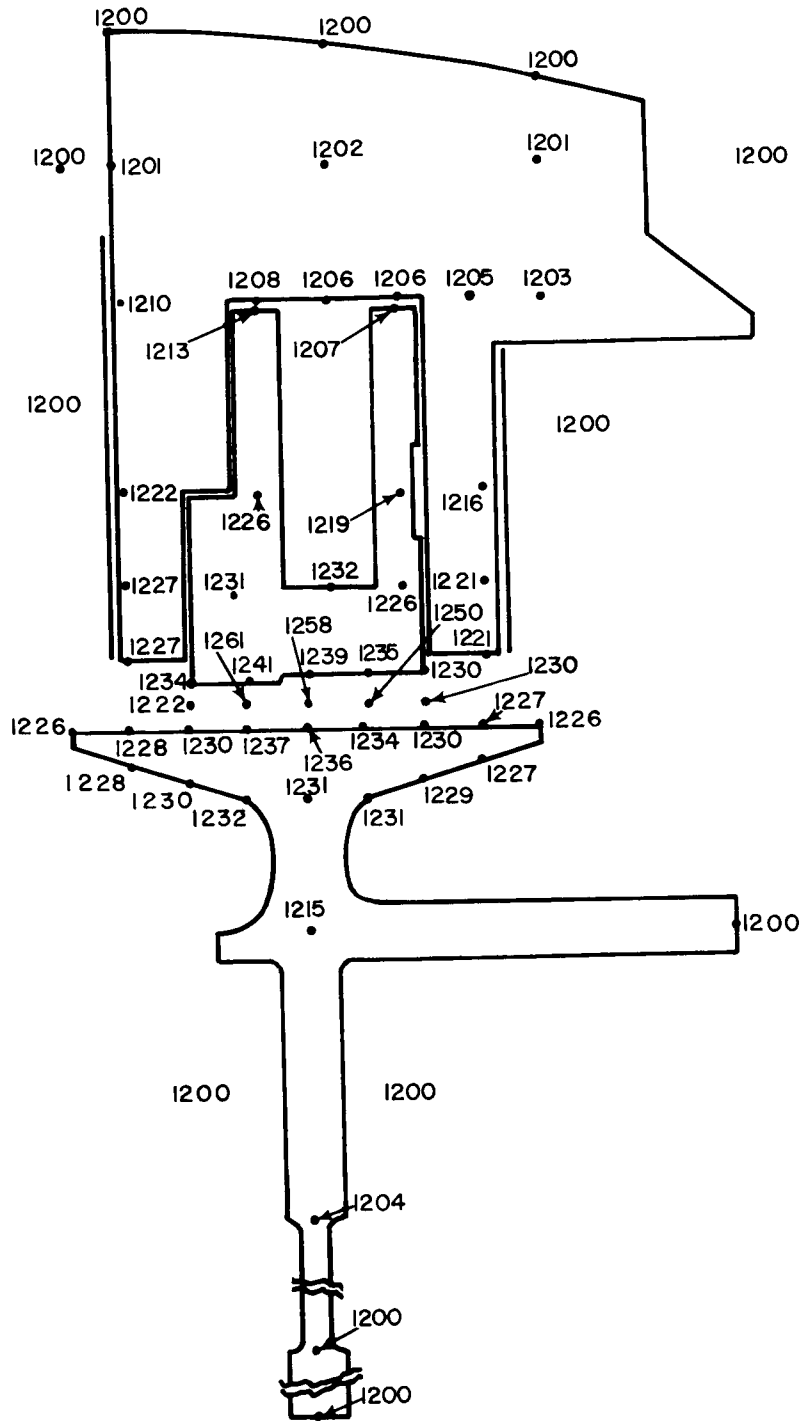


Figure 54 Temperature Distribution in Two-Side Floated Shoe Seal with Thermal Shunt in Runner. Thermal Conductivities 26.0 BTU/hr. ft. ² °F/ft. in Shunt, 13.0 BTU/hr. ft. ² °F/ft. elsewhere; 1200°F Core Machine. Temperature Shown in °F.

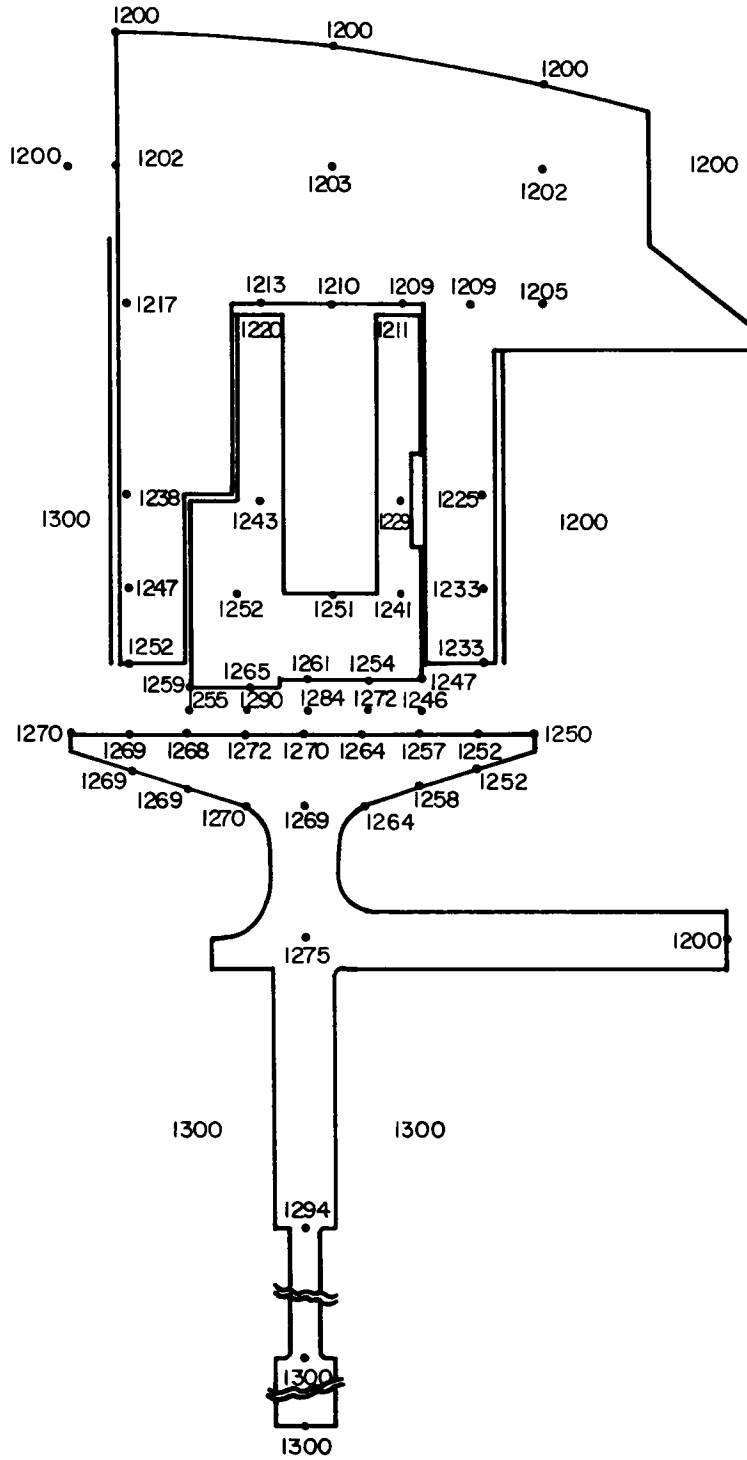


Figure 55 Temperature Distribution in Two-Side Floated Shoe Seal with Thermal Shunt in Runner. Thermal Conductivities 26.0 BTU/hr. ft.² °F/ft. in Shunt, 13.0 BTU/hr. ft.² °F/ft. elsewhere; 1300°F Core Machine. Temperatures Shown in °F.

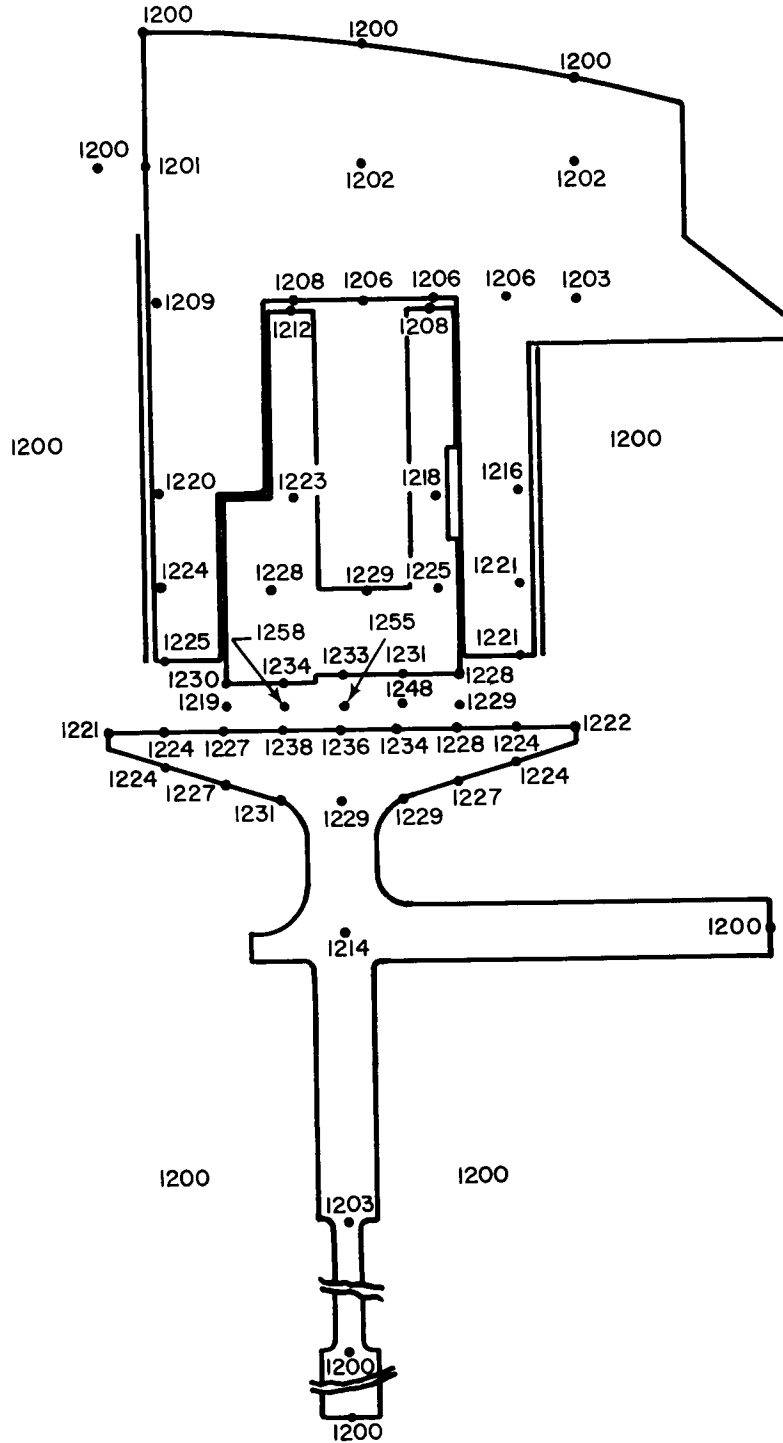


Figure 56 Temperature Distribution in Two-Side Floated Shoe Seal with Thermal Shunt in Seal Block. Thermal Conductivities 26.0 BTU/hr. ft.²°F/ft. in Shunt, 13.0 BTU/hr. ft.²°F/ft. elsewhere; 1200°F Core Machine. Temperatures Shown in °F.

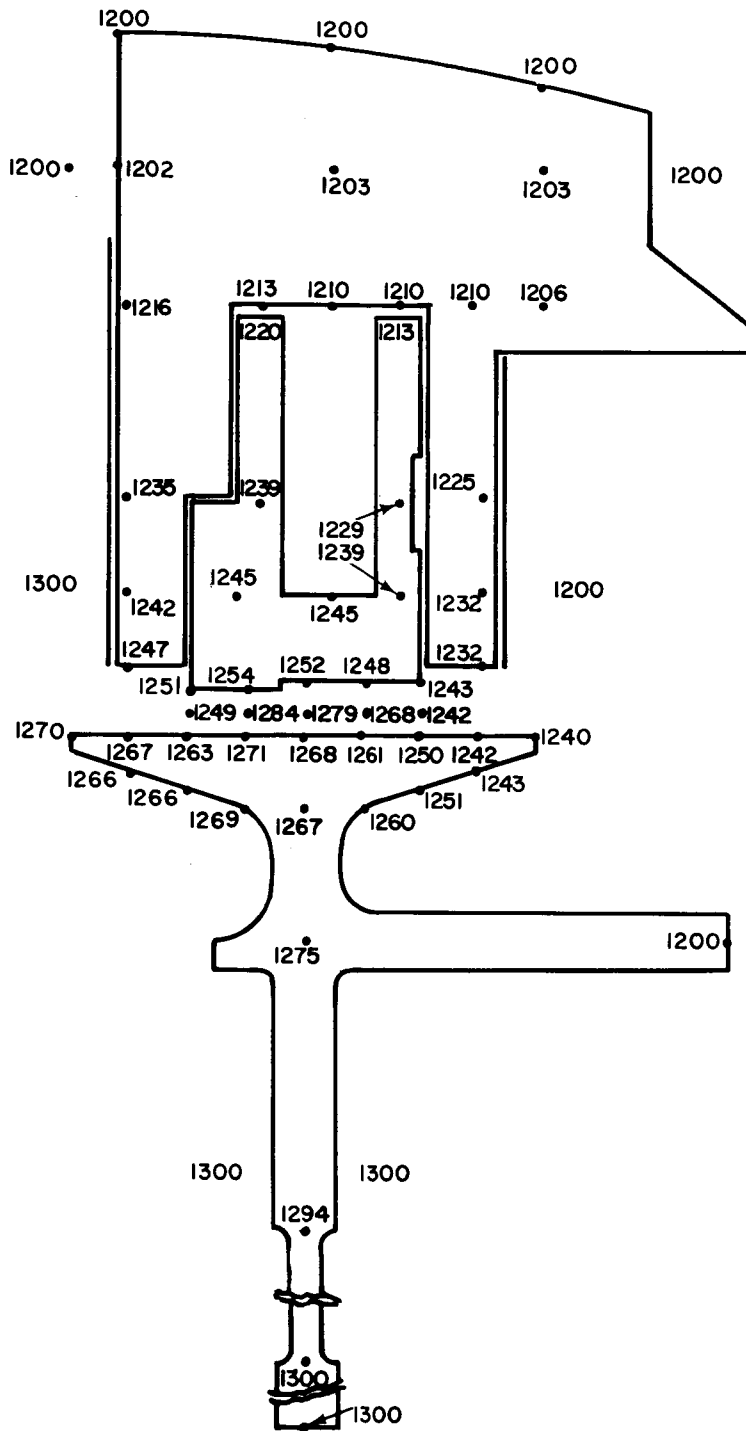


Figure 57 Temperature Distribution in Two-Side Floated Shoe Seal with Thermal Shunt in Seal Block. Thermal Conductivities 26.0 BTU/hr. ft.² °F/ft. in Shunt, 13.0 BTU/hr. ft.² °F/ft. elsewhere; 1300°F Core Machine. Temperatures Shown in °F.

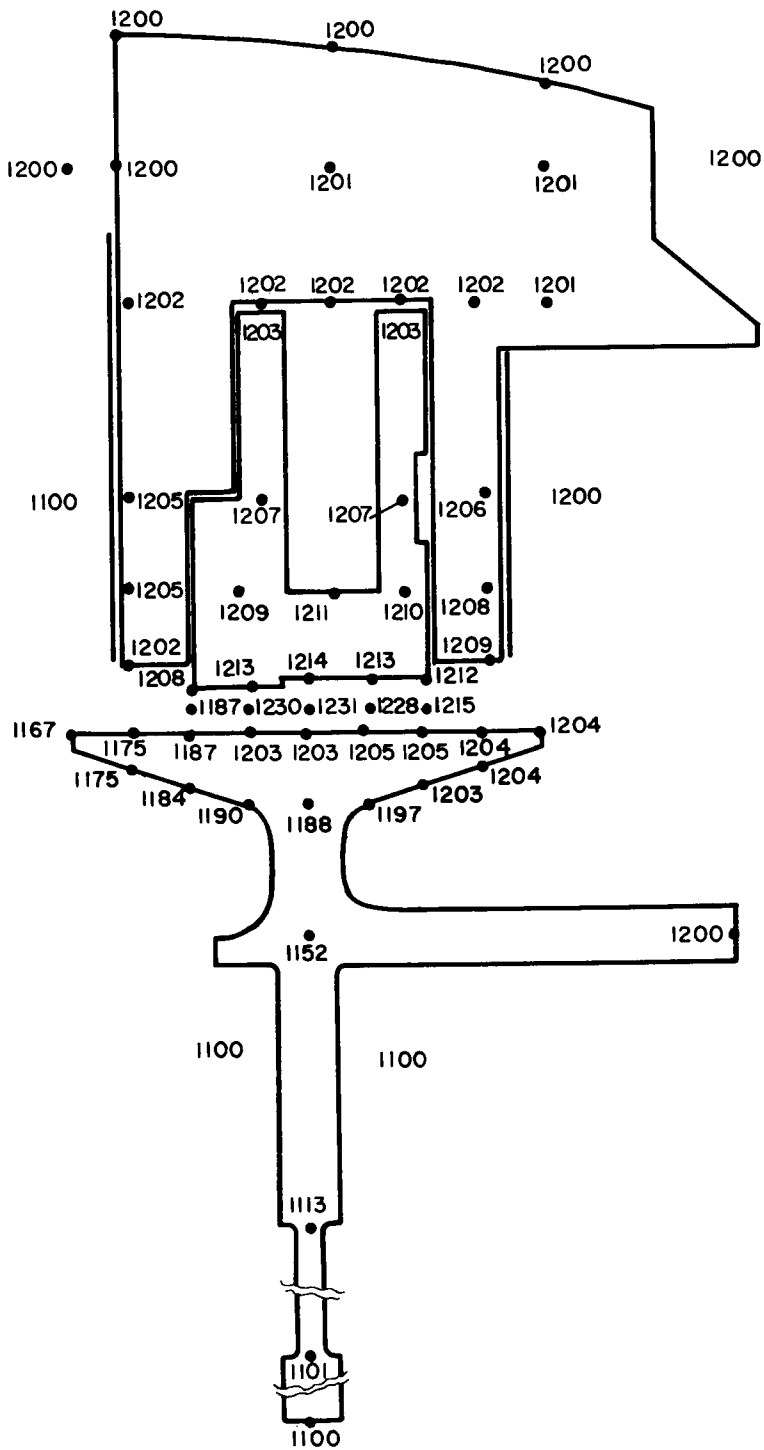


Figure 58 Temperature Distribution in Two-Side Floated Shoe Seal with Thermal Shunt in Seal Block. Thermal Conductivities 26.0 BTU/hr. ft² °F/ft. in Shunt, 13.0 BTU/hr. ft² °F/ft. elsewhere; 1100°F Core Machine. Temperatures Shown in °F.

TABLE XXIV

PHYSICAL PROPERTIES OF INCONEL-X, THE THERMAL SHUNTS, AND THE AIR USED IN THE THERMAL ANALYSIS

INCONEL-X

Thermal conductivity:

(i) Low value	$k = 7.1 \text{ BTU/hr ft}^2 \text{ }^\circ\text{F/ft}$
(ii) Average value at 1000 to 1200 degrees Fahrenheit	$k = 13.0 \text{ BTU/hr ft}^2 \text{ }^\circ\text{F/ft}$
Coefficient of thermal expansion	$\alpha = 9.0 \times 10^{-6} \text{ ft/ft }^\circ\text{F}$

THERMAL SHUNT

Effective thermal conductivity	$k = 26.0 \text{ BTU/hr ft}^2 \text{ }^\circ\text{F/ft}$
--------------------------------	--

AIR AT 1200 DEGREES FAHRENHEIT

Thermal conductivity	$k = 0.037 \text{ BTU/hr ft}^2 \text{ }^\circ\text{F/ft}$
Absolute viscosity,	$\mu = 2.29 \times 10^{-10} \frac{\text{lb}_f \text{ hr}}{\text{ft}^2}$
Specific heat at constant pressure	$C_p = 1.122 \times 10^8 \frac{\text{BTU ft}}{\text{lb}_f \text{ hr}^2 \text{ }^\circ\text{F}}$
Prandtl number	$\overline{Pr} = 0.6975$

3. DETAILS OF THERMAL ANALYSIS

a. TEMPERATURE DISTRIBUTION BY NUMERICAL METHOD

The circumferential symmetry of the seal assembly made a corresponding symmetry assumption possible for the temperature distribution. Consequently, the thermal analysis was simplified to that for a two-dimensional system with unit depth in the circumferential direction.

The determination of temperatures at specified points in the seal assembly was carried out by the conventional method of thermal network theory. The physical basis is the analogy to Kirchhoff's first law for electrical circuits. This law states that under steady-state conditions, the algebraic sum of heat flows into a junction point (nodal point) of the network is zero.

The seal assemblies were broken down into a number of contiguous subvolumes each of a shape suited to requirements for local temperature information and the overall geometry. For each internal or surface nodal point

$$\sum_j q_j = 0^{**}$$

As the temperatures between opposing surfaces across air gaps were always relatively small, no great loss in accuracy was incurred in neglecting radiative heat exchange. The equations representing heat flows into nodal points were therefore all linear and were composed of terms q ,

$$q = \frac{\Delta T}{\sum_j R_j^*}$$

for conduction and convection, and

$$q = mC_p \Delta T$$

for mass flow. The thermal resistances between nodal points were determined as the series sums of all local conductive and convective resistances which individually had the forms

$$R^* = \frac{L}{KA}$$

for conduction, and

$$R^* = \frac{1}{hA}$$

**NOTE: The symbols used are identified in Section 4 of this Appendix.

for convection.

The resultant systems of linear simultaneous equations describing the heat flows were then solved by computers using a standard matrix inversion routine.

b. AIR FLOW AND HEAT GENERATION IN THE GAPS BETWEEN SEAL BLOCK AND RUNNER AND SEAL BLOCK AND HOLDER

The basis of heat transfer computations in the gap between the seal block and runner were the results obtained in Reference 4 for combined axial flow and rotation through an annulus with an inner rotating cylinder.

Calculations showed that the air flow through the gap was laminar. This was concluded from a maximum tangential flow, a Reynolds number of less than 1000, an axial flow Reynolds number of less than 140, and a maximum modified Taylor number of less than 140. These dimensionless numbers were calculated from

$$\overline{Re} = \frac{R \omega h \rho}{\mu}$$

for tangential (Couette) flow,

$$\overline{Re} = \frac{\rho v h}{\mu}$$

for axial (Poiseuille) flow, and

$$\overline{Td} = \frac{\omega^2 R_m h^3}{\nu^2} \left(\frac{1}{F_g} \right)$$

The consequence of this conclusion that the flow is laminar is that the heat transfer regime in the seal block runner gap is by conduction only.

Similarly laminar flows and pure conduction regimes were found to occur in the clearances between the seal block and the seal holder.

The velocity profile in the seal block-runner gap in the tangential direction is linear

$$\frac{\partial U}{\partial r} = \frac{U}{h}$$

Consequently the heat generation per subvolume over the entire circumference is

$$q = \frac{8 \pi^3}{J} \mu R_r^3 N^2 \frac{b}{h}$$

and per subvolume per unit depth circumferentially

$$q = \frac{4\pi^2}{J} \mu R_r^2 N^2 \frac{b}{h}$$

The numerical values obtained are

$q = 18.1$ BTU's per hour for the 0.002 inch clearance, and

$q = 36.2$ BTU's per hour for the 0.001 inch clearance.

The local pressures in the seal block-runner gap were expressed by

$$p = \left\{ p_2^2 - \left(p_2^2 - p_s^2 \right) \frac{x}{b_2} \right\}^{1/2}$$

in the 0.002 inch gap $0 \leq x \leq b_2$ and by

$$p = \left\{ p_s^2 - \left(p_s^2 - p_1^2 \right) \left(\frac{x - b_2}{b_1} \right) \right\}^{1/2}$$

in the 0.001 inch gap between $b_2 \leq x \leq (b_2 + b_1)$. The pressure at the step was expressed by

$$p_s = p_2 \left\{ \frac{\left(\frac{p_1}{p_2} \right)^2 + \left(\frac{b_1}{b_2} \right) \left(\frac{h_2}{h_1} \right)^3}{1 + \left(\frac{b_1}{b_2} \right) \left(\frac{h_2}{h_1} \right)^3} \right\}^{1/2}$$

From the values of local pressure, the local density and consequently, the local velocity of axial (Poiseuille) flow were determined by

$$v = \frac{mRTg}{\rho A}$$

The local pressures and local axial flow velocities are shown in Figure 59. The curves indicate that in the 0.002 inch gap the flow is essentially incompressible, whereas in the downstream part of the 0.001 inch gap there is a substantial pressure and consequent density and volume change and a greatly accelerated flow.

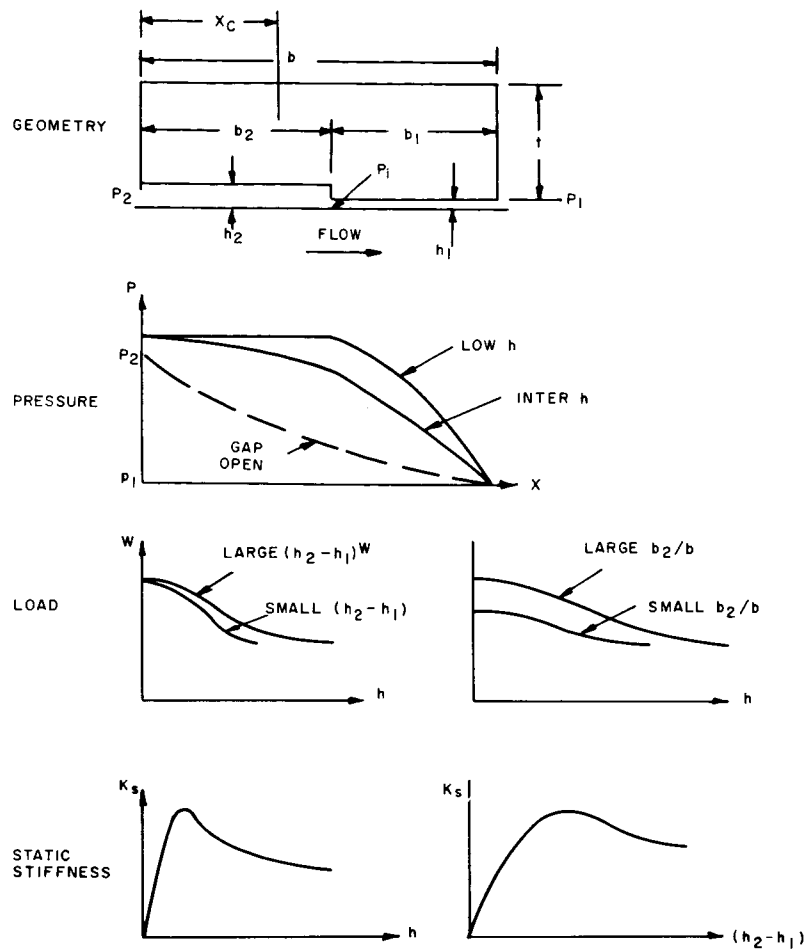


Figure 59 Hydrostatic Step Seal Parameters

The two extremes in possibilities for the gas temperature in the seal gap are:

- Isothermal analogous to a true throttling process
- Reducing static temperature as pressure drops analogous to a low speed throttling process superimposed on a compressible flow effect.

Since the difference in exit gas temperature between these two extremes is considerable, it was decided that the thermal analysis should use the one which would result in the largest thermal gradients: the second one. This would be conservative from the point of view that if thermal distortion requirements resulting from the second possibility could be met, then certainly the distortion resulting from the first possibility would be less severe. The first possibility is closer to reality.

The diffusion angle of the air jet from the seal block-runner gap was estimated to be about 8 degrees. This corresponds to half the angle of diffusion of a jet. This angle allows for only a very short length for the gap flow beyond the seal before it is disrupted. Consequently, nodal points beyond seal block-runner gap exit are not affected.

c. SURFACE COEFFICIENTS FOR CONVECTIVE HEAT TRANSFER

The surface coefficients of convective heat transfer on all surfaces of the seal assembly were computed by means of dimensionless expressions. These expressions are presented here in terms of Nusselt numbers as function of Reynolds and Prandtl numbers, and relate the nature of flow, the fluid properties and the surface geometry. They were chosen from a literature survey carried out earlier, and although originally derived for simpler configurations, correspond closely to the regimes expected on the seal assembly. Details are given below (refer to Figure 50 for corresponding locations).

- (a) Left hand face of runner skirt:
Turbulent flow.
Disk with central hole, no close obstruction.

$$\overline{Nu} = 0.0157 (\overline{Pr})^{1/3} (\overline{Re})^{0.8} \left\{ 1 + \left(\frac{R_i}{R_o} \right)^{0.6} \right\}$$

$$\overline{Nu} = \frac{\bar{h} R_o}{k}$$

$$\overline{Re} = \frac{\rho \omega R_o^2}{\mu}$$

$$\text{Surface coefficient } \bar{h} = 66 \text{ BTU/hr ft}^2 \text{ } ^\circ\text{F.}$$

- (b) Left hand inner face of runner.
Turbulent flow.
Horizontal rotating cylinder, no close obstruction.

$$\overline{Nu} = 0.073 (\overline{Re})^{0.7}$$

$$\overline{Nu} = \frac{\bar{h} D}{k}$$

$$\overline{Re} = \frac{\rho \omega D^2}{2 \mu}$$

Surface coefficient $\bar{h} = 37 \text{ BTU/hr ft}^2 \text{ }^\circ\text{F}$.

The expression used is actually for the outside surface of a horizontal rotating cylinder. Near the edge of a hollow cylinder, the inside and outside flow patterns are probably similar, despite the large angular acceleration forces. Sufficient accuracy is expected by using the outside form for a short inside portion near the cylinder edge.

- (c) Right hand face of runner skirt, inner and outer faces of runner support, and right hand inner face of runner.

Stagnation flow, because the air entrapped between surrounding surfaces rotates at the same constant angular velocity. The anticipated regime is that of free convection with slow circulation. The surface coefficient was estimated therefore by logic rather than by calculation. Surface coefficient $\bar{h} = 2 \text{ BTU/hr ft}^2 \text{ }^\circ\text{F}$.

- (d) Left hand outer face of runner - low pressure side.
Turbulent flow.

Horizontal rotating cylinder, no close obstruction.

Formulae as in (b).

Surface coefficient $\bar{h} = 61 \text{ BTU/hr ft}^2 \text{ }^\circ\text{F}$.

- (e) Runner and seal holder opposing face-low pressure side.
Turbulent flow.

Horizontal rotating cylinder within a concentric tube.

$$\overline{NU} = 0.350 \overline{NU}_{INITIAL} (\overline{TD})^{0.5}$$

$$\overline{NU} = \frac{\bar{h}D}{k}$$

$$\overline{NU}_{CRITICAL} = \frac{\frac{d}{R_i}}{\ln\left(1 + \frac{d}{R_i}\right)}$$

$$\overline{TD} = \frac{\rho \omega d R_i}{\mu} \left(\frac{d}{R_i}\right)^{0.5}$$

Surface coefficient $\bar{h} = 58 \text{ BTU/hr ft}^2 \text{ }^\circ\text{F}$.

- (f) Right hand outer face of runner - high pressure side.
Turbulent flow.
Horizontal rotating cylinder within concentric tube.
Formulae as in (e).
Surface coefficient $\bar{h} = 80 \text{ BTU/hr ft}^2 \text{ }^\circ\text{F}$.
- (g) Runner and seal holder opposing faces - high pressure side.
Turbulent flow.
Horizontal rotating cylinder within concentric tube.
Formulae as in (e).
Surface coefficient $\bar{h} = 131 \text{ BTU/hr ft}^2 \text{ }^\circ\text{F}$.
- (h) Left hand (low pressure) and right hand (high pressure) shrouded faces of seal holder.

No flow.

Stagnant air - conduction regime.

Surface coefficient $\bar{h} = 0.8 \text{ BTU/hr ft}^2 \text{ }^\circ\text{F}$.

- (i) Seal holder cylindrical face - high pressure side.
Turbulent flow.
Horizontal rotating cylinder within concentric tube.
Formulae as in (e).
Surface coefficient $\bar{h} = 103 \text{ BTU/hr ft}^2 \text{ }^\circ\text{F}$.

- (j) Seal holder radial face adjacent to the roots of the last stage blades.
Turbulent flow.
Disk rotating near a diaphragm.

$$\bar{Nu} = 0.0149 (\bar{Pr})^{1/3} (\bar{Re})^{0.8} \left\{ 1 + \left(\frac{R_i}{R_o} \right)^{0.5} \right\} \left(\frac{S}{R_o} \right)^{0.1}$$

$$\bar{Nu} = \frac{\bar{h} R_o}{k} ; \bar{Re} = \frac{\rho \omega R_o^2}{\mu}$$

Surface coefficient $\bar{h} = 164 \text{ BTU/hr ft}^2 \text{ }^\circ\text{F}$.

4. NOMENCLATURE

A = area, square feet

D = diameter, feet

F_g = geometric factor given by Reference 4

$$F_g = \left(\frac{\pi}{1697} \right) \left(1 - \frac{h}{2R_m} \right)^{-2} S^{-1}$$

J = mechanical equivalent of heat, foot-pounds per BTU

L = fixed length dimension, feet

$$S = 0.0571 \left\{ 1 - 0.652 \left(\frac{\frac{h}{R_m}}{1 - \frac{h}{2R_m}} \right) \right\} + 0.00056 \left\{ 1 - 0.652 \left(\frac{\frac{h}{R_m}}{1 - \frac{h}{2R_m}} \right) \right\}^{-1}$$

M = Mach number

\overline{Nu} = Nusselt number dimensionless

N = rate of rotation, revolutions per hour

P = pressure, pounds per square foot

P_H = pressure at high side, pounds per square foot

P_L = pressure at low side, pounds per square foot

P_S = pressure at seal block step, pounds per square foot

\overline{Pr} = Prandtl number (dimensionless)

R_t = thermal resistance hours - degrees Fahrenheit per BTU

R_i = inside radius feet

R_m = arithmetic mean radius of annulus between seal block and runner, feet

R_O = outside radius, feet

R_r = radius of runner, feet

\overline{Re} = Reynolds number (dimensionless)

$$R = \text{gas constant} = \frac{53.4 \text{ ft lb}}{\text{lb}_m \text{ } ^\circ\text{R}}$$

T = Temperature, degrees Fahrenheit

\overline{Ta} = Taylor number (dimensionless)

U = circumferential velocity of runner, feet per hour

V = mean axial velocity of flow, feet per hour

- a = local speed of sound, feet per hour
 b = width of subvolume, feet
 b_1 = width of 0.001" seal block-runner gap, feet
 b_2 = width of 0.002" seal block-runner gap, feet
 c_p = specific heat at constant pressure $\frac{\text{BTU ft}}{\text{lb}_f \text{ hr}^2 \text{ }^\circ\text{F}}$
 d = radial clearance, feet
 g_c = conversion coefficient = $32.2 \frac{\text{lb}_m \text{ ft}}{\text{lb}_f \text{ sec}^2}$
 h = clearance between seal block and runner, inches
 h_1 = clearance after step = 0.001 inches
 h = local heat transfer coefficient, BTU's per hour-square foot-degree Fahrenheit
 h_2 = clearance before step = 0.002 inches
 \bar{h} = average surface coefficient BTU's per hour-square foot-degree Fahrenheit
 j = index taking integral values 1, 2, 3, ---
 k = thermal conductivity, $\frac{\text{BTU}}{\text{hr ft } ^\circ\text{F}}$
 m = mass flow rate, $\frac{\text{lb}_f \text{ hr}}{\text{ft}}$
 q = heat flux BTU's per hour
 q = heat generation BTU's per hour
 r = variable length along radial coordinate, feet
 s = side clearance, feet
 X = variable length dimension, feet
 Δ = difference
 α = coefficient of thermal expansion, feet per foot - degree Fahrenheit

μ = absolute viscosity, $\frac{\text{lb}_f \text{ hr}}{\text{ft}^2}$

ν = kinematic viscosity, square feet per hour

ρ = density, $\frac{\text{lb}_f \text{ hr}^2}{\text{ft}^4}$

ω = angular velocity of runner, radians per hour

APPENDIX E.THERMAL ANALYSIS OF ONE-SIDE FLOATED SHOE
FACE SEAL

1. GEOMETRY AND BOUNDARY CONDITIONS

The bases for the calculations were the seals shown in Figures 4 and 8. Original and final clearances are shown in Figure 60. Figure 61 shows the numbered regions and nodes used in the calculations. Figures 62 through 64 show the results of the calculations.

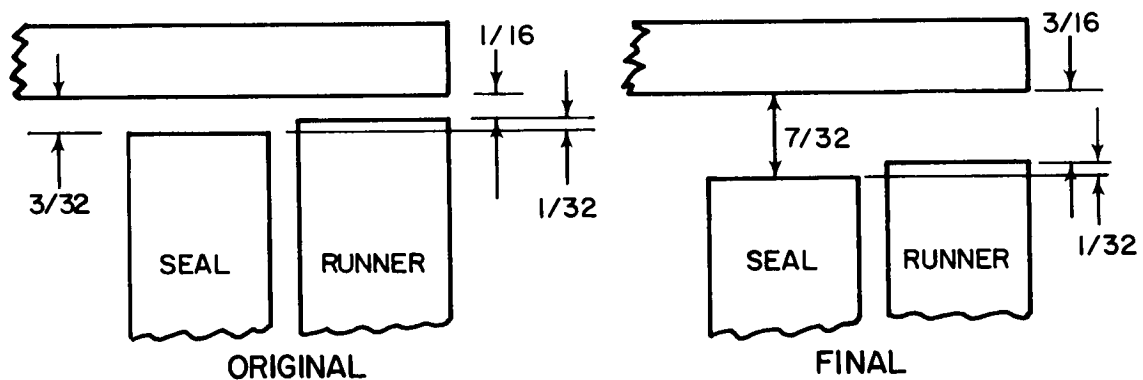


Figure 60 Original and Final Clearances of One-Side Floated Shoe Face Seal

After many of the calculations had been made, these dimensions were changed as indicated. Rather than change the geometry of some of the nodes, it was agreed to change only the values of the heat transfer coefficients to correspond to these new dimensions. Next, the location of the cylindrical skirt support was changed to intersect the runner disk one inch radially inward from the periphery of the runner.

These considerations are reflected in the attached simplified sketch (Figure 61). This figure shows the node number system and the regions (circled) for which film coefficients were computed. Finally, the upstream and downstream pressures were assumed to be 100 pounds per square inch absolute and 20 pounds per square inch absolute respectively for all calculations.

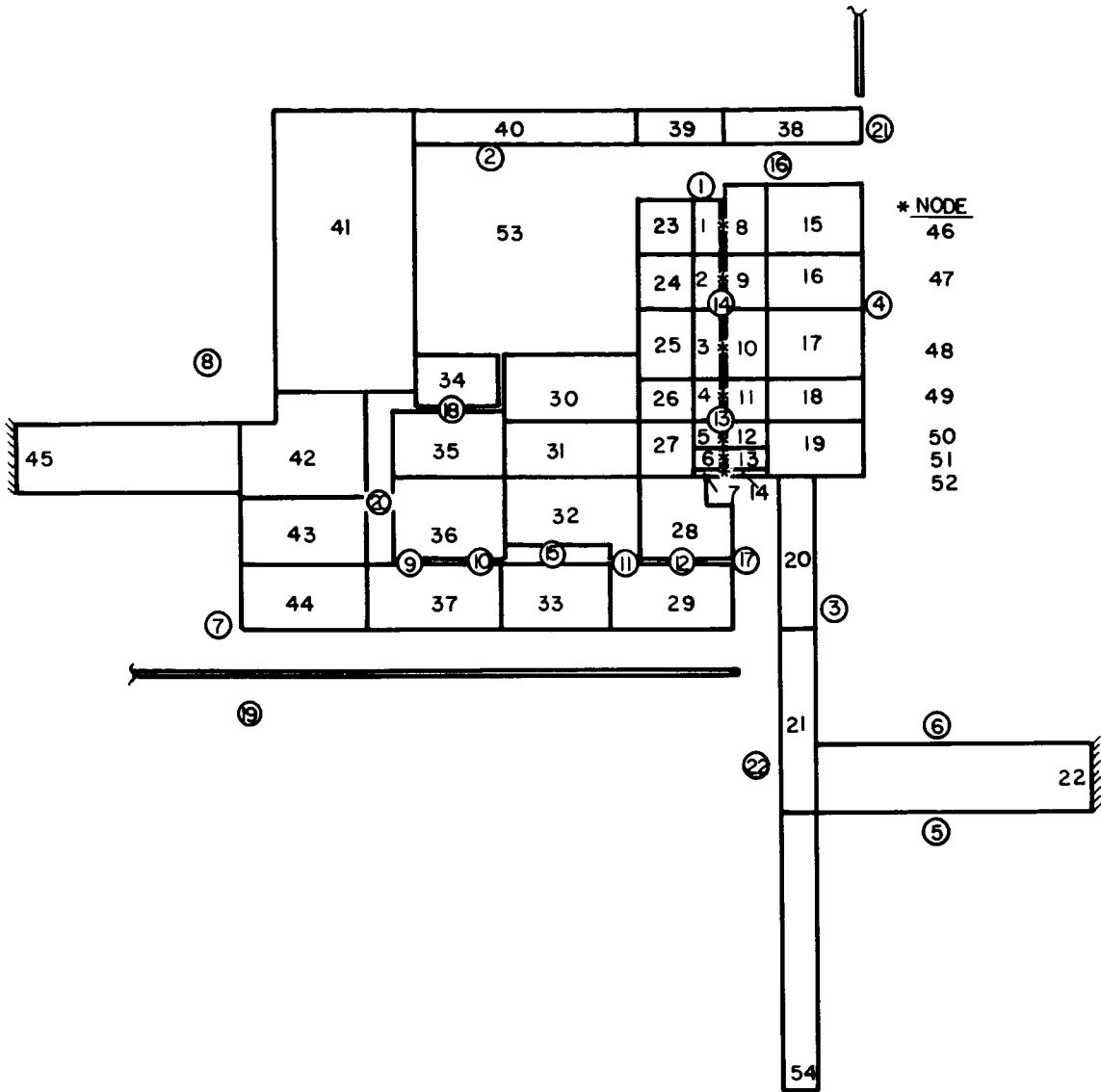


Figure 61 Node Number System for One-Side Floated Shoe Face Seal

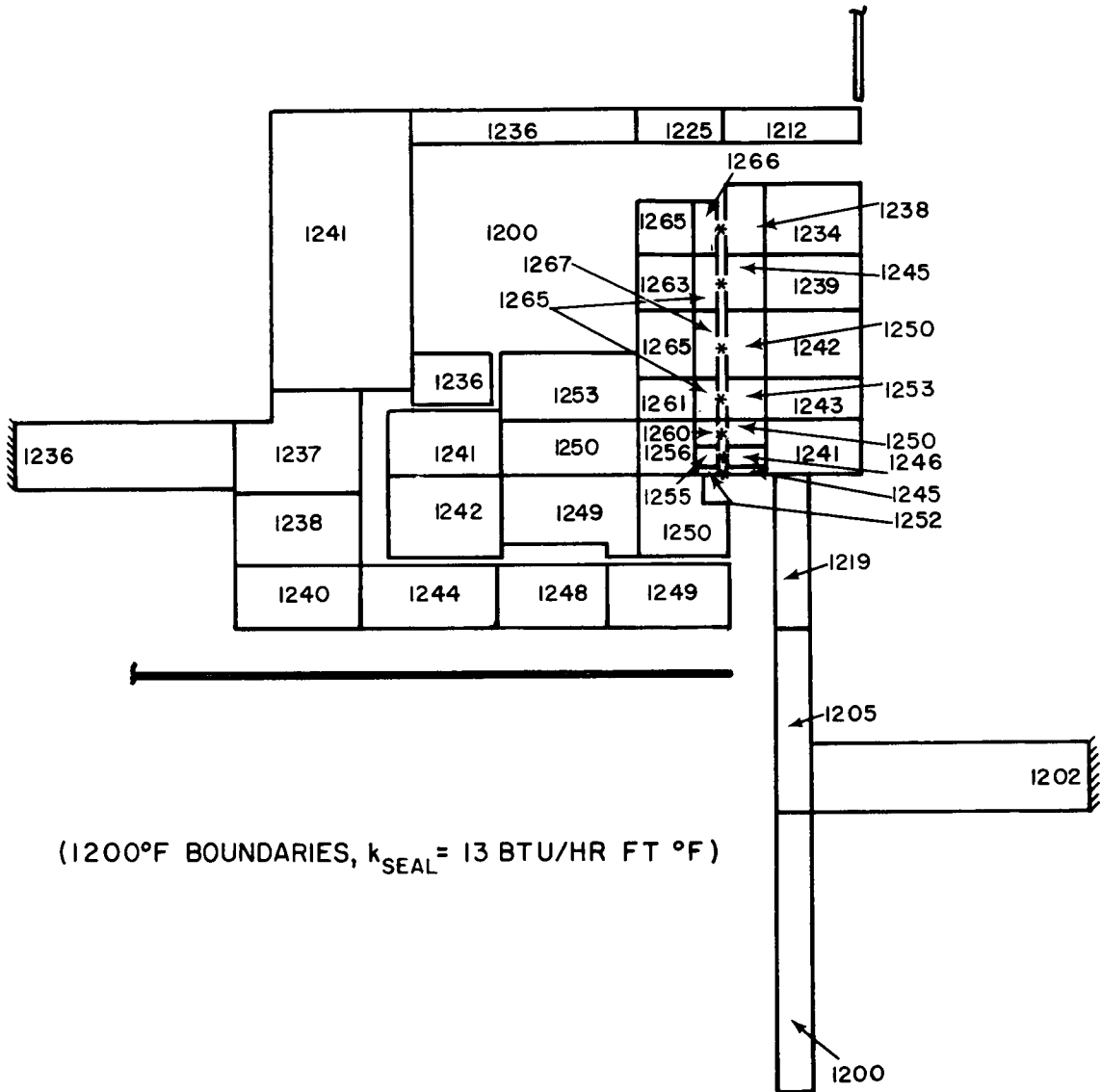


Figure 62 Temperature Distribution for Case A

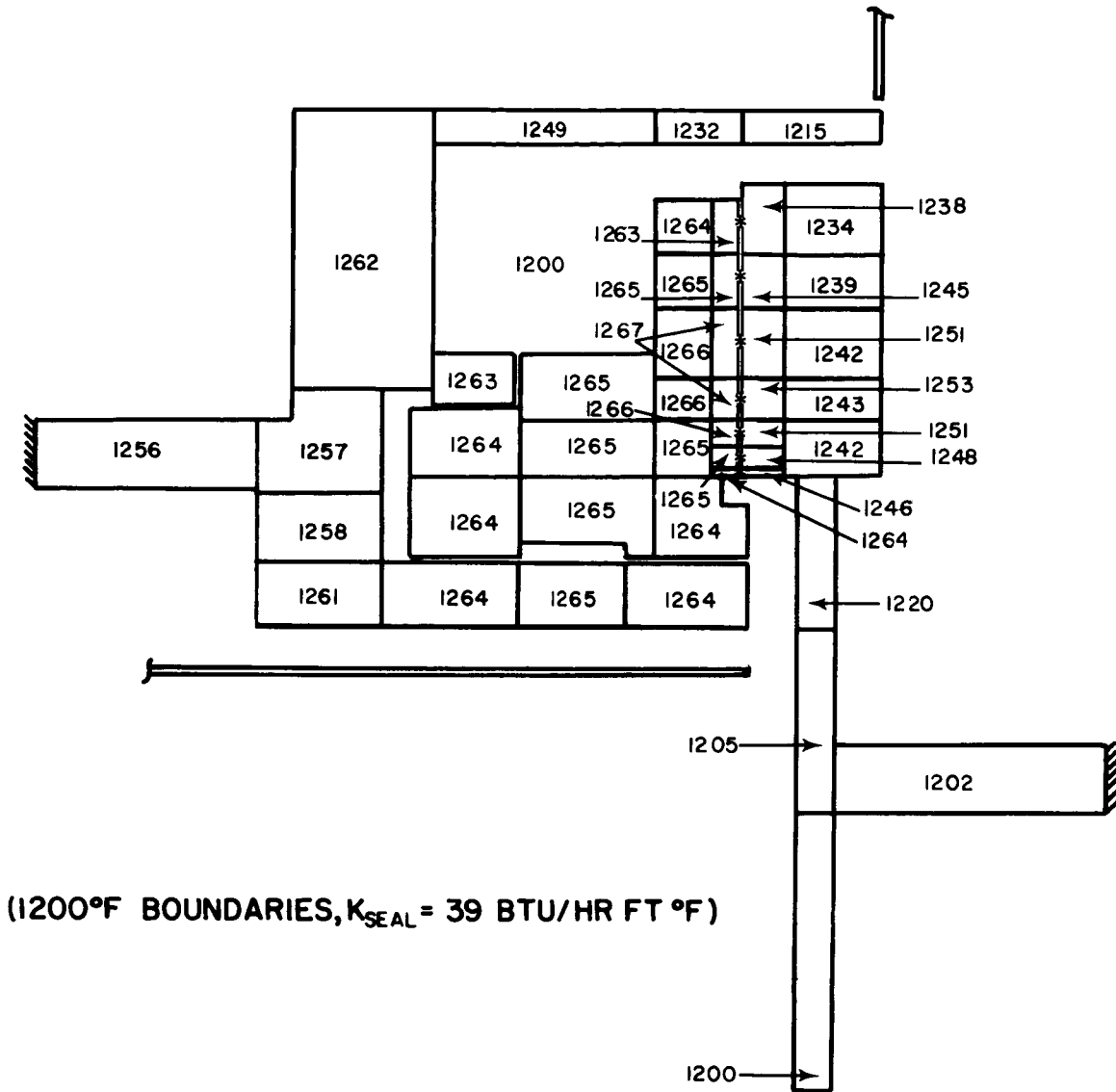


Figure 63 Temperature Distribution for Case B

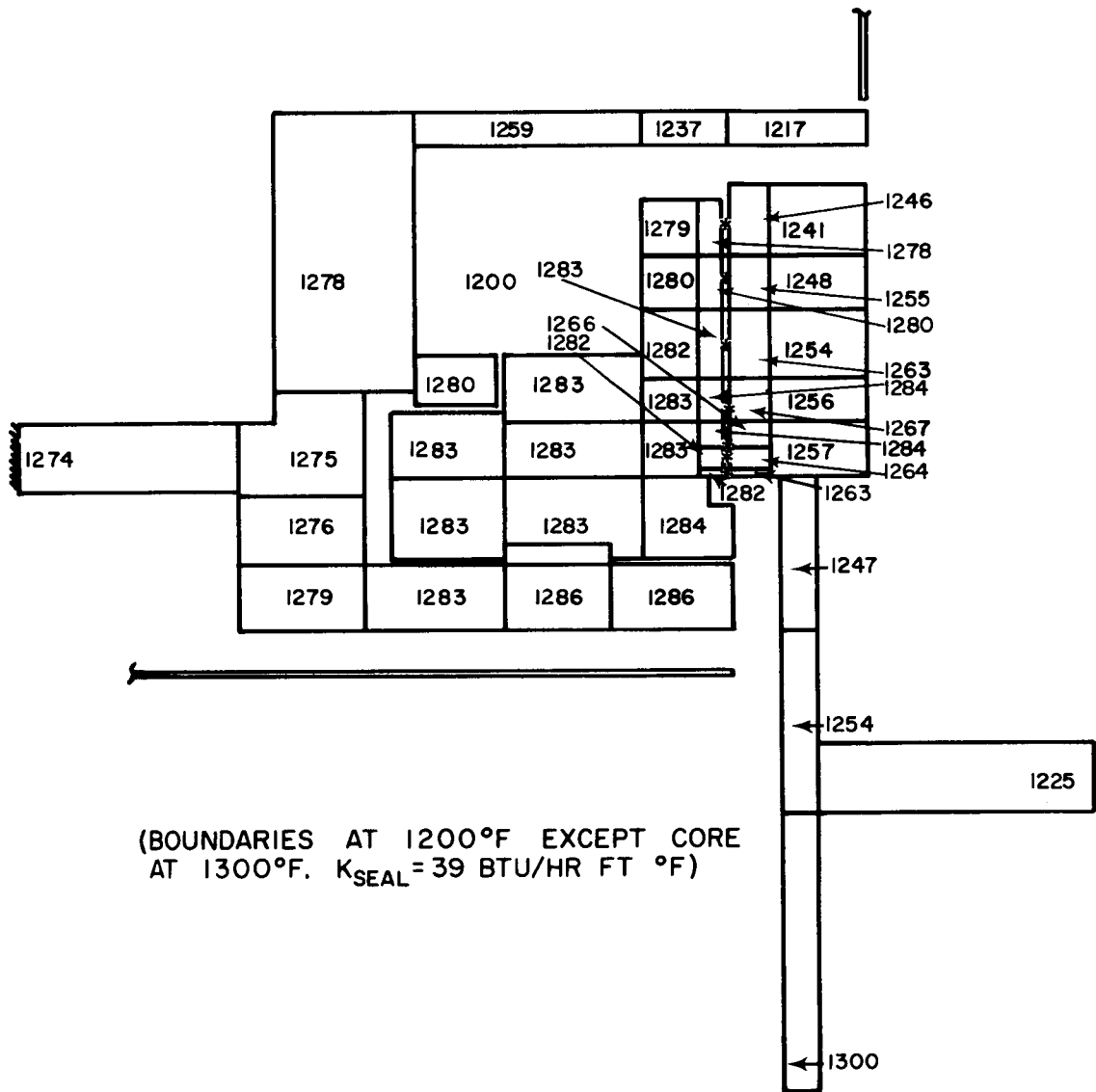


Figure 64 Temperature Distribution for Case C

2. SURFACE HEAT TRANSFER COEFFICIENTS

Values for Regions (1) and (2) in Figure 61 were determined as follows. First the volume flow due to pumping over the outer 1/32 inch of radius of the disk was calculated by modifying the boundary layer thickness equation of Reference 5 (pp. 432, 443, 445) to apply to an incomplete disk. For the surfaces of nodes 23 and 39 at Region (1), it was assumed that boundary layer flow exists all the way across the gap, so a reasonable assumption for one side is that the effective boundary layer thickness is one half the thickness of the gap (i. e., 7/64 inch.). From this, a flow area and an air velocity were computed. Next, (Reference 6, p. 224), treating the surfaces (nodes 23 and 29) as flat plates, it was found that these velocities would lead to laminar boundary conditions (Reynolds number much less than 80,000), and the resulting value of $h = 12 \text{ BTU/hr ft}^2 \text{ }^\circ\text{F}$ was computed treating the laminar flow heat transfer as pure conduction across the gap between nodes 23 and 39*:

$$h = k/t$$

Region (4) was treated as an incomplete disk with a close obstruction (Reference 5, pp. 445-447, and Reference 7). In this case the local Reynolds number was found to be about 7×10^6 , which is well into the turbulent range, and the value of the film coefficient was found to be $h = 120 \text{ BTU/hr ft}^2 \text{ }^\circ\text{F}$ from

$$\frac{\bar{h} R_r}{k} = \bar{Nu} = \left(1 + \left[\frac{R_i}{R_o} \right]^2 \right)^{1/2} \left[0.0149 \bar{Pr} \right] R_r^{4/5} \left[\frac{s}{r} \right]^{1/10}$$

At Region (3) the same equation applies, but a slightly lower value ($\bar{h} = 110 \text{ BTU/hr-ft}^2 \text{ }^\circ\text{F}$) was used, because there would be some tendency for solid rotation to occur. An even lower value ($\bar{h} = 50 \text{ BTU/hr-ft}^2 \text{ }^\circ\text{F}$) was assumed at Region (22) because of the much larger boundary layer which would exist, compared to Region (4), since there would be a tendency for the whole core to rotate.

Because the air at Region (5) is mostly enclosed between rotating elements, it was treated as laminar free convection in a high gravitational field (due to centrifugal acceleration) for a heated plate facing downward. For this case, the final equation (Reference 2, p. 180) for the coefficient is $h = 4.04 (\Delta T)^{1/4}$, where ΔT is the temperature difference between the inner surface of the skirt support and the air. For the temperature analysis, a value of $\Delta T = 10$ was assumed, yielding a coefficient of $h = 7 \text{ BTU/hr ft}^2 \text{ }^\circ\text{F}$.

* Nomenclature in this appendix is the same as that used in Appendix D.

Region (6) was treated as a cylindrical surface with no close obstructions (References 8 and 9). The turbulent flow heat transfer coefficient is defined by

$$\bar{Nu} = \frac{hD}{k} = 0.073 \bar{Re}^{0.7}$$

For well developed turbulence, the $h = 120 \text{ BTU/hr ft}^2 \text{ }^\circ\text{F}$. This value should be derated somewhat, however, because there is some tendency to get solid rotation due to the proximity of the runner disk and the last compressor stage disk. A value of $h = 100 \text{ BTU/hr ft}^2 \text{ }^\circ\text{F}$ was selected.

In the Regions (7) and (8), it was assumed that free convection dominates and thus values of $h = 1 \text{ BTU/hr ft}^2 \text{ }^\circ\text{F}$ were used (Reference 6, p. 167).

As an approximation, Region (16) was treated as a cylinder rotating within a concentric tube (Reference 10). For turbulent flow

$$\bar{Nu} = \frac{hd}{k} = \left[\frac{0.350 d/R}{\ln(1+d/R_i)} \right] \left[\bar{Ta} \right]^{\frac{1}{2}}$$

where

$$\bar{Ta} = \bar{Re} \left[\frac{d}{R_i} \right]^{\frac{1}{2}}$$

It is unlikely that a complete Taylor vortex pair could develop in this region because the gap thickness is almost as large as its axial length. A value of $h = 260 \text{ BTU/hr ft}^2 \text{ }^\circ\text{F}$ was obtained, and this is the value which was used in the temperature calculations. (The value due to laminar flow would be only $4.75 \text{ BTU/hr ft}^2 \text{ }^\circ\text{F}$.)

At Region (17), the equations for a partial disk with a close obstruction were used (Reference 5, p. 445-447, and Reference 7), assuming a gap width of $1/16 \text{ inch}$. The result was $h = 35 \text{ BTU/hr ft}^2 \text{ }^\circ\text{F}$.

For Region (22), the equations for an isolated partial disk were used (Reference 5, pp. 445-447, and Reference 11), yielding a value of $42 \text{ BTU/hr ft}^2 \text{ }^\circ\text{F}$. Here

$$\bar{Nu} = \frac{h R_o}{K} = \left[1 + \left(\frac{R_i}{R_o} \right)^6 \right] \left[0.0157 \right] \left[\bar{Pr} \right]^{\frac{1}{3}} \bar{Re}^{\frac{4}{5}}$$

It was assumed that the coefficient for all seal gaps (Regions (9) - (15), (18), (20), is the value which would result from pure conduction (or laminar flow). The following effective values of h were computed:

<u>Region</u>	<u>h (BTU/hr ft² °F)</u>
(9)	2960
(10)	1480 mean 2200
(11)	1480
(12)	2960 mean 2200
(13)	890
(14)	440
(15)	30
(18)	mean 24
(20)	18

3. MASS FLOW AT THE SEAL GAP

This quantity was calculated using the equation

$$m = \bar{M} \left(\frac{h_1^3}{24 \mu b} \right) \left(\frac{p_2^2}{RT_2} \right)$$

where \bar{M} = value from graphs from the first Semiannual Report (PWA-2752) = 2.43

Using the values $h_1 = 10^{-3}$ (inches)
 $\mu = 2.33 \times 10^{-10} \frac{\text{lb}_f \text{ hr}}{\text{ft}^3}$

$b = 5 \times 10^{-1}$ (inches)

$p_2 = 100$ (pounds per square inch, absolute)

$T_2 = 1660$ (degrees Rankine)

the mass flow through the seal gap, per inch of circumference, was found to be

$$m = 3.39 \times 10^{-8} \left(\frac{\text{lb}_f \text{ hr}}{\text{ft}^2} \right)$$

Thus, for an average radius of 14 inches,

$$m_{\text{TOTAL}} = \left(2.49 \times 10^{-7} \frac{\text{lb}_f \text{ hr}}{\text{ft}} \right) = \left(2.88 \times 10^{-2} \text{ lb}_m / \text{sec} \right) (16)$$

4. HEAT GENERATION IN THE SEAL GAP

Assuming Couette flow in the gap, the equation

$$q \text{ (BTU/HR)} = 8 \pi^3 N^2 \frac{\mu}{J} R_r^3 \frac{b}{h} = 0.00955 \frac{R_r^3 b}{h}$$

where R_r = mean radius of the node face, inches
 b = radial length of the node face, inches
 h = gap height, inches

q was obtained for the heat generation for any incremental area of node-face along the gap. Referring to Figure 61, the calculated values of q are as follows:

Nodes	q (BTU/HR)
46	1410
47	1385
48	1620
49	2320
50	1300
51	970
52	320

Total: 9325

5. PRESSURE AND VELOCITY DISTRIBUTION IN THE GAP

The pressures at various positions along the seal are shown in Figure 65.

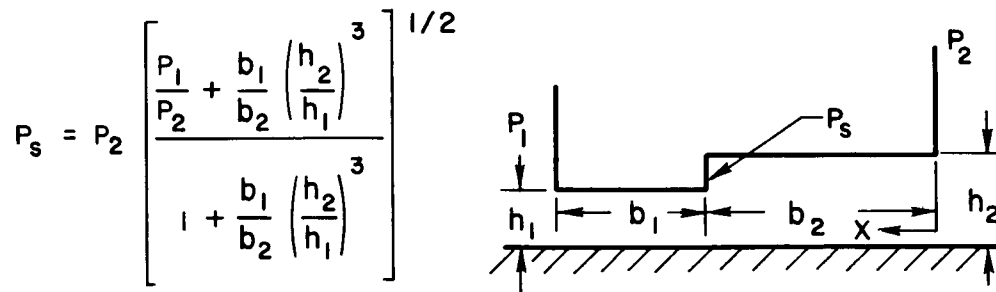


Figure 65 Pressures in One-Side Floated Shoe Face Seal Gap

$$p^2 \left[0 \leq x \leq b_2 \right] = p_2^2 - (p_2^2 - p_s^2) \frac{x}{b_2}$$

$$p^2 \left[b_2 \leq x \leq (b_2 + b_1) \right] = p_s^2 - (p_s^2 - p_1^2) \frac{x - b_2}{b_1}$$

This assumes isothermal flow.

The velocity in the gap was computed from

$$V = \frac{mRTg}{\rho A}$$

where

$$m = 2.49 \times 10^{-7} \frac{\text{LB}_f \text{ HR}}{\text{FT}} \text{ from Equation (16)}$$

This again assumes isothermal flow. In Appendix D it was stated that a temperature correction based on adiabatic flow theory should be applied to the primary film since it leads to a more conservative analysis of the temperature distribution in the seal. Similar adiabatic flow corrections were applied in the thermal analysis of the one side floated shoe seal.

The adiabatic temperature drop was computed from Reference 12, Table B2, using a value of "a" (speed of sound) of 7.2×10^6 feet per hour. Letting

$$b_1 = 0.175 \text{ inches}$$

$$b_2 = 0.325 \text{ inches}$$

$$p_1 = 20 \text{ pounds per square inch, absolute}$$

$$p_2 = 100 \text{ pounds per square inch, absolute}$$

$$h_1 = 0.001 \text{ inches}$$

$$h_2 = 0.002 \text{ inches}$$

the adiabatic temperature drop was computed, as shown in Table XXV.

TABLE XXV
ADIABATIC TEMPERATURE DROP

<u>X (in.)</u>	<u>P (psia).</u>	<u>ρ (lb_m/ft³)</u>	<u>$10^{-5} V$ (ft/hr)</u>	<u>M = V/Q</u>	<u>T (°R)</u>
0	100.0	0.156	5.30	0.074	1660
0.2	95.2	0.149	5.62	0.078	
0.325	92.2	0.144	5.88	0.082	1658
0.35	91.5	0.143	11.9	0.165	
0.4	71.0	0.111	15.6	0.217	1642
0.45	50.5	0.079	21.6	0.300	1630
0.475	39.4	0.062	27.5	0.382	1610
0.49	29.2	0.046	37.1	0.515	1575
0.50	20.0	0.031	55.0	0.765	1485

The value of T in the last column indicates the value to which the temperature at each x position has dropped due to adiabatic cooling. These values are included in the heat balance equations in the way described in the following section.

6. ADMITTANCE MATRIX AND HEAT BALANCE EQUATIONS

Three cases were considered. For Case A, it is assumed that the boundary temperature is 1200 degrees Fahrenheit and that the conductivity of the metal (at 1200 degrees Fahrenheit) is 13 BTU/hr ft °F. For Case B, the conductivity of the seal is raised to 39 BTU/hr ft °F. Case C included both the high conductivity seal and a 1300 degrees Fahrenheit core temperature. Temperature distributions for all three cases are shown in Figures 62 to 64.

The heat balance equation for the i^{th} node ($1 \leq i \leq 45$) is written in the following manner:

$$-q_i \text{ GENERATED} = (q_i \text{ IN} - q_i \text{ OUT})$$

or, because

$$\begin{aligned} (q_i \text{ IN} - q_i \text{ OUT}) &= \sum_j Y_{ij} (T_j - T_i) \\ &= -T_i \sum_j Y_{ij} + \sum_j Y_{ij} T_j \end{aligned}$$

Then

$$-q_{\text{GENERATED}} = -T_i \sum_j Y_{ij} + \sum_j Y_{ij} T_j$$

For nodes 46 through 52, which include heat generation, the corresponding equation is

$$-q_{\text{GENERATED}} = -T_i \sum_j Y_{ij} + \sum_j Y_{ij} T_j - q_i \text{ GAINED}$$

where $q_i \text{ GAINED} = C_p m (T_{i-1} - T_i)$

$$C_p = 113 \frac{\text{BTU FT}}{\text{°F LB}_f \text{ HR}^2} \text{ (AT 1200° F)}$$

$$m = 2.49 \times 10^{-7} \frac{\text{LB}_f \text{ HR}}{\text{FT}} \text{ (FROM EQ(16))}$$

The adiabatic cooling which was described in Appendix D is included in the heat balance equations in the following manner. At node 46, it is assumed that the inlet temperature is 1200 degrees Fahrenheit. The small amount of drop (1660 to 1658 degrees Rankin) is ignored for nodes 47 and 48. At node 49, ($0.325 \leq x \leq 0.4$), however, it is assumed that the inlet temperature is 18 degrees Fahrenheit lower than the temperature at node 48. In the same manner, then

<u>Node</u>	<u>Inlet Temperature</u>
49	$T_{48} - 18^\circ\text{F}$
50	$T_{49} - 12^\circ\text{F}$
51	$T_{50} - 55^\circ\text{F}$
52	$T_{51} - 90^\circ\text{F}$

Finally, nodes 53 and 54 are used to define boundary temperatures as shown below.

	<u>Case</u>		
	<u>A</u>	<u>B</u>	<u>C</u>
T_{53}	1200°F	1200°F	1200°F
T_{54}	1200°F	1300°F	1300°F

7. STEADY STATE TEMPERATURE DISTRIBUTIONS

The calculated steady state temperature for Cases A, B and C are shown in Figures 62 to 64. The heat generation (and adiabatic cooling) characteristics of the gap between the shoe and the runner are assumed to be the same in all three cases. The thermal conductivity of the shoe material is assumed to be

13 BTU/hr ft °F for Case A, but is 39 BTU/hr ft °F for Cases B and C. In addition, for Case C, the temperature of the core-air is defined to be 1300 rather than 1200 degrees Fahrenheit, which is used at all air-to-metal boundaries in Cases A and B.

APPENDIX FEFFECTIVE POLAR MOMENT OF INERTIA OF THIN OPEN SECTION

If the cross section of a bar is composed of many slender rectangular sections or thin curved sections, the value of J used in the torsional stiffness is usually known as the effective polar moment of inertia, which is much smaller than the true polar moment of inertia about the centroid.

The analysis and formulae for J for various thin open sections can be found in many stress analysis textbooks. The contractor has used the following expression for a section containing multiple thin rectangular sections.

$$J = \sum_{i=1}^n \frac{b_i t_i^3}{3}$$

where n is the total number of the thin rectangular sections, and b_i and t_i are the length and thickness of each section. This formula has been used to calculate the value of J of the primary seal ring for both the thin-strip piston-ring and the thin-strip C diaphragm seals. The effect of the small angular web in the cross section of the thin-strip piston-ring design is neglected, since its thickness is extremely small in comparison to the others, and they are located intermittently along the circumference.

APPENDIX GLEAKAGE RATE CALCULATIONS OF PRESENT LABYRINTH SEALS FOR
TEST RIG CONDITIONS

1. EGLI'S FORMULA

The general formula for calculation of leakage rate through a labyrinth, according to Egli, is:

$$W = A \phi \alpha \gamma \sqrt{g \frac{P_u}{V_u}} \quad (17)$$

where

W = Leakage flow, pounds per second

A = Leakage area, square inches

ϕ = Flow function

α = Flow coefficient

γ = Carry-over factor

g = Gravitational constant = 386.4 inches per second²

P_u = Absolute total pressure upstream of seal, pounds per square inch, absolute

V_u = Specific volume upstream of seal, cubic inches per pound

The flow function, ϕ , as given by Egli, is plotted in Figure 66.

where P_d = absolute total pressure downstream of seal, pounds per square inch absolute

N = number of seal blades

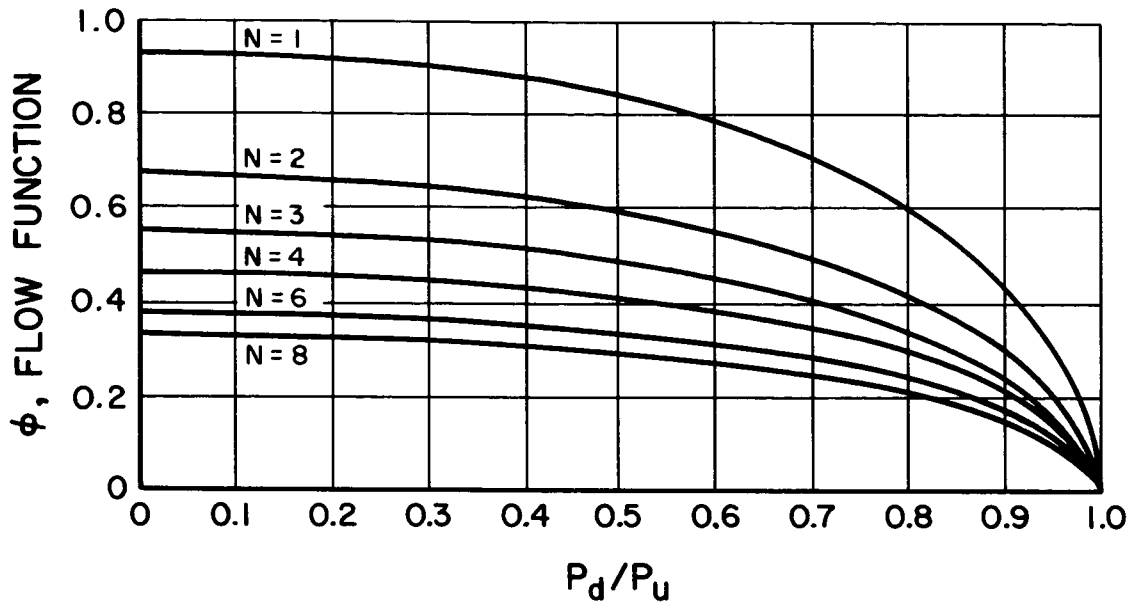


Figure 66 Labyrinth Seal Leakage Curves

The flow coefficient (α) can be determined from Figure 67 for a specified seal lip thickness (t) and clearance (e).

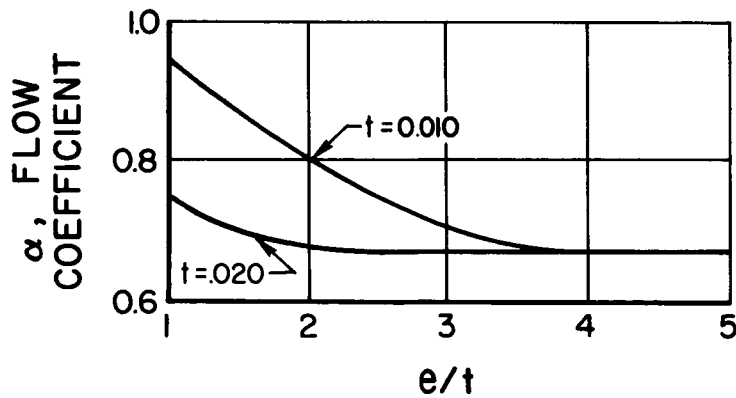


Figure 67 Flow Coefficient Curve

The carry-over factor, γ , for the present labyrinth seals is unity.

2. LEAKAGE RATES FOR END AND INTERSTAGE LABYRINTH SEALS

a. END SEAL (CRUISE CONDITION)

A typical configuration for the present engine end seal is shown in Figure 68. The inlet and exhaust pressures for the test rig are shown in Figure 10.

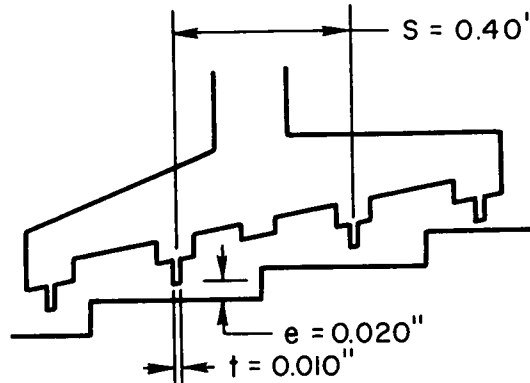


Figure 68 Current Engine End Seal

For $N = 4$ and $P_d/P_u = 0.2$, the flow function, ϕ , can be located in Figure 66.

$$\phi = 0.45$$

For $t = 0.010$ and $e/t = 2.0$, the value α , according to Figure 67, is 0.8. To calculate the other quantities in equation (17).

$$A = 2\pi R_f = 86.4 \times 0.018 = 1.555 \text{ square inches}$$

$$P_u = 100 \text{ pounds per square inch}$$

$$V_u = \frac{RT}{p \times 386} = \frac{2.47 \times 10^5 \times 1660}{100 \times 386} = 1.062 \times 10^4 \text{ cubic inches per pound}$$

Substituting these quantities in Equation (17), one obtains

$$W = 1.555 \times 0.45 \times 0.8 \times 1.0 \sqrt{386 \times \frac{100}{1.062 \times 10^4}} = 1.07 \text{ pounds per second}$$

for end seal cruise conditions.

b. END SEAL (TAKE-OFF CONDITION)

For the take-off, the following conditions are found,

$$P_u = 170 \text{ pounds per square inch}$$

$$T_u \text{ (upper stream temperature) } = 680 \text{ degrees Fahrenheit or } 1145 \text{ degrees Rankine}$$

$$P_d/P_u = \frac{20}{170} = 0.117$$

$$A = 1.555 \times \frac{.020}{.018} = 1.73 \text{ square inches}$$

$$\phi = 0.46$$

$$\alpha = 0.8$$

The flow rate according to Equation (17) is

$$W = 1.73 \times 0.46 \times 0.8 \times \sqrt{\frac{(386) (170)^2}{(1.062) (100) (10)^4} \left(\frac{1660}{1140} \right)}$$

$$= 2.5 \text{ pounds per second}$$

c. INTERSTAGE SEAL (CRUISE CONDITION)

A typical cross section of interstage seal can be seen in Figure 69.

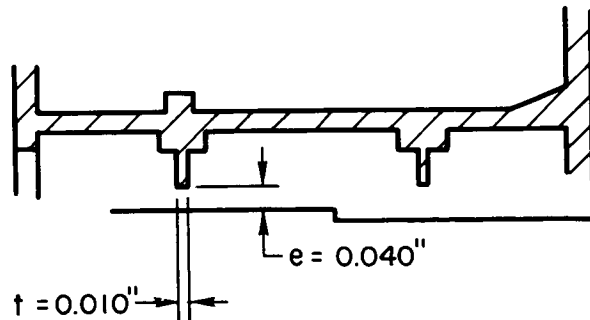


Figure 69 Current Interstage Seal

The leakage rate is determined as follows:

$$A = 2\pi R_f e = 3.45 \text{ square inches}$$

$$P_u = 100 \text{ pounds per square inch}$$

$$P_d = 75 \text{ pounds per square inch}$$

$$\phi = 0.455$$

$$C_d = 0.675$$

$$W = 3.45 \times 0.455 \times 0.675 \times 1.0 \times \sqrt{386 \times \frac{100}{1.062 \times 10^4}}$$

$$= 2.02 \text{ pounds per second}$$

d. INTERSTAGE SEAL (TAKE-OFF CONDITION)

$$e = 0.047$$

$$t = 0.010$$

$$\frac{e}{t} = 4.7$$

$$C_d = 0.675$$

$$A = 3.45 \times \frac{0.047}{0.04} = 4.05 \text{ square inches}$$

$$P_u = 170 \text{ pounds per square inch}$$

$$P_d = 120 \text{ pounds per square inch}$$

$$P_d / P_u = 0.705$$

$$\phi = 0.49$$

$$W = 4.05 \times 0.49 \times 0.675 \times 1.0 \times \sqrt{386 \times \frac{170^2}{1.062 \times 10^4 \times 100} \times \frac{1660}{1145}}$$

$$= 5.2 \text{ pounds per second}$$

BIBLIOGRAPHY

- Eckert, E. R. and Robert M. Drake, Jr., "Heat and Mass Transfer," McGraw-Hill Book Co., New York, 1959.
- Fuller, Dudley D., "Theory and Practice of Lubrication for Engineers," John Wiley & Sons, Inc. New York, 1956.
- Grassam, N. S. and J. W. Powell, "Gas Lubricated Bearings," Butterworth, Inc., London, 1964.
- Jakob, Max and George Hawkins, "Elements of Heat Transfer," third edition, John Wiley & Sons, Inc., New York, 1958.
- Lave, J. H., "Hydrostatic Gas Bearings," California Institute of Technology Progress Report No. 20-353 Pasadena, 1958.
- Pinkus, Oscar and Beno Sternlicht, "Theory of Hydrodynamic Lubrication," McGraw-Hill Book Co., New York, 1961.
- Shapiro, A. H., "The Dynamics and Thermodynamics of Compressible Fluid Flow, Vol. 1" The Ronald Press Co., New York, 1953.
- Wildman, M., "Grooved Plate Gas Lubricated Thrust Bearings, with Special References to the Spiral Groove Bearing," Ampex Corporation, Prepared under Contract No. NoNR-3815(00), Fluid Dynamics Branch, ONR, RR 64-1, Jan. 1964.
- Keenan, J. H. and J. Kaye, "Gas Tables", John Wiley & Sons, New York, 1961.
- Arwas, E. B. and Sternlicht, B., "Viscous Shear Compressor," Mechanical Technology Incorporated, Technical Report MTI 62TR21.
- Lund, J. W., "Gas Bearing Design Methods Vol. 2," Mechanical Technology Incorporated Technical Report, MTI 65TR5-II.
- Cheng, H. S., Chow, C. Y., and Murray S. F., "Gas Bearing Design Methods Vol. I", Mechanical Technology Incorporated Technical Report, MTI 65TR5-I.
- Hsing, F. and T. Chiang, "Discharge Coefficient of Orifices and Nozzles," Mechanical Technology Inc. Technical Memo MTI-65TM7.
- Castelli, V. and J. Pirvics, "Equilibrium Characteristics of Axial-Groove Gas-Lubricated Bearings," ASME 65-LUB-16, (1965).

REFERENCES

1. Hartog, Den. Mechanical Vibrations, 3rd edition. New York: McGraw-Hill
2. Tang, I. C., and Gross, W. A. "Analysis and Design of Externally Pressurized Gas Bearings". ASLE Transactions, Vol. 5, pp. 261-284. 1962
3. Timoshenko, S. Strength of Materials, Part II, 2nd Edition. New York: D. Van Nostrand Co., Inc., 1941
4. Becker, K. M., and Kaye, Joseph. "Measurements of Diabatic Flow in an Annulus with an Inner Rotating Cylinder", J. Heat Transfer, Trans. ASME, 84, 97-105, May 1962.
5. Schlichting, H. Boundary Layer Theory. New York: McGraw-Hill, 1955
6. McAdams, W. H. Heat Transmission, 3rd edition. New York: McGraw-Hill, 1954
7. Daily, J. W., and Nece, R. E. "Chamber Dimension Effects on Induced Flow and Frictional Resistance of Enclosed Rotating Discs", J. Basic Engineering, Trans. ASME, Vol. 82, p. 217, 1960.
8. Anderson and Saunders. "Connection from an Isolated Heated Rotating Cylinder Rotating about Its Axis," Proceedings of the Royal Society, Series A, Vol. 217, p. 555, 1953.
9. Bjorkland, Heat Transfer from Rotating Bodies - Single Cylinders and Concentric Cylinders, Technical Report No. 34, Dep't. of Mechanical Engineering. Stanford University. 1957
10. Bjorkland and Kays. Heat Transfer Between Concentric Rotating Cylinders, ASME Paper No. 58-A-99. 1958.
11. Theodorsen, T. and Reiger, A., "Experiments on Drag of Revolving Discs, Cylinders, and Streamline Rods of High Speeds," NACA Transactions, Vol. 796.
12. Shapiro, A. H. The Dynamics and Thermodynamics of Compressible Fluid Flow, Vol. I, Ronald Press Company. 1953

Semiannual Reports Distribution List
NAS 3-7605

Addressee

1. NASA-Lewis Research Center
Air Breathing Engine Procurement Section
Attention: John H. DeFord

2. NASA-Lewis Research Center
Air Breathing Engine Division
Attention: J. Howard Childs M. S. 60-4
 W. H. Roudebush M. S. 60-6
 D. P. Townsend (4) M. S. 60-6
 L. E. Macioce M. S. 60-6

3. NASA-Lewis Research Center
Technical Utilization Office
Attention: John Weber

4. NASA-Lewis Research Center
Reports Control Office

5. NASA-Lewis Research Center
Attention: Library

6. NASA-Scientific and Technical Information Facility (6)
Box 5700
Bethesda, Maryland
Attention: NASA Representative

7. NASA-Lewis Research Center
Fluid System Components Division
Attention: I. I. Pinkel
 E. E. Disson
 R. L. Johnson
 W. R. Loomis
 L. P. Ludwig
 N. A. Swikert
 T. B. Shillito
 H. J. Hartman

8. Air Force Materials Laboratory
Wright-Patterson Air Force Base, Ohio
Attention: MANL, R. Adamczak
 MANE, R. Headrick and J. N. Keible
 MAAE, P. House

9. Air Force Systems Engineering Group
Wright-Patterson Air Force Base, Ohio
Attention: SESMS, J. L. Wilkins
SEJPF, S. Prete

10. Air Force Aero Propulsion Laboratory
Wright-Patterson Air Force Base, Ohio
Attention: AFAPL (APFL), K. L. Berkey &
L. DeBrahum
AFAPL (APTC), C. Simpson
APTP, L. J. Gershon

11. FAA Headquarters
800 Independence Avenue, S. W.
Washington, D. C.
Attention: J. Chavkin SS/120
M. Lott FS/141

12. NASA Headquarters
Washington, D. C. 20546
Attention: N. F. Rekos (RAP)
A. J. Evans (RAD)
J. Maltz (RRM)

13. NASA-Langley Research Center
Langley Station
Hampton, Virginia 23365
Attention: Mark R. Nichols

14. Mechanical Technology Incorporated
968 Albany-Shaker Road
Latham, New York
Attention: D. Wilcock

15. Clevite Corporation
Cleveland Graphite Bronze Division
17000 St. Clair Avenue
Cleveland, Ohio 44110
Attention: T. H. Koenig

16. Koppers Company, Incorporated
Metal Products Division
Piston Ring and Seal Department
Baltimore 3, Maryland
Attention: T. C. Kuchler

17. Stein Seal Company
20th Street and Indiana Avenue
Philadelphia 32, Pennsylvania
Attention: Dr. P. C. Stein

18. Wright Aeronautical Division
Curtiss-Wright Corporation
333 West 1st Street
Dayton 2, Ohio
Attention: S. Lombardo

19. General Electric Company
Advanced Engine and Technology Department
Cincinnati, Ohio 45215
Attention: L. B. Venable
G. J. Wile
C. C. Moore H-25

20. Huyck Metals Company
P. O. Box 30
45 Woodmont Road
Milford, Connecticut
Attention: J. I. Fisher

21. Aerojet-General Corporation
20545 Center Ridge Road
Cleveland, Ohio 44116
Attention: W. L. Snapp

22. Lycoming Division
Avco Corporation
Stratford, Connecticut
Attention: R. Cuny

23. Battelle Memorial Institute
505 King Avenue
Columbus 1, Ohio
Attention: C. M. Allen

24. Bendix Corporation
Fisher Building
Detroit 2, Michigan
Attention: R. H. Isaccs

25. Boeing Aircraft Company
224 N. Wilkinson
Dayton, Ohio 45402
Attention: H. W. Walker

26. Douglas Aircraft Company
Holiday Office Center
16501 Brookpark Road
Cleveland, Ohio 44135
Attention: J. J. Pakiz

27. General Dynamics Corporation
16501 Brookpark Road
Cleveland, Ohio 44135
Attention: George Vila

28. General Motors Corporation
Allison Division
Plant #8
Indianapolis, Indiana
Attention: E. H. Deckman

29. Lockheed Aircraft Company
16501 Brookpark Road
Cleveland, Ohio 44135
Attention: Mr. L. Kelly

30. Martin Company
16501 Brookpark Road
Cleveland, Ohio 44135
Attention: Z. G. Horvath

31. North American Aviation
16501 Brookpark Road
Cleveland, Ohio 44135
Attention: George Bremer

32. Fairchild-Hiller Corporation
Republic Aviation Division
Farmingdale, Long Island
New York 11735
Attention: D. Schroeder

33. Westinghouse Electric Corporation
55 Public Square
Cleveland, Ohio 44113
Attention: Lynn Powers

34. I. I. T. Research Foundation
10 West 35 Street
Chicago, Illinois 60616
Attention: Dr. Strohmeler
35. Pesco Products Division
Borg-Warner Corporation
24700 N. Niles
Bedford, Ohio
36. Stanford Research Institute
Menlo Park, California
Attention: R. C. Fey
37. Franklin Institute Laboratories
20th and Parkway
Philadelphia 3, Pennsylvania
Attention: J. V. Carlson
38. Industrial Tectonics
Box 401
Hicksville, New York 11801
Attention: J. Cherubin
39. Sealol Incorporated
P. O. Box 2158
Providence 5, Rhode Island
Attention: Justus Stevens
40. Continental Aviation and Engineering
12700 Kercheval
Detroit 15, Michigan
Attention: A. J. Fallman
41. Northrop Corporation
1730 K. Street, N. W.
Suite 903-5
Washington 6, D. C.
Attention: S. W. Fowler, Jr.
42. Chicago Rawhide Manufacturing Company
1311 Elston Avenue
Chicago, Illinois
Attention: R. Blair

43. Midwest Research Institute
425 Volker Blvd.
Kansas City 10, Missouri
Attention: V. Hopkins

44. Southwest Research Institute
San Antonio, Texas
Attention: P. M. Ku

45. E. I. DuPont de Nemours and Company
1007 Market Street
Wilmington 98, Delaware
Attention: A. J. Cheney
R. J. Laux

46. Fairchild Engine and Airplane Corporation
Stratos Division
Bay Shore, New York

47. Borg-Warner Corporation
Roy C. Ingersoll Research Center
Wolf and Algonquin Roads
Des Plaines, Illinois

48. U. S. Naval Air Material Center
Aeronautical Engine Laboratory
Philadelphia 12, Pennsylvania
Attention: A. L. Lockwood

49. Department of the Navy
Bureau of Naval Weapons
Washington, D. C.
Attention: A. B. Nehman, RAAE-3
C. C. Singleterry, RAPP-4

50. Department of the Navy
Bureau of Ships
Washington, D. C.
Attention: Harry King, Code 634-A

51. SKF Industries, Incorporated
1100 First Avenue
King of Prussia, Pennsylvania
Attention: L. B. Sibley

52. Crane Packing Company
6400 W. Oakton Street
Norton Grove, Illinois
Attention: Harry Tankus
53. B. F. Goodrich Company
Aerospace and Defense Products Division
Troy, Ohio
Attention: L. S. Blaikowski
54. The University of Tennessee
Department of Mechanical and Aerospace
Engineering
Knoxville, Tennessee
Attention: Professor W. K. Stair
55. Hughes Aircraft Company
International Airport Station
P. O. Box 90515
Los Angeles 9, California
56. U. S. Navy Marine Engineering Lab.
Friction and Wear Division
Annapolis, Maryland
Attention: R. B. Snapp
57. Metal Bellows Corporation
20977 Knapp Street
Chatsworth, California
Attention: Sal Artino
58. Rocketdyne
6633 Canoga Avenue
Canoga Park, California
Attention: M. Butner
59. Carbon Products Division of Union Carbide
Corporation
270 Park Avenue
New York 17, New York
Attention: J. Curean
60. Garlock, Incorporated
Palmyra, New York 14522
Attention: E. W. Fisher

61. Chemicals Division of Union Carbide Corp.
Technical Service Lab.
P. O. Box 65
Tarrytown, New York
Attention: J. C. Haaga

62. Durametallic Corporation
Kalamazoo, Michigan
Attention: H. Hummer

63. Morganite, Incorporated
33-02 48th Avenue
L. I. C. 1, New York
Attention: S. A. Rokaw

64. United States Graphite Company
1621 Holland
Saginaw, Michigan
Attention: F. F. Ruhl

65. Cartiseal Corporation
3515 West Touhy
Lincolnwood, Illinois
Attention: R. Voitik

66. Department of the Army
U. S. Army Aviation Material Laboratory
Fort Eustis, Virginia 23604
Attention: John W. White, Chief
Propulsion Division

67. AVCOM
AMSAVEGTT
Mart Building
405 South 12th Street
St. Louis, Missouri 63100
Attention: E. England